

DUPLICATE COPY

2

GL-TR-89-0343
ENVIRONMENTAL RESEARCH PAPERS, NO. 1039

AD-A231 595

Development of a Cloud Forecast Scheme for the
GL Baseline Global Spectral Model

KENNETH E. MITCHELL
DOUGLAS C. HAHN



20 December 1989

DTIC
ELECTE
FEB 14 1991
S B D



Approved for public release; distribution unlimited.



ATMOSPHERIC SCIENCES DIVISION PROJECT 6670
GEOPHYSICS LABORATORY
HANSCOM AFB, MA 01731-5000

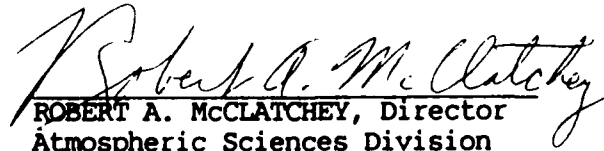
91 2 13 027

"This technical report has been reviewed and is approved for publication"

FOR THE COMMANDER



DONALD A. CHISHOLM, Chief
Atmospheric Prediction Branch



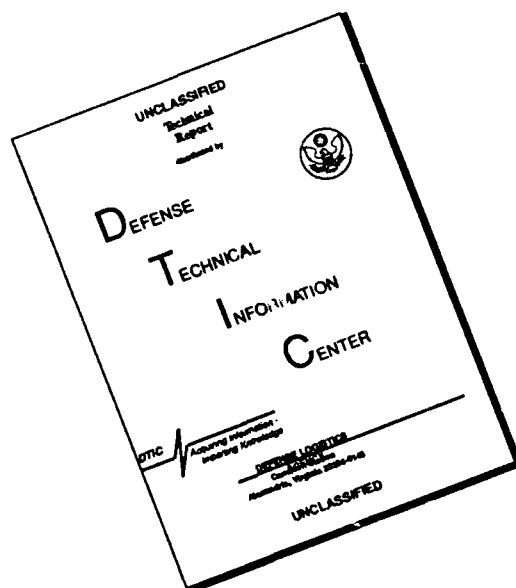
ROBERT A. McCLATCHEY, Director
Atmospheric Sciences Division

This document has been reviewed by the ESD Public Affairs Office (PA) and is releasable to the National Technical Information Service (NTIS).

Qualified requestors may obtain additional copies from the Defense Technical Information Center. All others should apply to the National Technical Information Service.

If your address has changed, or if you wish to be removed from the mailing list, or if the addressee is no longer employed by your organization, please notify AFGL/DAA, Hanscom AFB, MA 01731. This will assist us in maintaining a current mailing list.

DISCLAIMER NOTICE



THIS DOCUMENT IS BEST QUALITY AVAILABLE. THE COPY FURNISHED TO DTIC CONTAINED A SIGNIFICANT NUMBER OF PAGES WHICH DO NOT REPRODUCE LEGIBLY.

REPORT DOCUMENTATION PAGE

Form Approved
OMB No. 0704-0188

Public reporting for this collection of information is estimated to average 1 hour per response, including the time for reviewing instructions, searching existing data sources, gathering and maintaining the data needed, and completing and reviewing the collection of information. Send comments regarding this burden estimate or any other aspect of this collection of information, including suggestions for reducing this burden, to Washington Headquarters Services, Directorate for Information Operations and Reports, 1215 Jefferson Davis Highway, Suite 1204, Arlington, VA 22202-4302, and to the Office of Management and Budget, Paperwork Reduction Project (0704-0188), Washington, DC 20503.

1. AGENCY USE ONLY (Leave blank)		2. REPORT DATE 20 December 1989	3. REPORT TYPE AND DATES COVERED Final Report 01 Oct 87 to 30 Sep 89	
4. TITLE AND SUBTITLE Development of a Cloud Forecast Scheme for the GL Baseline Global Spectral Model			5. FUNDING NUMBERS 62101F PR 6670 TA 10 WU 19	
6. AUTHOR(S) Mitchell, Kenneth E. Hahn, Douglas C.				
7. PERFORMING ORGANIZATION NAME(S) AND ADDRESS(ES) Geophysics Laboratory (LYP) Hanscom Air Force Base Massachusetts 01731-5000			8. PERFORMING ORGANIZATION REPORT NUMBER GL-TR-89-0343 ERP, NO. 1039	
9. SPONSORING/MONITORING AGENCY NAME(S) AND ADDRESS(ES)			10. SPONSORING/MONITORING AGENCY REPORT NUMBER	
11. SUPPLEMENTARY NOTES				
12a. DISTRIBUTION/AVAILABILITY STATEMENT Approved for public release; distribution unlimited			12b. DISTRIBUTION CODE	
13. ABSTRACT (Maximum 200 words) Using forecast relative humidity (RH) from a global model, several pre-existing diagnostic RH-to-cloud schemes were tested to forecast global fractional cloud cover in a postprocessor format. Since none of the schemes tested provided a superior cloud forecast when compared to Air Force Global Weather Central's (AFGWC) operational 5LAYER cloud forecasts, a new RH-to-cloud scheme was developed by relating cumulative frequencies of forecast RH to cumulative frequencies of analyzed cloud cover from the AFGWC RTNEPH cloud analysis. This scheme creates a series of forecast time-dependent RH-to-cloud curves that can be temporally updated to account for changes in season, cloud analysis, or forecast model. The global model used was a spectral-type developed by the Geophysics Laboratory (GL) using parameterized diabatic physics presently incorporated in the operational GSM (global spectral model) at AFGWC.				
14. SUBJECT TERMS Numerical weather prediction Spectral atmospheric models			15. NUMBER OF PAGES 164	
Weather forecasting Cloud forecasting			16. PRICE CODE	
17. SECURITY CLASSIFICATION OF REPORT UNCLASSIFIED	18. SECURITY CLASSIFICATION OF THIS PAGE UNCLASSIFIED	19. SECURITY CLASSIFICATION OF ABSTRACT UNCLASSIFIED	20. LIMITATION OF ABSTRACT SAR	

Accession For	
NTIS GRA&I	<input checked="" type="checkbox"/>
DTIC TAB	<input type="checkbox"/>
Unannounced	<input type="checkbox"/>
Justification	
By _____	
Distribution/	
Availability Codes	
Dist	Avail and/or Special
A-1	



Preface

The authors wish to acknowledge several persons and groups who contributed to the development and preparation of this report. Several members of AFGWC sections SDDC and SDDN, especially Major Carol Belt and Mr. Ed Carr, carried out the rather arduous special archiving of AFGWC databases needed for this study. Mr. Don Norquist of GL derived and provided the data in Figure 2 and Table 4. Mr. Don Aiken of GL assisted in generating some of the computer graphics as well as managing and reading the many data tapes. The pursuit of the overall study benefited from the many discussions with and advice from our GL colleagues Mr. Don Norquist, Mr. Don Chisholm, Dr. C.-H. Yang, and Dr. H. Stuart Muench.

The new GL diagnostic cloud scheme described in Section 3.1.3 was first presented in December 1987 to the annual meeting of the GL and AWS Numerical Models Technical Exchange Group (NUMTEG). It is an empirical diagnostic cloud scheme that can be tuned for any given forecast model and can optionally include a real-time update feature, made possible by the real-time operation of AFGWC's automated cloud analysis model, known as the RTNEPH. The methodology of the GL cloud scheme evolved from steps to establish a critical value of relative humidity, RH_c , that defined a range of model forecast humidity (0 to RH_c) occurring with the same cumulative frequency as zero cloud cover in the verifying RTNEPH cloud analysis. By similarly repeating the procedure to establish critical humidity thresholds for nonzero RTNEPH cloud amounts, quasi-continuous empirical curves can be derived relating the full range of forecast humidity to the full range of fractional cloud cover. The development of this cloud scheme benefited from discussions with colleagues Dr. Ross Hoffman of AER, Inc. of Cambridge, MA and Lt Dave McDonald of AFGWC/SDDC.

At the time of this writing, a GL-funded contract effort at AFGWC has been initiated to perform an extensive follow-on study. This study will test and evaluate the new GL cloud scheme in the AFGWC operational global spectral model on a routine daily basis over a period of 6-12 months. In support of this contract effort, the present report is purposely rather

detailed, and hence probably longer than preferred by most readers. To this latter group we recommend Sections 1, 2.2, 3.1, the beginning of Section 3.2 (up to 3.2.1) and Section 4.

Finally, the latter third of this report was completed after the lead author had transferred from GL to a position at the National Meteorological Center beginning in November 1988. As a reserve officer with AFGWC, the lead author thanks AFGWC/SDD for permission during this period to complete portions of this report while on reserve duty.

Contents

1. INTRODUCTION	1
2. GLOBAL HUMIDITY ANALYSES AND FORECASTS	6
2.1 Global Humidity Analyses	7
2.1.1 Sources of the Humidity Analyses	7
2.1.2 Characteristics of the Humidity Analyses	15
2.2 Global Humidity Forecasts	29
3. EXPERIMENTAL GLOBAL CLOUD FORECASTS	52
3.1 Diagnostic Cloud Forecast Schemes	52
3.1.1 Global Cloud Forecast Procedures	53
3.1.2 Previous Diagnostic Cloud Schemes	55
3.1.3 The New GL Diagnostic Cloud Scheme	67
3.2 Performance of Global Cloud Forecasts	80
3.2.1 Parallel 5LAYER Model Forecasts	104
3.2.2 Previous Diagnostic Cloud Schemes	109
3.2.3 The New GL Diagnostic Cloud Scheme	128
4. SUMMARY AND CONCLUSIONS	138
REFERENCES	143
LIST OF ACRONYMS	146
APPENDIX A: THE VERTICAL CLOUD STACKING ALGORITHM	A1

Illustrations

1. Boundaries of the NH AFGWC Octagon Domain and the U.S. and Europe Verification Domains Used in this Study. (Shading key at lower right applies to cloud fields in Figures 30-47 and shows eight shading intensities, including blank, for eight cloud intervals). 13
2. (a) Zonal Time Average of RH for the FGGE Level II-B Rawinsonde Observations During 3-22 February 1979. In all plots of zonal average RH, the contour interval is five. (b) For the Seven Moist Layers of the GSM, the Number (X10) of Rawinsonde Observations of RH as Summed Over 10° Latitude Bands and Ten 00Z and 12Z Time Periods During 15-20 February 1979 (From the study of D. Norquist¹²). 16
3. (a) Zonal Time Average of RH for the 00Z and 12Z NMC FGGE III-A Objective Analyses During 3-22 February 1979. (b) Difference Between Zonal Time Average of RH in Figures 3a and 2a. (In all difference plots of zonal average RH, the contour interval is four and dashed contours denote negative values). 18
4. (a) Zonal Time Average of RH for the NMC Analysis for 00Z, 14 January 1982. (b) Difference Between Zonal Average of RH in Figures 4a and 2a. 20
5. (a) Zonal Time Average of RH from Eleven 00Z AFGWC Analyses During January 1985 (see Table 1 for dates). (b) Difference Between Zonal Time Average of RH in Figures 5a and 2a. 22
6. NH AFGWC 30 kPa RH Analysis for 00Z, 17 January 1985. (Shading key at lower right shows five shading intensities, including blank, for five RH intervals). 23
7. Schematic Diagram of the AFGWC Algorithm Which Infers Initial CPS Moisture Values for the AFGWC 5LAYER Forecast Model from the AFGWC RTNEPH Global Cloud Analysis. (See report by T. Crum⁴ for details). 24
8. Curves of the AFGWC CPS-cloud Amount Conversion Scheme Used in the CPS-cloud Conversion Step of Figure 7. 25

9. The Critical Relative Humidity (RH) as Derived from the CPS-cloud Curves of Figure 8, for the Lowest Six Mandatory Pressures, Assuming U.S. Standard Atmosphere Temperatures and Applying the 85 kPa and 30 kPa CPS-cloud Curves Also to the 100 kPa and 40 kPa Levels, Respectively.	26
10. (a) Zonal Average of RH from the Experimental Analysis of 3DNEPH-inferred RH Derived by Mitchell and Warburton ⁶ for 00Z, 14 January 82. (b) Difference Between Zonal Average of RH in Figures 10a and 2a.	28
11. NH Mean RH at Six Mandatory Pressures as a Function of Forecast Length in Four GSM Forecasts Initialized from Four Separate Initial Analyses as Labeled.	30
12. Vertical Profiles of the NH Mean RH at the (a) 0-hr Initial Time and (b) 96-hr Forecast Time for the Four GSM Forecast Cases in Figure 11. Also given as a reference is the vertical profile of NH mean RH as derived from the FGGE II-B zonal average RH values in Figure 2.	32
13. (a) Zonal Average of RH for the 48-hr GSM Forecast Initialized from the NMC Analysis of 00Z, 14 January 1982. (b) Difference Between the Above Average and that of the Corresponding Initial Analysis (Figure 4a).	34
14. (a) Zonal Average of RH for the 48-hr GSM Forecast Initialized from the AFGWC Analysis of 00Z, 17 January 1985. (b) Difference Between the Above Zonal Average and That of the Corresponding Initial Analysis.	35
15. NH NMC RH Analysis for 00Z, 14 January 1982 at Levels (a) 100, (b) 85, (c) 70, (d) 50, (e) 40 and (f) 30 kPa. (The shading key in Figure 6 applies to all shaded displays of <u>RH</u> fields).	37-39
16. NH GSM 48-hr RH Forecast at Levels (a) 100, (b) 85, (c) 70, (d) 50, (e) 40 and (f) 30 kPa for the Forecast Initialized From the NMC Analysis of Figure 15.	40-42
17. NH AFGWC RH Analysis for 00Z, 17 January 1985 at Levels (a) 100, (b) 85, (c) 70, (d) 50, (e) 40 and (f) 30 kPa. (The shading key in Figure 6 applies to all shaded displays of <u>RH</u> fields).	43-45
18. NH GSM 48-hr RH Forecast at Levels (a) 100, (b) 85, (c) 70, (d) 50, (e) 40 and (f) 30 kPa for the Forecast Initialized from the GSM Forecast Initialized from the AFGWC Analysis of Figure 17.	46-48
19. Percent Occurrence Over the NH Octagon Domain of (a) Moist RH Values (RH>82) and (b) Dry RH Values (RH<23) at the 50, 70, and 85 kPa Pressure Levels for the 0-, 48-, and 96-hour GSM Forecasts Initialized from the NMC Analysis of 00Z, 14 January 1982 (bottom) and the AFGWC Analysis of 00Z, 17 January 1985 (top).	50
20. Curves of the ECMWF Humidity-cloud Conversion Scheme of Eqs. (1)-(2) for Four Mandatory Pressures.	58
21. Critical Relative Humidity, RH _c , as a Function of Pressure for the Cloud Amount Thresholds of (a) 0 Percent and (b) 30 Percent for the ECMWF, AFGWC, NMC, and GL Humidity-cloud Conversion Schemes.	60
22. Curves of the ECMWF, AFGWC, NMC, and GL Humidity-cloud Conversion Schemes for the (a) 50 kPa and (b) 85 kPa Mandatory Pressures.	61
23. Curves of the NMC Humidity-cloud Conversion Scheme of Eq. (4) and Table 6 for the PBL, Low Middle, and High Pressure Regimes of Eq. (3).	64

24. Category (top) and Cumulative (bottom) Frequency of Occurrence (at one percent intervals) of RTNEPH Analyzed Cloud Amounts (Part a) and GSM 24-hour Forecast RH Amounts (Part b) at 70 kPa Over the NH Octagon, Valid at 00Z, 18 January 1985. At bottom, the one-to-one mapping of the RTNEPH observed cloud frequency onto the GSM forecast RH frequency yields one of the GL humidity-cloud conversion curves (solid) in Figure 25a.	69
25. Curves of the GL Humidity-cloud Conversion Scheme Derived for the GSM 24-hour Forecasts at (a) 70 kPa and (b) 30 kPa by Applying the Methodology of Figure 24 to Two Separate Samples (and their aggregate) of the Frequency Distributions of GSM Forecast RH and RTNEPH Verifying Cloud Over the NH Octagon.	71
26. Curves of the GL Humidity-cloud Conversion Scheme as a Function of GSM Forecast Length for (a) 70 kPa and (b) 30 kPa Mandatory Pressures. (Curves based on the aggregate NH octagon GSM RH/RTNEPH cloud frequency distributions for the 00Z, 17 and 24 January 1985 GSM forecast cases).	74
27. Curves of the GL Humidity-cloud Conversion Scheme as a Function of Mandatory Pressure for the GSM 0-hour and 48-hour Forecasts (based on aggregate sample as in Figure 26).	76
28. Curves of the Four-layer Version of the GL Humidity-cloud Conversion Scheme (see text) as a Function of Mandatory Pressure for the GSM 0-hour and 48-hour Forecasts (based on aggregate sample as in Figure 26).	78
29. The ECMWF Operational NH 12Z Analyses ³² of the 50 kPa Height Field (top) and Sea-level Pressure Field (bottom) for (a) 17 January and (b) 19 January 1985.	98
30. The RTNEPH 00Z Analysis of NH Octagon <u>Total</u> Cloud Amount for (a) 17 January and (b) 19 January 1985. (The shading key in Figure 1 applies to all shaded displays of cloud amount).	99
31. The RTNEPH 00Z Analysis of NH Octagon <u>Layer</u> Cloud Amount for (a) 17 January 1985 for the (a) Gradient, (b) 85, (c) 70 and (d) 30 kPa Layers. (The shading key in Figure 1 applies to all shaded displays of cloud amount).	100-101
32. The RTNEPH 00Z Analysis of NH Octagon <u>Layer</u> Cloud Amount for 19 January 1985 for the (a) Gradient, (b) 85, (c) 70 and (d) 30 kPa Layers. (The shading key in Figure 1 applies to all shaded displays of cloud amount).	102-103
33. The 5LAYER 45-hour Forecast of NH Octagon <u>Total</u> Cloud Amount Valid at 00Z, 19 January 1985.	105
34. The 5LAYER 45-hour Forecast of NH Octagon <u>Layer</u> Cloud Amount Valid at 00Z, 19 January 1985, for the (a) Gradient, (b) 85, (c) 70 and (d) 30 kPa Layers.	106-107
35. For the AFGWC Cloud Scheme, the GSM (a) 0-hour and (b) 48-hour Forecast of NH <u>Total</u> Cloud Amount Valid at 00Z on 17 and 19 January 1985, Respectively.	112
36. For the AFGWC Cloud Scheme, the GSM 0-hour Forecast of NH <u>Layer</u> Cloud Amount Valid at 00Z on 17 January 1985 for Layers Nominally Centered at the (a) 100, (b) 85, (c) 70 and (d) 30 kPa Pressure Levels.	113-114
37. For the AFGWC Cloud Scheme, the GSM 48-hour Forecast of NH <u>Layer</u> Cloud Amount Valid at 00Z on 19 January 1985 for Layers Nominally Centered at the (a) 100, (b) 85, (c) 70 and (d) 30 kPa Pressure Levels.	115-116
38. Schematic Illustration of the Major Static Preprocessing and Postprocessing Steps, which when Applied (Along with the Chosen Cloud Scheme as the Last Step) to an Input Humidity Analysis on Mandatory Pressure Levels Yield the So-called "Synthesized" GSM 0-hour Cloud Forecast.	118

39. For the NMC Cloud Scheme, the GSM (a) 0-hour and (b) 48-hour Forecast of NH <u>Total</u> Cloud Amount Valid at 00Z on 17 and 19 January 1985, Respectively.	121
40. For the NMC Cloud Scheme, the GSM 48-hour Forecast of NH <u>Layer</u> Cloud Amount Valid at 00Z on 19 January 1985 for Layers Nominally Centered at the (a) 100, (b) 85, (c) 70 and (d) 30 kPa Pressure Levels.	122-123
41. For the ECMWF Cloud Scheme, the GSM (a) 0-hour and (b) 48-hour Forecast of NH <u>Total</u> Cloud Amount Valid at 00Z on 17 and 19 January 1985, Respectively.	125
42. For the ECMWF Cloud Scheme, the GSM 48-hour Forecast of NH <u>Layer</u> Cloud Amount Valid at 00Z on 19 January 1985 for Layers Nominally Centered at the (a) 100, (b) 85, (c) 70 and (d) 30 kPa Pressure Levels.	126-127
43. For the GL6 Cloud Scheme, the GSM (a) 0-hour and (b) 48-hour Forecast of NH <u>Total</u> Cloud Amount Valid at 00Z on 17 and 19 January 1985, Respectively.	129
44. For the GL6 Cloud Scheme, the GSM 0-hour Forecast of NH <u>Layer</u> Cloud Amount Valid at 00Z on 17 January 1985 for Layers Nominally Centered at the (a) 100, (b) 85, (c) 70 and (d) 30 kPa Pressure Levels.	130-131
45. For the GL6 Cloud Scheme, the GSM 48-hour Forecast of NH <u>Layer</u> Cloud Amount Valid at 00Z on 19 January 1985 for Layers Nominally Centered at the (a) 100, (b) 85, (c) 70 and (d) 30 kPa Pressure Levels.	132-133
46. For the GL4 Cloud Scheme, the GSM (a) 0-hour and (b) 48-hour Forecast of NH <u>Total</u> Cloud Amount Valid at 00Z on 17 and 19 January 1985, Respectively.	134
47. For the GL4 Cloud Scheme, the GSM 48-hour Forecast of NH <u>Layer</u> Cloud Amount Valid at 00Z on 19 January 1985 for Layers Nominally Centered at the (a) Low and (b) High Cloud.	135

Tables

1. Attributes of the Global Analyses Used in Study (All analyses performed on mandatory pressure levels).	8
2. Main Differences Between Phase I and Phase II of AFGWC AWAPS Global 4-D Assimilation System.	11
3. Outline of AFGWC Pre-HIRAS Operational Global Moisture Analysis.	14
4. Statistics of Differences Between Relative Humidity Inferred from Cloud Amount and that Measured with Radiosondes (in %) (from Norquist ^{12,13}).	27
5. The σ -Structure of the Baseline GL GSM.	31
6. Parameters of the NMC/Tibaldi Humidity-Cloud Scheme.	65
7. Comparison of Critical Relative Humidity Values, RH _c , in Original and Modified ECMWF Humidity-Cloud Scheme (assume P* = 100 kPa).	68
8. Examples of Transformation $RH^* = 1 - \sqrt{1 - RH}$.	73
9. Mean Total Cloud Amount (percent) as a Function of Forecast Period Over the N.H. Octagon Domain for 00Z, 17 January 1985.	82
10. Total Cloud Forecast BIAS (in Percent Cloud Cover) for 10 Global Spectral (GSM) Cloud Schemes, the 5LAYER Model, and RTNEPH Persistence for the 00Z, 17 January 1985 Case Over the Three Areas of (A) NH, (B) U.S., and (C) Europe.	83
11. Total Cloud Forecast BIAS (in Percent Cloud Cover) for 10 Global Spectral Model (GSM) Cloud Schemes, the 5LAYER Model, and RTNEPH Persistence for the 00Z, 24 January 1985 Case Over the Three Areas of (A) NH, (B) U.S., and (C) Europe.	86

12. Total Cloud Forecast 20/20 Accuracy Score (Percent of Grid Points Correct to Within 20 Percent Cloud Cover) for Ten Global Spectral Model (GSM) Cloud Schemes, the 5LAYER Model, and RTNEPH Persistence for the 00Z, 17 January 1985 Case Over the Three Areas of (A) U.S., (B) Europe, and (C) NH (See text for connotation of brackets, parentheses, and underscores). 89
13. Total Cloud Forecast 20/20 Accuracy Score (Percent of Grid Points Correct to Within 20 Percent Cloud Cover) for Ten Global Spectral Model (GSM) Cloud Schemes, the 5LAYER Model, and RTNEPH Persistence for the 00Z, 24 January 1985 Case Over the Three Areas of (A) U.S., (B) Europe, and (C) NH (See text for connotation of brackets, parentheses, and underscores). 92

Development of a Cloud Forecast Scheme for the GL Baseline Global Spectral Model

1. INTRODUCTION

Numerical weather prediction groups generally incorporate cloud forecast schemes into global prediction models with one of two primary objectives in mind. The first and most common objective is to formulate a scheme suitable for interaction with the global model's parameterized diabatic physics, particularly radiation. These schemes are ultimately judged by their impact on the parameterized physics, such as their effect on the earth's radiation budget.¹ In this context, simple cloud schemes are often utilized. Some examples are prescribed zonal mean cloud amounts at every grid point or forecasts of "on-off" binary cloud amounts of 0 or 100 percent.

The second objective, which is the foremost objective here, is to forecast cloud cover for its own sake, that is, for its importance as a sensible weather element to end users of numerical

(Received for Publication 15 Dec. 1989)

¹ Geleyn, J.-F. (1981) *Some diagnostics of the cloud/radiation interaction in the ECMWF forecasting model*, ECMWF Workshop on Radiation and Cloud-Radiation Interaction in Numerical Modeling, 15-17 October 1980, European Centre for Medium Range Weather Forecasts, Reading, Berkshire, U.K., 135-162.

weather prediction (NWP) products.* Our specific goal here is to forecast grid-area values of horizontal fractional cloud cover (both total and layered) in the 0-4 day range. The purpose is to develop and demonstrate a cloud forecast scheme suitable for use in the operational global spectral model (GSM) of the Advanced Weather Analysis and Prediction System (AWAPS)² at Air Force Global Weather Central (AFGWC). The cloud cover forecasts must be sufficiently accurate to use in the operation of numerous Air Force missions that are sensitive to clouds, particularly their obstruction to clear lines of sight.

Clearly, the two cloud forecast objectives cited above are not mutually exclusive and modeling groups consider both simultaneously.³ However, the state of the art in modeling the hydrological cycle and other diabatic physics in global models is not sufficiently advanced to allow pursuing both objectives with equal priority. Therefore, in developing and testing cloud forecast schemes, modeling groups must sometimes adopt methods that further one objective to the detriment of the other. Over the long term, as modeling advances continue, the approaches to achieve these two cloud forecast objectives should converge. In the meantime, the near-term emphasis in the GL effort will remain accurate forecasts of fractional cloud cover.

Before the implementation of the AWAPS at AFGWC in October 1985, the AFGWC model known as 5LAYER was the only *moist* NWP forecast model executed by AFGWC. The 5LAYER model forecasts temperature, moisture, and precipitation by employing quasi-Lagrangian numerical methods, in which 3-hourly 3-D air parcel displacements or trajectories are computed from wind velocity forecasts input from a previously executed independent NWP forecast model.⁴ The AWS dry PE grid-point model served as the independent model prior to the AWAPS era.⁵ The AWS PE model, and thus also 5LAYER, was executed only out to 48 hours and only on extratropical domains.

With the advent of the AWAPS at AFGWC, the concurrent advent of a moist GSM provided AFGWC with a second moist model, which was also global in extent. Since the beginning of the AWAPS, AFGWC has continued to execute the 5LAYER model as its primary cloud forecast model, but now using the GSM wind velocity forecasts for its input winds. While executing the above GSM/5LAYER scenario, AWS and AFGWC have naturally considered the question of *whether the GSM, being a moist model, could be utilized directly to provide cloud forecasts, thus eliminating the need to execute 5LAYER as a follow-on cloud forecast model.* The present study

* (Note: all acronyms are defined in List of Acronyms)

² Stobie, J.G. (1986) *AFGWC's Advanced Weather Analysis Prediction System (AWAPS)*, AWS/TN-86-001, Air Weather Service, Scott AFB, IL, pp. 61.

³ Slingo, J. and Ritter, B. (1985) *Cloud Prediction in the ECMWF model*, ECMWF Tech. Rep. No., 46, European Centre for Medium Range Weather Forecasts, Reading, Berkshire, U.K., pp. 48.

⁴ Crum, T.D. (1987) *AFGWC Cloud Forecast Models*, AFGWC/TN-87-001, Air Force Global Weather Central, Offutt AFB, NE, pp. 66.

⁵ Tarbell, T. and Hoke, J. (1979) *The AFGWC Automated Analysis/Forecast Model System*, AFGWC-TN-79/004, Air Force Global Weather Central, Offutt AFB, NE, pp. 52.

addresses this question in the context of the resolution and physics of AFGWC's presently operational GSM.

The GSM cloud forecast experiments presented in this report are close follow-ons to the GSM experiments described in the paper by Mitchell and Warburton.⁶ We urge the reader to review that paper (hereafter denoted as MW) as a forerunner to this report. The GSM cloud forecast experiments in MW were performed at the National Meteorological Center (NMC) using the NMC GSM.

The present experiments utilize the GL global spectral model, described by Brenner et al.⁷ This model was developed at GL by closely following the NMC spectral model developed by J. Sela,⁸ who earlier in 1980 with other NMC staff provided the NMC GSM codes and substantial consultation to GL. In the GL spectral model, the formulation for the *adiabatic* dynamics of the NMC model was utilized, but was completely recoded by GL to increase the code modularity, flexibility, and portability desirable in R&D applications. The GL model can be configured easily to run in numerous horizontal and vertical resolutions and on various mainframe computers used by GL and GL contractors (see Brenner et al.⁷ for examples).

Unlike the adiabatic dynamics, whose formulation is now fairly fixed and has remained essentially unchanged since the recoding cited above, the GL GSM parameterizations for the diabatic physics (for example, boundary layer fluxes, precipitation, radiation) can follow any one of several packages. For the GSM experiments in this study, we used GL's "baseline" version of the parameterized physics. This version utilizes verbatim the parameterized physics subroutines presently used in the operational GSM in AFGWC's AWAPS. The latter operational model was delivered to AFGWC by NMC in 1983 and represents NMC's operational GSM as it stood at that time.

The decision to utilize the baseline physics for this study was motivated by the study objective cited earlier; namely, *to develop and demonstrate a cloud forecast scheme suitable for AFGWC's currently operational GSM*. Thus in the GSM experiments here, which were executed on the Air Force Supercomputer Center - Kirtland (AFSCC-K) CRAY-1/S computer, we took care to parallel the configuration of operational executions of AFGWC's GSM. Specifically, in addition to using the baseline (AFGWC) parameterized physics, we acquired and used AFGWC's prescribed GSM surface fields, which include terrain height, monthly mean sea-surface temperature, and surface-drag coefficients. Furthermore, we utilized the same externally specified control parameters (such as horizontal diffusion coefficients), 12-layer vertical σ -structure (N12), horizontal rhomboidal truncation at wavenumber 40 (R40), and nonlinear normal mode initialization package. Lastly, for the GSM initial conditions, we used AFGWC's operational 2.5° latitude/longitude global objective analysis (uninitialized). In later

⁶ Mitchell, K. and Warburton, J. (1983) *A comparison of cloud forecasts derived from the NMC and AFGWC operational hemisphere forecasts of moisture*, Proceedings of AMS Sixth Conference on Numerical Weather Prediction, 6-9 June 1983, Omaha, NE, pp. 66-73.

⁷ Brenner, S., Yang, C.-H., and Mitchell, K. (1984) *The AFGL Global Spectral Model: Expanded Resolution Baseline Version*, AFGL-TR-84-0308, ADA160370.

⁸ Sela, J. (1980) Spectral modeling at the National Meteorological Center, *Mon. Wea. Rev.*, **108**:1279-1292.

experiments, we also used several NMC global 2.5° analyses as GSM initial states, to highlight several serious deficiencies that we identified in the AFGWC global moisture analyses.

The possibility of future AFGWC application of the GSM cloud forecast algorithms tested in this report also motivated the decision to evaluate and compare the experimental GSM cloud forecasts against the operational cloud forecasts from the AFGWC 5LAYER model.⁴ The AFGWC global objective cloud analysis model, known as RTNEPH and described by Kiess and Cox,⁹ is used by AFGWC to routinely verify the cloud forecast skill of the 5LAYER model. Therefore, in this study, the experimental GSM cloud forecasts as well as the operational 5LAYER cloud forecasts for the same valid times are verified in parallel against the RTNEPH cloud analysis.

It is appropriate now to review the basic components of the "baseline" physics package in the GL GSM (or present AFGWC GSM). Following that, we will briefly review the considerable efforts at GL to develop substantially improved physical parameterizations for the GSM. In so doing, we shall clarify the context of the present study within the larger overall GSM development program at GL.

The baseline physical parameterizations include linear horizontal diffusion, moist convective adjustment following Kuo,¹⁰ dry convective adjustment, and a simple stable condensation scheme that immediately condenses out, as rain, all water vapor exceeding a relative humidity saturation criterion of 1.0 (0.90 in the lowest model layer). The evaporation of rainfall is included in subsaturated lower levels. The planetary boundary layer scheme is very simple and includes bulk aerodynamic surface fluxes of momentum, heat, and moisture in the first model layer (the surface exchange coefficients are not stability dependent). Over land the surface heat and moisture fluxes are assumed to be zero and over oceans they are computed using a specified monthly mean surface temperature. Finally, vertical diffusion is ignored everywhere above the first model layer and the effects of radiation are entirely neglected.

Since 1983 both GL and NMC have pursued comprehensive improvements to the baseline parameterized physics. The GL and NMC parameterization efforts are proceeding mostly independently, because of different priorities in the requirements to be satisfied by the respective GSMs and the available computer resources. However, a constant exchange of model development progress takes place routinely between NMC, GL, and AFGWC through periodic meetings of a Numerical Models Technical Exchange Group.

Within the GL parameterization program, more emphasis is being placed on both 1) the shorter range of 0-2 days (including the diurnal cycle) rather than the medium range of 3-10 days, and 2) the hydrological cycle, to provide a firm foundation for forecasting humidity, clouds, and precipitation. The latter fields are notoriously difficult to predict in global models, owing to the historically coarse resolution of such models. At NMC and other centers for example, emphasis on moisture-related fields is foremost in regional or limited-area models, but somewhat secondary in global models. GL also has an ongoing development

⁹ Kiess, R. and Cox, W. (1988) *The AFGWC Automated Real-Time Cloud Analysis Model*, AFGWC/TN-88-001, Air Force Global Weather Central, Offutt AFB, NE, pp. 82.

¹⁰ Kuo, H.L. (1965) On formation and intensification of tropical cyclones through latent heat release by cumulus convection, *J. Atmos. Sci.*, **22**:40-63.

program in regional and mesoscale modeling (for example, Halberstam et al.¹¹). However, because the USAF operates world-wide missions routinely, it may not always be feasible to provide explicit regional modeling support to all mission areas at all times. This emphasizes the need for the AFGWC GSM to be able to provide, as much as possible, regional support on the relatively short range and including detailed representation of the moist physical processes and parameters that strongly impact Air Force operations.

The development of GL's global objective analysis and 4-D data assimilation system (Norquist¹²) provides an example of the emphasis on humidity, clouds, and precipitation in GL's global modeling program. Through contracts, GL is pursuing global analysis/assimilation techniques tailored for moisture and alternative global data sources for moisture (Kaplan et al.¹³). Furthermore, in response to large moist biases in early GL assimilation experiments, GL developed improved methods for vertically interpolating moisture in 4-D assimilations (Mitchell and Yang¹⁴).

With a similar emphasis on moisture and clouds, GL has pursued its R&D in GSM physical parameterizations through contracts with three universities, one each in the areas of radiation (Liou et al.¹⁵), deep moist convection (Soong et al.¹⁶), and the planetary boundary layer or PBL (Mahrt et al.¹⁷). The PBL and convection initiatives in particular have emphasized moisture and hydrological aspects. In-house, GL is testing the three physical parameterizations together in the GL GSM and a first evaluation of their performance and impacts is given in Yang et al.¹⁸. Although the GSM cloud forecast scheme interacted with the physical parameterizations in these latter tests, the first evaluation by Yang et al.¹⁸ purposely did not examine point-wise cloud forecast accuracy. Nevertheless, as the new physical parameterizations are further extended and refined, ultimately a chief GL criterion for judging the new parameterizations will be the impact on accurate forecasts of fractional cloud cover (along with the closely associated relative humidity distribution). Thus, the present effort here, to determine the cloud forecast skill achievable in the GL GSM using the original

¹¹ Halberstam, I.M. (1988) *Objective Nephology, Section 1: Improved Regional Cloud Forecast Model*, AFGL-TR-88-0109, pp. 1-46, ADA200500.

¹² Norquist, D. (1986) *Alternative forms of moisture information in 4-D data assimilation*, AFGL-TR-86-0194, pp. 139, ADA179792.

¹³ Kaplan, L.D., Hoffman, R.N., Isaacs, R.G., Rosen, R.D., Salstein, D.A., and Wang, W.-C. (1983) *Outlook for Improved Numerical Weather Prediction Using Satellite Data with a Special Emphasis on the Hydrological Variables*, AFGL-TR-83-0305, pp.183, ADA141233.

¹⁴ Mitchell, K. and Yang, C.-H. (1985) *A Comparison of Moisture Variables in the Vertical Interpolations of a 4-D Assimilation System*, AFGL-TR-85-0090, pp. 77, ADA160464.

¹⁵ Liou, K.-N., Ou, S.C., Kinne, S., and Koenig, G. (1984) *Radiation Parameterization Programs for Use in General Circulation Models*, AFGL-TR-84-0217, ADA148015.

¹⁶ Soong, S.-T., Ogura, Y., and Kau, W.S. (1985) *Study of Cumulus Parameterization in a Global Circulation Model*, AFGL-TR-85-0160, pp. 122, ADA170137.

¹⁷ Mahrt, L., Pan, H.-L., Paumier, J. and Troen, I. (1984) *A Boundary Layer Parameterization Scheme for a General Circulation Model*, AFGL-TR-84-0063, pp. 169, ADA144224.

¹⁸ Yang, C.-H., Norquist, D., Yee, S.Y.K., and Mitchell, K. (1989) *Diagnostics for and Evaluations of New Physical Parameterization Schemes for Global NWP Models*, GL-TR-89-0158.

baseline physics, will provide a basis for comparing future cloud forecast experiments using the newer physical parameterizations.

We conclude this introduction with an overview of the sections that follow. In Section 2 we examine the GSM humidity forecasts. To do this in a complete sense, we first examine the AFGWC global humidity analyses used to initialize the GSM humidity forecasts. To document several substantial weaknesses in the AFGWC humidity analyses, key features of global relative humidity are derived from global radiosonde observations (RAOBs) and from NMC operational global moisture analyses. The above emphasis on humidity analyses and forecasts is a necessary forerunner to understand several central features of the experimental GSM cloud forecasts presented later in Section 3.

Section 3 begins with a description of several candidate empirical cloud schemes that relate large-scale humidity fields to fractional cloud cover. Three of these humidity-to-cloud schemes are previously known schemes obtained from operational NWP groups. A fourth empirical cloud scheme is highlighted here as it is a new scheme recently developed at GL as a part of this study. This new GL cloud forecast scheme is unique in that it is the first known scheme to be derived objectively from coincident samples of global gridded NWP humidity forecasts and global gridded objective cloud analyses (in this case AFGWC RTNEPH cloud analyses). Because the RTNEPH is a daily operational cloud analysis model at AFGWC, the method of deriving the empirical humidity-to-cloud relations in the new GL cloud scheme can optionally include real-time updates of the relations as part of the daily AFGWC analysis and forecast cycle. As a by-product of such a real-time update, the GL cloud scheme can adjust to changes in resolution, physics, or systematic trends in either the NWP model humidity forecasts or the RTNEPH cloud analyses. Also in Section 3, displays of the experimental GSM cloud forecasts are presented, as obtained by employing each of the four empirical cloud schemes in conjunction with 4-day GSM humidity forecasts. Finally, Section 3 presents the comparative 5LAYER and GSM cloud forecast accuracy statistics obtained by grid-to-grid objective verifications of the various cloud forecasts against the AFGWC RTNEPH cloud analysis. Section 4 closes out this report with conclusions and recommendations.

2. GLOBAL HUMIDITY ANALYSES AND FORECASTS

The various cloud forecast schemes documented in the literature fall into the two broad categories of 1) diagnostic schemes and 2) prognostic schemes. In prognostic schemes (for example, Sundqvist¹⁹) predictive equations are formulated and integrated to predict cloud water/ice content explicitly. In diagnostic schemes (for example, Slingo and Ritter³), desired cloud properties are diagnosed empirically or statistically from other model output fields, such as humidity, precipitation rate, and vertical velocity. In the present study, only diagnostic

¹⁹ Sundqvist, H. (1981) Prediction of stratiform clouds: results from a 5-day forecast with a global model, *Tellus*, **33**:242-253.

cloud schemes will be considered and tested. Although prognostic schemes are physically more pleasing, they are in the early stages of development, more difficult to verify, and more expensive computationally. More importantly, they typically introduce numerous arbitrary parameters to relate prognostic cloud quantities (cloud water) to desired cloud quantities (geometric cloud cover). Thus, there may be as much or more empirical or diagnostic character in predictive as in purely diagnostic cloud schemes.

Virtually all diagnostic cloud schemes depend foremost on the prediction model's relative humidity simulation. *To obtain a good diagnostic cloud forecast then, it is first imperative to achieve realistic humidity forecasts, regardless of the chosen diagnostic cloud scheme.* Thus, before applying several different diagnostic cloud schemes in Section 3, we first examine in this section the crucial characteristics of the initial global humidity analyses and follow-on GSM humidity forecasts.

2.1 Global Humidity Analyses

At the beginning of this study, the intent was to utilize only AFGWC global objective analyses to initialize and execute 4-day forecasts from GL's GSM (configured to be parallel to that of AFGWC). As the study progressed, unrealistic features were identified in the AFGWC humidity analyses. These poor initial humidity features and the GSM's large short-range humidity trends (shown later) that developed in response to these initial features necessitated the use of and comparison with alternative global humidity analyses.

2.1.1 SOURCES OF THE HUMIDITY ANALYSES

The various global analyses that were eventually considered are summarized in Table 1 and discussed further in this subsection. The collection of non AFGWC analyses in Table 1 is not exhaustive, but intentionally rather limited in number and source (NMC). The non-AFGWC analyses that were chosen here for consideration were largely determined by (1) the current availability of these analyses at GL and software to process them, and (2) the adequacy of these analyses in providing an intercomparison set sufficient to establish the major weaknesses in the AFGWC analyses.

Table 1. Attributes of the Global Analyses Used in Study
(All analyses performed on mandatory pressure levels).

DESIGNATION	SOURCE	DATES	ANALYZED VARIABLES	HORIZONTAL RESOLUTION
FGGE III-A	NMC	3-22 FEB 79	u, v, z, Q^+	2.5°
NMC/OP	NMC	00Z, 14 Jan 82	u, v, z, RH	24-wave
NMC/3DNEPH	NMC/GL	00Z, 14 Jan 82	u, v, z, RH	24-wave
AFGWC	AFGWC	00Z, Jan 85 (10-12, 16-19, 23-26)	u, v, z*, Q^+	2.5°

DESIGNATION	FIRST-GUESS FORECAST MODEL	MASS/MOTION ANALYSIS METHOD	HUMIDITY ANALYSIS METHOD
FGGE III-A	9-layer grid point	OI	OI
NMC/OP	12-layer spectral (R30)	Hough	Hough
NMC/3DNEPH	12-layer spectral (R30)	OI	3DNEPH/CPS
AFGWC	9-layer spectral (R20)	OI	Cressman

The primary reference set of non-AFGWC analyses in Table 1 is the FGGE III-A analyses. These are the optimal interpolation (OI) analyses (see Bergman²⁰) that were products of the "final update" (that is, run off of the latest data-cutoff time and using the global forecast model of Stackpole²¹ as the first-guess) of the NMC operational Global Data Assimilation

²⁰ Bergman, K.H. (1979) Multivariate analysis of temperature and winds using optimum interpolation, *Mon. Wea. Rev.*, **107**:1423-1444.

²¹ Stackpole, J.D. (1978) *The NMC 9-Layer Global Primitive Equation Model on a Latitude-Longitude Grid*, NMC Office Note 178, National Meteorological Center, Washington, D.C.

System²² (GDAS), as configured on the given analysis dates. The FGGE designation denotes First GARP Global Experiment, which refers to the internationally sponsored period (in 1979) of globally augmented conventional and satellite weather observing systems. The augmentation of observations during FGGE was especially significant during the Special Observing Period 1 (5 January 1979 - 5 March 1979) and Period 2 (5 May 1979 - 5 July 1979) which encompass the valid times of the FGGE III-A analyses in Table 1. Hence the NMC GDAS during these periods benefited from an expanded set of input observations.

The secondary set of non-AFGWC analyses in Table 1 is given by two NMC-based analyses for 00Z, 14 January 1982. These analyses were used and discussed in the previous study of MW.⁶ The analysis designated NMC/OP corresponds to the Hough-function based NMC operational global analysis used as the initial state for the NMC global forecast cycle (then called the "Large-Scale Cycle"). This analysis/forecast cycle was executed with an earlier data cutoff time than the OI-based final update cycle in the GDAS. The 6-hour GSM forecast from the GDAS OI analysis of the previous 6-hour cycle provided the first-guess for the Hough analysis. The Hough analysis is a spectral analysis (rhomboidally truncated at wavenumber 24) that uses spherical harmonic basis functions to fit available data by means of a global least squares technique.²³ Further details and limitations of the Hough analysis, especially as regards the humidity fields, are given in MW. With respect to the FGGE III-A analyses, it is important to emphasize that the NMC/OP analysis is from a different year and utilizes 1) a different analysis method, 2) an earlier data cutoff time, and 3) a later generation GDAS²⁴ (including the newer NMC GSM⁸ as the first-guess forecast model). Thus the NMC/OP analysis will serve as a useful cross reference to validate the robustness of the major zonal-mean humidity features that we shall first infer from the earlier FGGE III-A analyses.

The analysis designated NMC/3DNEPH is identical to the NMC/OP analysis for the variables u,v, and z. In NMC/3DNEPH however, the operational NMC relative humidity (RH) analysis of NMC/OP was replaced in the study of MW⁶ by an experimental RH analysis. The latter was derived by applying AFGWC's empirical humidity/cloud conversion scheme (known as the CPS scheme detailed later) to derive humidity profile estimates globally from the AFGWC 3DNEPH global cloud analysis. (The predecessor to the RTNEPH was the 3DNEPH,²⁵ which was executed operationally at AFGWC until August 1983.) The ultimate result of this application was a conversion of global 3DNEPH cloud amounts to a global 2.5° RH analysis at the lowest six mandatory pressure levels. Further details on the derivation of this humidity analysis are given in MW as well as below, when discussing the source of the AFGWC first-guess field for the AFGWC humidity analysis in Table 1. Both derivations are closely

²² McPherson, R.D., Bergman, K.H., Kistler, R.E., Rasch, G.E., and Gordon, D.S. (1979) The NMC operational global data assimilation system, *Mon. Wea. Rev.*, **107**:1445-1461.

²³ Flattery, T. (1971) *Spectral methods for global analysis and forecasting*, Proc. Sixth AWS Technical Exchange Conference, U.S. Naval Academy, 21-24 September 1970, AWS-TR-242, Air Weather Service, Scott AFB, IL, 42-54.

²⁴ Dey, C.H. and Morone, L.L. (1985) Evolution of the National Meteorological Center global data assimilation system: January 1982-December 1983., *Mon. Wea. Rev.*, **113**:304-318.

²⁵ Fye, F.K. (1978) *The AFGWC Automated Cloud Analysis Model*, AFGWC-TM-78-002, Air Force Global Weather Central, Offutt AFB, NE, pp. 97.

analogous. The experimental NMC/3DNEPH humidity analysis serves a crucial role in Section 2.1.2, as it illustrates the cause of a pervasive weakness in the AFGWC humidity analysis.

Lastly in Table 1 are the analyses designated AFGWC. These analyses were operational products of the AFGWC global 4-D assimilation system as configured during the January 1985 period denoted for them in Table 1. Except for the humidity analyses, the production AFGWC global analyses during this period were products of AFGWC's global OI analysis model known as HIRAS² and the AFGWC GSM first-guess model (obtained from NMC in 1983 and virtually identical to the GSM described by Sela⁸).

The AFGWC global 4-D data assimilation system is henceforth referred to simply as the HIRAS/GSM system. The HIRAS OI analysis model was developed, coded, and tested by AFGWC, but is a fairly close adaptation of the NMC OI analysis model described by Dey and Morone.²⁴ The AFGWC HIRAS/GSM system is well documented in the report by Stobie.² Furthermore, in a separate report Stobie et al.²⁶ describe (1) how the AFGWC OI model differs from the NMC version and (2) how the HIRAS/GSM system was implemented in two major phases. The dates of the AFGWC analyses in Table 1 are during the period of Phase I. It is important for this study to next describe the major differences between Phase I and Phase II, especially as regards the humidity fields. The period of Phase I extends from early 1984, when the HIRAS/GSM system was first implemented, until October 1985, when AFGWC acquired its CRAY X-MP/12 supercomputer. Thus Phase I is a pre-CRAY period wherein the HIRAS/GSM system operated in a substantially "scaled-down" mode as dictated by constrained computer resources. The important differences between Phase I and Phase II are listed in Table 2. These differences are self explanatory, except for the differences regarding the humidity analysis. This latter difference is explained below -- and necessarily in some detail.

²⁶ Stobie, J.G., Lewis, M.D., Langford, M.A., Tuell, J.P., and Carr, E.L. (1985) The use of optimum interpolation at AFGWC, *Preprints Seventh Conference on Numerical Weather Prediction*, Montreal, P.Q., Canada, Amer. Meteor. Soc., 43-49.

Table 2. Main Differences Between Phase I and Phase II of AFGWC AWAPS Global 4-D Assimilation System.

CHARACTERISTIC	PHASE I	PHASE II
Max. no. of obs analyzed per grid point	8 (u, v, z, Q)	35 (u, v, z) 20 (Q)
Spectral Resolution of Analysis	Rhomboidal-24	Rhomboidal-30
Resolution of GSM 6-hour first guess	Rhomboidal-20 9 vertical layers	Rhomboidal-30 12 vertical layers
Quality Control Steps	Gross check (No buddy check)	Gross check and buddy check
Humidity Analysis	Not stored into production database	Stored into production database
Resolution of 4-day production GSM forecast	Rhomboidal-20 9 vertical layers	Rhomboidal-40 12 vertical layers

During Phase I, the global moisture analysis produced by the GSM/HIRAS system was not stored into the production AFGWC database. That is, although the GSM/HIRAS cycle produced a global moisture analysis and although the 96-hour GSM moisture forecast was initialized with this moisture analysis, neither the HIRAS moisture analysis nor the GSM moisture forecast were stored into the production databases, that is, those databases accessed by follow-on applications, display, dissemination and archiving programs. This decision at AFGWC was based on the following two main reasons:

- 1 - Lack of evaluation during Phase I of the HIRAS/GSM moisture fields, owing to the higher priority evaluation requirements for the wind, height, and temperature fields.
- 2 - The poor Phase I spectral resolution of both the 6-hr GSM first-guess and the 96-hour GSM forecast. (Because of their greater spatial variance, upper-air humidity fields suffer greater deterioration from low spectral truncation than upper-air wind, height, or temperature fields.)

For the two reasons above, the AFGWC production 2.5° global moisture analyses during Phase I continued to be provided by the AFGWC moisture assimilation system that existed prior to the HIRAS/GSM era. There is no accepted name for this system, because it involved an array of models. Nevertheless, the system is documented in the report by Tarbell and Hoke⁵ and we shall refer to the system here simply as the pre-HIRAS moisture assimilation. The latter is a system that evolved over 15-20 years and accordingly is a system whose domain expanded in stages as computer resources expanded. Thus the pre-HIRAS moisture assimilation is not a straightforward unified global system; but rather it consists of separate surface and upper-air analysis models over separate tropical and extratropical domains.

In the tropical domain (on a Mercator projection extending from 30° N to 30° S latitude), the first-guess field for the moisture analysis is merely persistence of the previous analysis (hence the tropical first-guess moisture field is substantially dependent on a tropical moisture climatology, which was the first-guess for the first tropical moisture analysis). In the NH and SH extratropical domains (on a polar stereographic projection), the first-guess field for the moisture analysis is the 3-hour moisture forecast of AFGWC's NH and SH 5LAYER model.⁴ Figure 1 shows the boundaries of the NH octagon domain, mirrored by a companion SH octagon domain. Given their respective first-guess moisture fields, the separate tropical and extratropical moisture analysis models (known as TROPUA and MULTAN respectively⁵) applied a standard Cressman analysis scheme²⁷ to all available RAOBs of humidity. During Phase I, a utility program called DATFCH merged the separate tropical and extratropical humidity analyses. The latter program interpolated the several humidity analyses to a single global 2.5° latitude/longitude grid at the lowest six mandatory pressure levels, defaulting to the extratropical humidity analysis in areas of domain overlap (except along a fairly narrow latitude belt inside the octagon boundary where some blending with the tropical analysis occurred). The essential details of the above discussion are summarized in Table 3.

²⁷ Cressman, G.P. (1959) An operational objective analysis system, *Mon. Wea. Rev.*, **87**:367-374.

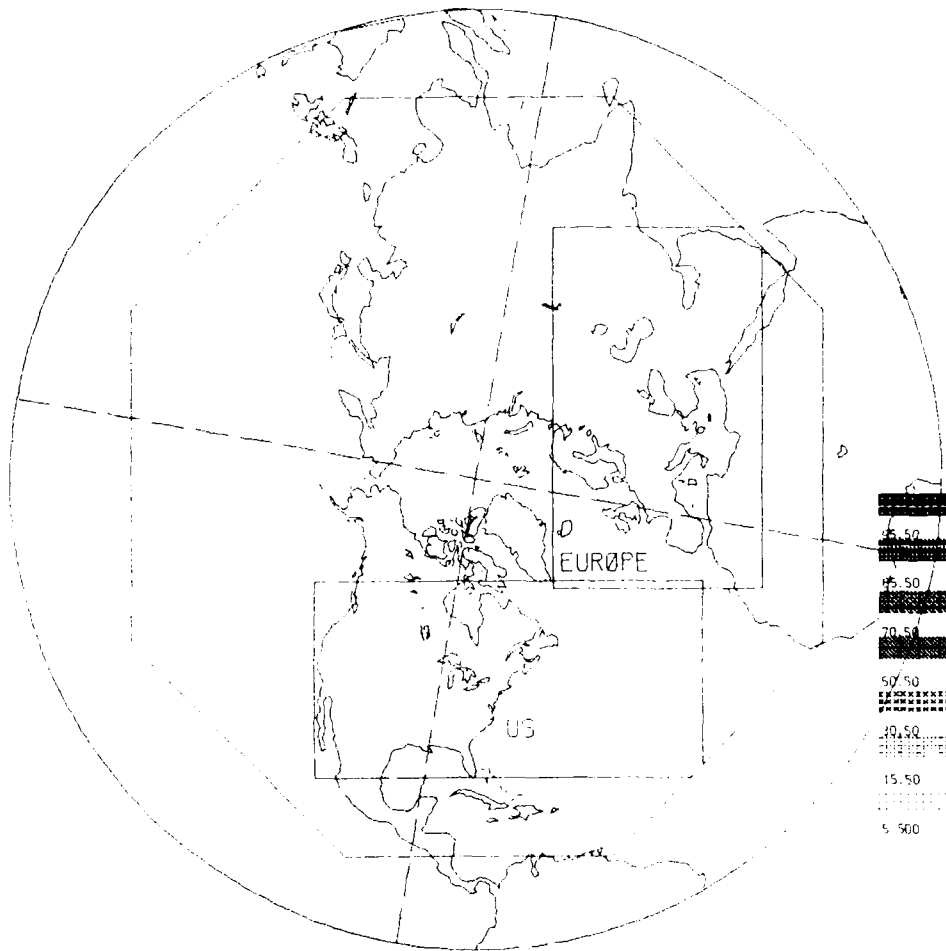


Figure 1. Boundaries of the NH AFGWC Octagon Domain and the U.S. and Europe Verification Domains Used in this Study. (Shading key at lower right applies to cloud fields in Figures 30-47 and shows eight shading intensities, including blank, for eight cloud intervals).

Table 3. Outline of AFGWC Pre-HIRAS Operational Global Moisture Analysis.

DOMAIN	RESOLUTION	AFGWC NAME	ANALYSIS METHOD	SOURCE OF FIRST-GUESS	SOURCE OF OBS
N.H. Octagon	whole-mesh	MULTAN	Cressman	3-hour 5LAYER fcst	RAOBs
S.H. Octagon	whole-mesh	MULTAN	Cressman	3-hour 5LAYER fcst	RAOBs
Tropics 30S-30N	whole-mesh	TROPUA	Cressman	Persistence and Climo.	RAOBs
The three separate analysis domains above are merged and interpolated to a global 2.5° lat/lon grid.					

In addition to the January 1985 cases for the AFGWC analyses in Table 1, AFGWC archived April, July, and October analyses during 1984 for GL use in this study. However, until corrected in late October 1984, a logic error in the DATFCH program cited above inadvertently resulted in zero humidity values being stored at all tropical points (that is, outside the NH and SH octagon domains) in the Phase I global humidity analyses. Hence the Phase I analyses archived before November 1984 were unusable in this study and are not listed in Table 1.

Despite yet other weaknesses in the January 1985 Phase I AFGWC global moisture analyses to be documented in Section 2.1.2, Section 3.2 demonstrates that beyond the 12- to 24-hour GSM forecast range, competitive and skillful global cloud forecasts are obtained from the GSM moisture forecasts initialized from these analyses. To fully measure the potential skill in GSM-based cloud forecasts from AFGWC's present AWAPS system, one obvious consideration was to extend the present study to the use of Phase II AFGWC global analyses, following October 1985 when the higher resolution AWAPS assimilation cycle was implemented and the GSM/HIRAS global moisture analysis was stored and archived as the production AFGWC global moisture analysis. However, the GL study of Mitchell and Yang¹⁴ indicated the strong likelihood of substantial systematic moist biases in the Phase II GSM/HIRAS moisture assimilation due to poor methods of vertically interpolating analyzed specific humidity (full values, not residuals) from the pressure surfaces of the HIRAS analysis to the σ -coordinate surfaces of the GSM forecast model and vice versa. This foreseen bias was fully substantiated by subsequent AFGWC evaluation of the Phase II moisture analyses, but the problem was not corrected until March 1988. All experiments for the present study had to be completed before the latter date. A second follow-on GSM cloud forecast study using Phase II AFGWC moisture analyses subsequent to March 1988 was initiated in July 1989.

There is another crucial reason why the present GSM cloud forecast study was carried through with AFGWC Phase I global moisture analyses. Unlike Phase II, the Phase I moisture

analyses implicitly utilized RTNEPH global cloud analyses as a source of estimated humidity observations. This was by virtue of the previously cited use of the 5LAYER model's moisture forecast as the Phase I first-guess humidity field in the extratropics. As detailed further in the next subsection, 5LAYER initial humidity fields are almost entirely inferred from the RTNEPH cloud analysis. In contrast, Phase II global moisture analyses utilize only RAOBs as a source of humidity observations. Therefore, to maximize the potential GSM cloud forecast skill in comparison to that of 5LAYER, especially in the short range, we felt it imperative that the GSM moisture forecast be initialized, like 5LAYER, from a moisture analysis/assimilation system that utilized the RTNEPH cloud analysis (and hence, indirectly, satellite cloud imagery and surface cloud reports) as a data source. This remains a real possibility, but not (as we shall show) using the faulty cloud-to-humidity inference methods employed in Phase I. In an important related study, Norquist^{12,28} demonstrated that the quality of global humidity analyses can be improved by assimilating humidity estimates inferred from RTNEPH cloud analyses, provided an appropriate cloud-to-humidity inference scheme is employed.

2.1.2 CHARACTERISTICS OF THE HUMIDITY ANALYSES

The previous section established that the humidity fields in the various global analyses in Table 1 were derived with several different first-guess forecast models, analysis methods, and data sources. Not surprisingly then, this section will demonstrate that the gross features of these humidity fields have some substantial differences from each other.

The differences are best understood by grouping the analyses in Table 1 into two sets -- Set A consisting of the NMC operational analyses (FGGE III-A and NMC/OP) and Set B consisting of the analyses (AFGWC and NMC/3DNEPH) that directly or indirectly utilize the 3DNEPH or RTNEPH cloud analysis database. Between the two sets, the general characteristics of the humidity fields show substantial differences, but within each set the characteristics are quite consistent. The emphasis in these comparisons will be on zonal mean humidity fields. In particular, the zonal mean features of the humidity analyses in Set A will be found to agree well with observations, despite the fact that the FGGE III-A and NMC/OP analyses utilized a different analysis method and first-guess model. The zonal mean features of the humidity analyses in Set B show substantial departures from the zonal means derived from observations and from Set A.

The background truth fields for this section are provided by the FGGE II-B RAOBs gathered during the period of 3-22 February 1979, which falls within FGGE Special Observing Period 1. The zonally and temporally averaged relative humidity (RH) field obtained from this nearly three-week dataset is given in Figure 2a. The corresponding depiction of RH observation frequency during five days within that period is given in Figure 2b. Figures 2a and 2b were taken from Figures 16 and 17 in the study by Norquist.¹² In that study, to obtain the zonal average in Figure 2a, all RAOBs were first grouped according to nearly equal-area grid cells of 10 degrees width in latitude, then the mean RH value for each grid cell was calculated, and

²⁸ Norquist, D. (1988) Alternative forms of humidity information in global data assimilation, *Mon. Wea. Rev.*, **116**:452-471.

lastly the zonal mean was computed from the mean grid-cell values. In this fashion, areas of high observation density were not given unduly large weight.

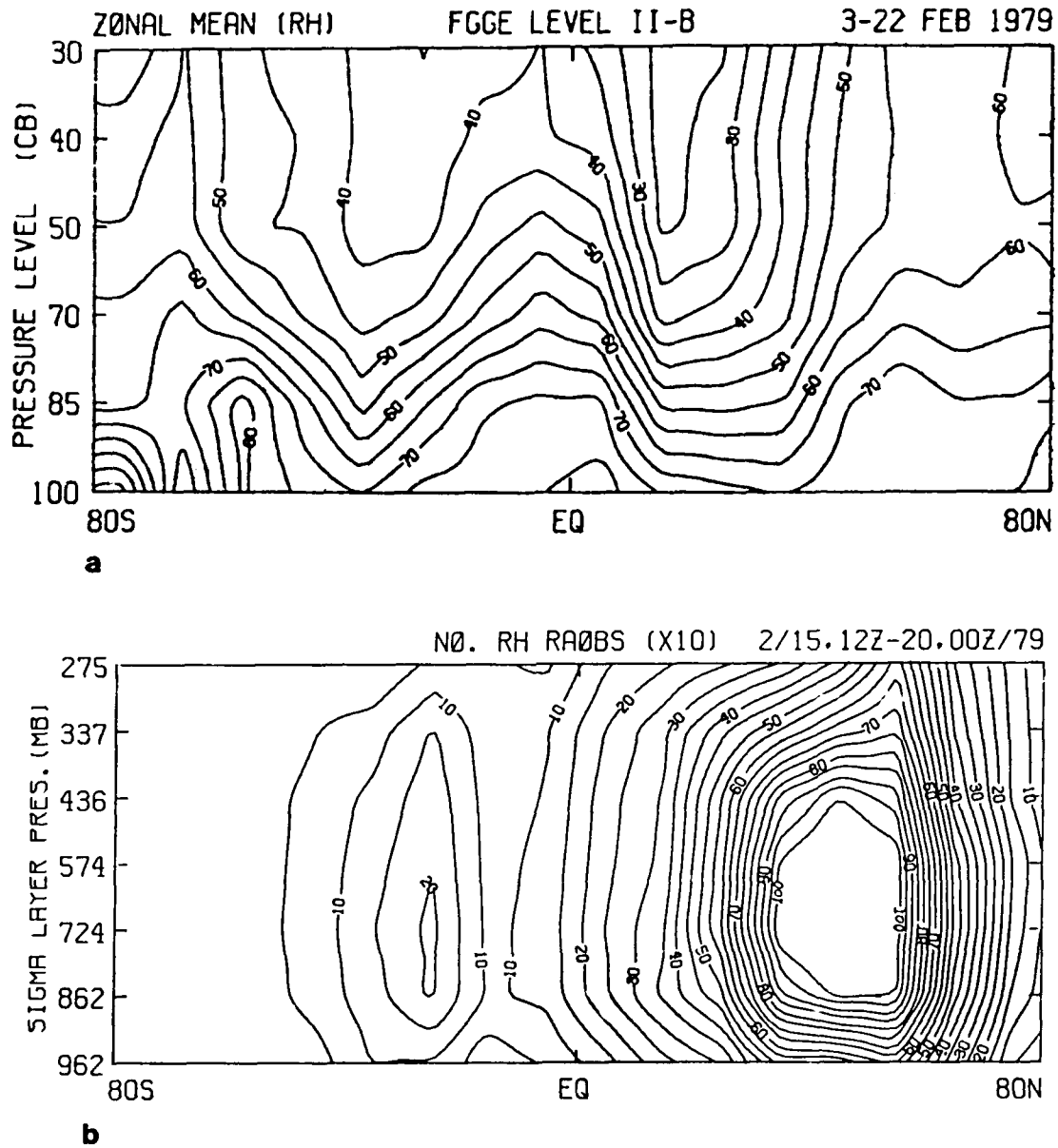


Figure 2. (a) Zonal Time Average of RH for the FGGE Level II-B Rawinsonde Observations During 3-22 February 1979. In all plots of zonal average RH, the contour interval is five. (b) For the Seven Moist Layers of the GSM, the Number (X10) of Rawinsonde Observations of RH as Summed Over 10° Latitude Bands and Ten 00Z and 12Z Time Periods During 15-20 February 1979 (From the study of D. Norquist¹²).

The distinctive features of Figure 2a are 1) the rather low mean humidity in the subtropical descending branches of the Hadley circulation, 2) the rather high mean humidity in the region of mean ascending motion around the Inter-Tropical Convergence Zone (ITCZ), and 3) the high mean humidities poleward of 40° latitude in both hemispheres, particularly in the NH (the high-latitude low-level anomalies of the SH are suspect because of the scarcity of observations there). To compare with Figure 2a, we first consider the corresponding FGGE III-A objective analyses, which are listed first in Table 1. Figure 3a is the zonal and temporal average of the daily 00Z and 12Z NMC operational global objective analyses (FGGE III-A) for the same period as Figure 2a. Figure 3a agrees well with Figure 2a, showing the same three general features cited above. Figure 3b provides a plot of the differences between Figures 3a and 2a. Except for the differences poleward of latitude 50° S (where Figure 2a is suspect), the zonal mean RH values in Figure 3a generally agree with those in Figure 2a to within 8 percent RH.

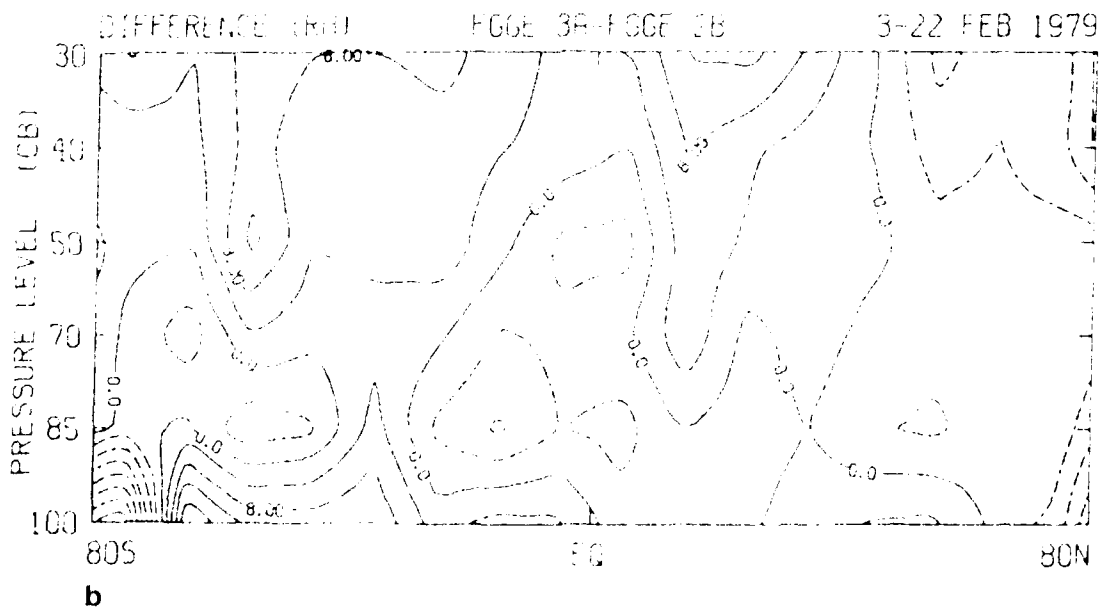
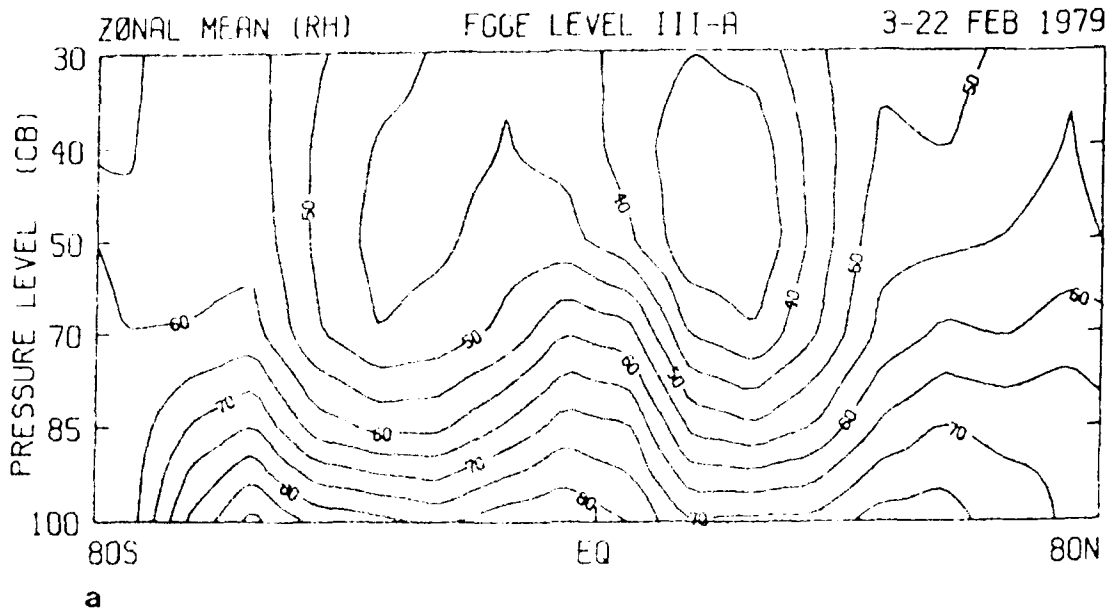


Figure 3. (a) Zonal Time Average of RH for the 00Z and 12Z NMC FGGE III-A Objective Analyses During 3-22 February 1979. (b) Difference Between Zonal Time Average of RH in Figures 3a and 2a. (In all difference plots of zonal average RH, the contour interval is four and dashed contours denote negative values).

Considering next the second source of objective analyses in Table 1, we turn to Figure 4a, which provides the zonal average of the NMC operational global analysis for 00Z on 14 January 1982 (this is the case highlighted in MW⁶). The similarity between Figure 4a and Figure 3a is striking, considering that Figure 4a is from a different year and from an earlier winter month. Moreover, the NMC analysis represented in Figure 4a utilized a different analysis method and a later generation NMC global data assimilation system (see Section 2.1.1) that included a different global forecast model for the first guess. The similarity between Figures 3a and 4a is further illustrated by comparing Figures 3b and 4b, where Figure 4b is the plot of the difference between Figure 4a and Figure 2a. The key purpose of Figure 4a is to demonstrate the interannual robustness of the pattern of NH winter season zonal mean RH depicted in Figures 2a or 3a.

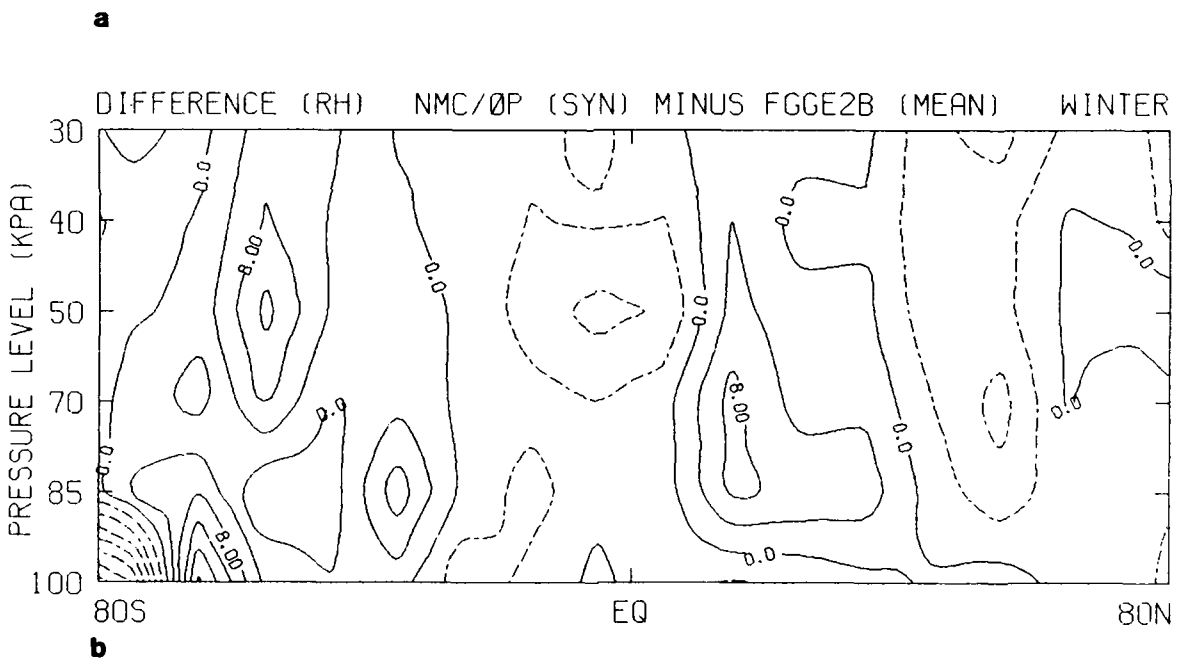
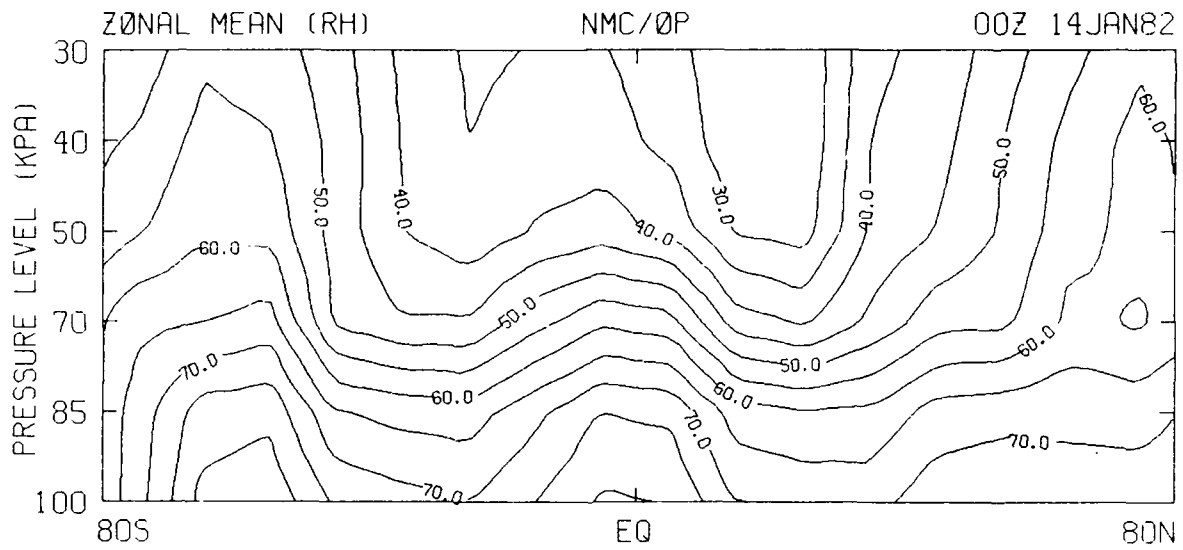
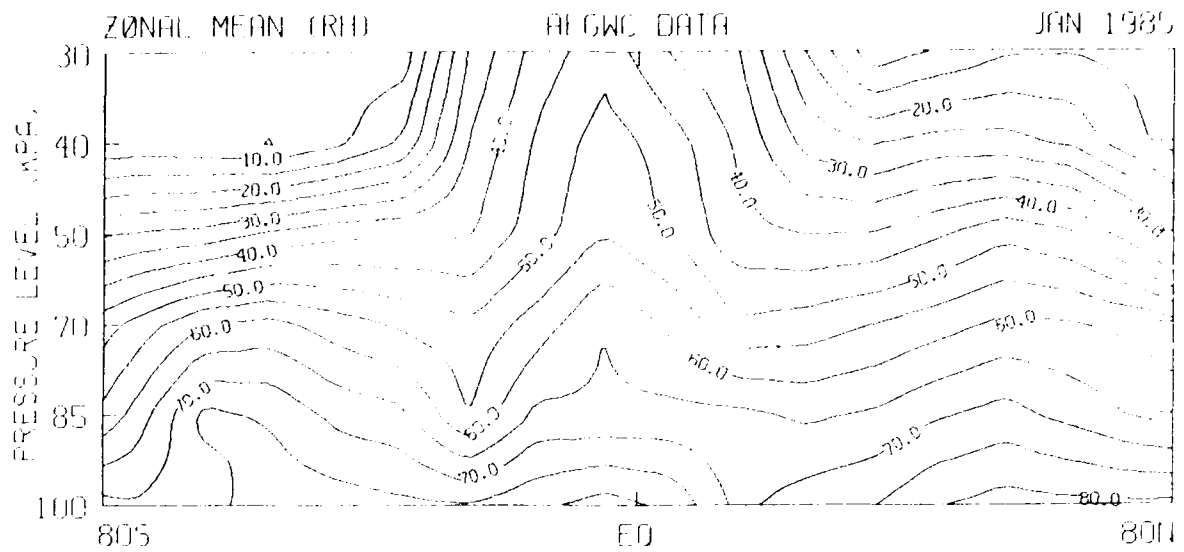
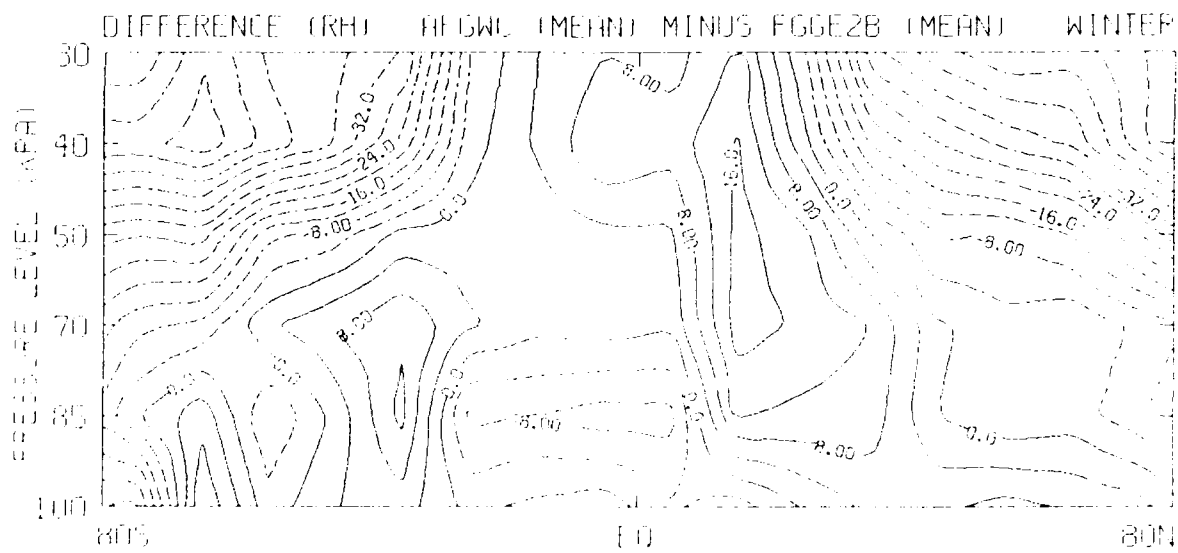


Figure 4. (a) Zonal Time Average of RH for the NMC Analysis for 00Z, 14 January 1982. (b) Difference Between Zonal Average of RH in Figures 4a and 2a.

Figures 2-4 provide a sufficient reference to compare against the zonal mean RH fields obtained from the AFGWC analyses in Table 1. For purposes of this comparison, Figure 5a provides the zonal and temporal average of the eleven 00Z January 1985 AFGWC RH analyses cited in Table 1. The plot of the difference between Figure 5a and Figure 2a is given in Figure 5b. Figure 5 shows large departures from Figures 2-4. The most outstanding feature of Figure 5 is the very dry and erroneous character of the AFGWC analysis in the upper-half of the troposphere in the extratropics of both hemispheres. The discussion below establishes and addresses the source of this error.



a



b

Figure 5. (a) Zonal Time Average of RH from Eleven 00Z AFGWC Analyses During January 1985 (see Table 1 for dates). (b) Difference Between Zonal Time Average of RH in Figures 5a and 2a.

Figure 6 provides a shaded display of the NH 30 kPa AFGWC RH analysis for 00Z on 17 January 1985. Superimposed on Figure 6 is the AFGWC octagon domain boundary of Figure 1. It is evident that the widespread region of uniformly low RH values in Figure 6 occurs over that region where the exclusive source of the AFGWC analysis is the extratropical octagon humidity analysis that utilizes the humidity forecast of the AFGWC 5LAYER model as the first-guess field. (See Table 3 and the earlier discussion of the AFGWC DATFCH program toward the end of Section 2.1.1.) It is also noteworthy in Figure 5a that the extratropical upper-level dry bias is more extreme in the SH (versus the NH) where Figure 2b shows considerably fewer RAOBs are available to correct the 5LAYER forecast first-guess field. These facts point to the 5LAYER first-guess field as the source of the upper-level extratropical dry bias in Figure 5. Additional facts supporting this supposition follow.

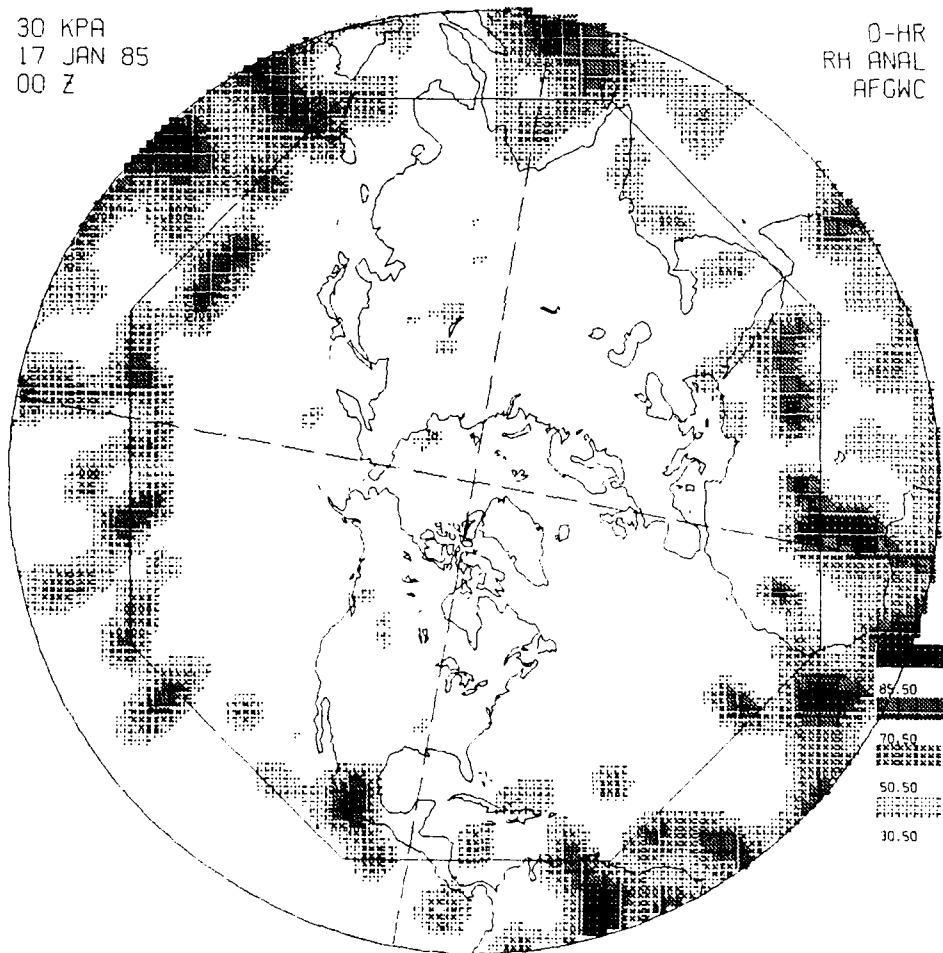


Figure 6. NH AFGWC 30 kPa RH Analysis for 00Z, 17 January 1985. (Shading key at lower right shows five shading intensities, including blank, for five RH intervals).

As shown in Table 3, the AFGWC 5LAYER first-guess humidity forecast for the extratropical AFGWC humidity analysis (MULTAN) is a three-hour short-range forecast. Hence the character of this first-guess humidity forecast is very similar to the initial 0-hour 5LAYER humidity analysis. The 5LAYER initial or 0-hour humidity analysis is unique in that it utilizes the AFGWC RTNEPH 3-D global cloud analysis as its primary humidity "data" source. Figure 7 provides a summary schematic of the procedure as applied in January 1985 (and as still applied at the time of this writing except for some changes in the details of the vertical compaction⁴). First, the high resolution 3-D RTNEPH cloud analysis is vertically compressed and horizontally averaged to yield a "compacted" 3-D cloud analysis on the coarser resolution grid of the 5LAYER forecast model. Secondly, the empirical cloud-to-humidity conversion curves in Figure 8, known as the "CPS" curves, are used to convert the compacted 3-D RTNEPH cloud amounts to inferred pseudo or surrogate initial humidity values. At grid points where the compacted 3-D RTNEPH cloud amounts are strictly zero (clear), the humidity analysis defaults to the drier of 1) the zero-cloud threshold value or critical value from Figure 8 or 2) the humidity value from the previous cycle's conventional MULTAN humidity analysis (Table 3).

CPS INITIALIZATION IN CLOUDY AREAS

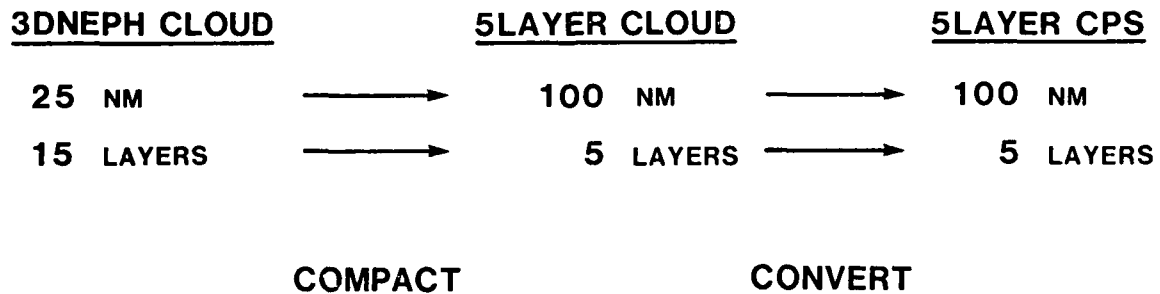


Figure 7. Schematic Diagram of the AFGWC Algorithm Which Infers Initial CPS Moisture Values for the AFGWC 5LAYER Forecast Model from the AFGWC RTNEPH Global Cloud Analysis. (See report by T. Crum⁴ for details).

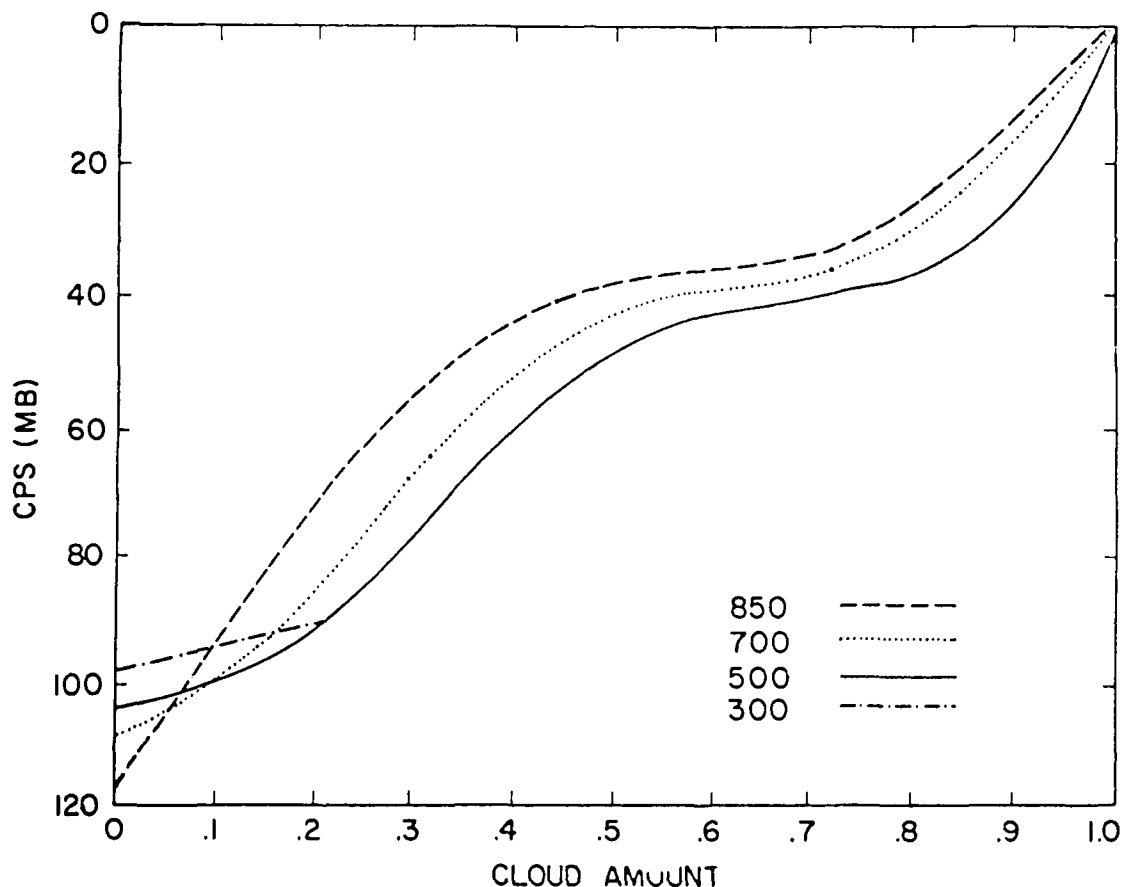


Figure 8. Curves of the AFGWC CPS-cloud Amount Conversion Scheme Used in the CPS-cloud Conversion Step of Figure 7.

The humidity-to-cloud curves in Figure 8 are defined in terms of the moisture variable called condensation pressure spread (CPS). For an air parcel having a given temperature and dewpoint, CPS is defined as the amount of upward dry adiabatic vertical displacement in millibars required for the parcel to reach saturation. Thus a zero CPS value denotes saturation (RH = 100 percent) and increasingly larger values of CPS denote increasingly drier air (analogous to dewpoint depression). The AFGWC CPS curves were originally derived by Air Weather Service in the early 1960's from a coincident sample of surface cloud reports (note: not 3DNEPH or RTNEPH cloud amounts) and RAOBs.²⁹ Unfortunately, no information remains on the nature of this coincident cloud/ humidity observation sample such as the time period, the region, or scatter plots.

²⁹ Edson, H. (1965) *Numerical Cloud and Icing Forecasts*, Scientific Services Technical Note 13, 3rd Weather Wing, Offutt AFB, NE, pp. 44.

Given a CPS value and a coincident temperature value, any of several other common moisture values, such as RH, may be derived. Using U.S. Standard Atmosphere temperatures, the critical CPS values for zero cloud amount in Figure 8 have been converted to their corresponding critical RH values (RHc) and plotted for the lowest six mandatory pressure levels in Figure 9. (To obtain the critical RH values for the 40 and 100 kPa levels in Figure 9, the 30 and 85 kPa critical CPS values from Figure 8 were assumed respectively, as the AFGWC CPS curves do not include separate curves for the 40 and 100 kPa levels.) The implied critical RH values in Figure 9 at and above 50 kPa are unexpectedly low.

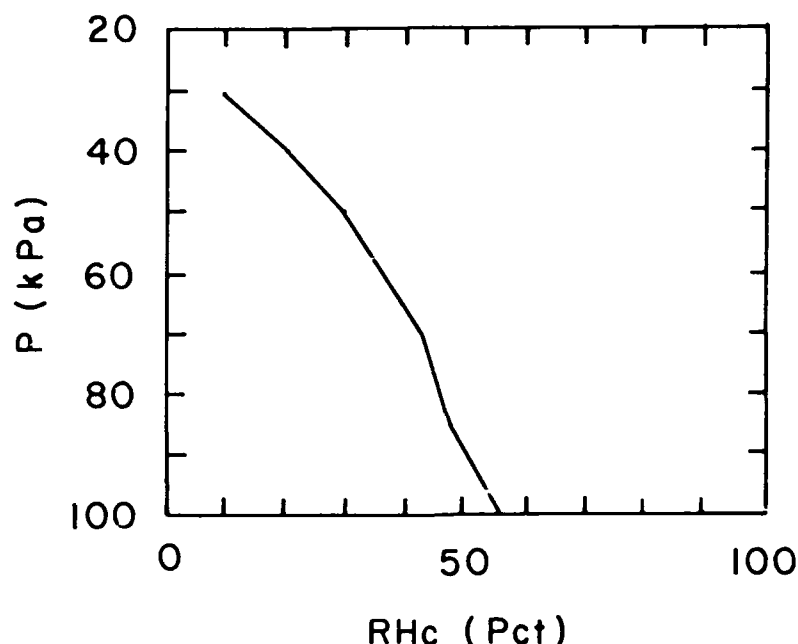


Figure 9. The Critical Relative Humidity (RH) as Derived from the CPS-cloud Curves of Figure 8, for the Lowest Six Mandatory Pressures, Assuming U.S. Standard Atmosphere Temperatures and Applying the 85 kPa and 30 kPa CPS-cloud Curves Also to the 100 kPa and 40 kPa Levels, Respectively.

On a separate but relevant matter, the studies by Hughes and Henderson-Sellers^{30,31} of the FGGE year climatology of the January and July 1979 3DNEPH cloud databases show that the mean amounts of high cloud in the 3DNEPH database are lower than several other independent cloud climatologies. (However, the 3DNEPH low, middle, and total cloud amounts

³⁰ Hughes, N.A. and Henderson-Sellers, A. (1985) Global 3-D nephanalysis of total cloud amount: climatology for 1979. *J. Climate Appl. Meteor.*, **24**:669-686.

³¹ Henderson-Sellers, A. (1986) Layer Cloud Amounts for January and July 1979 from 3D-Nephanalysis. *J. Climate Appl. Meteor.*, **25**:118-132.

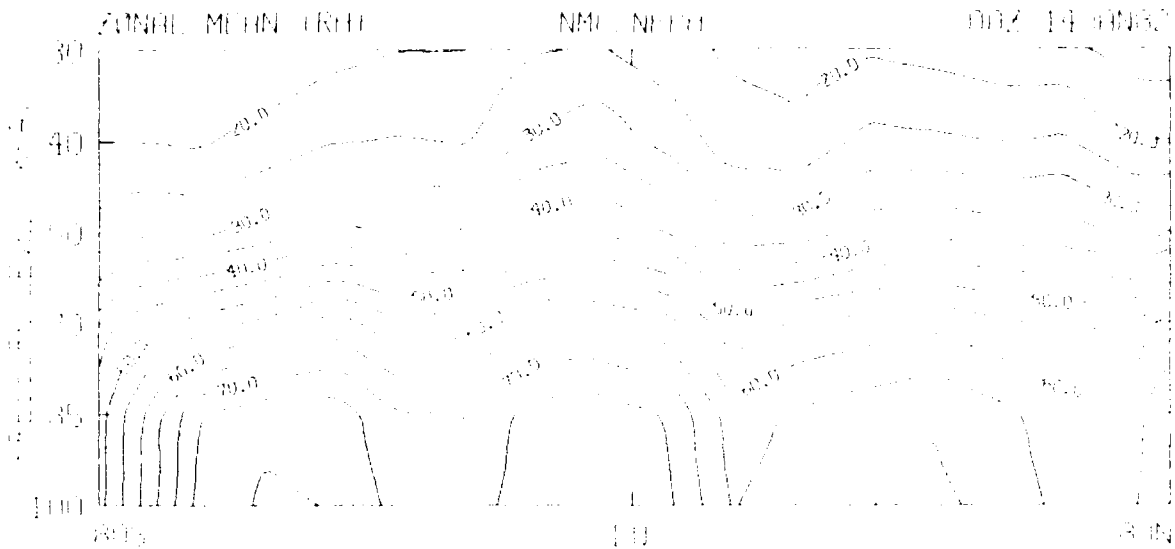
did compare favorably with other climatologies, except around the two polar regions and the summer Asian monsoon region.)

When the CPS curves are applied to 3DNEPH or RTNEPH cloud amounts to infer humidity estimates, the above two independent factors of 1) surprisingly low equivalent critical RH values from the upper-level CPS curves and 2) low mean amounts of high cloud in the 3DNEPH or RTNEPH database both contribute to yield erroneously low inferred humidity estimates. Most importantly, the conclusion that the 3DNEPH/RTNEPH-inferred humidity estimates at upper tropospheric levels are erroneously low is substantiated by the independent results of Table 4, obtained from the collocation study of Norquist.^{12,28} Table 4 shows a substantially dry bias in humidity estimates inferred from applying the upper-level CPS curves of Figure 8 to the upper-level February 1979 3DNEPH cloud amounts, relative to measured RH from collocated RAOBs for the same February 1979 winter period as Figures 2 and 3.

Table 4. Statistics of Differences Between Relative Humidity Inferred from Cloud Amount and that Measured with Radiosondes (in %) (from Norquist^{12,28}).

LEVEL (mb)	AFGWC		ECMWF		NMC	
	BIAS	RMS	BIAS	RMS	BIAS	RMS
850	1	21	10	22	-2	20
700	2	26	15	29	-4	25
500	-7	26	22	32	-5	24
400	-12	30	26	34	-5	23
300	-26	37	31	37	-5	21
The results are based on observations for the period 2/3/79 - 2/22/79 00Z						

Finally, Figure 10a shows the zonal average of the experimental humidity analysis of MW, wherein the operational NMC RH analysis of 00Z 14 January 1982 was completely replaced by an RH analysis derived from the 00Z 14 January 1982 3DNEPH analysis following the procedure of Figure 7. For further details on the derivation of this experimental analysis, see MW⁶ where it was first presented. Figure 10b gives the plot of differences between Figures 10a and 2a. It is clear that Figure 5a for the AFGWC RH analysis resembles Figure 10a far more closely than it resembles Figures 2-4 -- this despite the fact that RAOBs of RH were used in the AFGWC analysis of Figure 5 to correct a largely RTNEPH-based 5LAYER first-guess humidity forecast (within the octagon).



a



b

Figure 10. (a) Zonal Average of RH from the Experimental Analysis of 3DNEPH-inferred RH Derived by Mitchell and Warburton⁶ for 00Z, 14 January 82. (b) Difference Between Zonal Average of RH in Figures 10a and 2a.

The analysis of this subsection has led to several conclusions. First, on average, the AFGWC Phase I global humidity analyses are substantially too dry in the upper-half of the extratropical troposphere. Second, the cause of this upper-level dry bias is the overly dry upper-level 3DNEPH inferred humidity estimates used to initialize the 5LAYER three-hour first-guess humidity forecast. Lastly, the upper-level 3DNEPH inferred humidities are too dry because 1) the zero-cloud critical humidity values in the upper-level CPS curves are too low and 2) the mean upper-level 3DNEPH cloud amounts are too low. We contend that factor 1) dominates factor 2). To support this contention, Table 4 shows that Norquist^{12,28} found only a small upper-level dry bias in humidity values estimated from the RTNEPH using an alternative NMC cloud-to-humidity inference scheme -- a scheme originally developed for use with surface cloud reports. This latter scheme is considered further in Sections 3.1.2 and 3.2.2.

It is important to emphasize that the height, wind, and temperature fields of the AFGWC analyses in Table 1 were also examined and compared with those from other sources. From this comparison they were deemed to be of good quality. Though no details will be presented here for sake of brevity, the 50 kPa AFGWC height analyses in Table 1 compared surprisingly well with those published by the European Centre for Medium Range Weather Forecasts (ECMWF),³² especially considering the relatively poor resolution of the AWAPS Phase I AFGWC analyses and GSM forecast first-guess fields.

2.2 Global Humidity Forecasts

This section will examine the characteristics of the 4-day global humidity forecasts of the GL baseline GSM. Recall from Section 1 that the term "baseline" here refers to a particular configuration of the GL GSM that parallels the currently operational AFGWC GSM. Humidity fields from four GSM forecasts out to 96 hours are examined here. One GSM forecast is presented for each of the four types of GSM initial analysis sources listed in Table 1. Thus all four GSM forecasts are NH winter season cases. The basetime and source of the four initial analyses are shown in Figure 11.

³² Staff (1986) *Daily Global Analyses: Operational Data Assimilation System, January - March 1985*, European Center for Medium Range Weather Forecasts, Reading, Berkshire, U.K.

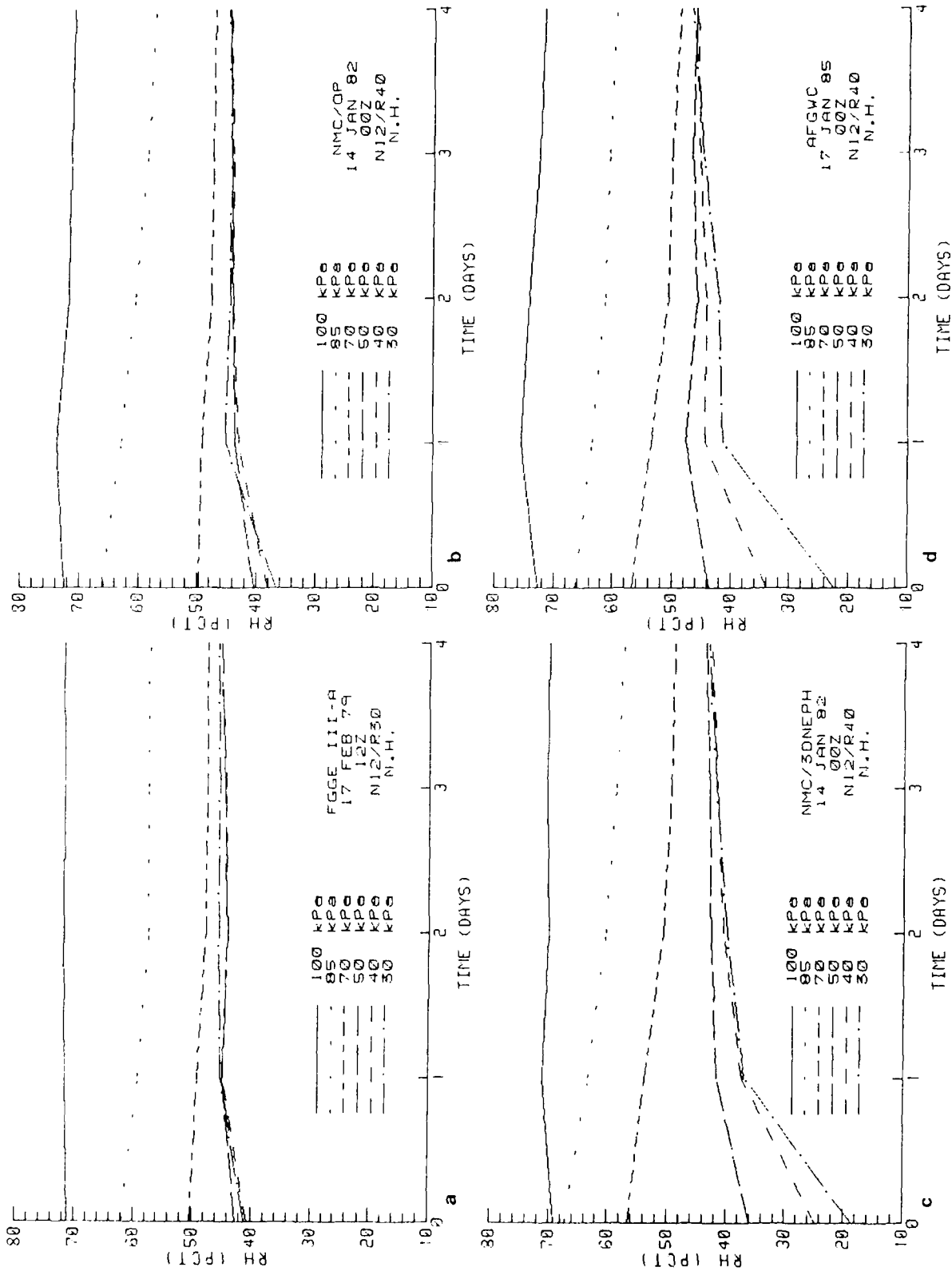


Figure 11. NH Mean RH at Six Mandatory Pressures as a Function of Forecast Length in Four GSM Forecasts Initialized from Four Separate Initial Analyses as Labeled.

Like the AFGWC GSM, the GL baseline GSM explicitly forecasts moisture on only the lowest 7 of the 12 model sigma layers, that is, on those sigma layers that are essentially contained in the troposphere as shown in Table 5. The GSM postprocessor eventually outputs the GSM RH forecast on the lowest six mandatory pressure surfaces. Figure 11 shows the 96-hour temporal trend of the NH mean RH at each of these six pressure surfaces. The examination in this section shall emphasize NH behavior, as the 5LAYER cloud forecasts used to compare with GSM cloud forecasts in Section 3.2 are exclusively NH forecasts.

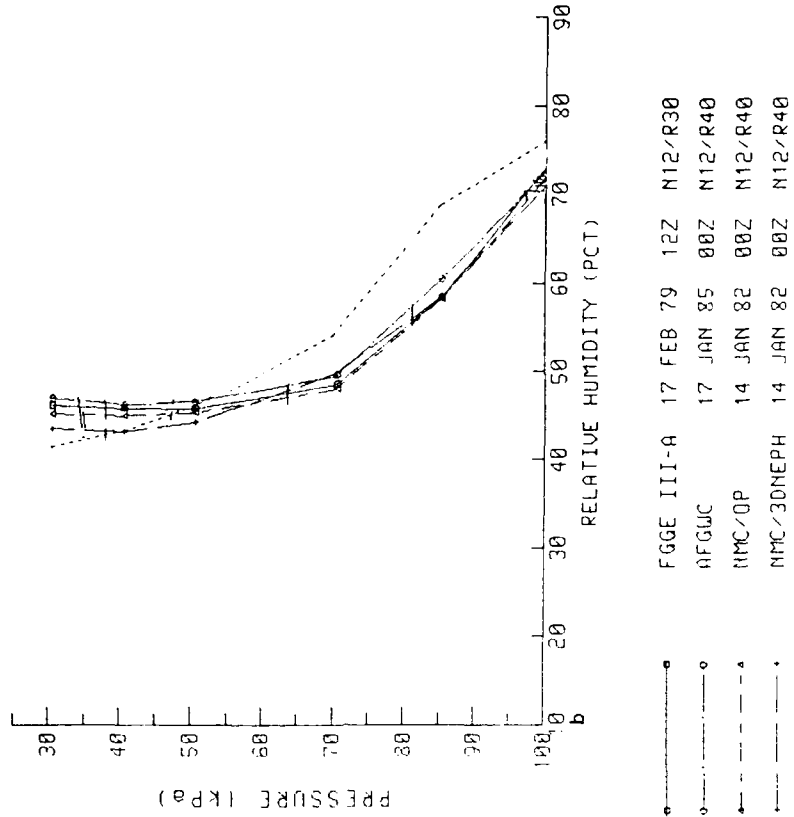
Note in Figure 11 that the lower (upper) two plots are for the two forecasts initialized from humidity analyses that directly or indirectly utilize (ignore) 3DNEPH/RTNEPH cloud data. Figure 12, generated from the data in Figure 11, shows the 0-hour and 96-hour vertical profiles of NH mean RH for the four GSM forecasts in Figure 11. Also as a reference, Figure 12 shows the vertical profile of the NH mean RH obtained from the FGGE II-B RAOB-based data in Figure 2a.

Table 5. The σ -structure of the Baseline GL GSM.

k INDEX	$\Delta\sigma$ THICKNESS	$\tilde{\sigma}$ INTERFACE	σ LAYER
		0.	
1	.050		.020747
		.050	
2	.050		.073986
		.100	
3	.050		.124400
		.150	
4	.050		.174573
		.200	
5	.050		.224668
		.250	
6*	.050		.274729
		.300	
7*	.075		.337003
		.375	
8*	.125		.436433
		.500	
9*	.150		.573831
		.650	
10*	.150		.724074
		.800	
11*	.125		.861960
		.925	
12*	.075		.962326
		1.000	

* Moisture bearing layer

96-HOUR FORECAST



0-HOUR ANALYSIS

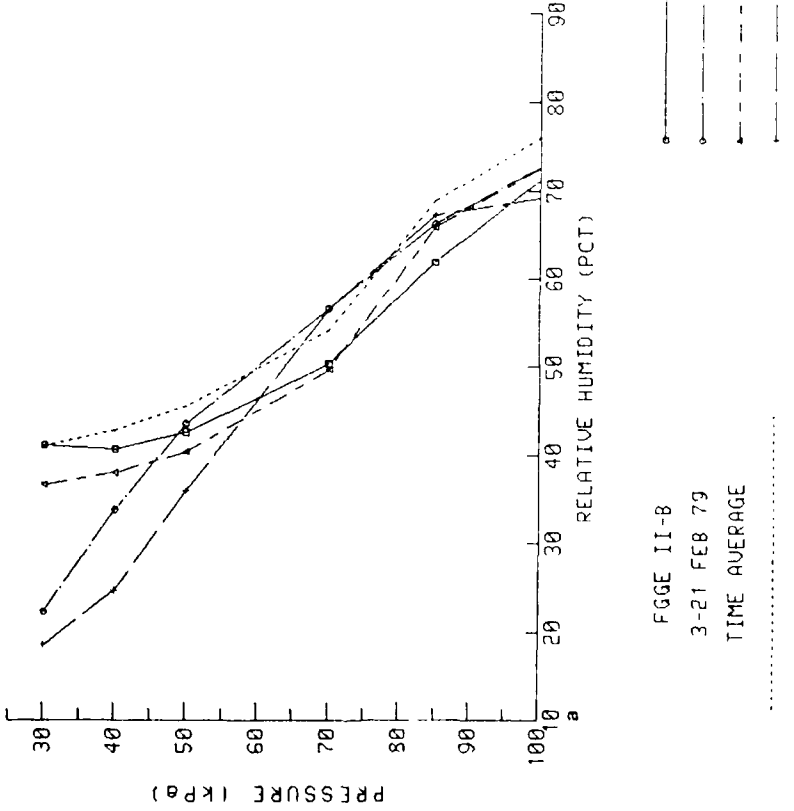


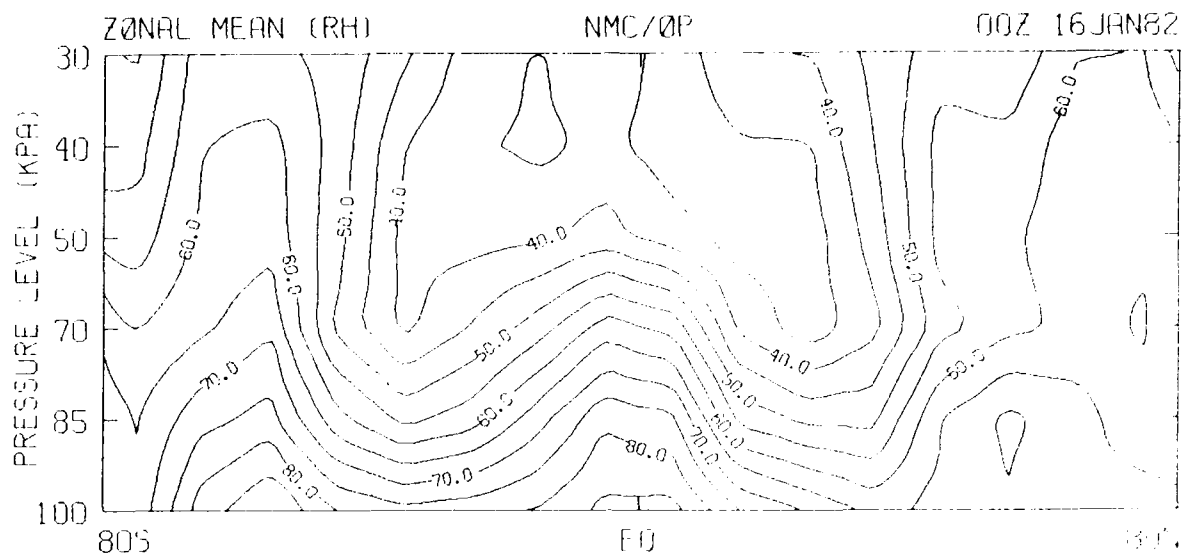
Figure 12. Vertical Profiles of the NH Mean RH at the (a) 0-hr Initial Time and (b) 96-hr Forecast Time for the Four GSM Forecast Cases in Figure 11. Also given as a reference is the vertical profile of NH mean RH as derived from the FGGE II-B zonal average RH values in Figure 2.

Several important features are apparent in Figures 11 and 12. First, reiterating several 0-hour characteristics noted earlier in Section 2.1.2, the two 3DNEPH/RTNEPH-influenced 0-hour humidity analyses are much drier in the mean at 30 and 40 kPa than the other two analyses. Of these two dry upper-level analyses, the NMC/3DNEPH analysis is the driest, presumably because unlike the AFGWC analysis, it has not been "corrected" by actual humidity RAOBs. At 50 kPa, the 0-hour mean RH values of all but the NMC/3DNEPH analysis agree fairly closely with each other. At the 70 and 85 kPa levels, the two 3DNEPH/RTNEPH-influenced analyses are somewhat more moist (compare again Figures 4b and 5b). Lastly at the 100 kPa level, the mean RH values of all four analyses are in near agreement.

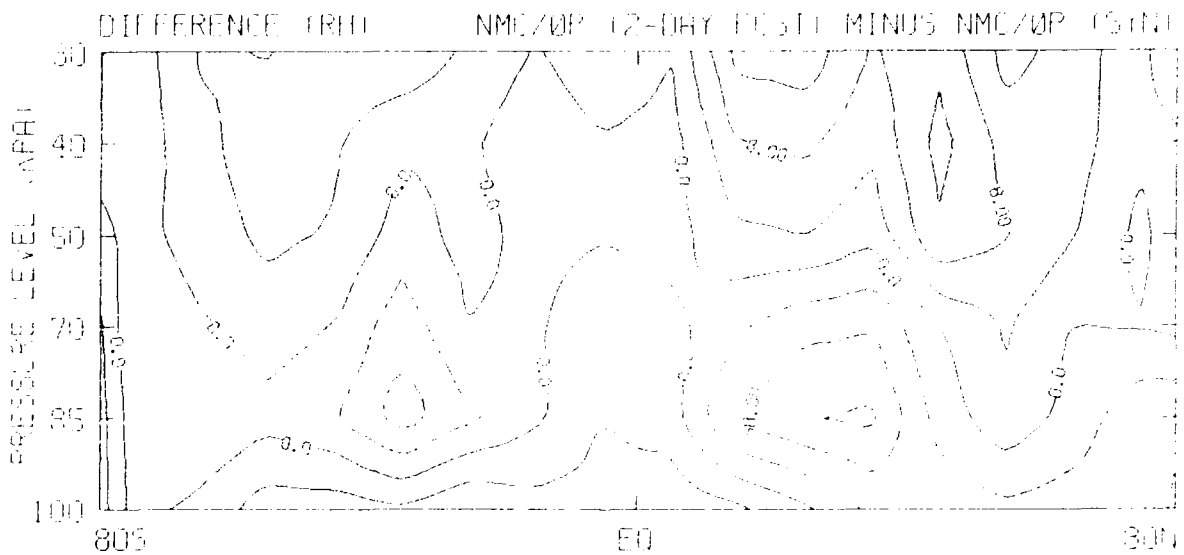
Of greater interest in this section are the distinct GSM forecast trends apparent in Figures 11 and 12. Most notably, the GSM quickly evolves or adjusts at all levels toward what we shall refer to here as the model's preferred mean humidity state. This asymptotic, mean GSM humidity state is somewhat dry (moist) at levels below (above) 50 kPa, compared to the RAOB mean state. More importantly here, the 96-hour vertical profile of GSM hemispheric mean RH values is largely independent of the 0-hour initial humidity profile. This type of behavior in forecast mean RH fields is a common characteristic in large-scale forecast models as a class.³³ There is clearly strong forcing of the GSM forecast humidity distribution due to modeled internal vertical motions and diabatic physics. The majority of the adjustment of GSM mean humidity occurs in the first 24 (48) hours in the upper (lower) levels. Not surprisingly, the magnitude of this rapid initial humidity adjustment is largest in the upper levels of the forecasts from the AFGWC and NMC/3DNEPH analyses, as these levels depart more from both the observations and the GSM's preferred mean humidity state.

It is instructive to examine the GSM temporal humidity trends in greater detail across the model's horizontal spatial domain. Corresponding to Figures 11b and 11d, Figures 13 and 14 show the zonally-averaged 48-hour RH forecast and forecast trends (forecast minus analysis) for the NMC/OP and AFGWC cases, respectively. Note that Figure 13b is the difference of Figure 13a and Figure 4a; and similarly, Figure 14b is the difference of Figure 14a and the corresponding single initial analysis field taken from the eleven analysis fields averaged in Figure 5a.

³³ Lejenas, H. (1979) Initialization of moisture in primitive equation models, *Mon. Wea. Rev.*, 107:1299-1305.

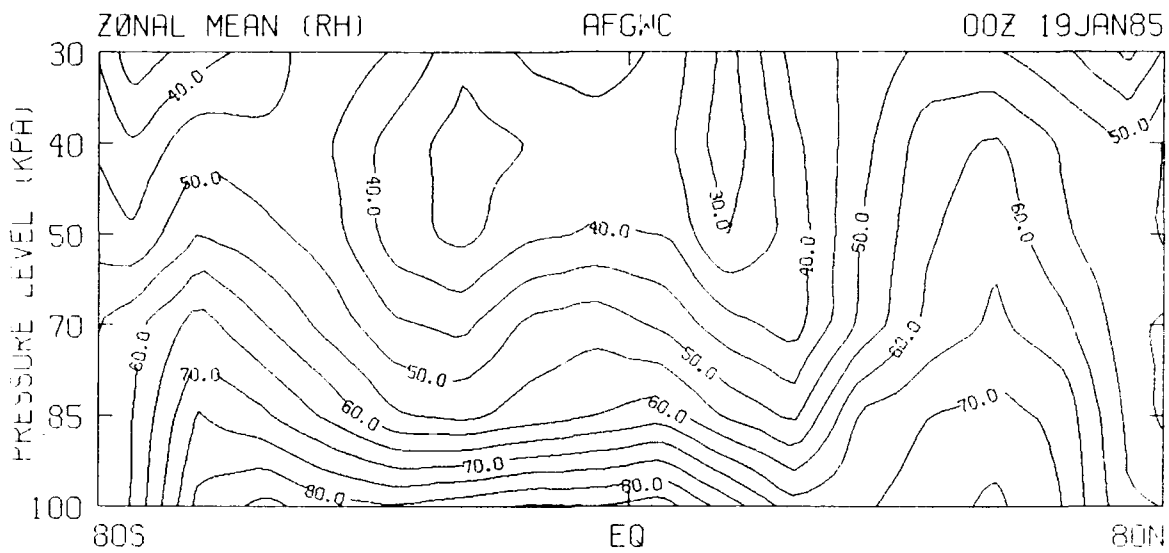


a

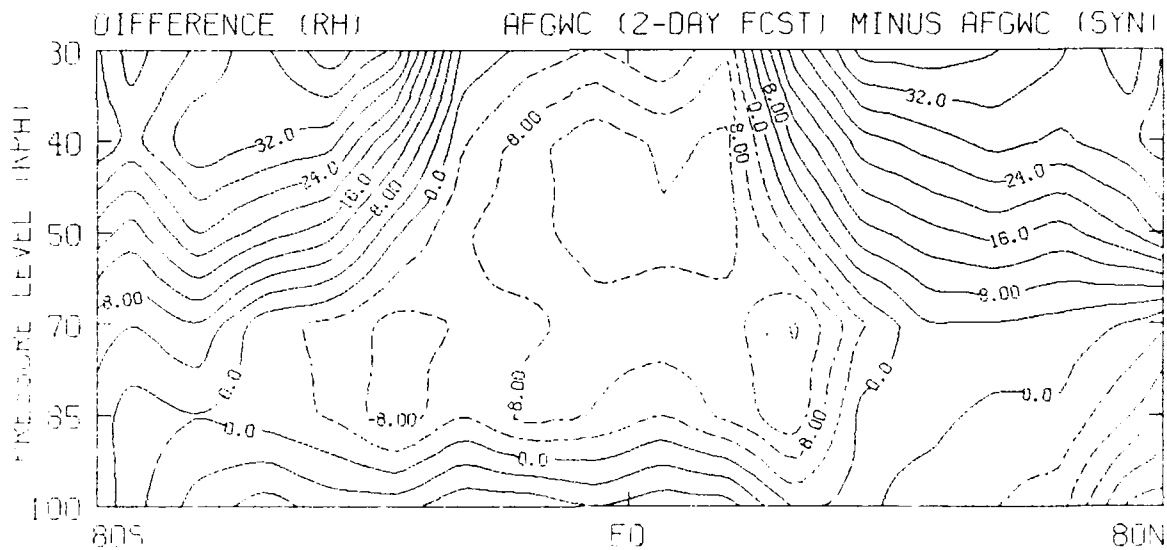


b

Figure 13. (a) Zonal Average of RH for the 48-hr GSM Forecast Initialized from the NMC Analysis of 00Z, 14 January 1982. (b) Difference Between the Above Zonal Average and that of the Corresponding Initial Analysis (Figure 4a).



a



b

Figure 14. (a) Zonal Average of RH From the 48-hr GSM Forecast Initialized From the AFGWC Analysis of 00Z, 17 January 1985. (b) Difference Between the Above Zonal Average and That of the Corresponding Initial Analysis.

In the NMC/OP case of Figure 13, the modest increase in mean RH above 50 kPa is pervasive across virtually all NH latitudes. The general NH drying at 70-85 kPa in Figure 13 is interrupted at a few latitudes by moistening. Though not shown, the zonal mean RH trends in the GSM forecast from the 17 February 1979 NMC FGGE III-A analysis are very similar to those in Figure 13. The RH trends in Figures 11a-11b and Figure 13 are very likely representative of the mean RH trends AFGWC will observe in its GSM forecasts initialized from the AWAPS Phase II moisture analyses after March 1988, because then the AFGWC RH observation sources (RAOBs) and global data assimilation forecast model (GSM) are very similar to those represented in Figure 13.

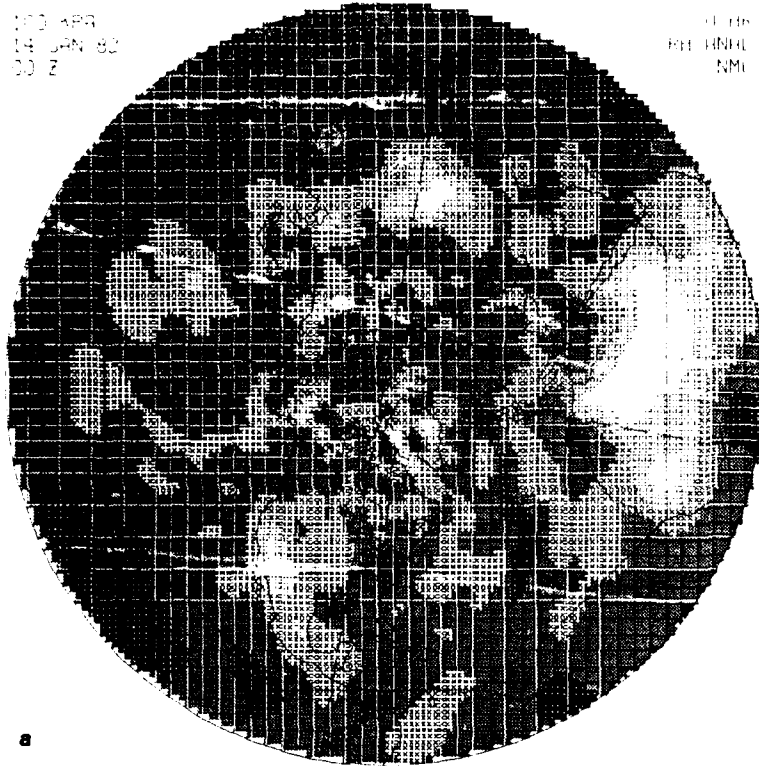
As expected from Figure 11, the Figure 14 RH trends in the GSM forecast from the AFGWC analysis are much larger than those of the NMC/OP case in Figure 13. The RH trends evident in Figure 14 are very significant to the experimental GSM cloud forecasts presented in Section 3, as all of these GSM cloud forecasts are executed from January 1985 AFGWC analyses in order to allow comparisons with the January 1985 5LAYER cloud forecasts archived for this study. In Figure 14 the large moistening at upper-level extratropical locations (that is, within the octagon domain) increases with height and dominates all trends. Also of note, the RH trends at the 70 - 100 kPa levels at latitudes within the NH octagon show a modest drying on average.

Comparing Figure 14 with Figure 5, it is important to recognize that in the zonal mean sense, the GSM RH forecast is actually a significant improvement over the initial AFGWC RH analysis. Figures 14b and 5b show that the GSM RH forecast is growing more moist (more dry) primarily in those areas where the AFGWC RH analysis is erroneously too dry (too moist) with respect to the FGGE II-B observed zonal mean moisture distribution. That is, the forecast RH mean state in Figure 14a agrees more closely with the observed RH mean state in Figure 2a than does the AFGWC analyzed mean state of Figure 5a. This characteristic whereby the 0-48 hour GSM RH zonal mean forecast trends are large (especially at upper levels within the octagon) because the forecast needs to correct errors in the mean state of the AFGWC RH analysis is a serious detriment to the ability of the GSM to yield short-range competitive cloud forecasts in Section 3.2.

Next, Figures 15-18 expand the present focus on the temporal trends of the GSM humidity forecast to the model's entire horizontal domain. For the NMC/OP case, Figures 15 and 16 provide NH shaded displays of the 0-hour NMC RH analysis and the associated 48-hour GSM RH forecast, respectively, for all six moist mandatory levels. Figures 17 and 18 provide the corresponding displays for the AFGWC case. A comparison of Figures 15e-f and 17e-f vividly depicts the pervasiveness of the very dry character of the AFGWC 30-40 kPa analyses within the AFGWC octagon domain. The 48-hour RH forecasts at 30 kPa in Figures 16e-f and 18e-f show how quickly the GSM 48-hour RH forecast from the AFGWC RH analysis has recovered from the initial dry bias and produced an RH forecast field whose overall synoptic character is already remarkably similar to the 48-hour RH forecast from the NMC/OP case.

100 KPA
14 JAN 82
00 Z

11 15
011 11011
NMI



85 KPA
14 JAN 82
00 Z

11 15
011 11011
NMI

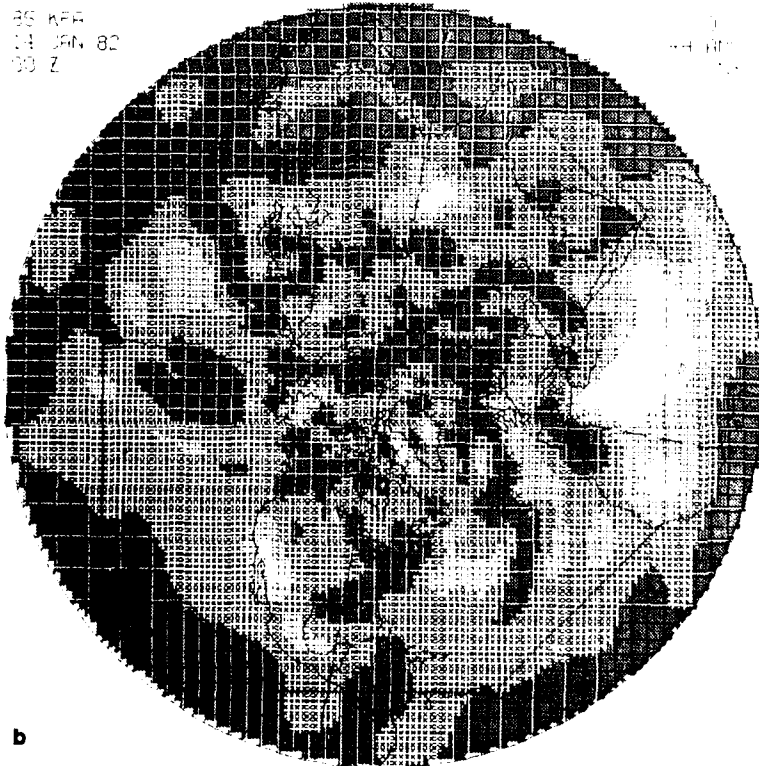
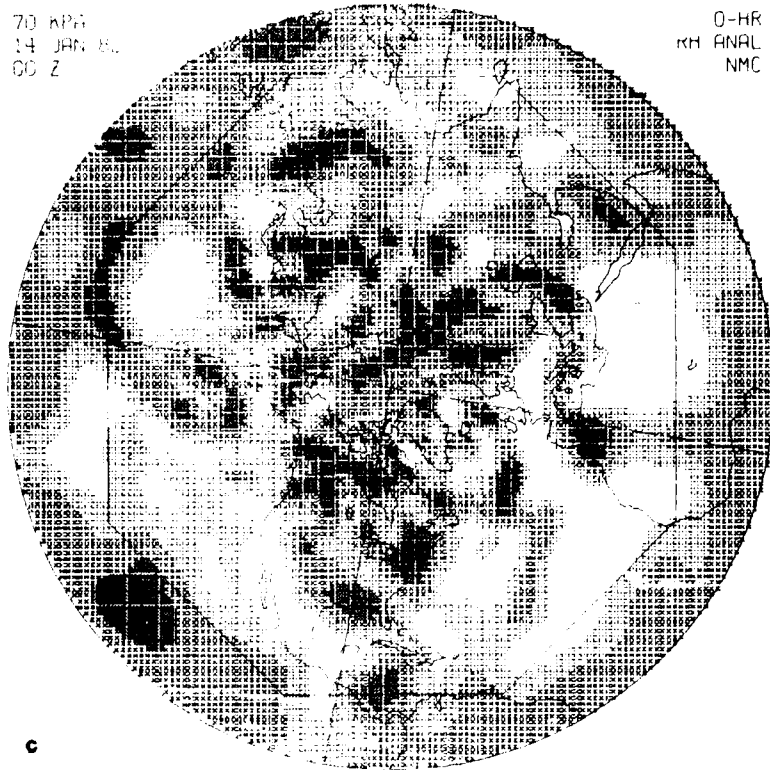


Figure 15. NH NMC RH Analysis for 00Z, 14 January 1982 at Levels (a) 100, (b) 85, (c) 70, (d) 50, (e) 40 and (f) 30 kPa. (The shading key in Figure 6 applies to all shaded displays of RH fields).

70 KPH
14 JAN 82
00 Z

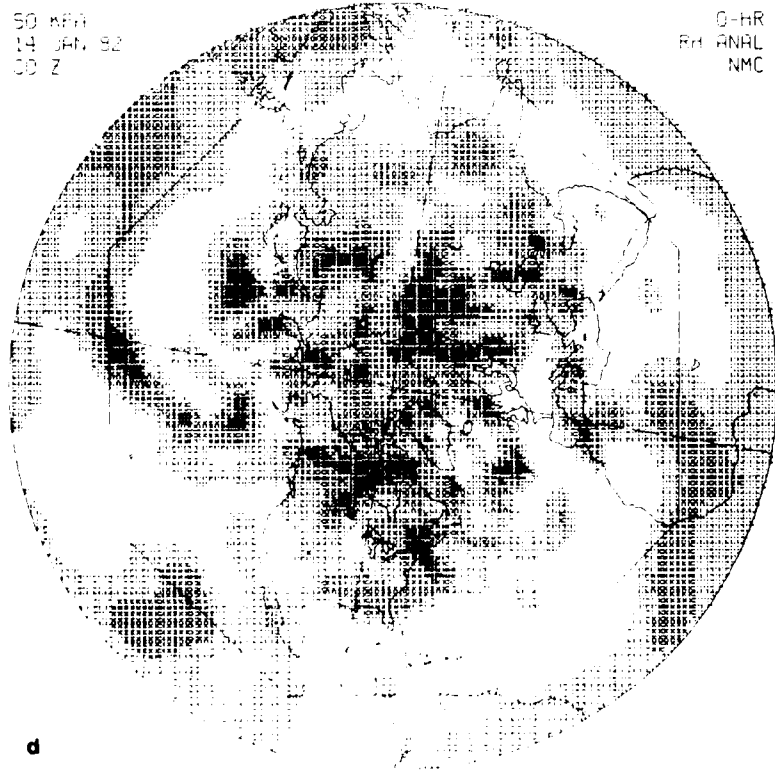
0-HR
RH ANAL
NMC



c

50 KPH
14 JAN 82
00 Z

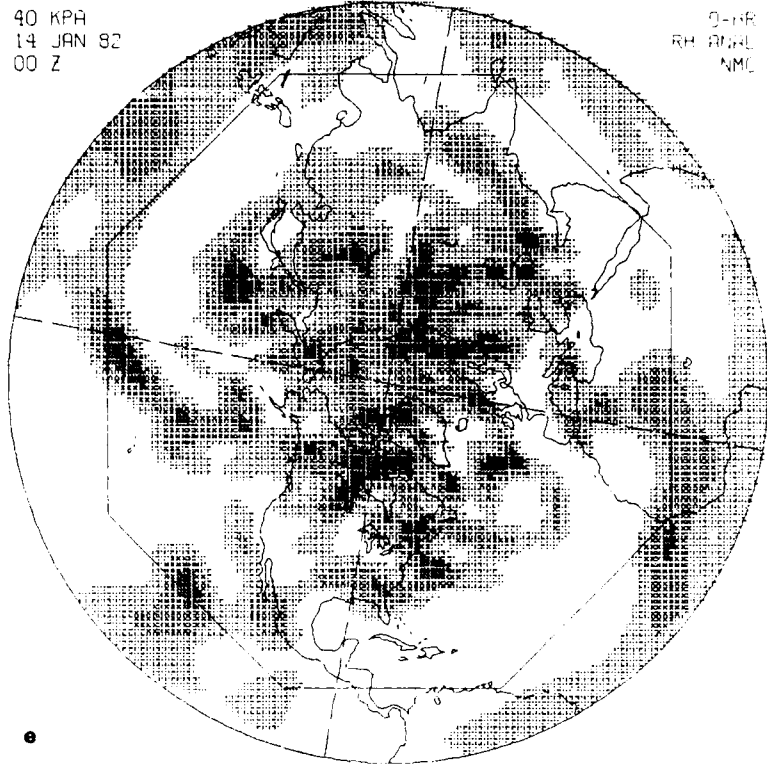
0-HR
RH ANAL
NMC



d

40 KPA
14 JAN 82
00 Z

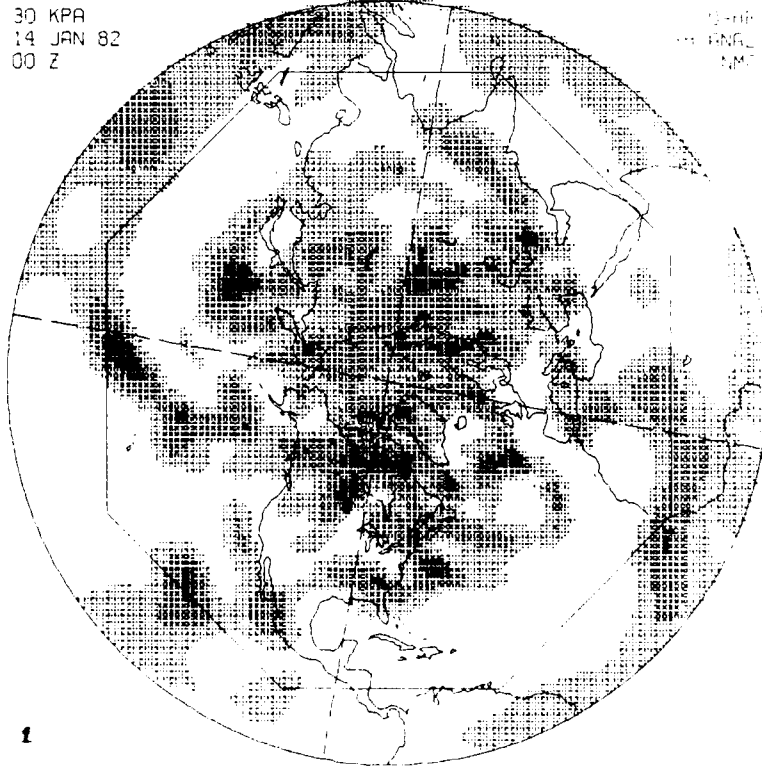
0-RR
RH RNL
NML



e

30 KPA
14 JAN 82
00 Z

0-RR
RH RNL
NML



f

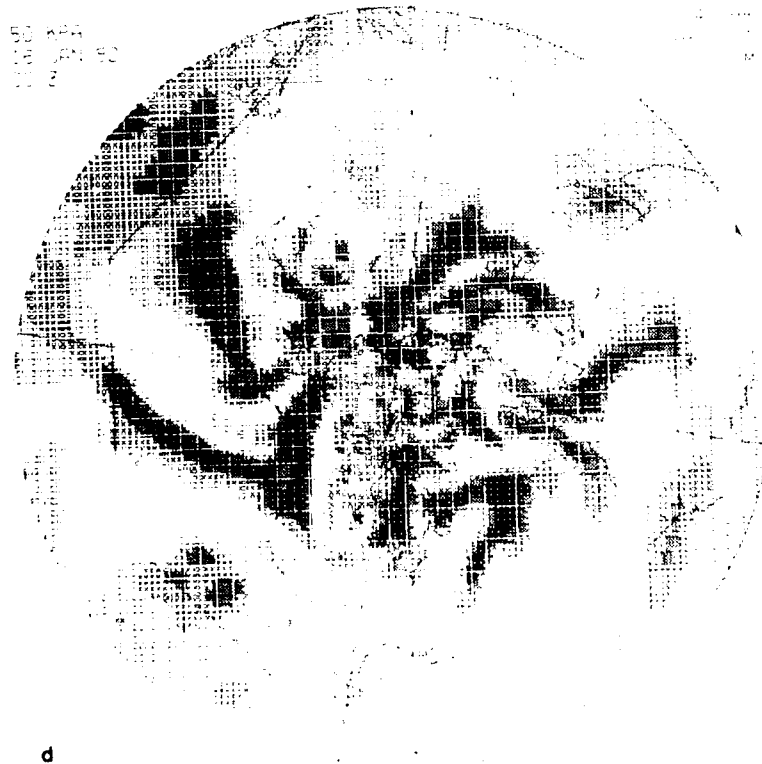
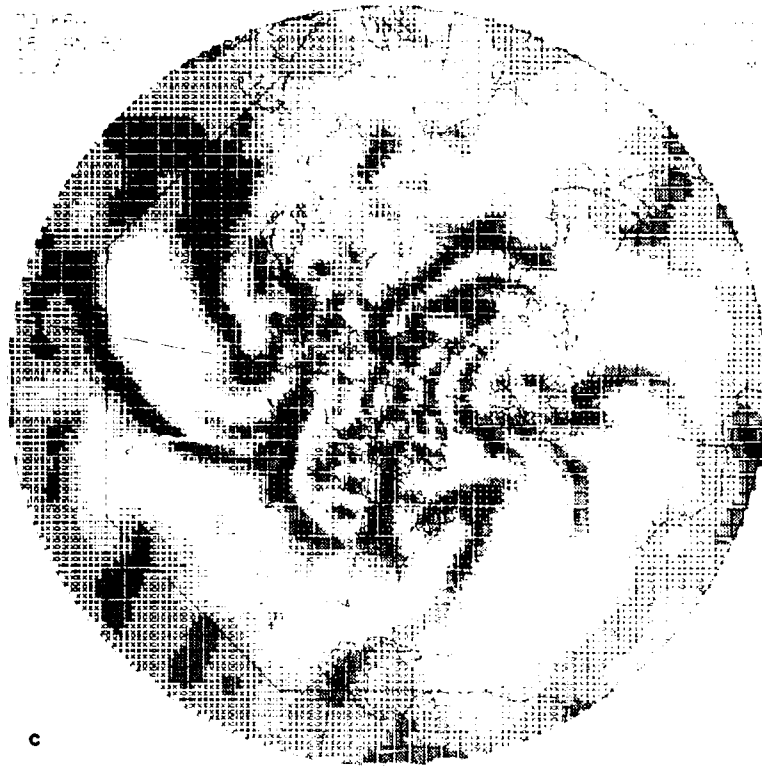


a



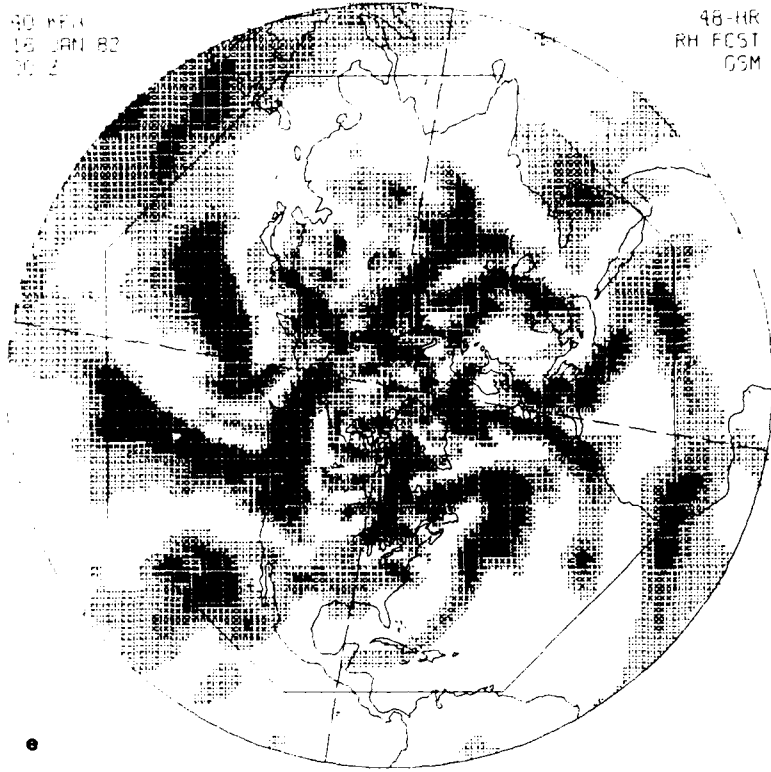
b

Figure 16. NH GSM 48-hr RH Forecast at Levels (a) 100, (b) 85, (c) 70, (d) 50, (e) 40 and (f) 30 kPa for the Forecast Initialized From the NMC Analysis of Figure 15.



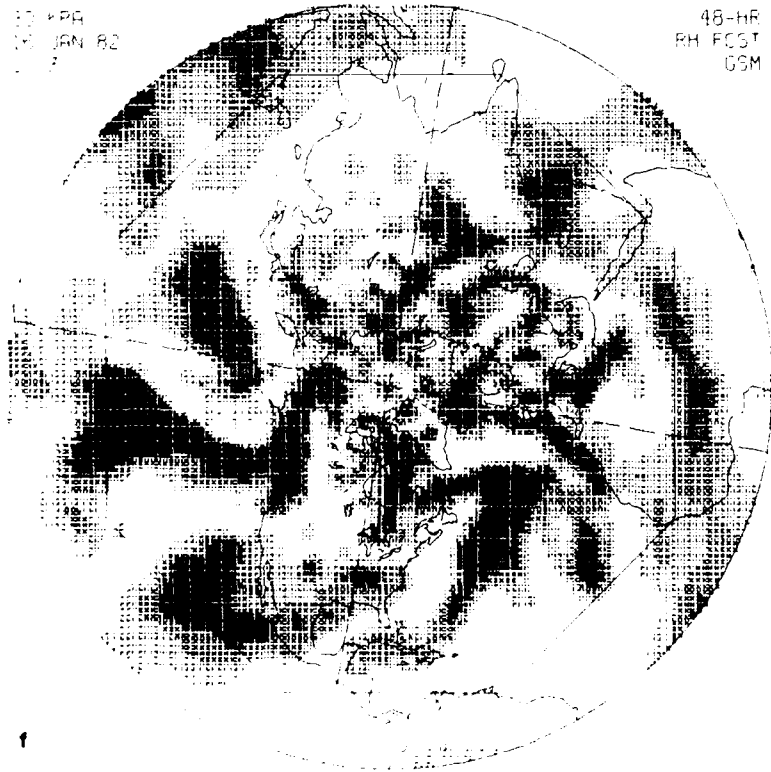
80 KPA
15 JAN 82
00 Z

48-HR
RH FCST
GSM



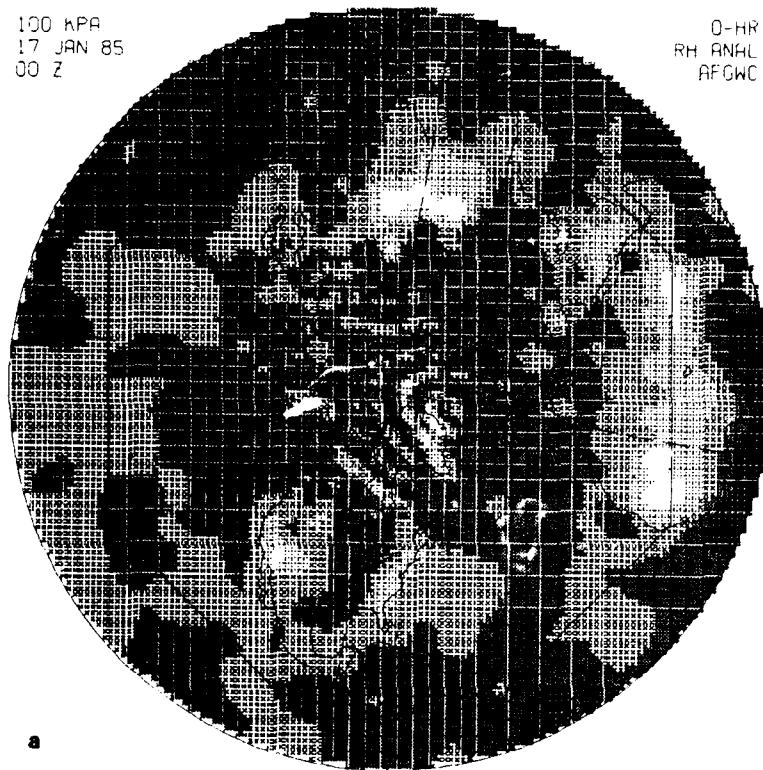
80 KPA
15 JAN 82
00 Z

48-HR
RH FCST
GSM



100 KPA
17 JAN 85
00 Z

0-HR
RH ANAL
AFGWC



85 KPA
17 JAN 85
00 Z

0-HR
RH ANAL
AFGWC

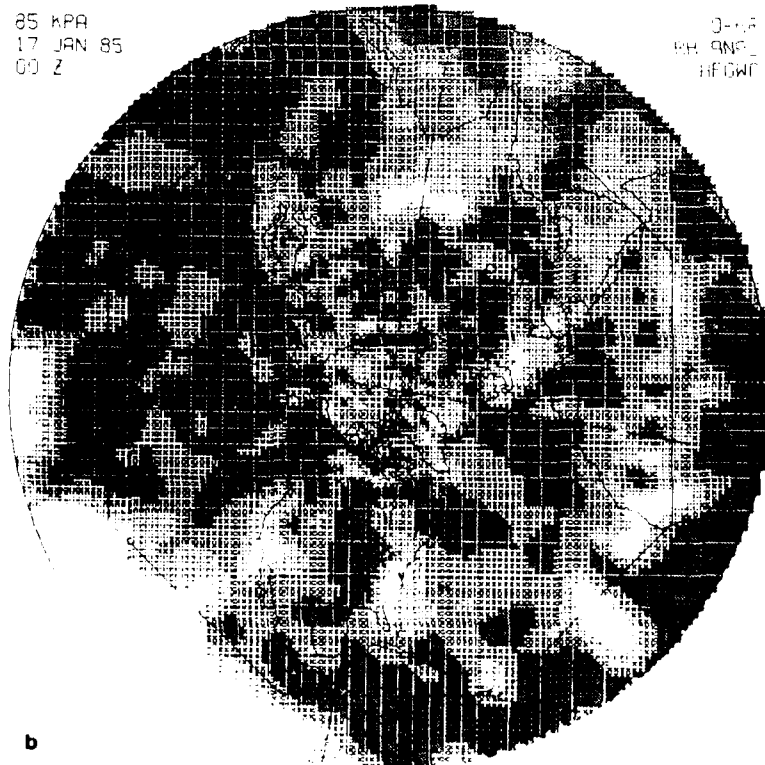
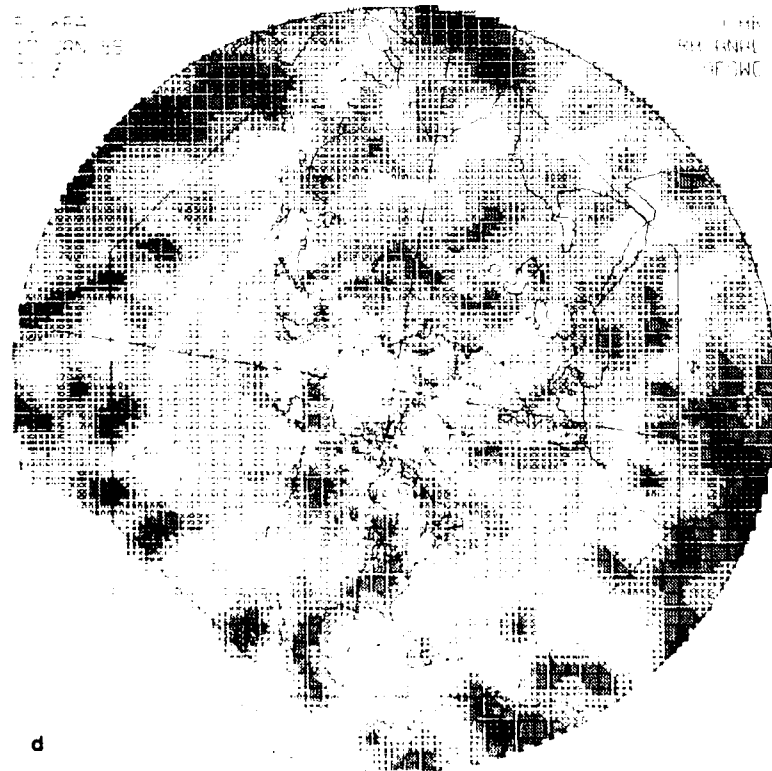
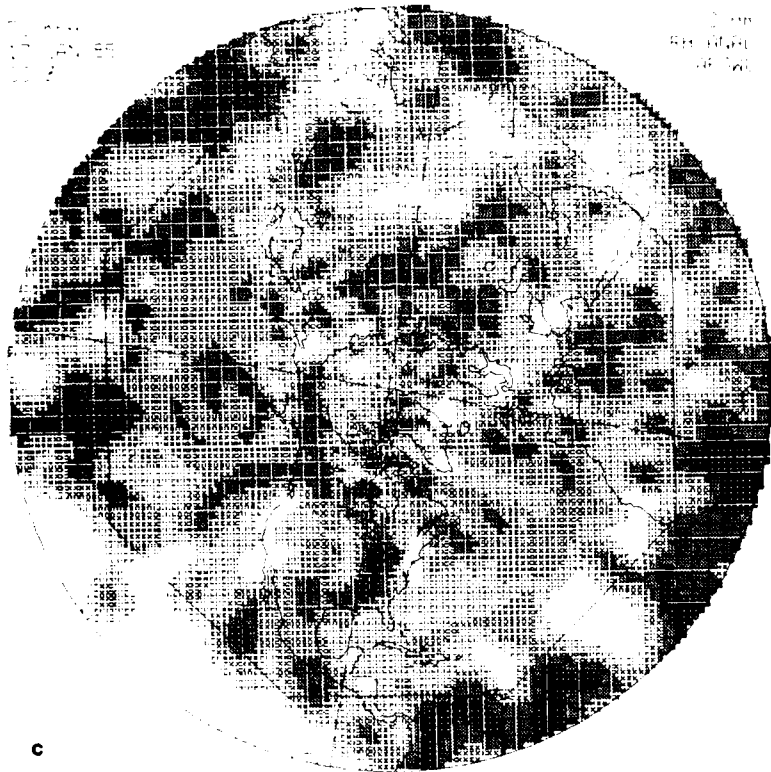
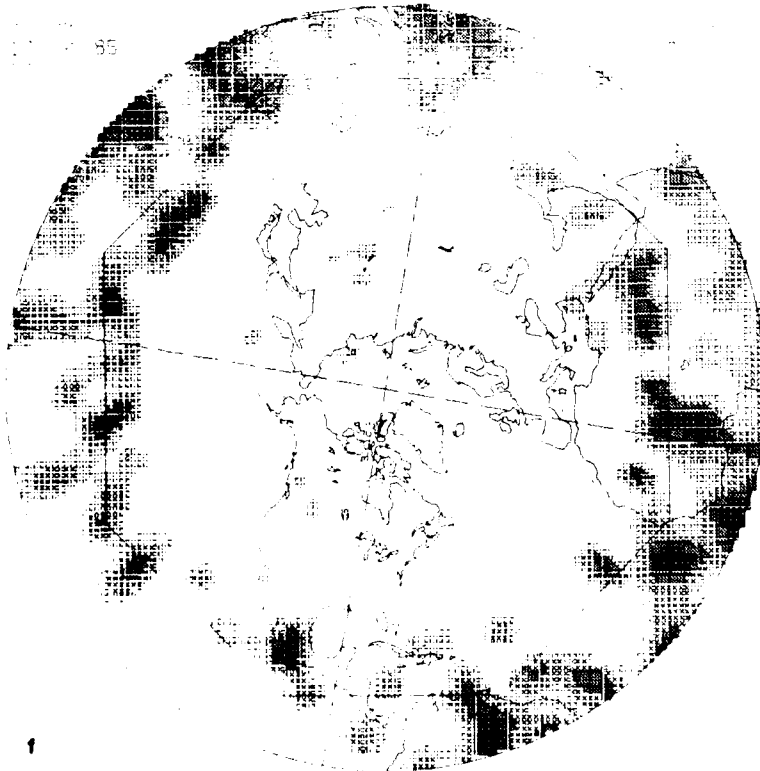
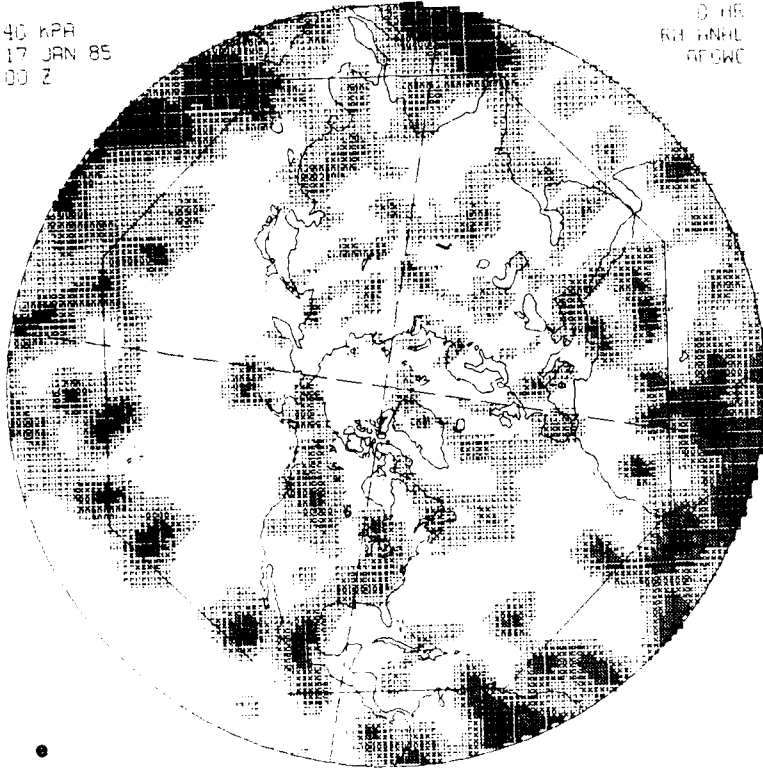


Figure 17. NH AFGWC RH Analysis for 00Z, 17 January 1985 at Levels (a) 100, (b) 85, (c) 70, (d) 50, (e) 40 and (f) 30 kPa. (The shading key in Figure 5 applies to all shaded displays of RH fields).



40 KPA
17 JAN 85
00 Z

0 HE
R1 GNHL
RFQWC



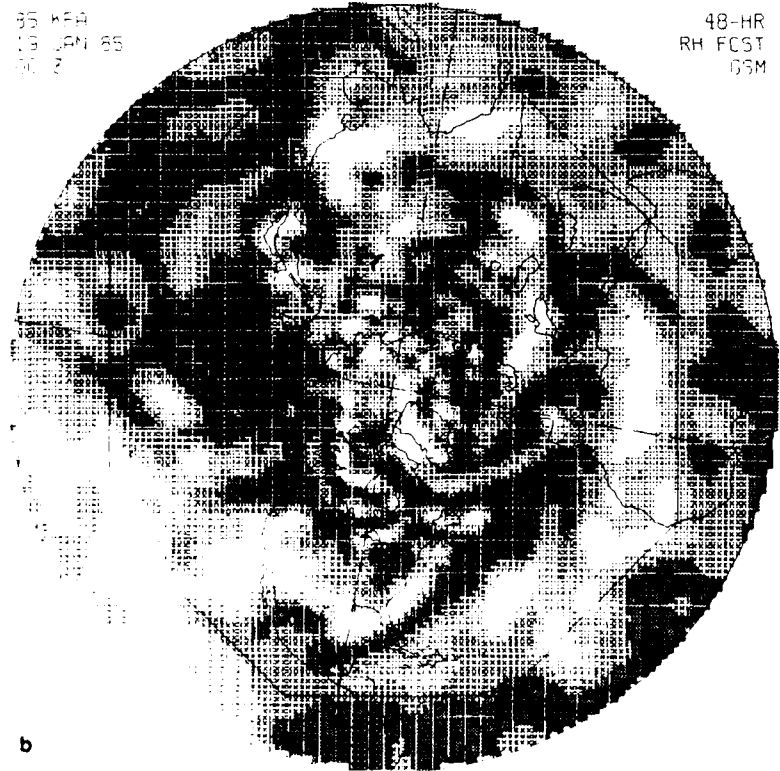
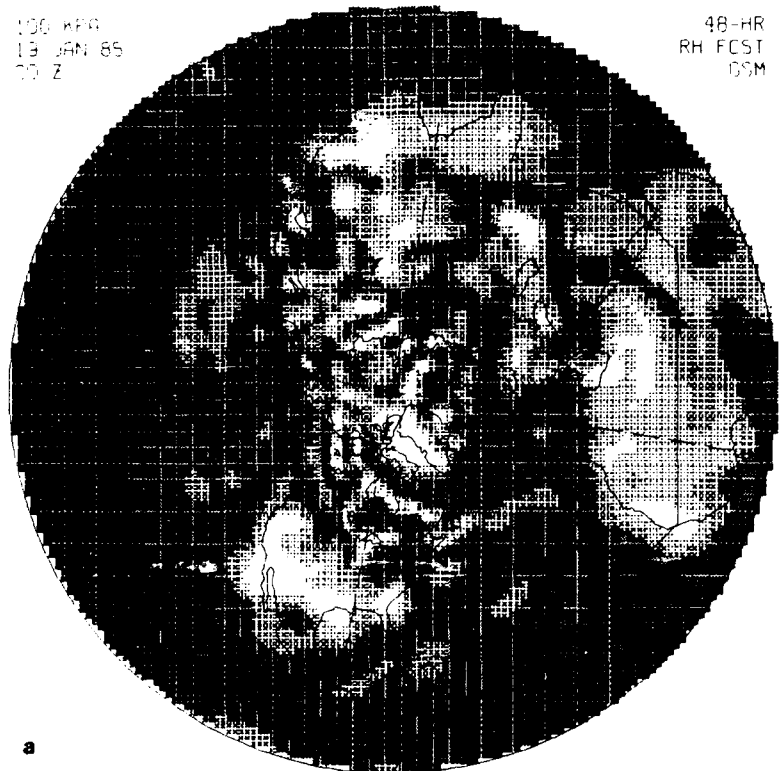
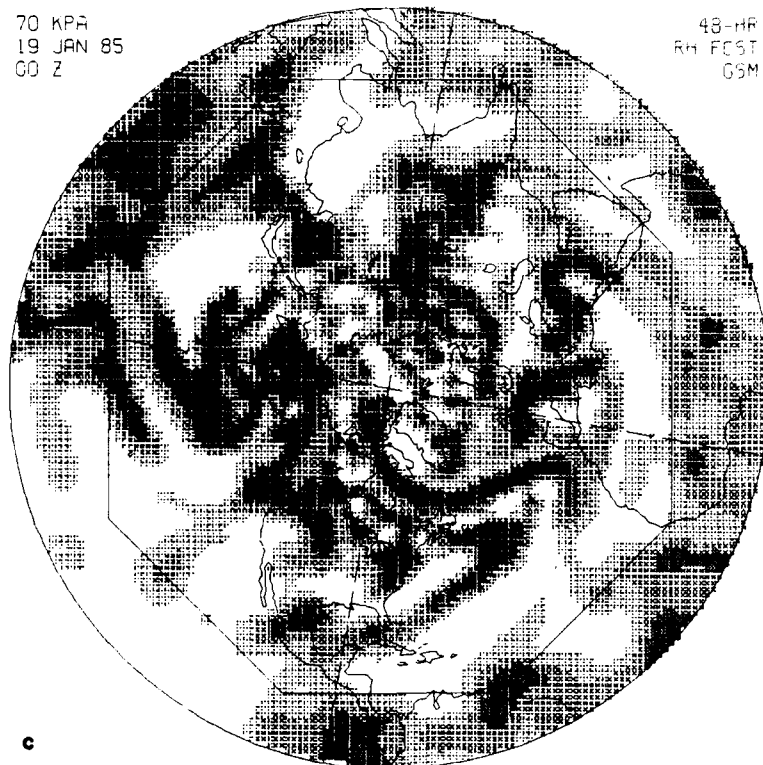


Figure 18. NH GSM 48-hr RH Forecast at Levels (a) 100, (b) 85, (c) 70, (d) 50, (e) 40 and (f) 30 kPa for the Forecast Initialized from the GSM Forecast Initialized from the AFGWC Analysis of Figure 17.

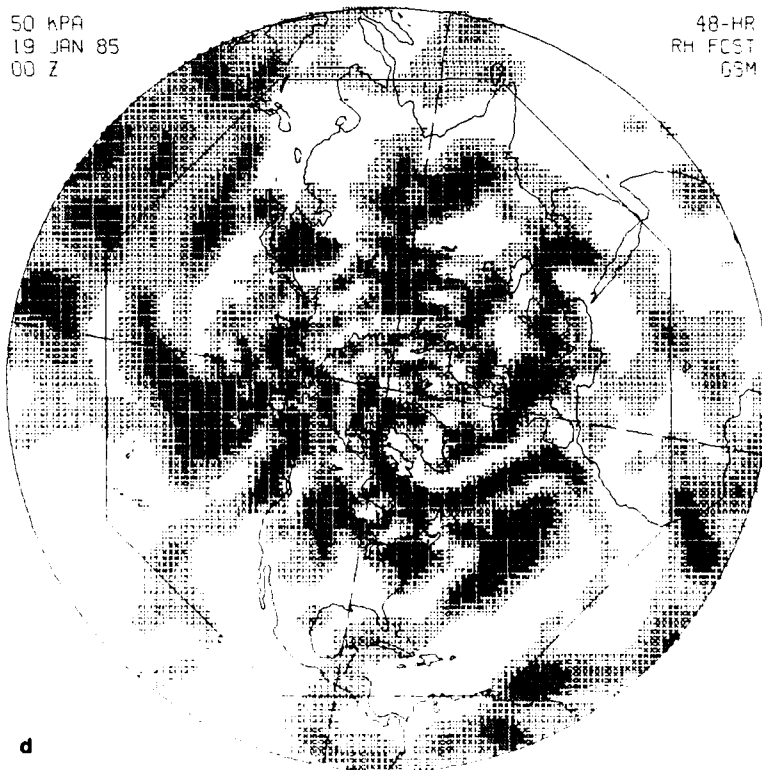
70 KPA
19 JAN 85
00 Z

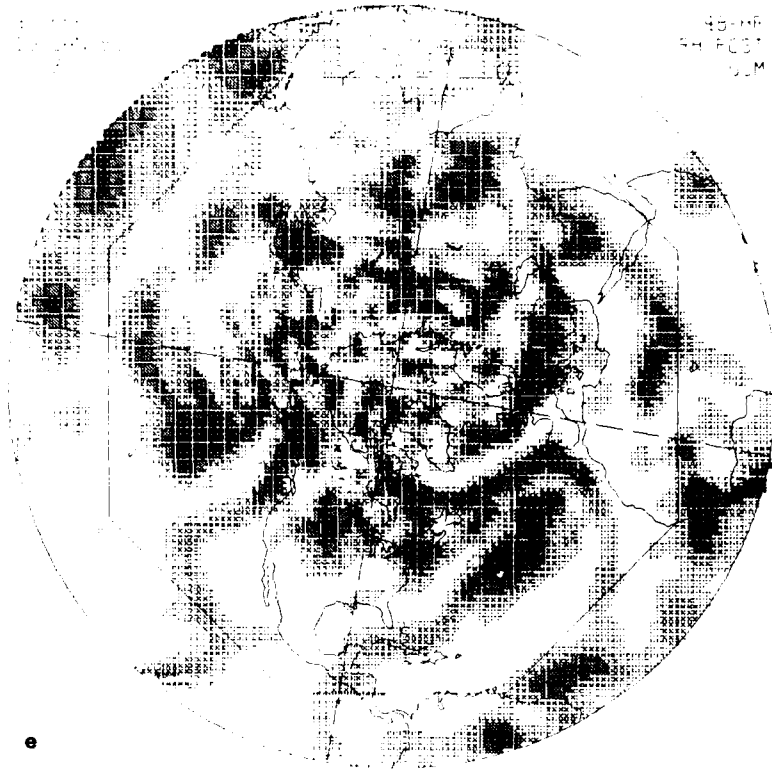
48-HR
RH FCST
GSM



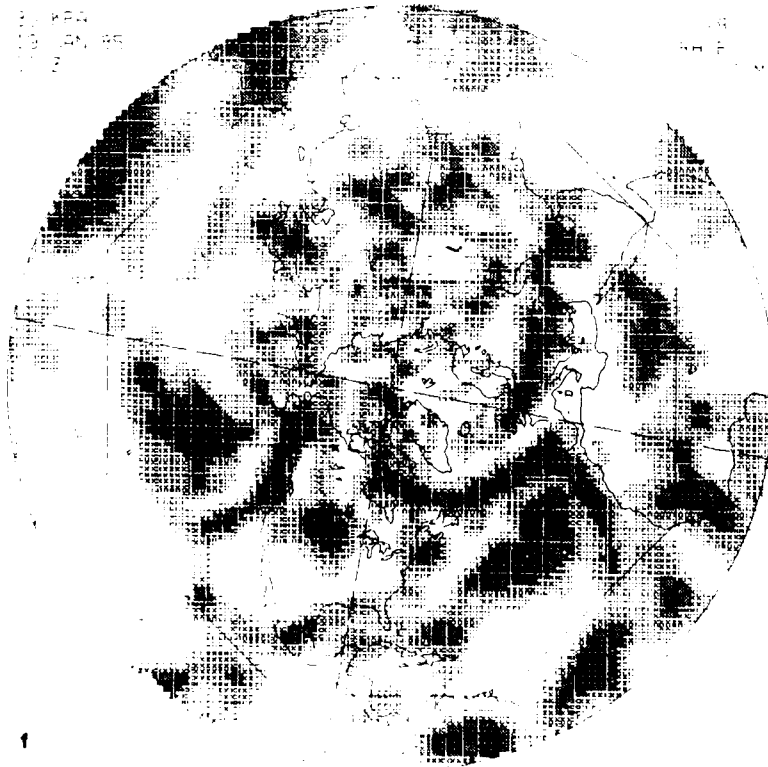
50 KPA
19 JAN 85
00 Z

48-HR
RH FCST
GSM





e



f

But the primary interest here in Figures 15-18 is the 100, 85, and 70 kPa levels, where some new characteristics not evident in Figures 11-14 are revealed. By comparing Figures 15b-c to Figures 16b-c and Figures 17b-c to Figures 18b-c, one notes that both 48-hour forecast fields show higher "contrast" within the display field than their 0-hour analysis counterparts. That is, the RH forecast displays show more areas at the dry and moist ends of the humidity range and sharper gradients between these moist and dry areas than the RH analysis displays. Most significant is the vivid synoptic patterns of narrow moist frontal bands and post-frontal "dry tongues" that have accompanied the emergence of more extreme wet and dry areas in the GSM forecast.

Quantitatively, this increase in contrast of the RH display in the GSM forecast shows up in terms of a changing frequency distribution of RH during the forecast. As an example, for the NH octagon domain, Figure 19 shows the temporal change toward an increase in the percent frequency of occurrence of GSM RH forecast values in both the moist and dry intervals of the RH range for the 85, 70, and 50 kPa levels in both the NMC/OP and AFGWC forecast cases. The above occurs, of course, at the expense of fewer RH values occurring in the intermediate humidity categories (not shown). In Figure 19, the tendency of the GSM to drive the moisture distribution toward the dry and moist ends simultaneously is particularly highlighted by the 85 and 70 kPa levels, where there is, in fact, a modest decrease in the octagon mean RH value (not shown) during the forecast period.

NH OCTAGON

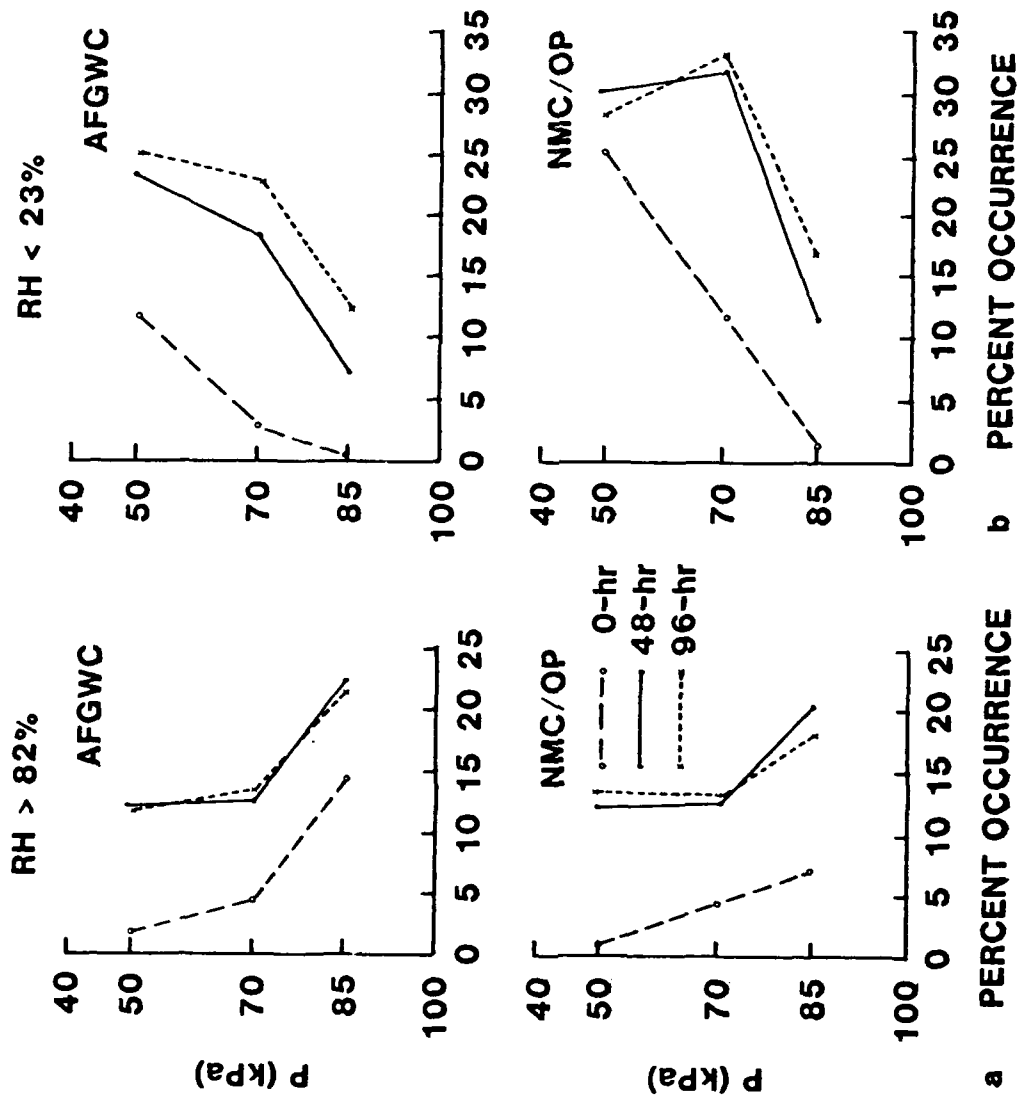


Figure 19. Percent Occurrence Over the NH Octagon Domain of (a) Moist RH Values (RH>82) and (b) Dry RH Values (RH<23) at the 50, 70, and 85 kPa Pressure Levels for the 0-, 48-, and 96-hour GSM Forecasts Initialized from the NMC Analysis of 00Z, 14 January 1982 (bottom) and the AFGWC Analysis of 00Z, 17 January 1985 (top).

The above spin-up of the GSM toward a more widespread occurrence of extremes in the moisture field is essentially accomplished by 48 hours in Figure 19. This result is a classic manifestation of the well-known "spin-up" period associated with large-scale models. The GL and AFGWC GSMs, like virtually all present-day large-scale models, begin with a quasi-balanced, quasi-nondivergent initial wind analysis, owing to the application of a nonlinear normal mode initialization to eliminate spurious large-amplitude gravity waves. Because of the largely nondivergent initial wind fields, the short range (0-6 hours) GSM vertical motion fields and frontal convergence zones are relatively weak, but subsequently intensify as the dynamics of the forecast model act to increase the magnitude of the horizontal divergence (see Brenner et al.⁷). As the GSM forecast proceeds, the attendant increase in the magnitudes of the vertical velocities and their organization into synoptic patterns (at least at extratropical latitudes) results in the aforementioned development of distinct synoptic frontal structures in the forecast RH field. Indeed, it is the vividness of the synoptic frontal patterns in Figures 16b-c and 18b-c that leads us in the first place to attempt cloud forecasting with a large-scale global forecast model.

Further examination of the moist frontal bands in Figures 16 and 18 reveals an unexpectedly deep vertical extent to these bands. The occurrence of a saturated band at one layer appears highly correlated with the simultaneous presence of a similar band at virtually all other tropospheric layers above and below. The moist band over the west coast of Canada in Figure 16 represents one of many extratropical examples in Figures 16 and 18. Outside the tropics in winter, we can rule out deep convection as a dominant process. Hence we conclude that the deep character of the extratropical saturated fronts in the GSM is a systematic error. Such deeply saturated fronts are substantially less frequent in the initial RH analyses of Figures 15 and 17, even in data rich areas. A similar systematic trend toward overdeveloping the vertical extent of moist frontal bands has been noted also in the ECMWF global model.³ The trend observed in the present study likely contributes to the lack of a vertical gradient in mean RH between the levels of 70 and 30 kPa in the GSM 96-hour NH mean RH profiles in Figure 12b.

To conclude this section, we focus on a systematic RH forecast trend apparent at 100 kPa over tropical and subtropical oceans, especially away from coastlines where air of continental origin may suppress the trend. Comparing Figure 15a to Figure 16a and Figure 17a to Figure 18a, we observe in these warm ocean areas an increase in RH to virtually saturated values in just 48 hours. Some of these very moist low-latitude ocean areas extend northward of the octagon boundary and will affect the cloud forecasts verified over the octagon in Section 3.2.

The cause of this systematic trend is the absence of a representation of vertical diffusion above the lowermost model level in the baseline GSM. In the bottom level of the GSM, surface evaporation over oceans occurs at the potential rate, as governed by a standard bulk aerodynamic drag formula and the specified sea-surface temperatures.⁸ Over warmer low-latitude waters this evaporation rate can be substantial, if the air is not already near saturation. As the evaporation proceeds, the lowest model layer continues to moisten rapidly (until the approach to saturation shuts the evaporation down), because no vertical diffusion is present in the GSM above the first layer. Such a vertical diffusion, if it were present, would

act as a continual sink of surface layer water vapor owing to the vertical turbulent flux to overlying layers.

Over land the GSM layer-one mean RH trend is reversed, as there the GSM ignores surface evaporation, yet precipitation still acts as a moisture sink. These reverse trends at 100 kPa over land and water undoubtedly cancel each other to a significant degree in the NH mean trends shown at 100 kPa in Figures 11 and 12. However, in Figures 13b and 14b, between latitudes 40S and 20N, where the percentage of land area is small, the mean moistening over oceans at 100 kPa during the forecast is evident, particularly in the January 1985 case of Figure 14. This latter case is one of the two cloud forecast cases presented later in Section 3.2.

3. EXPERIMENTAL GLOBAL CLOUD FORECASTS

3.1 Diagnostic Cloud Forecast Schemes

There are a myriad of challenging difficulties and issues in developing a cloud forecast scheme for a large-scale NWP model. The NWP model cloud forecast studies by J.M. Slingo^{3,34,35} provide excellent discussions and examples of these problems and issues and the reader is encouraged to review these references. For the reasons emphasized at the beginning of Section 2 and following the recommendation of Slingo, this study will examine only diagnostic cloud forecast schemes; that is, schemes that diagnose cloud properties (in this case layer and total fractional coverage) empirically or statistically from other model output fields.

Diagnostic cloud forecast schemes themselves encompass two broad types, which are 1) schemes that utilize only the model's forecast humidity field and 2) schemes that utilize both the humidity field and additional model output fields such as vertical velocity, convective and non-convective precipitation rates, vertical temperature and moisture gradients in the PBL, and surface fluxes of moisture and heat, among others. A diagnostic scheme of type 1 was used in the ECMWF global forecast model until May 1985; and the performance of this cloud scheme, known as the Geleyn scheme¹, is well documented by Slingo.³ Since May 1985, a diagnostic scheme of type 2 has been used in the ECMWF model, and the performance of this cloud scheme, known as the Slingo scheme, is also well documented by Slingo.³⁵

The choice of which type of diagnostic cloud scheme to employ in a given large-scale model is dictated for the most part by the complexity and veracity of the model's parameterized physical processes. Type-2 diagnostic schemes require fairly reliable deep and shallow convection schemes, fairly complex PBL schemes that employ at least three or four model

³⁴ Slingo, J. (1980) A cloud parametrization scheme derived from GATE data for use with a numerical model, *Q.J.R. Met. Soc.*, **106**:747-770.

³⁵ Slingo, J. (1987) The development and verification of a cloud prediction scheme for the ECMWF model, *Q.J.R. Met. Soc.*, **113**:899-927.

layers in the lowest kilometer, and radiative forcing schemes with a diurnal cycle. As detailed in the introduction, AFGWC's currently operational GSM (and hence GL's baseline GSM used here) lacks such physical complexity. Although the AFGWC GSM does include a deep convection scheme patterned after the widely used parameterization of Kuo,¹⁰ it also includes several additional constraints on the occurrence of deep convection not found in Kuo's original scheme. Examination by GL¹⁸ of the resulting convective precipitation rates and frequency of convective points showed vastly smaller, almost negligible, time and space averaged values for these quantities in the AFGWC GSM (or baseline GL GSM) compared to other models and estimated climatologies.

As a consequence of these baseline GL GSM characteristics, all experimental GSM cloud forecast schemes tested in this study and presented in this section were purposely limited to type-1 diagnostic schemes. Because of the limitations in GSM parameterized physics, we cannot expect the GSM cloud forecasts presented here to perform well depicting most tropical cloud regimes (which are dominated by deep and shallow convection and have a strong diurnal character over land) or those low cloud regimes that are driven by local PBL processes and their interaction with terrain and radiation (such as fair weather "popcorn" cumulus or persistent marine stratocumulus). But the AFGWC 5LAYER model, which also uses a type-1 diagnostic cloud scheme, similarly lacks an ability to forecast such tropical, convective, or PBL cloud regimes, as it too lacks physical treatments of convection, radiation, and the PBL.⁴

In terms of cloud forecast skill then, the strong suit of both the baseline GSM and 5LAYER models is expected to be prediction of the extratropical large-scale cloud organizations associated with synoptic circulations -- an association often observed in satellite imagery. Certainly in the case of the baseline GSM, synoptic patterns were distinctly present in the RH forecast displays of Figures 16 and 18. Because of some similarity in the strengths and weaknesses of the baseline GSM and 5LAYER models (and recalling that 5LAYER uses as input the GSM's horizontal and vertical wind velocity forecast), it is reasonable to expect baseline GSM cloud forecasts to be competitive with 5LAYER cloud forecasts.

3.1.1 GLOBAL CLOUD FORECAST PROCEDURES

The use of a type-1 diagnostic cloud scheme, which again utilizes only the model's moisture forecast (plus possibly the temperature forecast to allow conversion to other moisture variables), offers one important expedient advantage over more complex schemes. Namely, since a model's moisture and temperature forecast are standard model output fields, a type-1 diagnostic cloud scheme can be run as a "cloud postprocessor", executed external to the GSM model (even on a separate computer system). The type-1 diagnostic cloud schemes tested here indeed were executed as a separate cloud postprocessor after executing the baseline GL GSM.

Specifically, after GSM execution, the first task was to execute the standard non-cloud GSM postprocessor wherein (1) GSM forecast spectral coefficients of temperature (T) and specific humidity (Q) were transformed to a 2.5° latitude/longitude grid (following the AFGWC grid convention) on the GSM's seven moist sigma surfaces, (2) T and Q at each grid point were converted to RH (which due to well known moisture spectral truncation errors was then

checked and constrained to be between 1 and 100 percent), and (3) T and RH were vertically interpolated from sigma surfaces to the lowest six mandatory pressure surfaces. After the standard GSM postprocessor executed these three steps, the cloud postprocessor was executed, which involved four steps. First, the T and RH fields on the six pressure surfaces from step 3 above were input and biquadratically interpolated to AFGWC's fully hemispheric 1/2-mesh 129 X 129 grid (it is the RH fields from this step that are displayed in Figures 15-18). Next, RH was converted, if necessary, to another moisture variable (using T when needed). Then, the chosen type-1 diagnostic cloud scheme was applied to convert the moisture variable to a cloud amount at each moist pressure surface. Finally, a vertical stacking algorithm was applied to the layer cloud amounts to obtain a total cloud amount. In the second step, we *implicitly* view the GSM forecast moisture value at a given pressure level as a mean *layer* value for the corresponding layer centered around the given pressure level and hence view the resulting cloud amount as a layer cloud amount. The same vertical stacking algorithm, details of which are given in Appendix A, was used for all the cloud schemes (with minor variations described in Appendix A). In the stacking algorithm, whenever a given pressure level is found to be below the terrain height defined on AFGWC's 129 X 129 grid, the layer cloud amount is set to zero.

The AFGWC 93 X 101 5LAYER octagon 1/2-mesh grid is an exact pointwise subset of the 129 X 129 hemispheric 1/2-mesh grid cited above. All the total cloud forecast verification statistics presented later were computed on the 5LAYER 1/2-mesh grid, as the verifying RTNEPH cloud analyses archived for this study were also represented on this grid.

In any future follow-on study, one is strongly urged to reduce postprocessing error by reducing and modifying the above steps as follows: carry out the σ -surface horizontal spectral transform to a finer scale (that is, 1.0 or 0.5°) rather than 2.5° latitude/longitude grid before interpolating to the verifying 1/2-mesh grid and remain on the GSM σ -surfaces, thereby eliminating the errors of vertical interpolation to pressure surfaces (also the grouping of σ -layers into cloud layers can occur then on physical grounds rather than according to the arbitrary location of pressure surfaces). Presently, AFGWC does not store the original GSM forecast spectral coefficients on σ -surfaces beyond 12 hours (the storage from 0-12 hours is for the global data assimilation cycle). In the present study, we chose to utilize only GL GSM output fields corresponding to those routinely stored by AFGWC GSM postprocessing.

To provide the 5LAYER cloud forecasts for GSM comparison purposes in this study, AFGWC originally archived and provided GL with 12 NH 5LAYER 48-hour forecast cases (three each during the AWAPS Phase I months of April, July, and October 1984, and January 1985). As companion data sets, AFGWC also archived the corresponding 12 AWAPS global objective analyses to be used as the initial conditions (except for humidity) for the subsequent off-line GL GSM cloud forecast experiments for this study. Before examining these GL GSM cloud forecasts here, it is important to emphasize why this study did not simply use the archived data (in a type-1 diagnostic cloud postprocessor) from the operational AFGWC AWAPS GSM temperature and humidity forecasts for the above 12 cases. The reasons were fourfold:

- 1) The quality of the AWAPS Phase I humidity analyses used as initial moisture conditions for the AWAPS GSM forecasts was poor for the several reasons detailed in Section 2.1.1.

2) The AWAPS Phase I initial humidity analyses, unlike the 5LAYER initial humidity analyses, neglected to utilize RTNEPH cloud data as a surrogate humidity data source. A priori, this was viewed as giving 5LAYER an unfair advantage over the GSM, especially in the short range, since the RTNEPH was to be used as the cloud verification database.

3) The effective horizontal spatial resolution of the AWAPS Phase I GSM (rhomboidal 20) was considerably coarser than that of 5LAYER (1/2-mesh or 100 nm at 60° N) or that of AFGWC's present Phase II GSM (rhomboidal 40).

4) The study of Mitchell and Yang¹⁴ showed that the methods of vertically interpolating moisture fields between pressure and sigma surfaces in the preprocessor and postprocessor of the AWAPS Phase I GSM were sources of significant GSM moisture forecast error, especially in the short range.

For the above reasons, this study utilized separate GL GSM forecasts, executed off-line on the AFSCC-K CRAY-1/S and designed to mitigate these four factors. The GL GSM horizontal resolution was increased to rhomboidal-40 and the preprocessor and postprocessor were changed to utilize the vertical moisture interpolation methods recommended by Mitchell and Yang.¹⁴ Most importantly, as described in Section 2.1.1, the AWAPS Phase I humidity analyses were replaced here with AFGWC's alternative global humidity analyses that utilized RTNEPH cloud data via a 5LAYER first-guess and therefore more closely resembled the initial humidity analyses of 5LAYER.

Despite the good intentions of using AFGWC's non-AWAPS global moisture analyses, the results of Section 2.1.2 show that the latter analyses suffer from their own unique problems, including a severe extratropical upper-level dry bias. More pertinent here is the additional problem described in Section 2.1.1 whereby the nine April through October 1984 cases proved to be unusable in the parallel GL GSM cloud forecast experiments owing to the zero humidities stored at all tropical points. This in fact left only the three January 1985 cases as candidates for further GSM and 5LAYER comparisons.

In the end, only the two 5LAYER cases for 00Z on 17 January and 24 January 1985 were accessible for the comparisons here (physical errors on the archive tape prevented use of the third January 1985 case). Recall that as background for the GL GSM cloud forecasts to be examined for these two cases below, the GL GSM humidity forecasts for the 17 January case were examined in detail in Section 2.2.

3.1.2 PREVIOUS DIAGNOSTIC CLOUD SCHEMES

In the steps of the cloud postprocessor described in the previous section, the central step invokes the chosen type-1 diagnostic cloud scheme. This study will test and examine four such schemes. The first three schemes, which are considered in this section, are previously available schemes currently or formerly used by other NWF centers — specifically one scheme each from AFGWC, NMC, and ECMWF. The fourth scheme, which has two variants, is a new GL cloud scheme developed specifically as a product of this study and is described separately in Section 3.1.3.

Since the experimental GSM cloud forecasts are to be compared with the cloud forecasts of the AFGWC 5LAYER model, an obvious first candidate for a GSM cloud scheme is the diagnostic scheme used by the 5LAYER model. The latter scheme is the previously introduced AFGWC CPS-cloud scheme given in Figure 8. In the 5LAYER model code, the CPS-cloud curves in Figure 8 are actually represented as four look-up tables (one for each level in Figure 8) specified in increments of one percent cloud amount (see Appendix B of Crum⁴).

In its treatment of moisture, precipitation and clouds, the 5LAYER model includes explicit prognostic equations only for the moisture variable CPS (defined earlier in Section 2.1.2). CPS is forecast at five layers whose mid-points are given by the four constant pressure levels of 85, 70, 50, and 30 kPa plus a so-called "gradient" level, which is a terrain following lower level defined to be at 6 kPa above the surface. At each of these five layers, the 5LAYER model applies the respective curve in Figure 8 to empirically convert each CPS forecast value to a cloud amount. For the gradient layer, the 85 kPa CPS-cloud curve is utilized. Finally, total cloud is derived in 5LAYER by applying a vertical stacking algorithm as given in Appendix A.

In the GSM application here of the AFGWC cloud scheme, the GSM cloud postprocessor derives forecast CPS values at all six moist mandatory pressure levels from the GSM forecast values of RH and T. Then the AFGWC CPS-cloud curves are applied to obtain the corresponding cloud amounts. The 30 and 85 kPa CPS-cloud curves also are applied to the 40 and 100 kPa levels, respectively. (In this regard, recall the very close similarity in Figure 8 between the 50 and 30 kPa curves and the 5LAYER model use of the 85 kPa curve with the gradient level.)

Looking ahead to the quality of the GSM cloud forecasts obtained with the AFGWC scheme, we recall from Figure 9 that this scheme yields very low values of the critical relative humidity, RH_c, in the range $10 \leq \text{RH}_c \leq 30$ percent for the 30-50 kPa regime. As will be shown, these critical values are far below those obtained from the other cloud schemes to be considered here and, as previously shown in Section 2.1.2, contributed substantially to the significantly dry nature of the AFGWC upper-level humidity analysis within the NH octagon domain. In contrast, Figure 11 showed that the GSM NH mean RH forecast value in the 30-50 kPa regime is between 40 and 50 percent after 24 hours, even when the GSM is initialized from the overly dry upper-level AFGWC analysis. More importantly, Figure 12 established that the vertical profile of the NH mean RH of the GSM forecast agrees fairly closely with the observation-based vertical profile, although showing a modest moist bias at the upper levels.

Not surprisingly then, when applied to the GSM the AFGWC CPS-cloud scheme yields very large upper-level (and hence total) forecast cloud amounts showing a severe positive bias. This is illustrated later in Section 3.2 and in the forerunner study of MW.⁶ The AFGWC CPS-cloud scheme was the *only* cloud scheme tested in the forerunner GSM cloud forecast experiments of MW. Despite its poor performance in that study, it is tested again here for the sake of completeness and to serve as one of several examples demonstrating a major point to unfold in the present study -- namely, *a type 1 diagnostic cloud scheme developed and tuned for use in one NWP model will not perform well when applied to an independent NWP model unless the two models have closely similar, level by level, humidity forecast characteristics for 1) the domain mean value and 2) the frequency distribution of humidity.* To further demonstrate the above point, we proceed to consider and apply two additional previous type-1 cloud schemes from other NWP centers.

The next such scheme is that scheme used operationally by the ECMWF until May 1985.³ This scheme relates cloud amount, CL_k , at a given layer k , to the layer relative humidity, RH_k , by

$$CL_k = \left\{ \text{Max} \left[0, \left(\frac{RH_k - RHc_k}{1 - RHc_k} \right) \right] \right\}^2 \quad (1)$$

where RHc_k , the layer-dependent critical relative humidity for the onset of nonzero cloud, is specified by:

$$RHc_k = 1 - 2\sigma_k + 2\sigma_k^2 + \sqrt{3\sigma_k} (1 - 3\sigma_k + 2\sigma_k^2) \quad (2)$$

in which $\sigma_k = P_k/P_*$, the ratio of the mid-layer pressure, P_k , to the surface pressure, P_* . Equations (1)-(2) assume that RH and CL are expressed as fractional values in the range 0 to 1. To apply Eqs. (1)-(2) in the cloud postprocessor, we set P_k to the mandatory level pressure and P_* to 100 kPa. Figure 20 shows the RH -cloud curves thus obtained from Eqs. (1)-(2) for four mandatory levels.

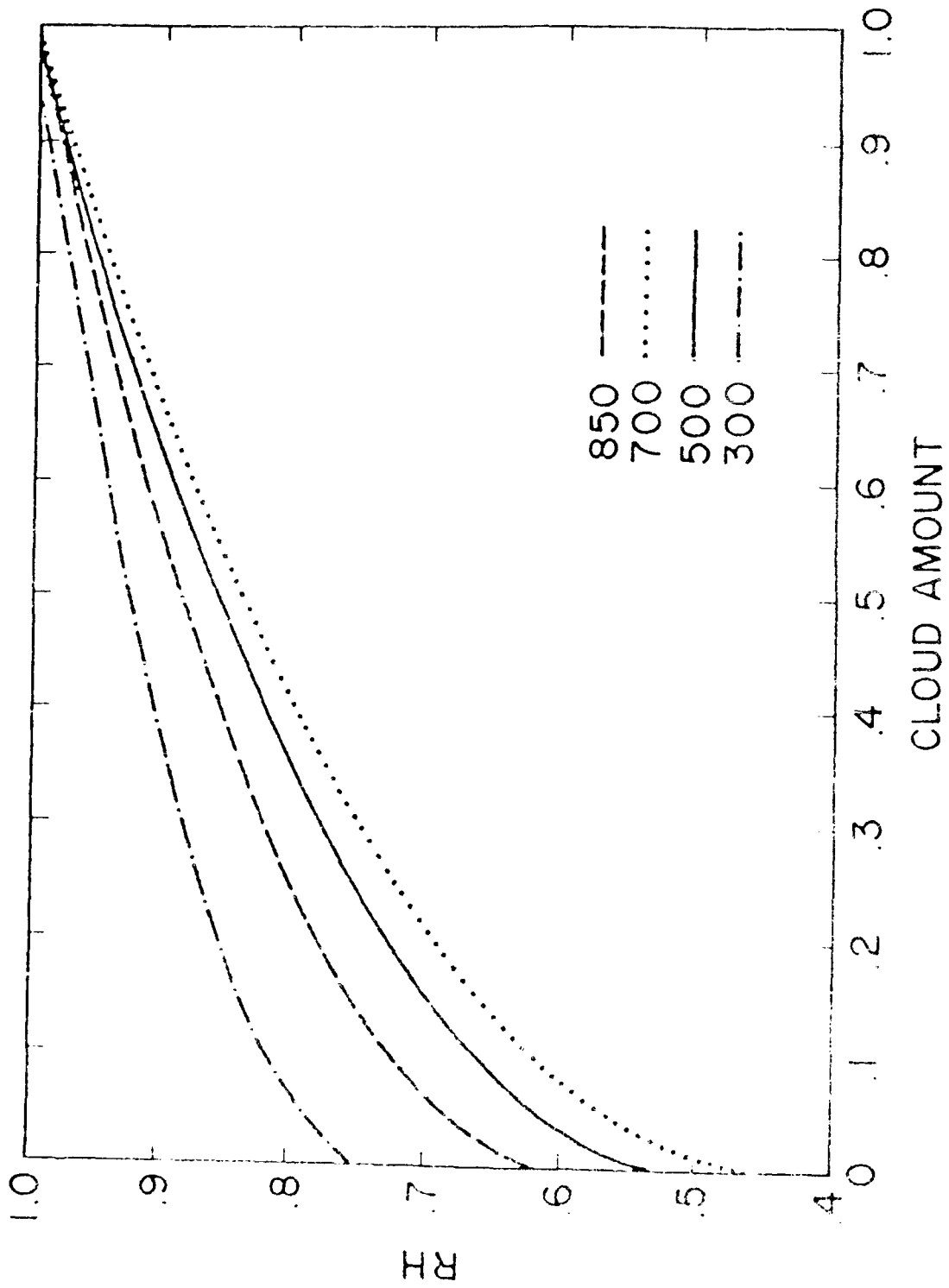


Figure 20. Curves of the ECMWF Humidity-cloud Conversion Scheme of Eqs. (1)-(2) for Four Mandatory Pressures.

Figure 21 compares the critical relative humidities of the AFGWC and ECMWF schemes as a function of pressure. Figure 21a compares the standard critical value, RH_c , for the zero-cloud threshold, while Figure 21b compares the critical RH value for the 30 percent cloud threshold. Figure 22 compares the AFGWC and ECMWF humidity-cloud curves for the 85 and 50 kPa levels over the full range of cloud amounts. To express the AFGWC curves in terms of RH for the purposes of Figures 21 and 22, U.S. Standard Atmosphere temperatures were again used to convert CPS to RH. Also represented in Figures 21 and 22 are the NMC and GL cloud schemes described later.

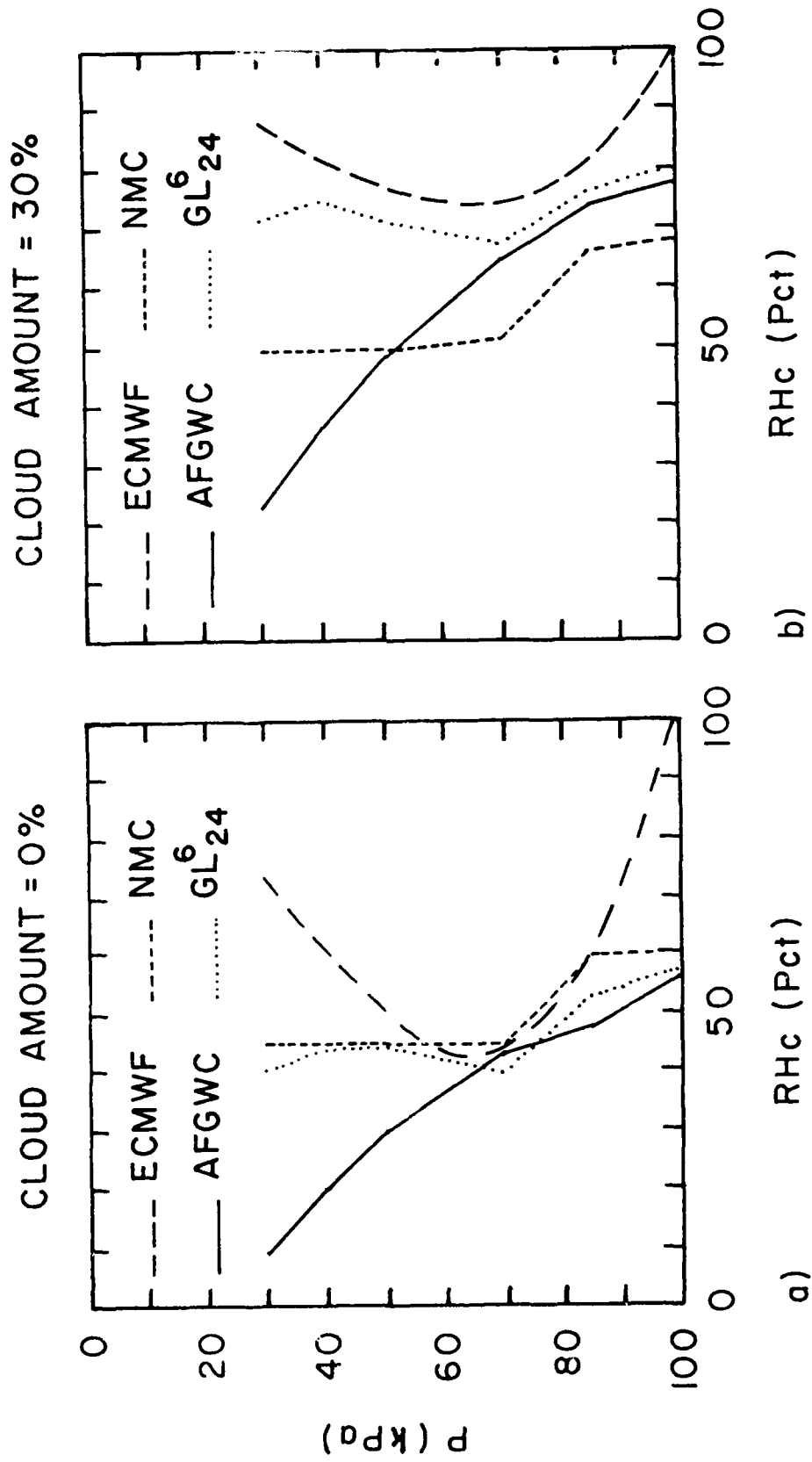


Figure 21. Critical Relative Humidity, RHc, as a Function of Pressure for the Cloud Amount Thresholds of (a) 0 Percent and (b) 30 Percent for the ECMWF, AFGWC, NMC, and GL Humidity-cloud Conversion Schemes.

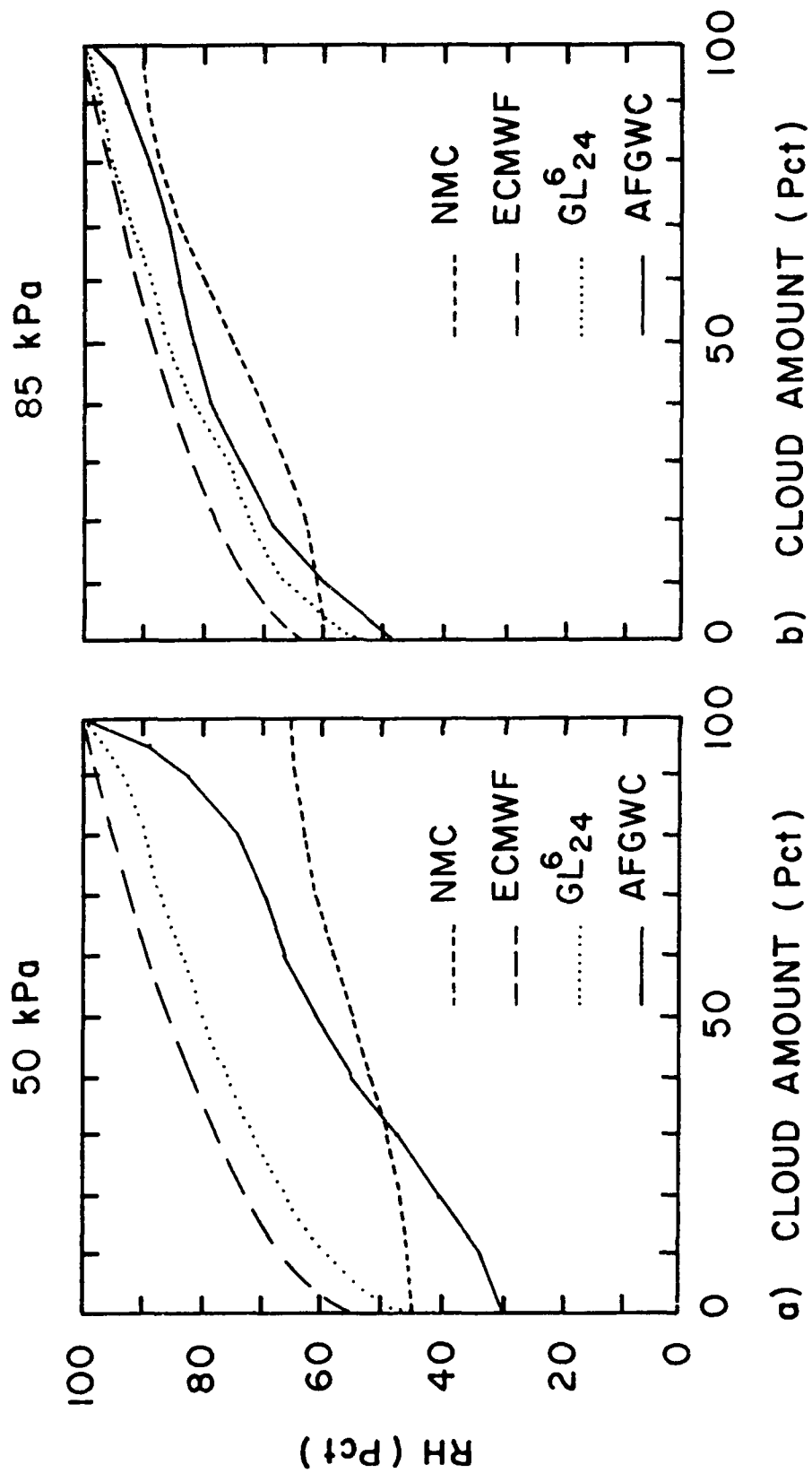


Figure 22. Curves of the ECMWF, AFGWC, NMC, and GL Humidity-cloud Conversion Schemes for the (a) 50 kPa and (b) 85 kPa Mandatory Pressures.

In Figure 21a, the AFGWC scheme yields the smallest RHC values of all the four cloud schemes at nearly every level. In contrast, the ECMWF scheme generally yields the largest RHC values, most particularly at the lowest and highest levels. The type-1 cloud scheme in Eqs. (1)-(2) was finalized after *adjustments* to give reasonable agreement between the *total* cloud forecasts of the ECMWF model and observed total cloud amounts (in terms of cloud climatologies and subjective comparisons with satellite imagery).¹ One can speculate that the adoption of large RHC values at low and high levels in the ECMWF scheme was a response to significant moist biases in the model's humidity forecasts at those levels. Recall from Section 2.2 that Slingo and Ritter³ found the ECMWF model to be considerably too moist in the model's lowest σ -layer, especially over the oceans. Further examination of Figures 20-22 shows the ECMWF scheme yields the largest critical humidities for virtually all cloud amount thresholds (30,50,70). Not surprisingly then, in Section 3.2 the layer and total GSM cloud forecasts based on the ECMWF scheme will depict too *little* layer and total cloud.

The large critical humidities in the ECMWF scheme are also manifest in the results of the study by Norquist^{12,28}. Using Eqs. (1)-(2) in the inverse sense to infer humidity estimates for an objective humidity analysis from 3DNEPH analyzed layer cloud amounts, Norquist found the ECMWF inferred humidities to be too high (substantial positive bias) compared with collocated RAOBs as shown in Table 4 -- this despite the fact that at low and middle levels, at least, the 3DNEPH mean cloud amounts during the Norquist study period were shown to be in fair agreement with other cloud climatologies.³¹

The latter experience illustrates the following important point: an empirical humidity-cloud relationship originally derived for use in a forecast model to infer cloud amounts from forecast humidity will likely not perform well in the inverse sense to infer humidity estimates from observed cloud amounts for use in an objective humidity analysis. One reason for this is that the mean values and frequency distributions of humidity in model forecasts can depart substantially from those obtained from observations. Such departures occur because of 1) differences in size and time span of the atmospheric volume or grid cell represented by the forecast versus observations, that is, "sampling" differences, and 2) erroneous systematic errors in the forecast model.³¹ For these same reasons, an empirical humidity-cloud scheme developed originally for the purpose of inferring humidity estimates from observed cloud amounts for use in an objective humidity analysis, likely will not perform well when inverted to infer cloud amounts from humidity forecasts in a forecast model. The next and last previous diagnostic humidity-cloud scheme to be considered here, namely the NMC scheme, is such an example.

The NMC humidity-cloud scheme was first described in the NMC report by Chu and Barnhart, and later applied by ECMWF as described by Tibaldi.³⁷ This scheme consists of two

¹ Chu, R. and Barnhart, D. (1977) *Humidity analyses for operational prediction models at the National Meteorological Center*, NMC Office Note 140, National Meteorological Center, Washington, DC.

³⁷ Tibaldi, S. (1982) The ECMWF humidity analysis and its general impact on global forecasts and on the forecast in the Mediterranean area in particular, *Rivista di Meteorologia Aeronomica*, 42:309-328. (portion used in this report also available in the book *Atmospheric Water Vapor* (1980) Academic Press, ISBN 0-12-208440-3).

parts that respectively infer relative humidity in several vertical layers from a) observed present weather and b) observed layer cloud amount. In the former's usual application in objective humidity analysis, the observed quantities in parts (a) and (b) are taken from reported surface observations. In the application of part (b) of the scheme in the humidity analysis study by Norquist^{14, 25}, layer cloud amount was taken from the 3DNEPH analysis. As shown in Table 4, the resulting inferred humidity estimates yielded the smallest errors (notably small bias) among all three humidity level schemes tested by Norquist against collocated RAOBS. This hopeful result encouraged an attempt here to invert part (b) of the NMC scheme to infer cloud amounts from the GEM humidity forecast.

The NMC scheme is defined over four layers, roughly equivalent to a PBL layer and a low, middle, and high cloud layer. The four layers are specified (primarily) by the five levels below

$$\begin{aligned}
 P_1 &= P_s \text{ (surface pressure)} \\
 P_2 &= P_1 - 5 \text{ kPa} \\
 P_3 &= P_2 - 1/3(P_2 - P_1) \\
 P_4 &= P_3 - 1/3(P_3 - P_2) \\
 P_5 &= 30 \text{ kPa}
 \end{aligned}
 \tag{3}$$

At a given layer k , part (b) of the NMC scheme can be used to infer the humidity, RH_k , or cloud cover, CL_k , by

$$RH_k = M_k^{-1} [A_k + B_k(CL_k)^2 + C_k P_k]
 \tag{4}$$

In which RH_k and CL_k are respectively relative humidity and cloud cover in layer k . Figure 23 shows the four layers defined by the five levels above. The coefficients A_k , B_k , and C_k in the four layers in Table 4, following the usual convention, are defined by $CL_k=0$ and $CL_k=100$ in turn into the above equation. The coefficients A_k , B_k , and C_k are the overcast cloud cover, the overcast humidity, and the overcast temperature, respectively, also verified by inspection of Figure 23.

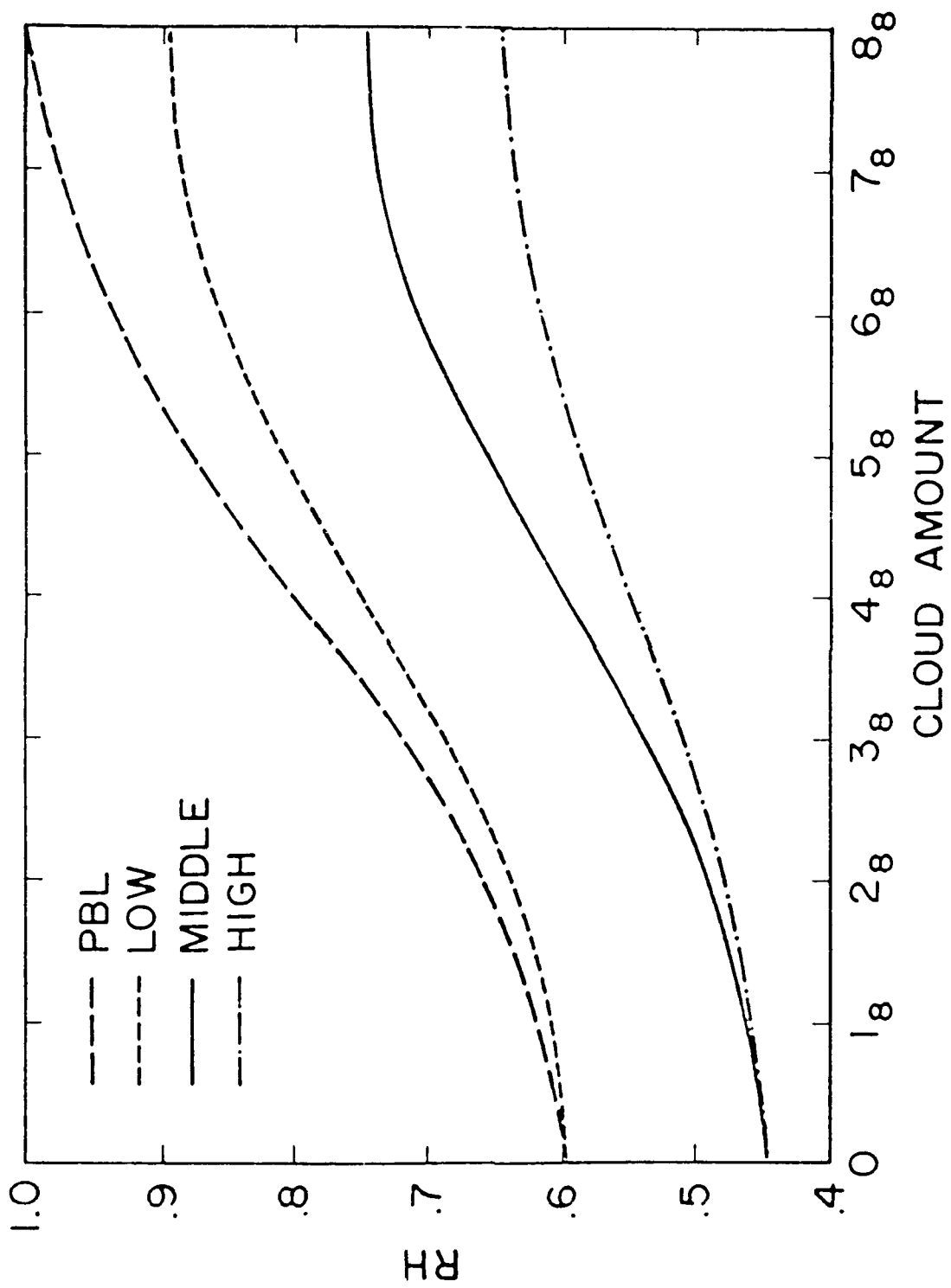


Figure 23. Curves of the NMC Humidity-cloud Conversion Scheme of Eq. (4) and Table 6 for the PBL, Low, Middle, and High Pressure Regimes of Eq. (3).

Table 6. Parameters of the NMC/Tibaldi Humidity-Cloud Scheme.

LAYER	LAYER INTERFACES FOR P*=101 kPa (kPa)	LEVELS OF APPLICATION IN GL GSM POST-PROCESSING (kPa)	$RHc_k = M_k - A_k$ $RHm_k = M_k + A_k$			
			M_k (%)	A_k (%)	RHc_k (%)	RHm_k (%)
PBL	101-96	100	80	20	60	100
Low	96-74	85	75	15	60	90
Middle	74-52	70	60	15	45	75
High	52-30	50,40,30	55	10	45	65

To apply Eq. (4) in the forecast context of the GSM cloud postprocessor, one must invert Eq. (4) and solve for CL_k as a function of RH_k , which yields

$$CL_k = (100/\pi) \{ \text{ARCCOS} [(M_k - RH_k)/A_k] \}, \quad (5)$$

$$M_k - A_k = RHc_k \leq RH_k \leq RHm_k = M_k + A_k$$

Since the function $\text{ARCCOS}(\alpha)$ is defined only for the argument range $-1 \leq \alpha \leq 1$, the input value of RH_k in the above is constrained to the given range. In practice then, we default to $CL_k=0$ when $RH_k < RHc_k$ and $CL_k=100$ when $RH_k > RHm_k$.

In the GSM application here, where we are constrained to operate with forecast RH on six mandatory pressure levels, we set $P_*=101$ kPa in Eq. (3). Table 6 shows the specific layer interfaces that result and the mandatory pressure levels that each layer spans. To implement this scheme in the cloud postprocessor, we chose to apply Eq. (5) for a given layer k to each mandatory pressure level spanned by that layer.

It is instructive to compare the NMC scheme with the previous AFGWC and ECMWF schemes. A review of Figures 8, 20, and 23 shows the NMC scheme is the only scheme that yields 100 percent cloud cover for $RH < 100$, that is, the only scheme in which RHm_k , the critical value for 100 percent overcast, satisfies $RHm_k < 100$. From a conceptual or intuitive view, this is not necessarily unreasonable, as cloud layers in the atmosphere are often quite thin and thus vertically "subgrid-scale" with respect to the larger layer thicknesses typical in forecast or objective analysis models. Equivalently stated, thin cloudy layers can be imbedded in thicker atmospheric layers whose vertically averaged RH is below 100 percent. However, the degree to which RHm_k falls below 100 percent in Table 6 is disturbingly large, especially for the middle and high layers. In this regard it is not surprising that in the results of the study by Norquist in Table 4, the bias of the humidities inferred from the NMC scheme is

negative (albeit modest) with respect to calibrated LADTs, as the humidities inferred at middle and upper levels from the NMC scheme will never exceed 75 and 65 percent respectively.

As a result of RH_{crit} = 100 in the NMC scheme, Figure 21 demonstrates that the critical humidities in the NMC scheme, though intermediate between those of the AFGWC and ECMWF schemes for the zero cloud threshold, become the lowest critical humidities as one considers larger cloud amount thresholds of say 30, 50, or 70 percent. Consequently, Section 3.2 will show that when applied to the USM RH forecast, the NMC scheme thus yields unacceptably large mean layer cloud amounts.

A second diagram, Figure 22, of the NMC scheme is shown in Figure 23 as the RH range over which the entire spectrum of cloud amount is covered, that is, the growing range of $RH_{crit} - RH_{crit} = RH_{crit} - RH_{crit}$ for cloud amount thresholds of 30, 50, and 75 percent, respectively. The growing interval occurs near the middle of the RH spectrum, and is centered about 75 percent. The narrow range of $RH_{crit} - RH_{crit}$ in the NMC scheme may be compared to that of the scheme as used as intended to date, which is the growing range of cloud amount forecast from following on forecast models and is centered on the middle of the growing RH range, thereby reflecting the relative insensitivity of cloud amount at the middle and ends of the humidity spectrum. However, in particular, for the lower RH values, as shown in Figure 14 (see above), the NMC scheme tends to extremes of the RH range. Section 3.2 shows that the cloud amount forecast standard forecast tends to shift, wherein all areas tend to be either cloud-free or saturated, as previously noted. ECMWF chose to use the ECMWF four-stage cloud scheme in its global forecast model,³ but chose to use the NMC four-stage cloud scheme in its global humidity analysis.⁴

This concludes the technical matter that the fundamental features of three previous diagnostic humidity schemes are fully represented in the two new schemes, in that the ECMWF scheme was chosen as the basis for the NMC scheme. The NMC scheme was developed for use in a predictive form, that is, for use in a model, and is used in both analysis and forecast applications. The NMC scheme is a four-stage scheme, with critical humidities which are both intermediate and intermediate to the AFGWC scheme, over which the full cloud amount spectrum is covered, and is centered about the middle of the RH spectrum, roughly as defined by the AFGWC scheme. Most importantly, none of the three new schemes is a four-stage scheme, as the NMC scheme is a four-stage scheme.

As a final point, it is noted that the NMC scheme is a four-stage scheme, as a function of NMC model forecast length, and is a four-stage scheme, as a function of the substantial spin-up characteristics of the NMC scheme, and is a four-stage scheme, as a function of sufficient temporal diffusion of the NMC scheme, and is a four-stage scheme, as a function of the ECMWF global model forecast length, and is a four-stage scheme, as a function of the

3.1.3 THE NEW GL DIAGNOSTIC CLOUD SCHEME

The disappointing performance of the previous diagnostic cloud schemes (demonstrated later in Section 3.2) led to the conclusion that a diagnostic humidity cloud scheme for a given forecast model must be developed specifically for that model. The development of the scheme must account for two major properties of the forecast model's humidity fields: a) the domain-mean humidity and b) the frequency distribution of humidity. In particular, Section 2.2 demonstrated that these two humidity properties (1) change significantly during a model spin-up period, (2) achieve by the end of the spin-up period fairly stable model-pertinent values that are largely independent of initial conditions, (3) vary with height, and (4) vary with geographic region (especially land versus ocean at low levels). The GL diagnostic cloud scheme here will be developed specifically for the baseline GL GSM and will explicitly account for factors (1)-(3) above. This new scheme can also account for the fourth factor, but the number of forecast cases available to this study was too limited to exercise this potential.

An instructive approach to describing the scheme is to review the unloading elements that led to its development. Of the *previous* cloud schemes, the ECMWF scheme will be shown to give the best (though still disappointing) cloud forecast results when used with the baseline GL GSM. This result led to a number of attempts to adjust or tune the ECMWF scheme. For this purpose, one can express Eq. (1) in a more general form as follows:

$$CL_k = \begin{cases} \frac{RH_k - RHc_k}{RHm_k - RHc_k}^{P_k} & , 0 \leq RHc_k \leq RH_k \leq RHm_k \leq 1 \end{cases} \quad (5)$$

where k is the level index, RHc_k and RHm_k are the zero-cloud and overcast cloud thresholds, and P_k is the exponent of nonlinearity (the special case of $P_k = 1$ yielding a linear curve). Eq. (5) serves to illustrate that there are at least four degrees of freedom or address in loading the cloud curves, namely, RHc_k , RHm_k , P_k , and k (vertical level). One can envision at least three degrees of freedom wherein P_k varies within the range of RHc_k to RHm_k (loading as in the changes in nonlinearity in Figure 8) and all parameters vary as a function of time (as well) in response to temporal changes in the statistical character of the forecast field.

The initial tuning attempts with the ECMWF scheme were of a mild, conservative, "tweaking" nature and aimed only at decreasing the RHc_k values in the ECMWF scheme to reduce the substantial negative bias in the cloud forecasts with that scheme. The GLSWC of two test verifications from one somewhat successful such trial are presented in Figure 2. This trial compares the RHc values for the original and "modified" ECMWF scheme. Other minor, essential and error modifications to the ECMWF scheme also tested changes to the P_k exponent in Eq. (6) (for example, $P_k = 1, 2.5, 4$), but without noteworthy success.

Table 7. Comparison of Critical Relative Humidity Values, RH_c, in Original and Modified ECMWF Humidity-Cloud Scheme (assume P* = 100 kPa).

P (kPa)	ECMWF ORIGINAL RH _c	ECMWF MODIFIED RH _c
30	0.73	0.65
40	0.61	0.55
50	0.50	0.50
70	0.44	0.40
85	0.61	0.55
100	1.00	0.85

Because the number of degrees of freedom in Eq. (6) is formidable, we sought objective approaches to specifying them. We were crucially aided here by the fact that the RTN_{EPH} is an objective, gridded, global 3-D cloud analysis database (as opposed to merely a satellite image or a zonal average cloud climatology). The key objective application here was to calculate and compare frequency distributions of 1) RH from the GSM forecasts and 2) layer cloud amounts from the verifying RTN_{EPH} cloud analysis. The top of Figure 24b shows as an example frequency distribution for the GL GSM RH forecast at 70 kPa over the NH octagon for the 24-hour forecast initialized from the AFGWC analysis of 00Z, 17 January 1985. The bottom of Figure 24b shows the corresponding *cumulative* frequency distribution of RH (that is, for a given RH value r , the percent frequency of RH values in the range $0 \leq \text{RH} \leq r$). The top of Figure 24a shows the cloud frequency distribution from the verifying RTN_{EPH} 70 kPa layer cloud analysis for the NH octagon. The bottom of Figure 24a shows the corresponding *cumulative* cloud frequency distribution. Both the RH and cloud distributions in Figure 24 were computed in terms of 101 categories at 1-percent intervals from 0 to 100.

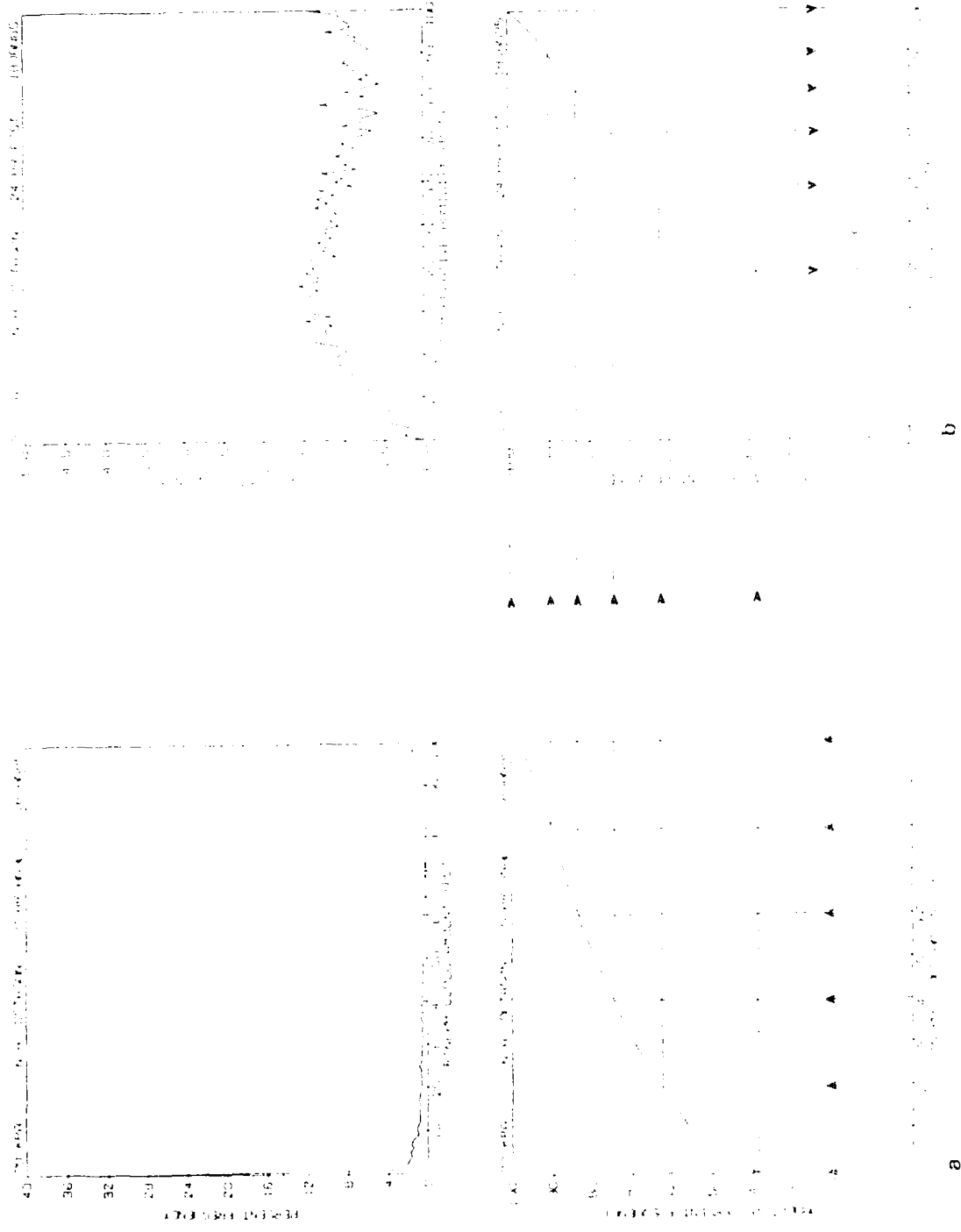


Figure 24. Category (top) and Cumulative (bottom) Frequency of Occurrence (at one percent intervals) of RTNeph Analyzed Cloud Amounts (Part a) and GSM 24-hour Forecast RH Amounts (Part b) at 70 kPa Over the NH Octagon. Valid at 00Z, 18 January 1985. At bottom, the one-to-one mapping of the RTNeph observed cloud frequency onto the GSM forecast RH frequency yields one of the GL humidity-cloud conversion curves (solid) in Figure 25a.

The first use of these RH and cloud frequency distributions at each level was to determine an appropriately tuned critical value of RHc_k , obtained objectively by "mapping" the value of the zero-cloud cumulative frequency to the same cumulative frequency value in the RH distribution, as illustrated by the lowermost horizontal directional arrow in Figure 24. A similar mapping of the cumulative frequency values for each 1-percent cloud interval onto the RH cumulative frequency yields a complete quasi-continuous empirical humidity-cloud curve relating the entire range of fractional cloud cover to an appropriate range of RHc_k to RHm_k -- a procedure that can be repeated level by level over the desired GSM forecast intervals. We shall henceforth call this procedure the GL humidity-cloud scheme.

Figure 25a shows the explicit 70 kPa RH-cloud curve (solid curve) that results from the mapping illustrated in the bottom of Figure 24. The dashed curve in Figure 25a shows the corresponding 70 kPa curve that results from the 24-hour GSM forecast (and verifying RTNEPH layer cloud analysis) initialized from the 00Z, 24 January 1985 AFGWC analysis. The dotted curve in Figure 25a shows the "aggregate" 24-hour 70 kPa RH-cloud curve that results from first combining the individual samples of the 70 kPa 17 and 24 January GSM 24-hour RH forecast and then verifying RTNEPH layer cloud analysis into a single aggregate sample, from which the requisite cumulative frequency distributions of RH and cloud is then computed. Figure 25b shows the corresponding three curves derived from the 24-hour GSM RH forecasts and layer RTNEPH cloud analyses at the 30 kPa level. As expected, the aggregate curves fall between the two separate curves for the individual forecast cases.

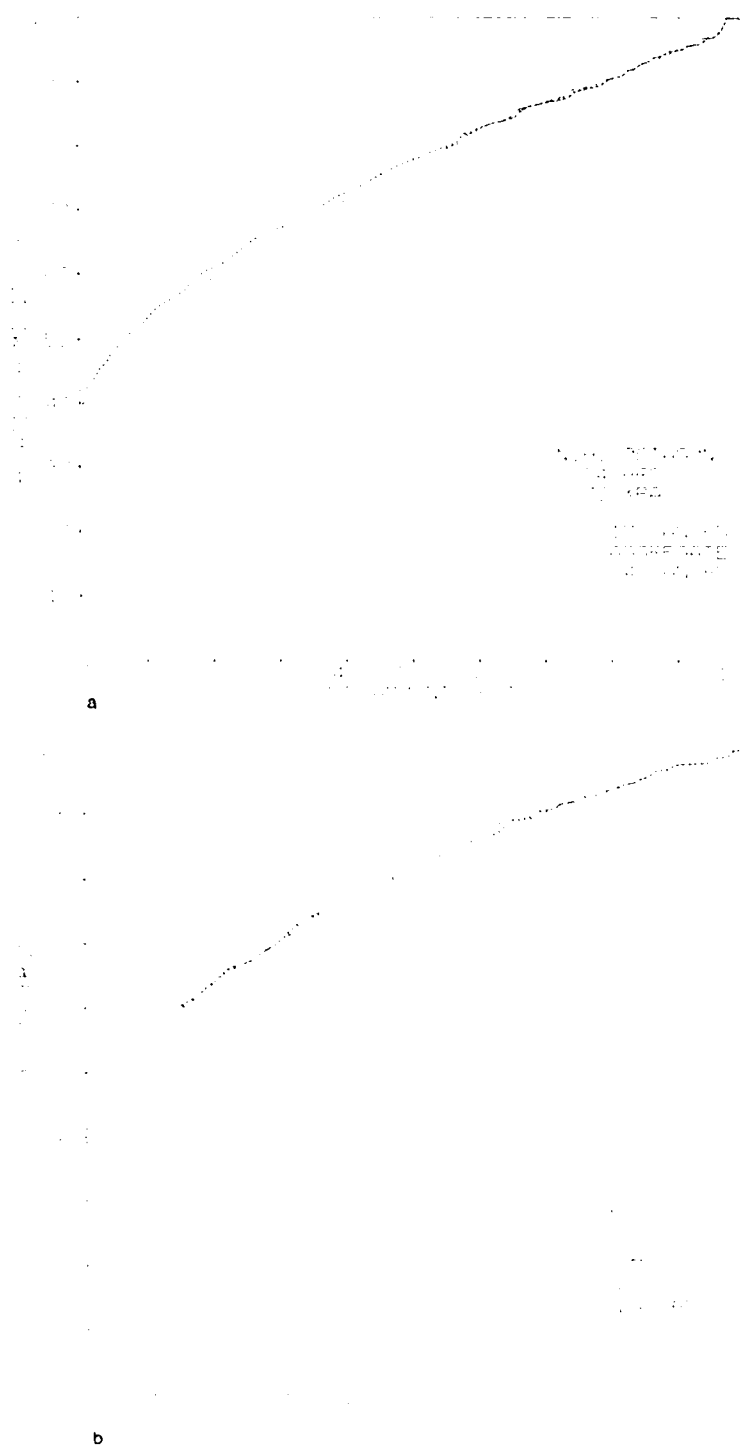


Figure 25. Curves of the GL Humidity-cloud Conversion Scheme Derived for the GSM 24-hour Forecasts at (a) 70 kPa and (b) 30 kPa by Applying the Methodology of Figure 24 to Two Separate Samples (and their aggregate) of the Frequency Distributions of GSM Forecast RH and RTNEPH Verifying Cloud Over the NH Octagon.

The important result of Figure 25 is the close similarity of the curves of the individual cases and the aggregate case. This indicates that, on a given level, and over a sufficiently horizontal domain (the octagon in this case), the relative frequency distributions of analyzed layer RTNEPH cloud amount and RTNEPH RH (for a fixed forecast length) remain essentially unchanged over the period of several weeks or so. This strongly suggests that, as operational practice, AFGWC could benefit from the use of cloud curves developed from frequency distributions of GSM forecast RH values and analyzed cloud gathered over a recent past time period (say the previous 3-4 weeks) and applying them to the GSM RH forecasts of the current period to obtain GSM cloud forecasts. This would involve *maintaining a running update (a week or more) of the forecast RH and analyzed cloud frequency distributions as part of its operational scheme*. AFGWC could maintain current *lookup tables* that automatically account for (1) actual seasonal changes in cloud frequency and (2) changes to the physics (and systematic errors) or resolution of the GSM or RTNEPH.

One notable refinement to the forecasting procedure presented in Figure 24 must be described. As a preliminary, we note in the lower half of Figure 24 that the zero-percent RH range occurs as frequently as the zero cloud category in the RTNEPH cloud distribution. Later results show this "zero-to-1" RH interval is never smaller than about 0.50 percent, at any level for forecasts beyond 12 hours. Given this, we sought to expand the resolution (or "microscope" the scale) of the RH range to enhance the sensitivity of the mapping of the frequencies of the non-zero cloud categories. To do this, we adopted the nonlinear transformation of RH to RH^* as introduced by Rasmussen³⁸ and given by

$$RH^* = 1 - (1 - RH)^2 \quad \text{OR} \quad RH = 1 - \sqrt{1 - RH^*} \quad (17)$$

Table 8 shows the values of RH^* corresponding to under a three parts of RH. At the extrema $RH=0$ and $RH=1$, we see that $RH^*=RH$ holds. In between the extrema, the transformation stretches the right end of the RH range and compresses the distance. For the above transformation to be most effective, the precision of the input RH value should be at least six significant digits, that is, preferably more than the three significant digits presently stored by AFGWC.

TABLE 2. Examples of Transformation $RH^* = 1 - (1 - RH)^2$.

RH	RH^*
1.0	1.0
0.90	0.68
0.80	0.55
0.70	0.45
0.60	0.37
0.50	0.29
0.40	0.23
0.30	0.16
0.20	0.11
0.10	0.05
0.00	0.00

In practice, the GSM forecast RH was converted to RH^* . Then the calculation of frequency distributions, mapping of those distributions, and resulting humidity-cloud curves were all defined in terms of RH^* . However, all related plots presented here in this study are depicted in terms of the normal RH, since the reader is hopefully more familiar with its range and since it makes it easier to compare with previous studies. In the case of the GL humidity-cloud scheme with the GSM, this study found the 12-h forecast skill scores to be slightly better using the curves derived from RH^* than using those derived from RH. Given only two forecast cases, this slight skill improvement may be fortuitous. Nevertheless, we proceeded to use RH^* routinely. All the GL RH-cloud curves presented in this report were derived using RH^* .

We next extend the examples of the GL cloud scheme to other forecast times and the remaining levels. The real value of the GL cloud scheme is its ability to respond and adjust to the GSM split-up period. By repeating the procedure of Figure 24 for the GSM RH frequency distribution valid for each GSM forecast interval (12-hourly here), one can derive RH-cloud curves that vary as a function of GSM forecast length. Figure 25 shows the 12-hourly 70 kPa and 30 kPa RH-cloud curves thus obtained. As expected, the biggest change occurs in the first 12 hours, but by 48-hours the curves have asymptotically approached a fairly constant temporal configuration. Marking the end of this asymptote is, interestingly, the early change in the 70 kPa curves in Figure 26a. The fact that the 30 kPa or nonlinearity of the curves, reflected by the substantial 0.05 increase in the 70 kPa RH frequency distribution (Figure 19) between the 12-hour and 48-hour forecast cases, is exceeded by only a modest 6% increase in the 30 kPa frequency distribution (Figure 18) between the 12-hour and 48-hour forecast cases. The RH value at 70 kPa increases 1.5 times between the 12-hour and 48-hour forecast cases. The change in the 30 kPa curves in Figure 26b is also due to the rapid increase in the RH value between the 12-hour and 48-hour forecast cases.

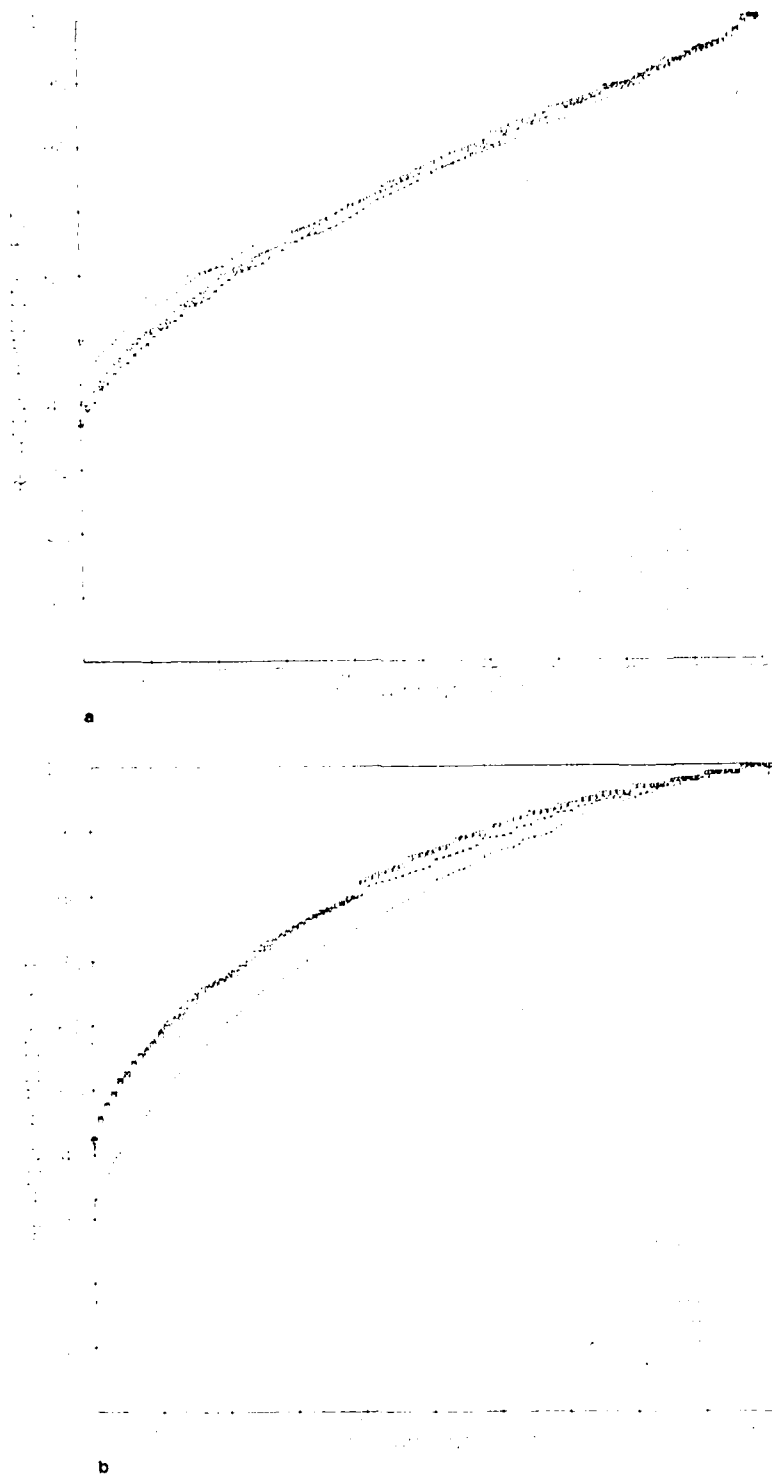


Figure 26. Curves of the GL Humidity-cloud Conversion Scheme as a Function of GSM Forecast Length for (a) 70 kPa and (b) 30 kPa Mandatory Pressures. (Curves based on the aggregate NH octagon GSM RH/RTNEPH cloud frequency distributions for the 00Z, 17 and 24 January 1985 GSM forecast cases).

Figure 26 offers a vivid demonstration of the GL humidity-cloud scheme adaptability to the temporal changes in the gross character of the GSM RH forecasts. As demonstrated in Section 3.2, a chief outcome of this adaptability is the capability of the GL scheme to provide short-range total cloud forecasts whose *octagon* domain-mean cloud amounts are substantially invariant in time during the GSM spin-up period and whose octagon bias with respect to the verifying RTNEPH total cloud analysis is small. (What total cloud bias there is enters from the vertical stacking algorithm of Appendix A, as the GL scheme effectively guarantees that the octagon domain-mean *layer* cloud forecast will have virtually zero bias against the RTNEPH. The occurrence of some total cloud bias prompted the vertical stacking experiments presented later in Section 3.2, as well as the variant of the GL cloud scheme described next.)

Figure 27 shows the GL RH-cloud curves obtained for the 0-hour and 48-hour GSM RH forecasts at all six moist mandatory levels. It must be reiterated here that this study utilized RTNEPH fields archived in the spatially compacted format of the 5LAYER grid (see Figure 7), that is, on the 1/2-mesh NH octagon grid at the vertical levels (layers) of 30, 50, 70, and 85 kPa and the gradient level. Thus to derive the GL RH-cloud curves for the GSM levels of 40 and 100 kPa in Fig. 27, we had to accept some mismatch between these two GSM output levels and the RTNEPH compacted (5LAYER) levels. As a compromise, we used the RTNEPH cloud frequency distributions at the gradient and 30 kPa levels to derive the 100 and 40 kPa GSM RH-cloud curves, respectively.

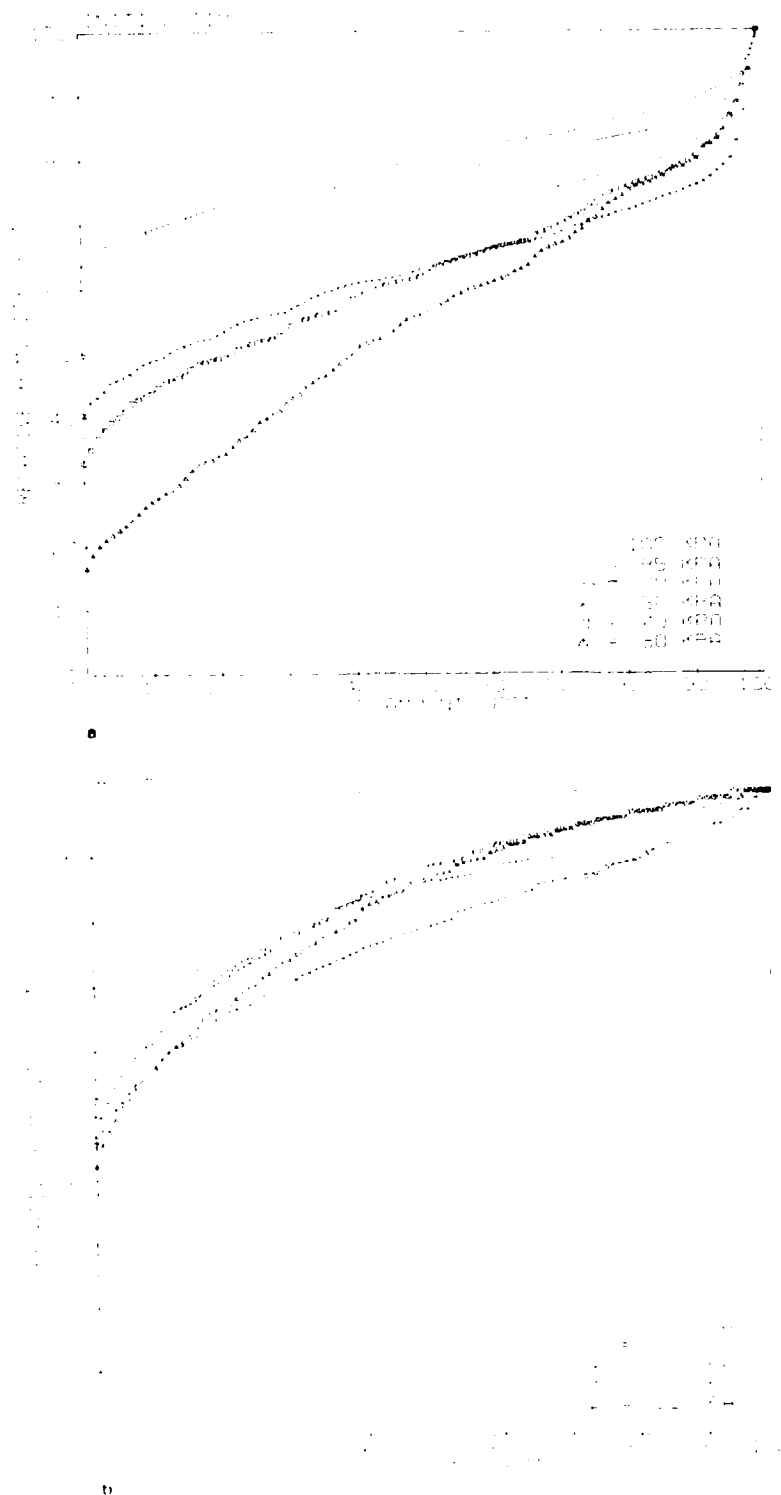


Figure 27. Curves of the GL Humidity-cloud Conversion Scheme as a Function of March 76 x Pressure for the GSM 0-hour and 48-hour Forecasts (based on aggregate sample as in Figure 26).

The above "pairings" dilemma was an unavoidable consequence of the structure of the data bases at our disposal. In a follow-on study, which would anticipate the development of RH cloud curves following the GL procedure, one would prefer to work with GSM RH forecasts directly on GSM σ -layers and

(1) ignore the lowest σ -layer (much too moist over oceans as cited in Section 2.2),

(2) group the remaining six moist GSM σ -layers into three pairs corresponding to low, middle, and high cloud layers,

(3) choose the maximum RH in each pair of σ -layers to represent the GSM RH forecast for the combined layer, and finally

(4) map the RH frequency distributions from these low, middle, and high GSM layers to the frequency distributions for low, middle, and high cloud layers obtained from a suitably matched vertical compaction of the original RTNEPH layers.

The modest real vertical resolution of the RTNEPH and the high vertical correlation of the RH forecasts of adjacent GSM layers (as shown in Section 2.2) does not encourage more than the three layers recommended here.

The present study could not follow the above procedure. Nevertheless, an appropriate rendition was pursued by developing a four-layer variant of the six curves in Figure 27. These four curves are given in Figure 28. The 50 and 70 kPa curves in Figure 28 are unchanged from those in Figure 27. The RH-cloud curve designated "high" in Figure 28 was developed by mapping the frequency distribution of the RTNEPH 30 kPa cloud analysis to the RH frequency distribution obtained by taking the maximum of the 30 and 40 kPa GSM RH forecast values at each grid point.

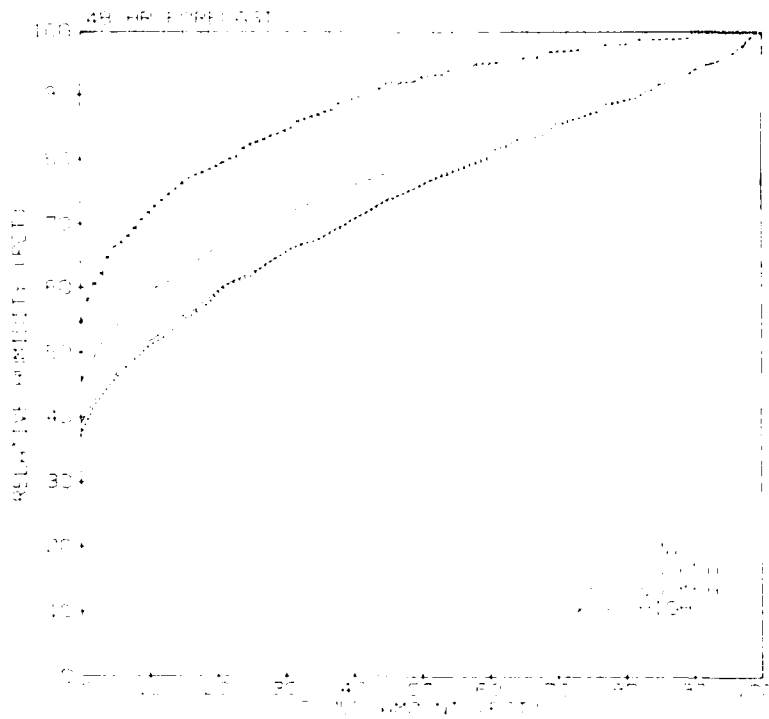
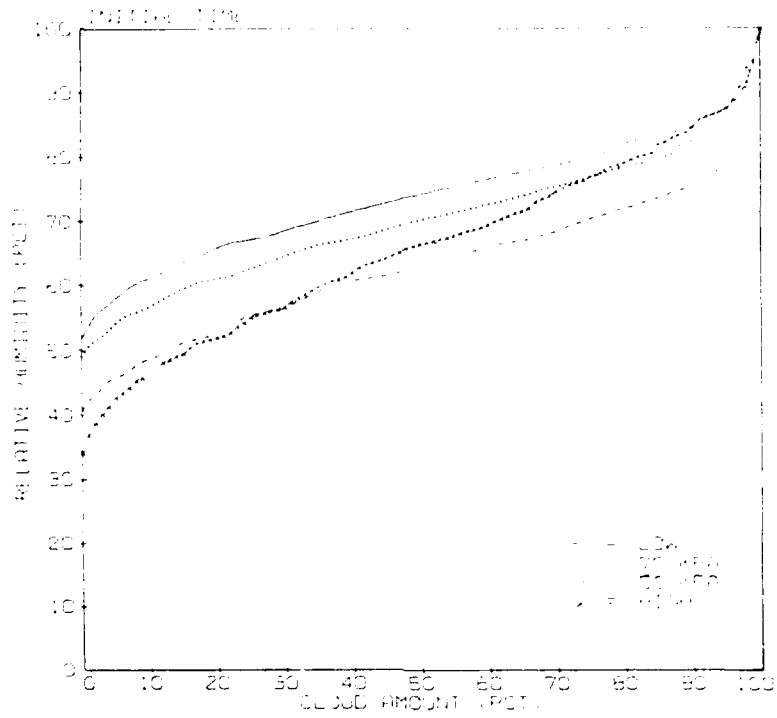


Figure 28. Curves of the Four-layer Version of the GL Humidity-cloud Conversion Scheme (see text) as a Function of Mandatory Pressure for the GSM 0-hour and 48-hour Forecasts (based on aggregate sample as in Figure 26).

The RH-cloud curve designated "low" in Figure 28 was developed by taking the maximum RTNEPH cloud amount of the gradient and 85 kPa levels at each grid point and mapping the resulting cloud distribution to the RH distribution of the 85 kPa GSM RH forecast. The 100 kPa GSM RH forecast is purposely ignored, because Figures 16 and 18 show it suffers from a severe moist bias over oceans. The vertical cloud stacking algorithm for the four-layer GL cloud scheme is described in Appendix A. The six-layer and four-layer GL cloud schemes will henceforth be designated as GL6 and GL4, sometimes with an additional subscript to denote a specific GSM forecast length in hours (for example, GL6₂₄ or GL4₂₄). The performance of both the GL6 and GL4 schemes will be examined in Section 3.2.

In concluding this section, it is useful to consider the GL humidity-cloud scheme as represented in Figure 27 in relation to the free parameters introduced earlier in presenting Eq. (6). Figure 27 (and its counterparts for the other GSM 12-hourly forecast times, not shown) explicitly specifies RHc_k and RHm_k (the latter always turns out to be 100 percent) as a function of level k and forecast length. Furthermore, the nonlinearity exponent, P_k , and its variation within the range $RHc_k - RHm_k$, though not explicitly obtained by the GL procedure, is nonetheless implicitly embodied in the specification of the GL curves; that is, in the six (GL6) or four (GL4) look-up tables defined for each desired GSM forecast length in terms of 101 one-percent cloud categories. Thus the GL scheme embraces all six degrees of freedom cited in the discussion following Eq. (6).

To conclude this section, we examine in Figures 21 and 22 the comparison of the GL RH-cloud scheme to the three previous diagnostic cloud schemes of Section 3.1.2. These figures show the GL6 scheme at the 24-hour forecast time (GL6₂₄), which is after the majority of the GSM spin-up is completed (at least on the extratropical octagon domain). The zero-cloud critical humidity profile of the GL scheme shows moderate values that do not vary drastically with height. These values lie between those of the AFGWC and ECMWF schemes and fairly closely follow the profile of NMC zero-cloud critical humidity values. Figure 22 shows that, in agreement with the AFGWC and ECMWF schemes (but unlike the NMC scheme), the overcast-cloud threshold of the GL6₂₄ scheme is $RHm_k=100$.

Rather interestingly in Figure 22, the overall shape of the GL6₂₄ curves is fairly similar to that of the ECMWF curves, and thus reasonably described by a quadratic function. Thus after the GSM spin-up at forecast times of 24 hours and beyond, the GL6 curves could be analytically approximated by Eq. (6) with $RHm_k=1$, $P_k=2$, and RHc_k as given for the GL6₂₄ scheme in Figure 21a (normalized by 100). Furthermore, it is interesting to compare the objectively derived values of RHc_k for the GL6₂₄ scheme in Figure 21a to the subjectively (trial and error) derived values of RHc_k for the "modified" ECMWF scheme in Table 7. The fixed analytical representation of Eq. (6) was not further pursued here for the GL schemes, as we wanted to tap the full capability of the GL schemes to adjust to the short-range GSM spin-up behavior.

3.2.2. Performance of Global Cloud Forecasts

The previous section examined and compared the formulations of six diagnostic cloud schemes denoted as the AFGWC, NMC, ECMWF, modified ECMWF, GL6, and GL4 schemes. This section examines the cloud forecast performance of these six schemes when applied to the humidity forecasts of the baseline GL GSM. The GSM results from these six schemes, respectively, shall be denoted in tables and figures as GSM/A, GSM/N, GSM/E, GSM/EM, GSM/GL6, and GSM/GL4. Cloud forecast performance will be examined quantitatively and subjectively for two NH winter GL GSM forecast cases -- namely, the GSM forecasts initialized from the operational AFGWC global analyses for 00Z, 17 January 1985 (designated Case I) and 00Z, 24 January 1985 (designated Case II). As a standard for comparison, this section also examines the cloud forecast performance of AFGWC's operational 5LAYER model for Cases I and II. An important background for the GSM cloud forecasts, Sections 2.1.2 and 2.2 earlier examined the corresponding relative humidity analyses and forecasts for Case I.

The quantitative performance of the GSM and 5LAYER total cloud forecasts (as well as RTNEPH persistence -- denoted PERS) are measured here following AFGWC operational practice; that is, by pointwise grid-to-grid verifications against the AFGWC operational RTNEPH total cloud analysis. This verification is performed on the 93 X 101 AFGWC NH 1/2-mesh octagon grid. This grid is 1) a one-to-one subset of the 129 X 129 1/2-mesh geographic output grid of the GSM cloud postprocessor (Section 3.1.1) and 2) the grid of the operational spatially compacted RTNEPH cloud analysis, produced by the spatial compaction step shown on the left of Figure 7.

More notably, this grid is also the operational grid of the 5LAYER model. We recall from Figure 7 that the compacted RTNEPH cloud analysis is identical to the 5LAYER 0-hour initial cloud fields (both layer and total). Hence by definition, the 0-hour 5LAYER cloud "forecast" verification scores will be perfect. Even beyond the 0-hour, one might argue that performing the verification directly on the 5LAYER grid will naturally favor 5LAYER over GSM forecasts. However, despite the area-averaging in the cited compaction step, the resolution of the compacted RTNEPH used for the verification is substantially higher than the 2.5° latitude/longitude output grid of the AFGWC GSM. Hence in considering the replacement of 5LAYER cloud forecasts with GSM cloud forecasts, one must demonstrate the GSM capability to perform the higher-resolution framework used to routinely assess 5LAYER skill. This is done in the subsequent steps of Section 3.1.1 included an interpolation of the compacted RTNEPH longitude grid to 1/2-mesh.

The cloud verification statistics obtained here will include 1) the bias in percent cloud cover and 2) accuracy as measured as the 20/20 score. This score is the traditional AFGWC cloud forecast accuracy score, defined as the percent of grid points where the forecast of cloud cover is within 20 percent or differ by less than 20 percent. A perfect 20/20 score is 100 percent. The bias and 20/20 score will be derived only for the total cloud forecasts, as the pointwise reliability of the verifying RTNEPH cloud

analysis is substantially better for total cloud than layer cloud. Both total and layer cloud forecasts will be examined here subjectively from example displays

All of the diagnostic cloud schemes detailed in Section 3.1 provide only layer cloud forecasts at the moist mandatory pressure levels of the GSM output. To obtain total cloud forecasts, the layer cloud forecasts are passed through a vertical stacking algorithm to obtain a total cloud amount. The vertical cloud stacking is described in detail in Appendix A. The reader is urged to review Appendix A, as several stacking issues will be addressed in this section.

We shall center the examination of cloud forecast performance on Tables 9 through 13. Table 9 shows the mean (area-averaged) total cloud amount as a function of forecast length in Case I for the NH octagon domain for ten GSM cloud schemes, plus the 5LAYER model and the verifying RTNEPH analysis. For Case I and Case II, respectively, Tables 10 and 11 show the total cloud forecast bias as a function of forecast length for the NH octagon and the regions denoted "U.S." and "Europe" in Figure 1 for the same ten GSM cloud schemes, plus the 5LAYER forecast and RTNEPH persistence.

Table 9. Mean Total Cloud Amount (percent) as a Function of Forecast Period Over the N.H. Octagon Domain for 00Z, 17 January 1985.

PERIOD CLOUD SCHEME	00-HR	12-HR	24-HR	36-HR	48-HR
Verification (RTNEPH)	48.0	50.2	45.1	47.0	42.7
Pers (RTNEPH)	48.0	48.0	48.0	48.0	48.0
5LAYER	48.0	47.4	46.0	43.1	41.6
GSM/A	58.8	74.4	79.9	77.5	78.2
GSM/N	59.6	71.4	74.3	72.8	73.0
GSM/E	19.5	32.8	32.7	31.2	31.6
GSM/EM	21.6	35.3	36.0	35.0	35.4
GSM/GL6	50.9	54.0	54.4	52.1	52.9
GSM/GL6A	55.2	57.9	58.1	56.0	56.6
GSM/GL6B	38.8	43.1	42.2	40.9	39.7
GSM/GL6C	43.8	47.6	46.5	45.3	43.8
GSM/GL4	44.5	46.9	46.8	44.6	43.1
GSM/GL4A	49.1	51.3	50.8	48.9	47.2

Table 10. Total Cloud Forecast BIAS (in Percent Cloud Cover) for 10 Global Spectral Model (GSM) Cloud Schemes, the 5LAYER Model, and RTNEPH Persistence for the 00Z, 17 January 1985 Case Over the Three Areas of (A) NH, (B) U.S., and (C) Europe.

(A) NH		BIAS			00Z, 17 January 1985	
PERIOD	00-HR	12-HR	24-HR	36-HR	48-HR	
CLOUD SCHEME						
Persistence	0.0	-2.3	2.2	0.8	4.1	
5LAYER	[0.0]	[-4.1]	[1.1]	-5.5	[-4.4]	
GSM/A	10.8	24.7	33.1	30.9	34.9	
GSM/N	11.7	21.4	28.1	25.8	30.3	
GSM/E	-28.5	-17.0	-13.4	-15.0	-10.1	
GSM/EM	-26.4	-14.4	-10.0	-11.2	-6.6	
GSM/GL6	[2.9]	[4.5]	8.3	5.7	9.9	
GSM/GL6A	7.2	8.4	12.1	9.7	14.2	
GSM/GL6B	-9.2	-6.6	[-4.0]	-5.5	[-1.2]	
GSM/GL6C	[-4.2]	[-2.0]	[0.3]	[-0.9]	[3.6]	
GSM/GL4	[-3.5]	[-2.5]	[0.6]	[-1.4]	[2.6]	
GSM/GL4A	[1.1]	[1.9]	[4.7]	[2.9]	7.3	
Percent of Timely Area	N/A	84	77	86	69	

Brackets denote values less than 5 percent in magnitude (Part A only).

Table 10. Total Cloud Forecast BIAS (in Percent Cloud Cover) for 10 Global Spectral Model (GSM) Cloud Schemes, the 5LAYER Model, and RTNEPH Persistence for the 00Z, 17 January 1985 Case Over the Three Areas of (A) NH, (B) U.S., and (C) Europe. (Continued).

(B) U.S.		BIAS				00Z, 17 January 1985
PERIOD	00-HR	12-HR	24-HR	36-HR	48-HR	
CLOUD SCHEME						
Persistence	0.0	-2.0	2.6	7.2	8.8	
5LAYER	0.0	-7.2	-5.5	-1.0	-6.7	
GSM/A	-4.0	14.7	22.0	31.8	31.3	
GSM/N	-2.0	12.3	18.0	26.9	27.5	
GSM/E	-40.0	-23.8	-19.6	-13.2	-10.1	
GSM/EM	-38.2	-21.3	-16.8	-9.2	-6.8	
GSM/GL6	-12.9	-2.7	-0.2	8.1	7.7	
GSM/GL6A	-8.7	1.0	3.3	12.1	11.5	
GSM/GL6B	-24.6	-14.7	-10.8	-3.5	-1.3	
GSM/GL6C	-19.7	-10.2	-6.8	1.1	3.0	
GSM/GL4	-17.2	-11.1	-7.5	-1.3	0.7	
GSM/GL4A	-12.8	-6.7	-3.8	3.1	4.7	
Percent of Timely Area	N/A	90	80	94	62	

Table 10. Total Cloud Forecast BIAS (in Percent Cloud Cover) for 10 Global Spectral Model (GSM) Cloud Schemes, the 5LAYER Model, and RTNEPH Persistence for the 00Z, 17 January 1985 Case Over the Three Areas of (A) NH, (B) U.S., and (C) Europe. (Continued).

(C) Europe		BIAS			00Z, 17 January 1985	
PERIOD	00-HR	12-HR	24-HR	36-HR	48-HR	
CLOUD SCHEME						
Persistence	0.0	-1.2	-3.0	-1.2	-0.2	
5LAYER	0.0	2.2	8.6	-2.8	2.3	
GSM/A	5.1	14.3	22.4	20.6	23.8	
GSM/N	5.0	9.6	18.9	15.8	17.7	
GSM/E	-37.6	-23.2	-17.6	-18.6	-18.1	
GSM/EM	-35.5	-20.8	-15.1	-15.0	-15.3	
GSM/GL6	-2.6	-4.6	-2.5	3.9	3.8	
GSM/GL6A	1.7	-1.3	1.7	0.1	0.4	
GSM/GL6B	-19.1	-14.2	-7.8	-9.7	-9.8	
GSM/GL6C	-13.6	-10.2	-3.1	-5.2	-5.1	
GSM/GL4	-13.9	-9.9	-3.7	-5.5	-5.9	
GSM/GL4A	-8.4	-5.9	0.7	-1.5	-1.3	
Percent of Timely Area	N/A	79	71	85	69	

Table 11. Total Cloud Forecast BIAS (in Percent Cloud Cover) for 10 Global Spectral Model (GSM) Cloud Schemes, the 5LAYER Model, and RTNEPH Persistence for the 00Z, 24 January 1985 Case Over the Three Areas of (A) NH, (B) U.S., and (C) Europe.

(A) NH		BIAS				00Z, 24 January 1985
PERIOD	00-HR	12-HR	24-HR	36-HR	48-HR	
CLOUD SCHEME						
Persistence	0.0	-3.7	-4.3	-4.9	-6.3	
5LAYER	[0.0]	[-4.2]	-7.4	-7.9	-9.8	
GSM/A	17.8	27.0	26.7	30.4	28.0	
GSM/N	18.1	24.3	22.6	26.0	24.0	
GSM/E	-22.6	-16.2	-17.2	-15.6	-14.9	
GSM/EM	-20.6	-13.6	-14.2	-11.8	-11.5	
GSM/GL6	10.4	5.8	[2.8]	5.5	[3.4]	
GSM/GL6A	14.5	10.2	6.8	9.8	7.4	
GSM/GL6B	[-2.3]	[-4.9]	-7.6	-5.1	-6.5	
GSM/GL6C	[2.6]	[0.2]	[-2.8]	[-0.3]	[-2.1]	
GSM/GL4	[3.6]	[0.0]	[-2.2]	[-1.5]	[-2.9]	
GSM/GL4A	8.0	[4.7]	[2.2]	[3.1]	[1.4]	
Percent of Timely Area	N/A	88	62	85	73	

Brackets denote values less than 5 percent in magnitude (Part A only).

Table 11. Total Cloud Forecast BIAS (in Percent Cloud Cover) for 10 Global Spectral Model (GSM) Cloud Schemes, the 5LAYER Model, and RTNEPH Persistence for the 00Z, 24 January 1985 Case Over the Three Areas of (A) NH, (B) U.S., and (C) Europe. (Continued).

(B) U.S.		BIAS				00Z, 24 January 1985
PERIOD	00-HR	12-HR	24-HR	36-HR	48-HR	
CLOUD SCHEME						
Persistence	0.0	-0.4	3.3	5.2	9.6	
5LAYER	0.0	-7.9	-6.5	-10.4	-7.5	
GSM/A	-5.1	10.2	17.8	24.5	27.5	
GSM/N	-5.9	6.6	15.6	20.1	21.8	
GSM/E	-43.9	-31.4	-21.2	-23.0	-18.4	
GSM/EM	-42.3	-29.0	-18.4	-19.0	-15.0	
GSM/GL6	-12.8	-11.2	-3.3	-1.3	2.8	
GSM/GL6A	-9.4	-7.3	1.1	3.1	6.7	
GSM/GL6B	-28.7	-21.4	-11.5	-12.0	-10.1	
GSM/GL6C	-24.3	-16.8	-6.7	-7.1	-6.0	
GSM/GL4	-19.5	-15.5	-6.3	-8.4	-6.3	
GSM/GL4A	-15.9	-11.1	-1.8	-3.7	-2.1	
Percent of Timely Area	N/A	98	76	99	87	

Table 11. Total Cloud Forecast BIAS (in Percent Cloud Cover) for 10 Global Spectral Model (GSM) Cloud Schemes, the 5LAYER Model, and RTNEPH Persistence for the 00Z, 24 January 1985 Case Over the Three Areas of (A) NH, (B) U.S., and (C) Europe. (Continued).

(C) Europe		BIAS				00Z, 24 January 1985
PERIOD	00-HR	12-HR	24-HR	36-HR	48-HR	
CLOUD SCHEME						
Persistence	0.0	-11.0	-6.1	-15.7	-12.1	
5LAYER	0.0	-3.6	5.2	-7.8	-3.8	
GSM/A	13.2	17.2	26.3	18.0	22.0	
GSM/N	14.4	14.0	23.4	14.2	18.8	
GSM/E	-25.1	-20.3	-10.9	-20.5	-14.8	
GSM/EM	-23.4	-18.1	-8.2	-17.7	-12.3	
GSM/GL6	5.1	-3.3	2.6	-6.8	-1.7	
GSM/GL6A	9.0	0.8	6.7	-2.6	2.0	
GSM/GL6B	-7.9	-10.2	-1.4	-10.5	-6.6	
GSM/GL6C	-2.9	-5.3	3.2	-6.0	-2.5	
GSM/GL4	-2.7	-6.6	1.4	-8.0	-4.2	
GSM/GL4A	1.9	-2.2	5.5	-3.6	-0.2	
Percent of Timely Area	N/A	78	63	78	75	

Table 12. Total Cloud Forecast 20/20 Accuracy Score (Percent of Grid Points Correct to Within 20 Percent Cloud Cover) for Ten Global Spectral Model (GSM) Cloud Schemes, the 5LAYER Model, and RTNEPH Persistence for the 00Z, 17 January 1985 Case Over the Three Areas of (A) U.S., (B) Europe, and (C) NH (See text for connotation of brackets, parentheses, and underscores). (Continued).

PERIOD CLOUD SCHEME	20/20 Score				00Z, 17 January 1985
	00-HR	12-HR	24-HR	36-HR	48-HR
Persistence	100.0	52.5	48.1	39.7	39.5
5LAYER	[100.0]	[62.4]	[54.9]	49.5	45.5
GSM/A	50.2	(55.9)	48.9	50.2	44.7
GSM/N	51.4	55.7	49.3	50.9	44.6
GSM/E	35.6	44.0	48.1	45.7	46.9
GSM/EM	36.1	45.9	49.3	46.3	47.3
GSM/GL6	54.6	52.0	<u>52.8</u>	<u>50.7</u>	<u>50.1</u>
GSM/GL6A	<u>57.2</u>	53.5	(53.5)	[51.0]	(50.9)
GSM/GL6B	49.3	50.7	48.8	47.8	50.0
GSM/GL6C	53.4	52.5	49.8	47.4	[51.0]
GSM/GL4	54.5	51.6	50.9	49.8	49.7
GSM/GL4A	(57.9)	<u>54.1</u>	50.6	49.4	50.1
Percent of Timely Area	N/A	79	71	85	69

Table 12. Total Cloud Forecast 20/20 Accuracy Score (Percent of Grid Points Correct to Within 20 Percent Cloud Cover) for Ten Global Spectral Model (GSM) Cloud Schemes, the 5LAYER Model, and RTNEPH Persistence for the 00Z, 17 January 1985 Case Over the Three Areas of (A) U.S., (B) Europe, and (C) NH (See text for connotation of brackets, parentheses, and underscores). (Continued).

(C) NH	20/20 Score			00Z, 17 January 1985	
PERIOD	00-HR	12-HR	24-HR	36-HR	48-HR
CLOUD SCHEME					
Persistence	100.0	54.8	52.3	47.4	47.7
5LAYER	[100.0]	[56.6]	(52.0)	[50.8]	(47.5)
GSM/A	41.4	45.2	39.0	40.4	38.0
GSM/N	42.5	44.7	39.8	42.4	37.5
GSM/E	38.6	45.9	[52.1]	<u>50.1</u>	[47.9]
GSM/EM	38.9	46.6	51.9	49.7	47.0
GSM/GL6	44.7	<u>49.1</u>	46.8	46.2	43.8
GSM/GL6A	45.8	49.3	46.8	46.2	43.7
GSM/GL6B	44.7	47.9	49.7	49.9	47.2
GSM/GL6C	46.4	48.7	49.8	50.1	47.0
GSM/GL4	<u>47.8</u>	<u>49.1</u>	<u>50.6</u>	(50.6)	<u>47.4</u>
GSM/GL4A	(49.0)	(49.7)	<u>49.9</u>	<u>50.0</u>	46.8
Percent of Timely Area	N/A	84	77	86	69

Table 13. Total Cloud Forecast 20/20 Accuracy Score (Percent of Grid Points Correct to Within 20 Percent Cloud Cover) for Ten Global Spectral Model (GSM) Cloud Schemes, the 5LAYER Model, and RTNEPH Persistence for the 00Z, 24 January 1985 Case Over the Three Areas of (A) U.S., (B) Europe, and (C) NH (See text for connotation of brackets, parentheses, and underscores).

(A) U.S.		20/20 Score			00Z, 24 January 1985	
PERIOD	00-HR	12-HR	24-HR	36-HR	48-HR	
CLOUD SCHEME						
Persistence	100.0	56.4	49.6	40.7	43.6	
5LAYER	[100.0]	[51.7]	<u>48.3</u>	(42.5)	42.7	
GSM/A	(49.6)	(46.4)	46.2	41.4	42.3	
GSM/N	<u>47.0</u>	45.7	46.3	41.3	41.6	
GSM/E	25.7	33.0	42.5	39.5	47.9	
GSM/EM	51.5	34.5	44.2	40.7	49.2	
GSM/GL6	45.0	43.3	46.3	41.8	45.7	
GSM/GL6A	46.2	<u>46.2</u>	<u>48.2</u>	42.3	44.9	
GSM/GL6B	39.4	38.6	47.9	42.4	[50.5]	
GSM/GL6C	41.6	42.4	[50.5]	[42.6]	<u>49.9</u>	
GSM/GL4	45.2	41.1	47.5	41.8	(50.0)	
GSM/GL4A	<u>46.6</u>	42.8	(50.0)	<u>42.2</u>	49.5	
Percent of Timely Area	N/A	98	76	99	87	

Table 13. Total Cloud Forecast 20/20 Accuracy Score (Percent of Grid Points Correct to Within 20 Percent Cloud Cover) for Ten Global Spectral Model (GSM) Cloud Schemes, the 5LAYER Model, and RTNEPH Persistence for the 00Z, 24 January 1985 Case Over the Three Areas of (A) U.S., (B) Europe, and (C) NH (See text for connotation of brackets, parentheses, and underscores). (Continued).

(B) Europe		20/20 Score			00Z, 24 January 1985	
PERIOD	00-HR	12-HR	24-HR	36-HR	48-HR	
CLOUD SCHEME						
Persistence	100.0	51.3	53.2	43.5	41.3	
5LAYER	[100.0]	(60.1)	<u>52.3</u>	46.3	[46.2]	
GSM/A	51.0	58.0	44.3	(53.0)	27.5	
GSM/N	49.3	58.5	46.8	[53.6]	(45.8)	
GSM/E	47.1	54.3	50.1	43.4	40.4	
GSM/EM	48.3	48.5	50.4	41.8	40.6	
GSM/GL6	52.7	[60.2]	[52.9]	50.7	44.8	
GSM/GL6A	53.3	<u>59.9</u>	<u>51.5</u>	<u>51.6</u>	<u>45.2</u>	
GSM/GL6B	56.0	57.0	51.3	48.4	42.7	
GSM/GL6C	56.2	58.2	50.3	49.6	42.9	
GSM/GL4	(57.2)	58.4	(52.4)	49.8	43.8	
GSM/GL4A	<u>56.6</u>	<u>58.8</u>	<u>51.4</u>	<u>51.5</u>	<u>44.5</u>	
Percent of Timely Area	N/A	78	63	78	75	

Table 13. Total Cloud Forecas: 20/20 Accuracy Score (Percent of Grid Points Correct to Within 20 Percent Cloud Cover) for Ten Global Spectral Model (GSM) Cloud Schemes, the 5LAYER Model, and RTNEPH Persistence for the 00Z, 24 January 1985 Case Over the Three Areas of (A) U.S., (B) Europe, and (C) NH (See text for connotation of brackets, parentheses, and underscores). (Continued).

(C) NH		20/20 Score			00Z, 24 January 1985	
PERIOD	00-HR	12-HR	24-HR	36-HR	48-HR	
CLOUD SCHEME						
Persistence	100.0	56.4	54.5	46.3	48.0	
5LAYER	[100.0]	[58.1]	[53.4]	[46.3]	44.7	
GSM/A	41.3	41.1	42.4	39.8	40.9	
GSM/N	41.1	41.4	42.8	40.3	40.3	
GSM/E	42.5	45.2	47.7	44.4	45.7	
GSM/EM	42.9	45.6	48.1	44.1	45.5	
GSM/GL6	44.4	47.7	<u>48.4</u>	42.3	43.8	
GSM/GL6A	45.4	47.7	48.0	42.2	43.7	
GSM/GL6B	46.1	48.2	<u>49.4</u>	44.6	(46.5)	
GSM/GL6C	47.3	<u>48.8</u>	(49.9)	<u>44.8</u>	[46.5]	
GSM/GL4	<u>48.7</u>	<u>48.6</u>	48.0	<u>45.1</u>	<u>46.4</u>	
GSM/GL4A	(49.1)	(48.9)	<u>48.1</u>	(45.2)	<u>46.2</u>	
Percent of Timeiy Area	N/A	88	62	85	73	

The cloud schemes designated GL6A, GL6B, GL6C, and GL4A in Tables 9-13 represent sensitivity tests of variations in the baseline vertical stacking algorithm (Appendix A) used in GL6 and GL4. In the schemes GL4A, GL6A, and GL6C, random vertical stacking was used (i.e. $R=1$ in layer Combinations I, II, and III of Appendix A), while scheme GL6B used the standard values of vertical stacking (that is, $0 \leq R \leq 1$ as given for layer Combinations I, II, and III in Appendix A). In the schemes GL6B and GL6C, the GSM layer cloud amounts at 100 kPa were set to zero. The motivation for these stacking experiments will be presented in Section 3.2.3.

Although the GSM forecasts were executed out to 96 hours, (for example, Figures 11 and 12), the verifications in Tables 10-13 were carried out to only 48 hours. The latter is the forecast length of the operational 5LAYER model in the NH, and therefore AFGWC archived RTNEPH verifying cloud analyses only out to 48 hours for this study.

To better show overall systematic trends, the calculation of mean total cloud amounts in Table 9 utilized every 1/2-mesh grid point in the NH octagon. Tables 10-13 on the other hand, focus on pointwise cloud forecast accuracy, particularly Tables 12-13. Hence the computations yielding the statistics of Tables 10-13 ignored grid points where the verifying RTNEPH cloud analysis was more than three hours old (for example, in surface data sparse regions between successive orbiting satellite passes). For this purpose, the RTNEPH database includes pointwise "time flags" indicating the timeliness of the analyzed cloud amount at each grid point.

Thus the sample of points verified within a given area differed somewhat over the various forecast times. However, for a given forecast time, all the cloud forecast schemes in the tables were verified at exactly the same sample of timely points. The percent of timely area is given in the Tables 10-13 to explain some of the temporal idiosyncrasies in the statistics.

We consider first the results in Table 9. Over an area as large as the NH octagon, a good cloud forecast scheme should exhibit a mean cloud amount that (1) is nearly constant over the entire forecast period (adjusts to the model's spin-up behavior in RH) and (2) agrees closely with the verifying mean cloud amount (negligible bias). The first criterion is justified by the RTNEPH mean cloud amounts at the top of Table 9, which show a quasi-constant mean cloud cover of about 47 percent, with 12-hourly deviations within about plus or minus 4 percent. The deviations in the bias of RTNEPH persistence over the NH octagon in Tables 10a and 11a, which represent two cases, also reflect small temporal changes in observed total cloud cover over a hemispheric domain. We shall view temporal deviations in forecast mean cloud cover over the octagon as acceptable if bounded by this observed variability of about 5 percent. The bracketed bias values in Tables 10A and 11A denote those instances in which forecast bias over the octagon was 5 percent or less. (The 5 percent bias threshold was not highlighted for the U.S. and European regions; because for a single forecast case over a limited area, diurnal variations or translating weather systems can affect the calculated bias irrespective of the model's systematic trend -- hence only substantially large biases are meaningful in the regional bias statistics in Tables 10-11.)

Turning to Tables 12-13, we have highlighted certain values of the 20/20 score in these tables. Scores in brackets and parentheses denote the first and second highest forecast model scores, respectively, for each forecast time. Underlined scores represent "honorable mentions"

to help identify cloud schemes that are consistently providing competitive scores, albeit not always the best scores. Bold persistence scores indicate when persistence beat all model forecasts. Also of note in Tables 12 and 13, we purposely first present and henceforth emphasize the U.S. and European regional 20/20 scores instead of the NH octagon scores. Though the scores for the GSM cloud schemes are admittedly less competitive over the octagon, here we justify the emphasis on regional comparisons for the following reasons:

- (1) the greater availability of surface reports to augment satellite data, thereby increasing the accuracy of the verifying RTNEPH,
- (2) the greater availability of RAOBs to correct the severe upper-level dry bias in the first-guess forecast used by the AFGWC moisture analysis over the octagon (Sec. 2.1),
- (3) the greater relevance of the chosen regions to the preponderance of Air Force operations.

The results of Tables 9-13 and example displays of cloud forecast fields will be assessed in detail in the following sections according to three groupings of forecasts: 5LAYER and RTNEPH persistence in Section 3.2.1, GSM using previous diagnostic cloud schemes in Section 3.2.2, and GSM using the GL cloud schemes in Section 3.2.3. As a starting point, we list below the major conclusions to be drawn from the tables and later cloud displays:

- (1) The margin of skill over persistence in both the 5LAYER and GSM cloud schemes is disappointingly small. The accuracy of persistence is rather hard to surpass at 24 hours or less. Even at 48 hours, the margin of GSM and 5LAYER forecast skill over persistence is lackluster. The small margin of 5LAYER and GSM skill over persistence was also seen in the nine winter forecast cases in the forerunner study by MW⁶.
- (2) The surprisingly low absolute accuracy of 5LAYER and GSM cloud forecasts at 24-48 hours, with 20/20 scores only in the range of 40-55 percent, despite the fact that the definition of the score allows a 20 percent cloud cover forecast error in a "hit" is another disappointment. Even at the short 12-hour range, accuracy scores much above 60 percent are rare. These low scores reflect the quasi-binary nature of the verifying cloud fields (either mostly clear or mostly cloudy), which increases the chances of large forecast busts.

(3) The 5LAYER forecasts:

(a) show an acceptably small but steady decrease in NH mean cloud amount over time and hence small but generally increasing negative biases; (b) show a consistent monotonic decrease in 20/20 score or accuracy with forecast time, but nevertheless exhibit the highest 12-hour accuracy scores and often the highest 24-hour accuracy scores; (c) compared to the GSM/GL4 scheme in the U.S. and European areas, exhibit 36- and 48-hour accuracy scores that are always lower in Case I and usually lower in Case II.

(4) The GSM forecasts using previous cloud schemes:

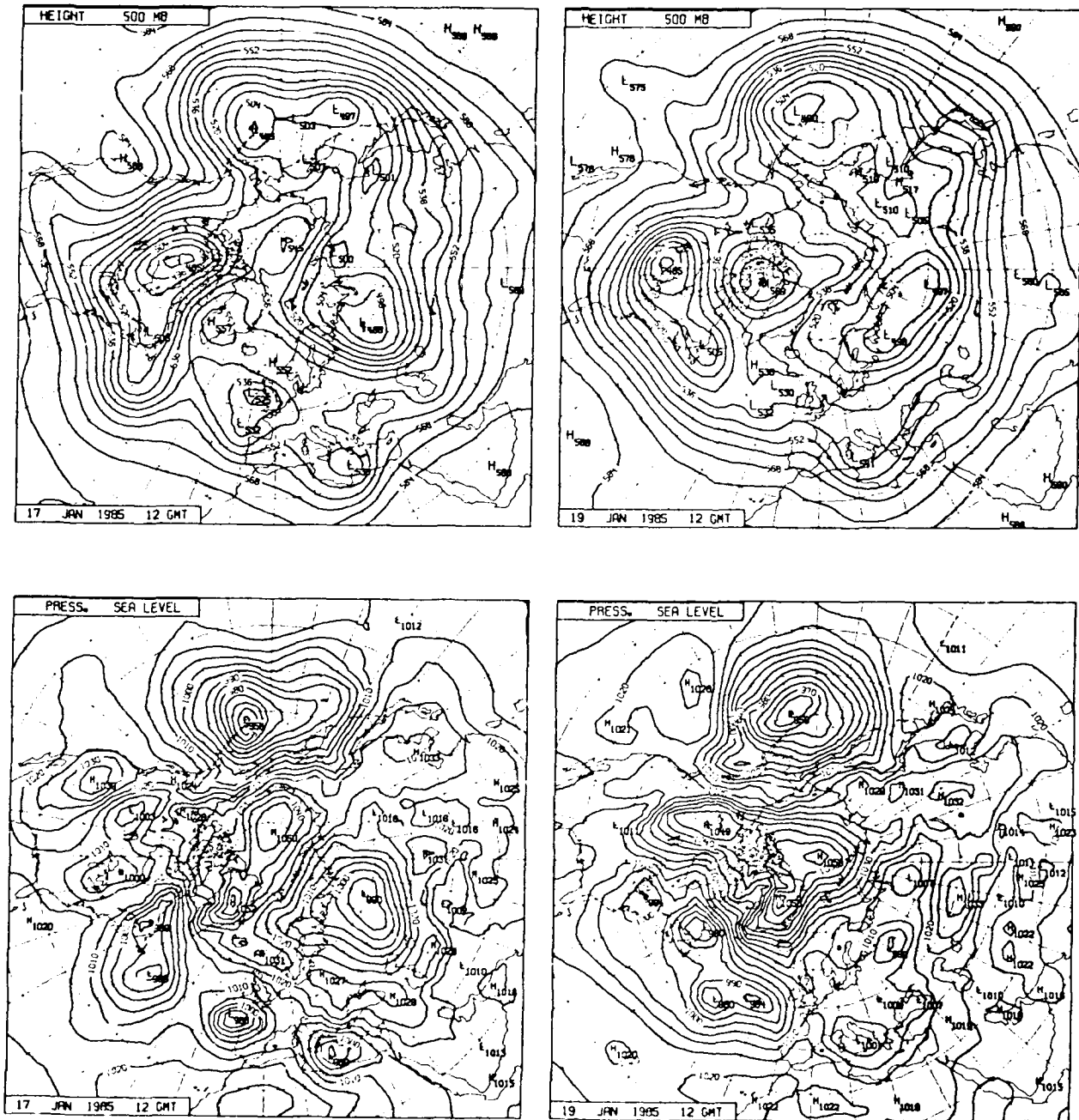
(a) show a very large spin-up (increase) in cloud amounts in the first 24 hours; (b) show unacceptably large positive or negative biases; (c) do not surpass either 5LAYER or GSM/GL schemes in accuracy with any consistency whatsoever.

(5) The GSM forecasts using the GL cloud schemes:

(a) in the case of the GL4 scheme, show strikingly negligible spin-up behavior, nearly steady NH mean cloud amounts, and small NH octagon biases (this despite the huge spin-up noted in Section 2.2 in the GSM upper-level RH forecasts); (b) in the case of the GL6 scheme, also show small spin-up behavior, but an unexpected nontrivial bias (positive) (The latter result prompted the cloud stacking experiments embodied in the GL6A, GL6B, and GL6C schemes); (c) consistently provide more accuracy at all times than the GSM forecasts using previous cloud schemes, and often surpass 5LAYER accuracy at 24 hours and beyond over the U.S. and European areas; (d) show such disappointingly low accuracy at the initial (0-hour) time that accuracy actually increases during the first 12, 24, or even 36 hours; (e) show rather impressive accuracy scores at 48 hours relative to 5LAYER in several instances.

In the following sections, we examine displays of the 5LAYER and GSM layer and total cloud fields over the NH for Case I. These forecasts will be compared to each other and to displays of the verifying RTNEPH cloud analyses. As our reference point, we begin by examining the latter analyses in Figure 30 (total cloud) and Figures 31 and 32 (layer cloud), which show the RTNEPH in Case I at basetime and 48 hours later. (The shading intensity key of Figure 1 applies to these and all later cloud displays.) To provide a further reference and an

aid in synoptic interpretation, we provide in Figure 29 the ECMWF operational 12Z analyses³² of the 50 kPa height field and sea-level pressure field at the 12- and 60-hour points of Case I.



a

b

Figure 29. The ECMWF Operational NH 12Z Analyses³² of the 50 kPa Height Field (top) and Sea-level Pressure Field (bottom) for (a) 17 January and (b) 19 January 1985.

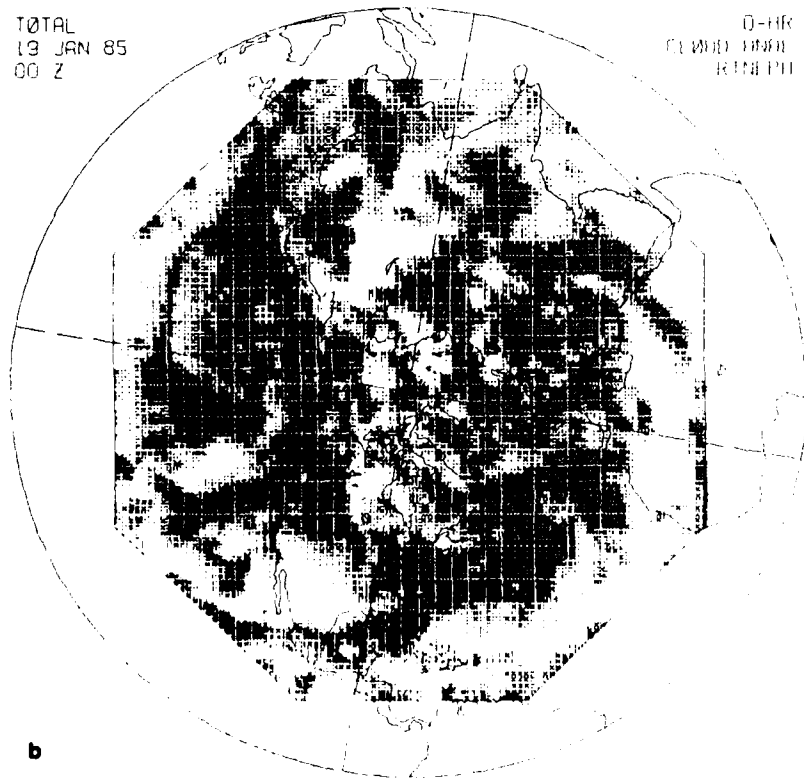
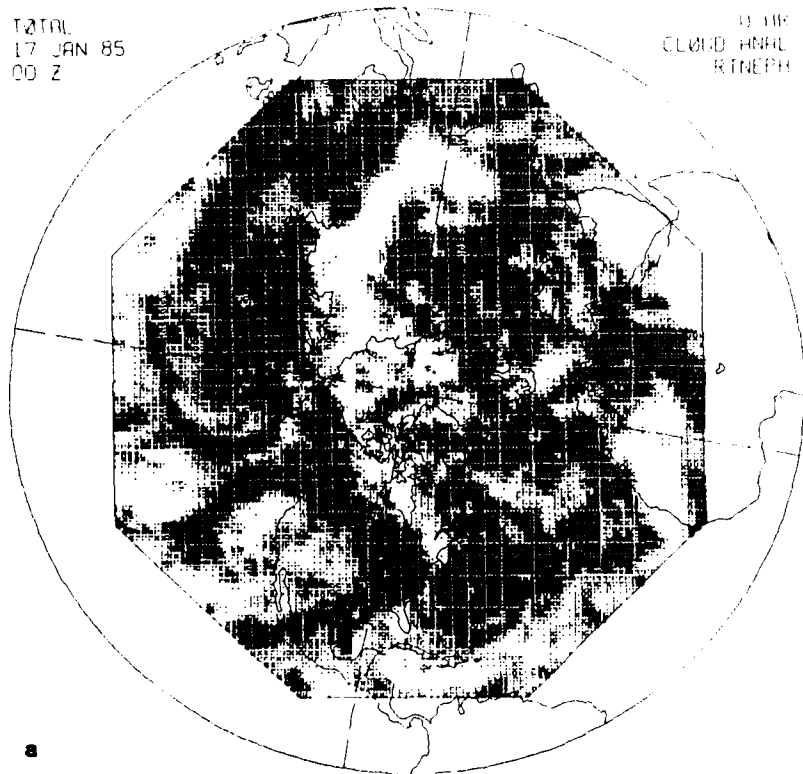
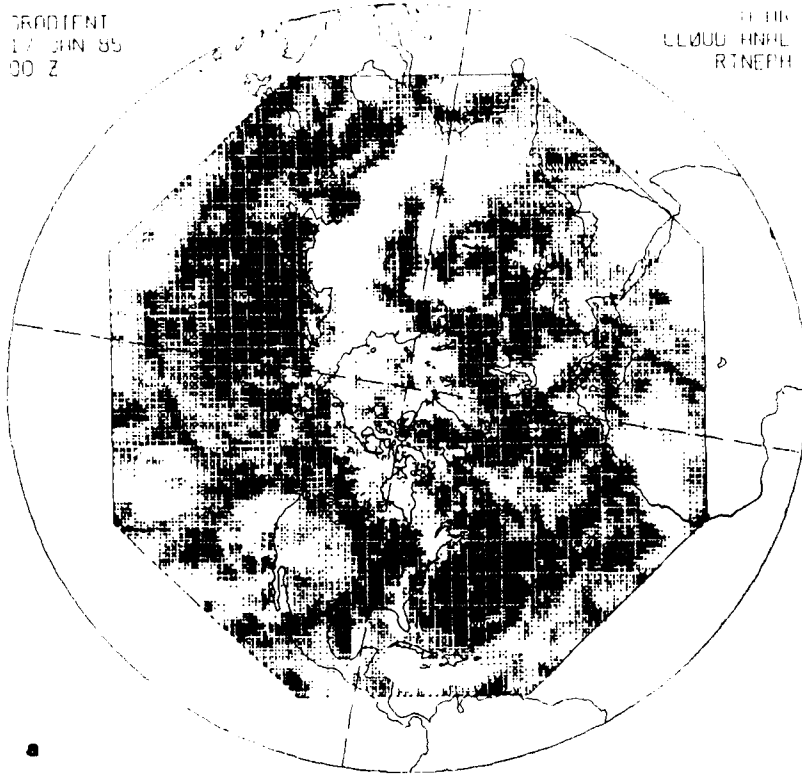


Figure 30. The RTNEPH 00Z Analysis of NH Octagon Total Cloud Amount for (a) 17 January and (b) 19 January 1985. (The shading key in Figure 1 applies to all shaded displays of cloud amount).

GRADIENT
17 JAN 85
00 Z

0-HR
CLOUD ANAL
RTNEPH



85 KPA
17 JAN 85
00 Z

0-HR
CLOUD ANAL
RTNEPH

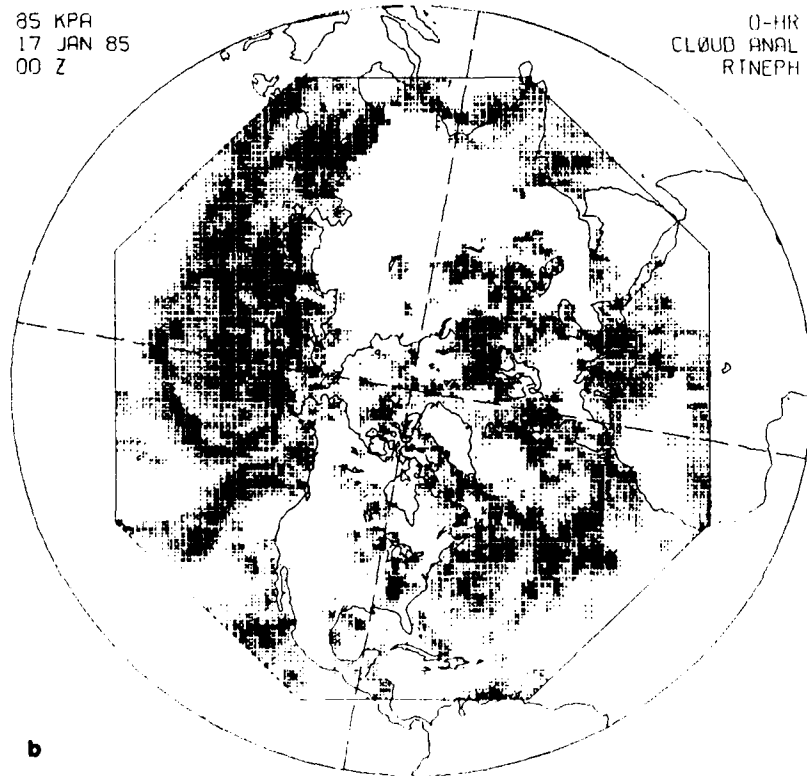
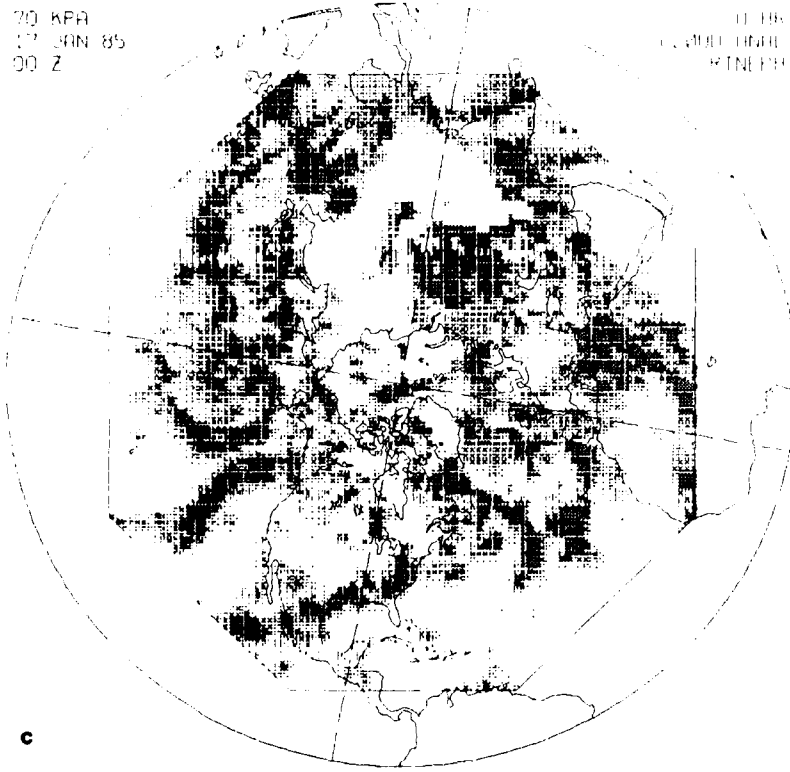


Figure 31. The RTNEPH 00Z Analysis of NH Octagon Layer Cloud Amount for 17 January 1985 for the (a) Gradient, (b) 85, (c) 70 and (d) 30 kPa Layers. (The shading key in Figure 1 applies to all shaded displays of cloud amount).

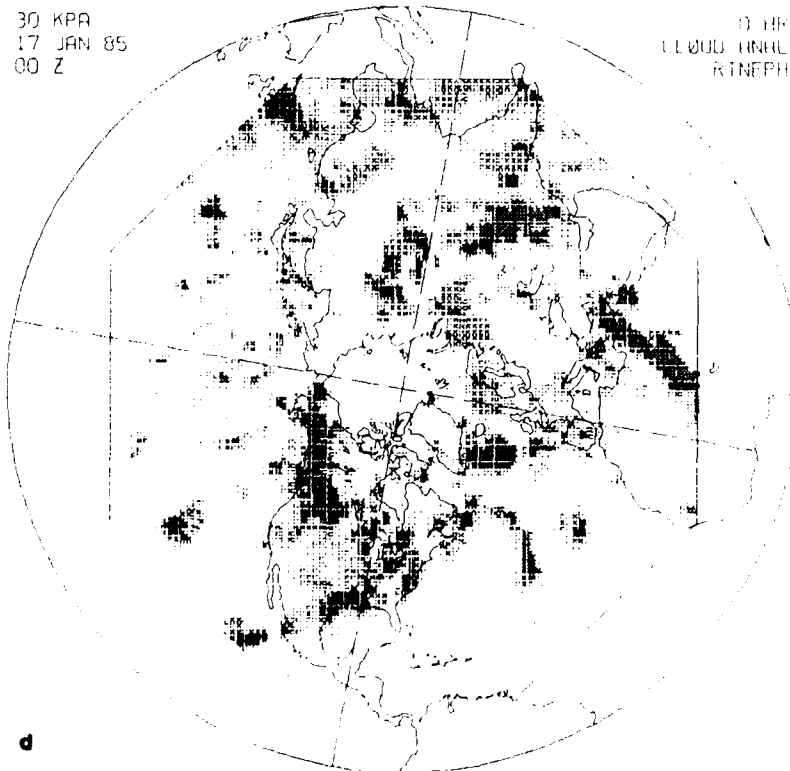
70 KPA
17 JAN 85
00 Z

0.10
CLOUD THICK
RTNEPH



30 KPA
17 JAN 85
00 Z

0.10
CLOUD THICK
RTNEPH



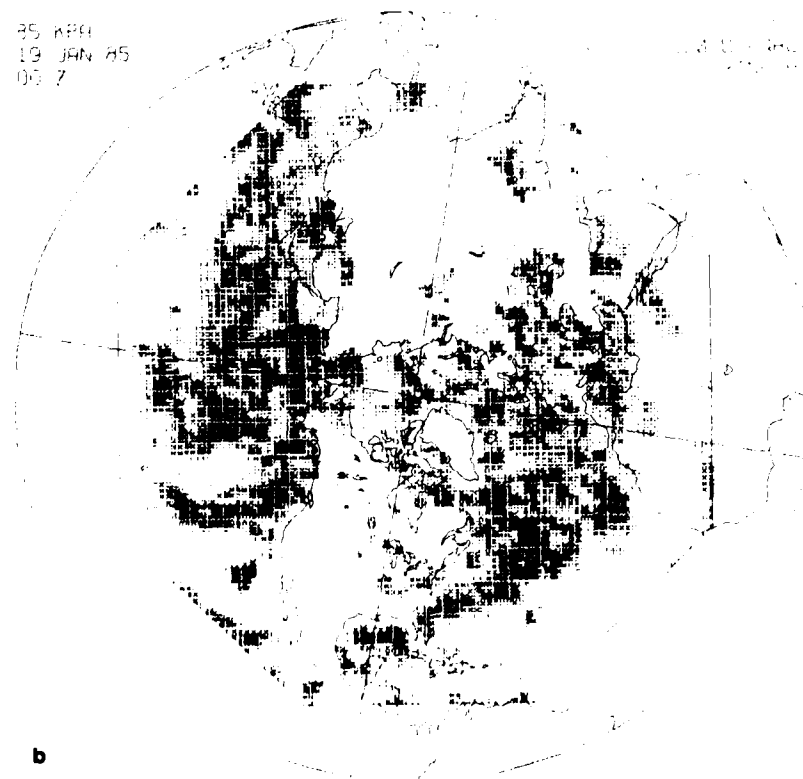
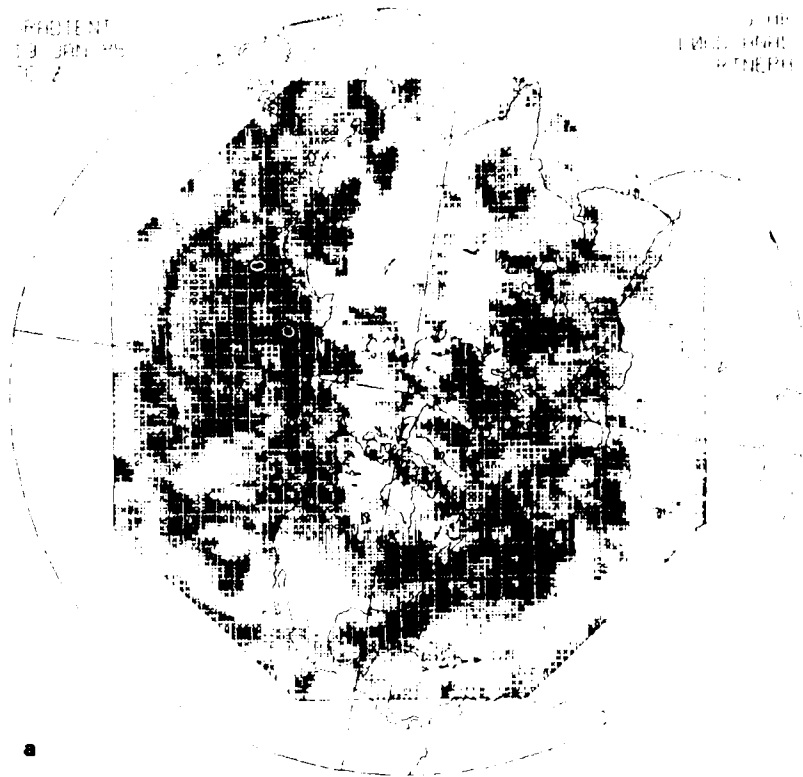
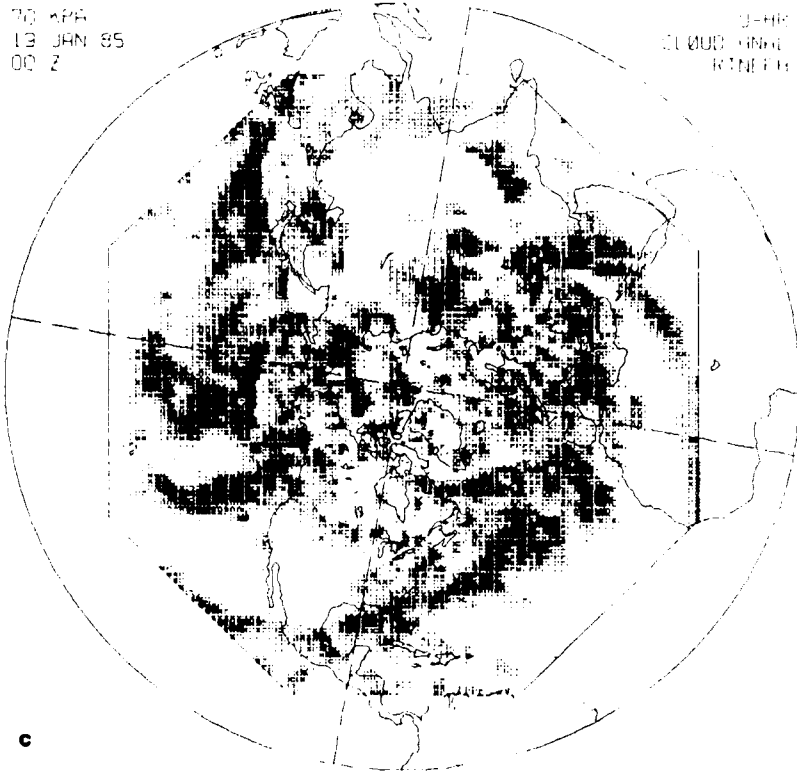


Figure 32. The RTNEPH 00Z Analysis of NH Octagon Layer Cloud Amount for 19 January 1985 for the (a) Gradient, (b) 85, (c) 70 and (d) 30 kPa Layers. (The shading key in Figure 1 applies to all shaded displays of cloud amount).

70 HPA
13 JAN 85
00 Z

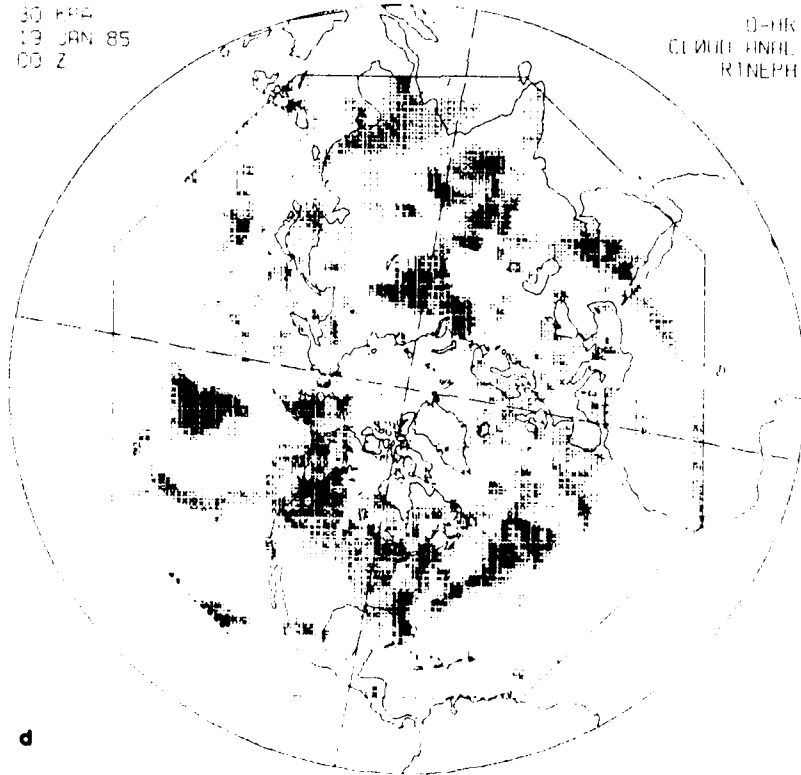
0-HR
CL WUEI ANFL
RTNEPH



c

30 HPA
13 JAN 85
00 Z

0-HR
CL WUEI ANFL
RTNEPH



d

The distinctive features of the total cloud analyses in Figure 30 are 1) the distinctive frontal bands in certain areas (such as, the eastern Pacific), 2) the persistent cloud-free character of the trade wind and desert areas of the subtropical Atlantic and Pacific, North Africa, and the southwest U.S., and 3) the preponderance of cloud over the extratropical oceans.

The foremost feature of the layer cloud analyses of Figures 31 and 32 is the significantly greater extent of cloud cover in the lower layers. (The RTNEPH analyses of cloud cover at 50 kPa, not shown, appear similar to the given 30 kPa analyses). This preponderance of low-level versus high-level cloud is observationally realistic and is a characteristic common to other cloud databases, as described in the study of Henderson-Sellers.³¹ Finally, Figures 31-32 show that the larger total cloud amounts over the oceans noted in Figure 30 stem largely from clouds in the lower layers. The overall dominance of low-level clouds in these RTNEPH analyses demonstrate that for a consistently good total cloud forecast, it is virtually essential to have a good low-level cloud forecast.

Following on this latter point, it is crucial to note that the vertical compaction (Figure 7) of the originally retrieved RTNEPH cloud layers to the five layers of the 5LAYER model includes, as a check, an application of the cloud stacking algorithm in Appendix A. This check is followed if necessary by an iterative adjustment of the compacted layer cloud amounts until the cloud stacking gives a total cloud amount that agrees within a few percent of the independently obtained RTNEPH 1/2-mesh total cloud amount.

The aforementioned study of Henderson-Sellers³¹ and the companion study of Hughes and Henderson-Sellers³⁰ examined the AFGWC cloud analyses of January and July 1979 from the 3DNEPH model²⁵ (the direct RTNEPH predecessor which used very similar cloud retrieval algorithms). These studies concluded that the 3DNEPH provides reliable cloud distributions agreeing with known features of the general circulation and other cloud databases, except for 1) some misrepresentation of cloud cover over the immediate polar regions (not included in the U.S. and European areas here), 2) somewhat underestimation of high clouds in general and stratus clouds at low levels over oceans, and 3) overestimation of clouds associated with the NH summer monsoon (not present in the NH winter cases considered here). Despite the above modest weaknesses, daily operational experience with the RTNEPH and its regular comparison with satellite cloud imagery at AFGWC show it to be vastly more accurate than the cloud model forecasts and hence a fundamental tool in the assessment of cloud model forecast accuracy.

3.2.1 PARALLEL 5LAYER MODEL FORECASTS

The cloud forecast fields of the AFGWC operational 5LAYER model valid at 48-hours in Case I are given in Figure 33 (total cloud) and Figure 34 (layer cloud). In AFGWC parlance, and strictly speaking, the 5LAYER forecasts in Figures 33 and 34 are 45-hour forecasts, because they represent the results of a quasi-Lagrangian temporal integration over 15 3-hour time steps starting from a nominal RTNEPH basetime of 03Z rather than 00Z on 17 January 1985. However, as justified below, these same 5LAYER forecasts can be viewed also as 48-hour

forecasts starting from a 00Z basetime, which is the view we chose to adopt for convenience in labeling the 5LAYER statistics in Tables 9-12. An understanding of this ambiguity reveals one of the two dominant factors leading to the clear superiority of 5LAYER over the GSM cloud schemes in 20/20 scores over the 0-12 or 0-24 hour periods in Tables 12-13.

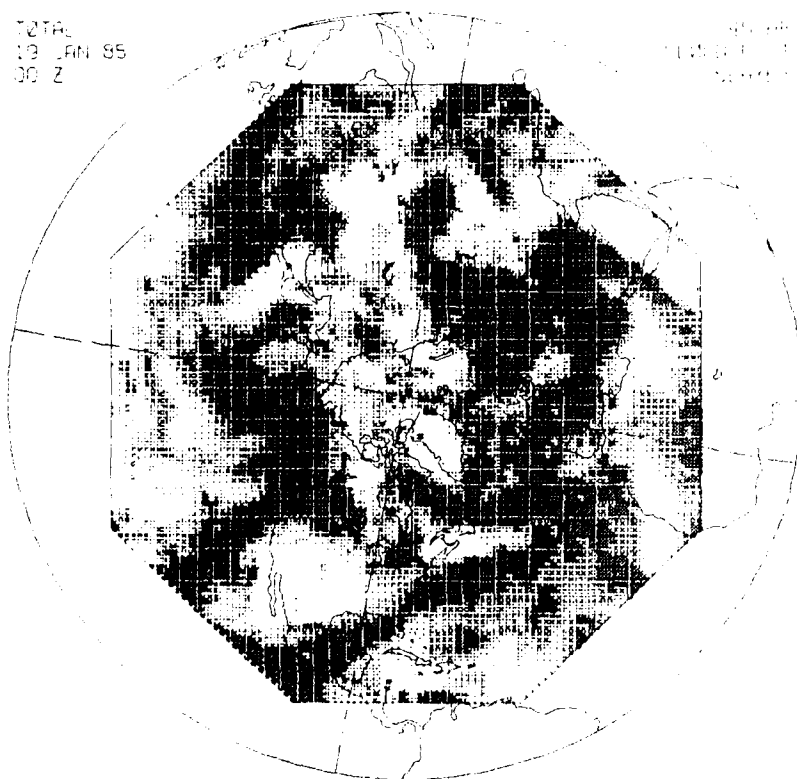
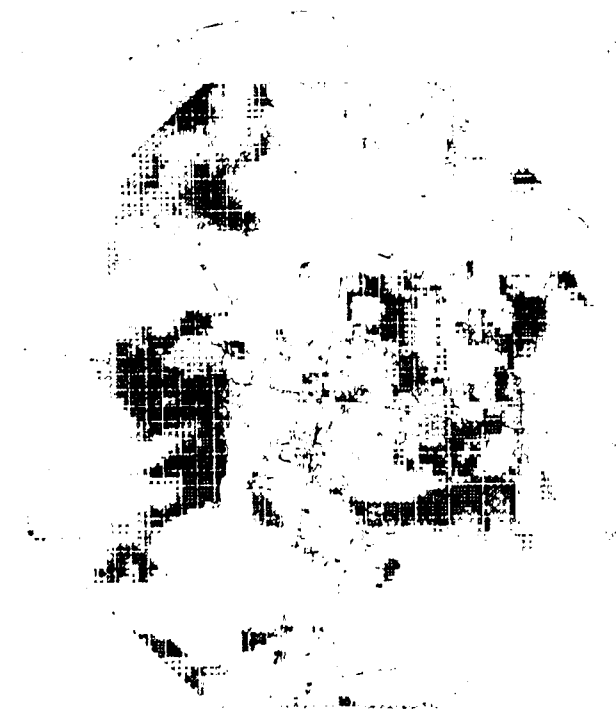


Figure 33. The 5LAYER 45-hour Forecast of NH Octagon Total Cloud Amount Valid at 00Z, 19 January 1985.



a



b

Figure 34. The 5LAYER 45-hour Forecast of NH Octagon Layer Cloud Amount valid at 00Z, 19 January 1985, for the (a) Gradient, (b) 85, (c) 70 and (d) 30 kPa Layers.



c



d

To sort out the ambiguity, recall from Section 1 that the 5LAYER model calculates its quasi-Lagrangian air parcel trajectories from the 3-D wind velocity forecasts of a previous execution of the AFGWC GSM. The AFGWC 48-hour GSM forecast, which is executed along with its predecessor HIRAS analysis on a 6-hourly cycle or four times daily, finishes at about 5 hours after basetime as depicted in Figures 4-7 of Stoble,² that is, 5 hours after 0, 6, 12, and 18Z. In contrast, the quasi-Lagrangian efficiency and quick execution of the 5LAYER model allows it to start by 2 hours after a given basetime and finish 1/2 hour later. Owing to the latter execution efficiency, the RTNEPH/5LAYER pair execute on a 3-hourly cycle, that is, finishing 2.5 hours after 0, 3, 6, 9, 12, 15, 18, and 21Z. Therefore, a new 03Z RTNEPH analysis is available and input to the first 5LAYER execution able to make use of the GSM wind forecast from 00Z. The official basetime given to this 5LAYER execution is 03Z -- the nominal time of the input RTNEPH, which is used in the manner of Figure 7 to directly initialize the 5LAYER initial CPS moisture field. However, the initial temperature field for the 03Z 5LAYER run is a persistence of the 00Z HIRAS temperature analysis used by the 00Z GSM. Finally, the octagon-wide time average of the RTNEPH point-wise time flags would typically yield a mean valid time of say 1-2 hours before 03Z. In summary then, the 45-hour forecast of the 03Z 5LAYER has used 1) a 48-hour GSM wind forecast from 00Z, 2) an initial temperature analysis of 00Z, and 3) an RTNEPH analysis valid in an area-mean sense somewhat before 03Z.

The key revelation of the above discussion is that owing to the quick execution time of the RTNEPH/5LAYER cycle (three hourly) relative to the HIRAS/GSM cycle (6-hourly), the 5LAYER run most closely parallel to a given GSM run is able to begin with initial moisture fields derived from an RTNEPH 6-hours more current than the RTNEPH, influencing the initial AFGWC moisture analyses used to initialize the GSM runs in this study. To see this, we recall from Section 2.1 that the first-guess moisture forecast for the 00Z AFGWC moisture analyses used in the 00Z GSM runs here was the 3-hour 5LAYER forecast from the 21Z RTNEPH analysis. Hence the one dominant factor in the superiority of 5LAYER short-range cloud forecasts versus the GSM is that its superior execution efficiency allows it to utilize a more current RTNEPH analysis. (Even if the 00Z RTNEPH were used directly as a pseudo moisture observation source in the 00Z HIRAS moisture analysis of today, the 06Z RTNEPH for the 06Z 5LAYER run would still be 6 hours more current than the 00Z RTNEPH input to the 00Z HIRAS. It is not until 11Z that the next 48-hour GSM forecast would be available from the 06Z GSM run.

Furthermore, as illustrated later in Section 3.2.2, an equally dominant factor in 5LAYER short-range superiority in this GSM comparison is the extremely direct and fairly high resolution processing route illustrated in Figure 7 from a 1/2-mesh RTNEPH layer cloud analysis to the initial 5LAYER layer CPS humidity field, and the counterpart short and direct inverse route from 5LAYER CPS forecasts to 1/2-mesh layer clouds. In the GSM case (recall Section 3.1 and see later in Section 3.2.2), this preprocessing/postprocessing circuit involves significantly more transformation steps, some occurring at resolutions worse than 1/2-mesh. In summary then, the paramount strengths of the 5LAYER model for short-range cloud forecasting (0-12 hours) are its direct and timely use of the RTNEPH cloud analysis in deriving its initial moisture field.

Surprisingly, this short-range advantage of 5LAYER is realized despite the pervasive upper-troposphere dry bias in the initial 5LAYER CPS fields -- a bias clearly demonstrated in Section 2.1.2 and arising from 1) the somewhat underestimated high cloud amounts in the RTNEPH and 2) the very low critical humidity values (RHc) implicit in the CPS curves (Figure 21). The answer to this crucial contradiction is that 5LAYER sustains its initial dry bias throughout the forecast. Thus, while any user retrieving 5LAYER's upper-level CPS humidity forecasts would find them very poor (much too dry) compared to RAOBs, the 5LAYER layer cloud forec. and hence total cloud forecasts remain satisfactory, because 5LAYER does not significantly moisten or dry any of its layers. Hence, because the same CPS curves with the same critical humidity values are applied in the inverse sense at forecast time to get layer clouds from forecast layer CPS, the resulting cloud amounts remain reasonable showing little bias with respect to the RTNEPH layer cloud amounts.

These latter observations are substantiated by the 5LAYER layer cloud forecast displays of Figure 34d, which show that while 5LAYER yields a more coherent frontal or banded structure than the RTNEPH analyses at the various levels, it does not show a significantly increased or decreased cloud amount over the domain as a whole. Similarly, the 5LAYER mean total cloud amounts in Table 9 and total cloud biases in Tables 10 and 11 show only a small decrease in total cloud cover with forecast time. Hence 5LAYER does not exhibit a large spin-up behavior, despite its dry upper-level initial state.

Although the decrease in 5LAYER total cloud cover over 48-hours is only 6.4 percent in Table 9, there are well-known physical reasons for this small drying tendency in 5LAYER. Specifically, the 5LAYER model includes precipitation processes in saturated ascending parcels as a moisture sink, but it ignores surface evaporation as a counterpart moisture source.⁴ At the precipitation-prone lower levels of 85 and 70 kPa, a comparison of the 5LAYER forecasts in Figures 34b and 34c with the RTNEPH analyses at those levels in Figures 32b and 32c suggests a small decrease in cloud amount at these levels during the 5LAYER forecast.

Overall, there is an impressive similarity in the character of the 5LAYER forecast total cloud field in Figure 33 and the verifying RTNEPH total cloud in Figure 30b. The sharp gradients in cloud amounts, the relative size of large synoptic patterns, the ragged appearance of cloud shield edges, and the location of persistently clear areas in the RTNEPH analysis are reproduced well by 5LAYER. Stated alternatively, the subjective impression imparted by the 5LAYER cloud displays is that the fractal character or geometry of the 5LAYER total cloud forecast agrees well with that of the RTNEPH analysis.

As a final point, a physical overlay of Figure 31b onto Figure 31a (say via transparencies) highlights the persistent nature of several large cloud-free and cloudy regions. This illustrates the difficult challenge of surpassing persistence skill in Tables 12-13.

3.2.2 PREVIOUS DIAGNOSTIC CLOUD SCHEMES

Tables 9-13 showed that cloud forecasts from the GSM using the previous diagnostic cloud schemes suffered from a large spin-up behavior of increasing cloud amounts, large biases, and generally lower accuracy scores. We will investigate example displays of these GSM total and

layer cloud forecasts in Case I to substantiate this behavior and illustrate important characteristics therein.

The fundamental basis for the above spin-up and bias behavior goes back to the central features of the GSM relative humidity forecasts documented in Section 2.2, which the reader is urged to review. The central feature was the rapid spin-up of the GSM RH forecasts by 48 hours to a distinct model preferred mean state -- a mean state by and large independent of the initial mean state of the input humidity analysis. This was clearly illustrated in Figures 11-14.

As a close corollary, the magnitude or degree of the spin-up will depend on how closely the mean state of the initial humidity analysis agrees with the model-preferred state. The latter also was strikingly demonstrated in Figures 11-14. For example, in Case I and II, the magnitude of GSM spin-up at the 30 and 40 kPa levels is notably large and reflects substantial moistening, because the AFGWC humidity analyses at these levels are much drier than the GSM-preferred humidity state (and drier than observations as well). In contrast, at 100 kPa, where the AFGWC RH analysis over the octagon agreed fairly well in a zonal mean sense with observations and two independent analyses (Figures 4, 5, and 12), the GSM 100 kPa RH forecast develops a large positive forecast bias over oceans, due to a systematic error in the parameterized physics of the surface fluxes and vertical diffusion of water vapor in the GSM (Section 2.2, Figures 17a and 18a).

Then as a second corollary, it follows that the model-preferred forecast mean humidity state may (1) not agree with the observed mean state and (2) not agree with the preferred mean state of a separate forecast model. Consequently, the previous diagnostic cloud schemes of GSM/A (AFGWC CPS curves of Figure 8 from the 5LAYER model) and GSM/E (the ECMWF curves of Figure 20 from the ECMWF model prior to May 1985), which were both developed for other models, or GSM/N (curves of Figure 23 used in the moisture analyses of first NMC and second ECMWF) which was developed for use with surface cloud observations in an objective analysis model, have strikingly different critical values of RH for the onset of various cloud amount thresholds (Figure 21).

Because the latter critical values were not tuned for the particular model-preferred humidity state of the GL baseline GSM here, their use with this GSM yields the large cloud amount biases given for these schemes in Tables 9-11. Lastly, these previous cloud schemes are fixed schemes, and thus they cannot adjust in forecast time for the large Case I and II spin-up in (1) mean RH amount (Figure 10 and bottom right of Figure 11) and (2) RH frequency distribution (Figure 19). Thus these previous schemes yield large temporal changes in forecast values of mean cloud amount (Table 9).

The cloud forecasts in Case I from the GSM/A scheme (Figure 8) are displayed for the 0- and 48-hour times in Figure 35 (total cloud) and Figures 36-37 (layer cloud). As shown by these displays, one advantage of the GSM over 5LAYER is the GSM's ability to provide fully hemispheric (or global) cloud forecasts, unlike the octagon domain limitation of 5LAYER in Figures 33 and 34. However, we limit our assessment of GSM cloud forecast quality to the octagon, as that is the domain limit of the verifying compacted RTNEPH analyses in Figures 30-32. In Figures 36 and 37, and all later GSM layer cloud forecast displays, for brevity we show only four of the six output mandatory pressure levels, as the 50 and 40 kPa

cloud fields appear very similar to the 70 and 30 kPa fields, respectively, especially at 48 hours (for example, compare the 70 and 50 kPa levels and the 40 and 30 kPa levels in the GSM RH displays of Figure 18).

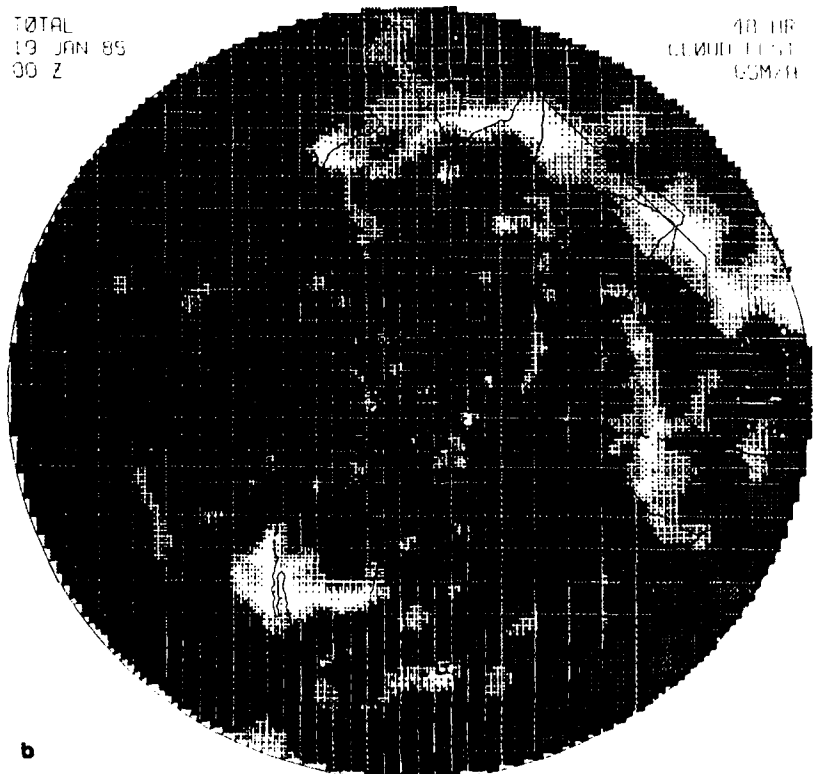
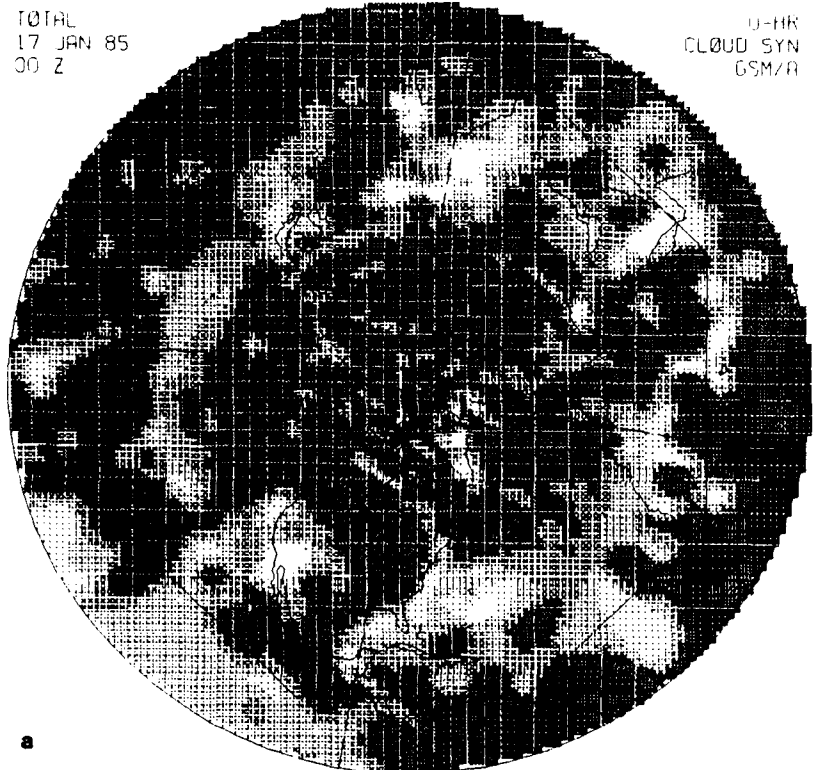
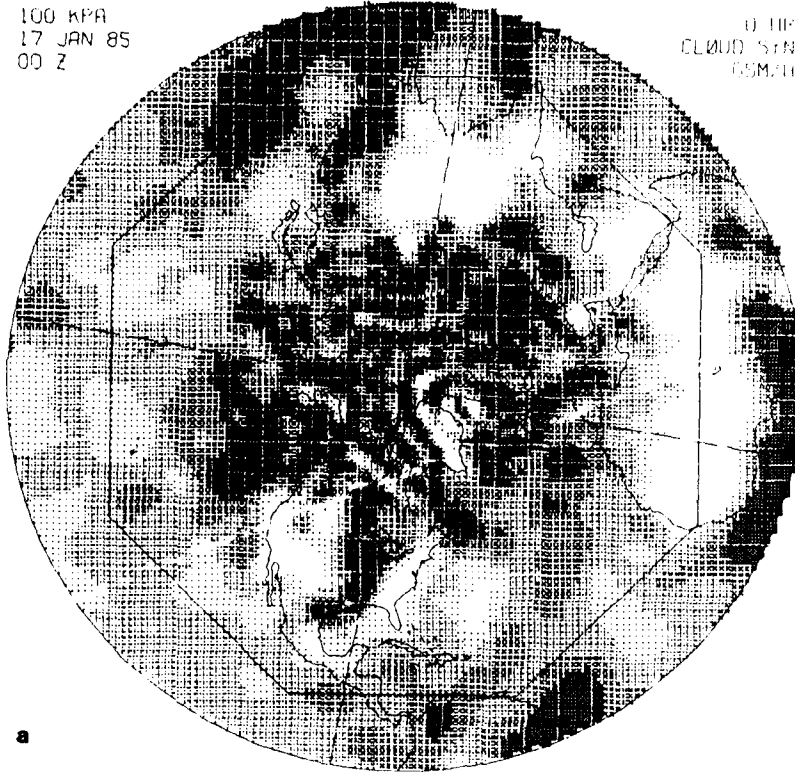


Figure 35. For the AFGWC Cloud Scheme, the GSM (a) 0-hour and (b) 48-hour Forecast of NH Total Cloud Amount Valid at 00Z on 17 and 19 January 1985, Respectively.

100 KPA
17 JAN 85
00 Z

0 HR
CLOUD SYN
GSM/11



85 KPA
17 JAN 85
00 Z

0 HR
CLOUD SYN
GSM/11

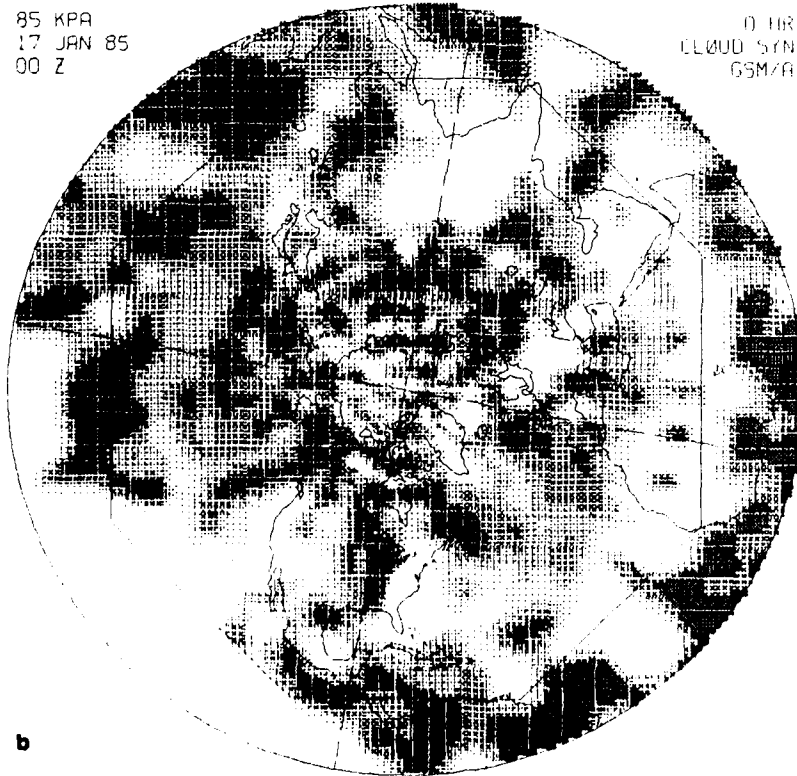
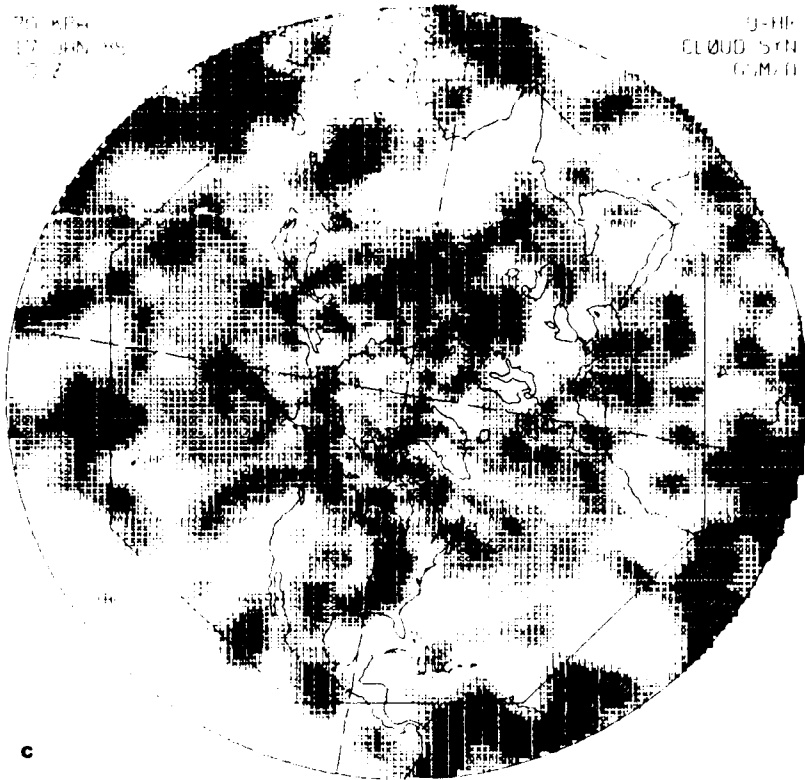


Figure 36. For the AFGWC Cloud Scheme, the GSM 0-hour Forecast of NH Layer Cloud Amount Valid at 00Z on 17 January 1985 for Layers Nominally Centered at the (a) 100, (b) 85, (c) 70 and (d) 30 kPa Pressure Levels.

700 MB
17 JUN 85
07Z

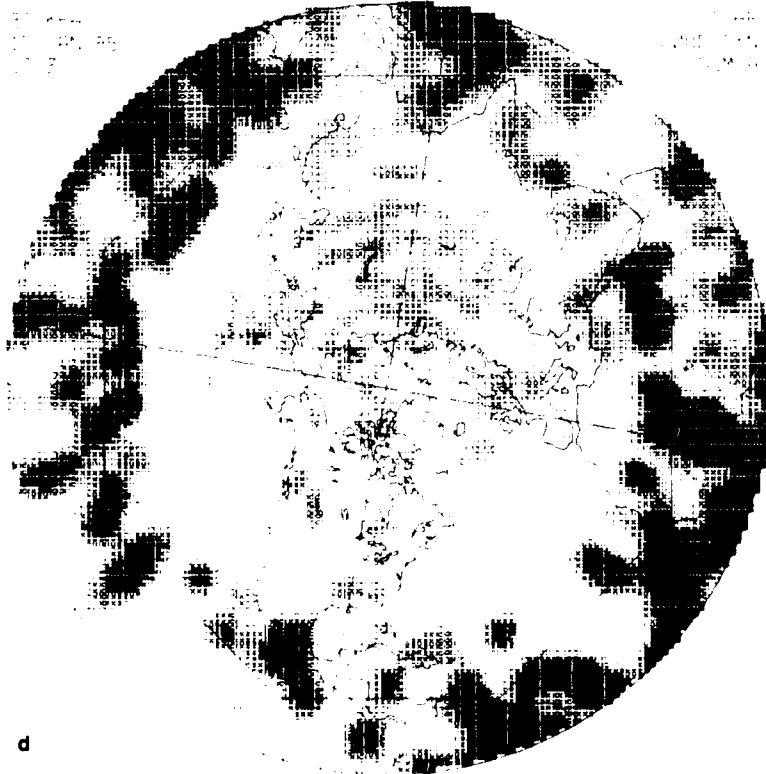
3-HP
CLOUD SYN
G.M.T.



c

700 MB
17 JUN 85
07Z

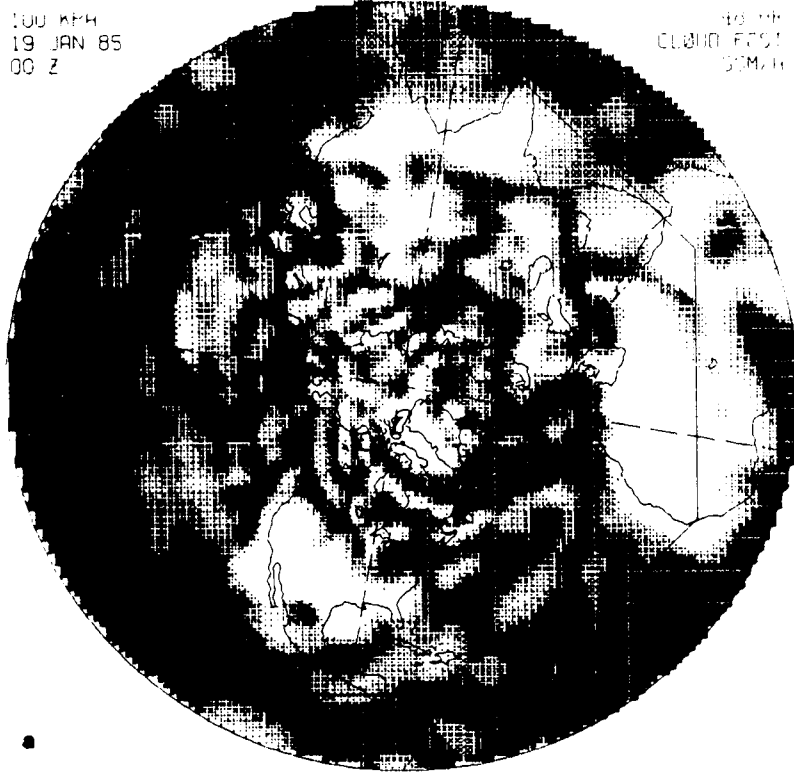
3-HP
CLOUD SYN
G.M.T.



d

100 KPA
19 JAN 85
00 Z

48 HR
CLOUD FST
GSM/4



85 KPA
19 JAN 85
00 Z

48 HR
CLOUD FST
GSM/4

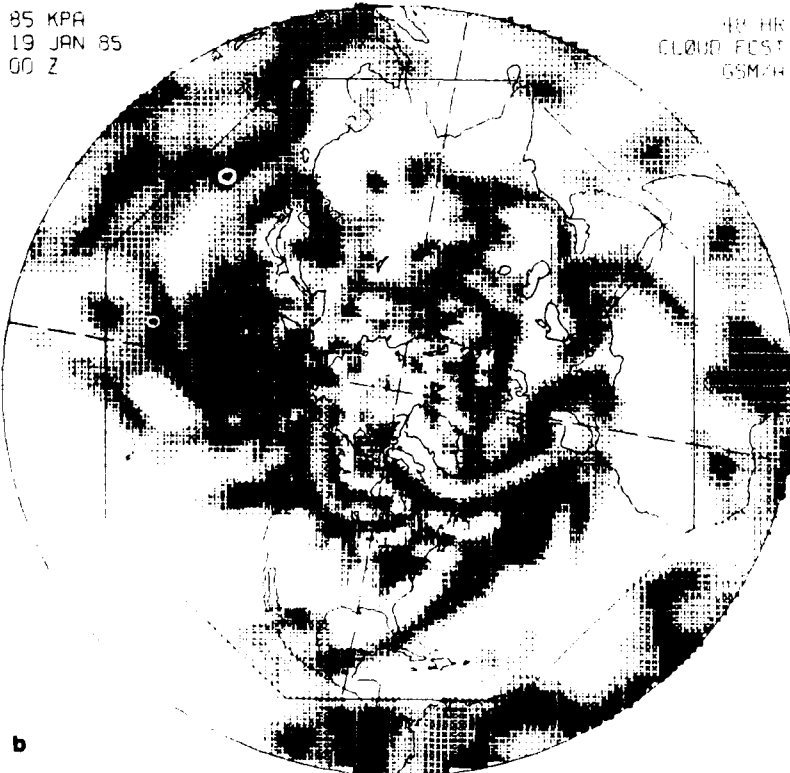
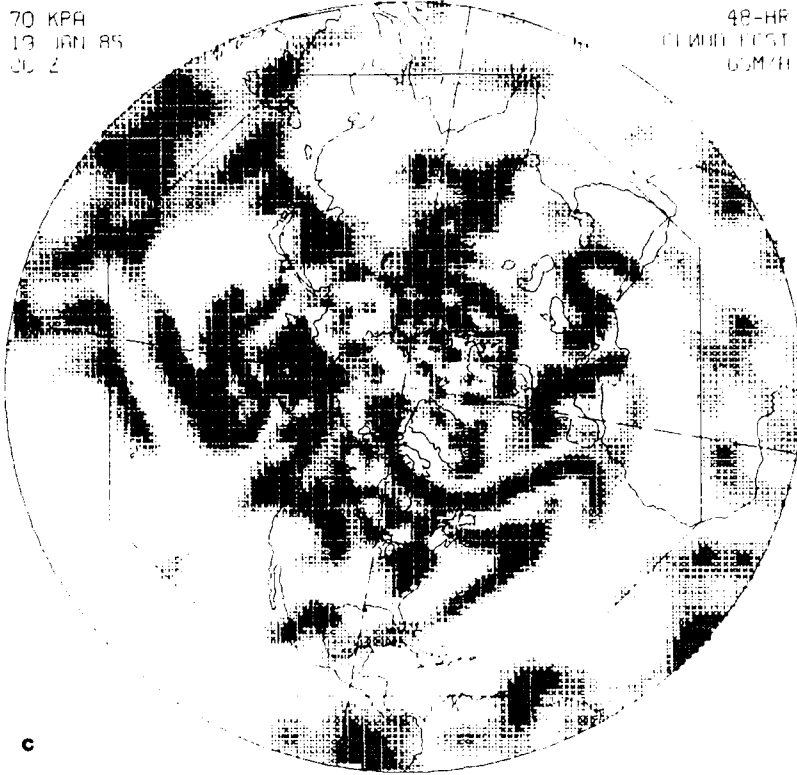


Figure 37. For the AFGWC Cloud Scheme, the GSM 48-hour Forecast of NH Layer Cloud Amount Valid at 00Z on 19 January 1985 for Layers Nominally Centered at the (a) 100, (b) 85, (c) 70 and (d) 80 kPa Pressure Levels.

70 KPA
19 JAN 85
00 Z

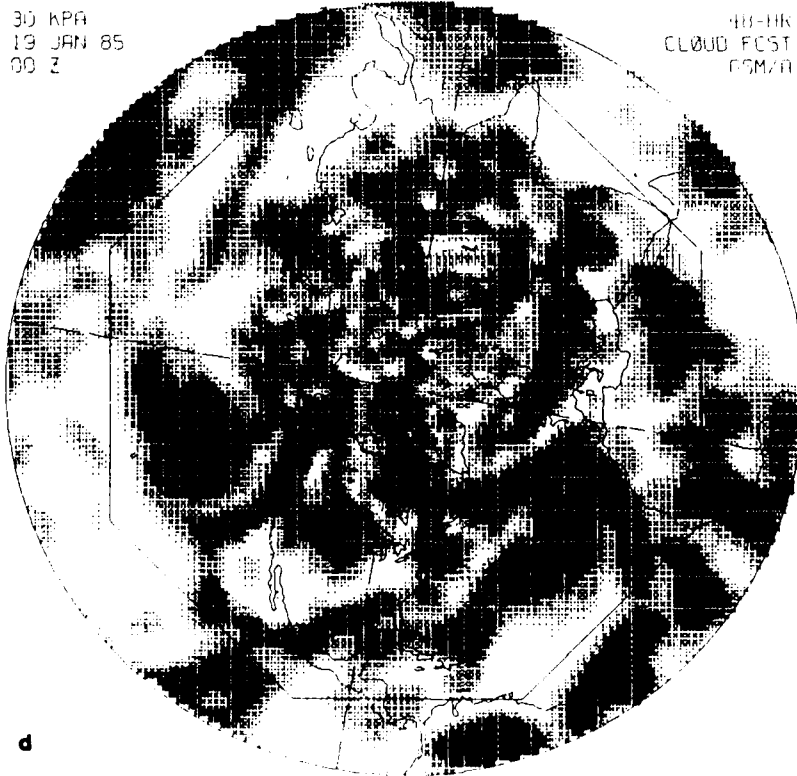
48-HR
CLOUD FCST
GCM/RR



c

30 KPA
19 JAN 85
00 Z

48-HR
CLOUD FCST
GCM/RR



d

The GSM/A scheme is characterized by a dramatic and erroneous increase in total cloud amount, vividly portrayed in Figure 35 and Tables 9, 10A, and 11A. Figures 36 and 37 show that the greatest layer cloud increase occurs at the upper levels, since the critical RH values for these levels in the GSM/A (that is, CPS) scheme are simply much too low relative to the GSM-preferred upper-level RH mean state (Figure 12). The 85 and 70 kPa levels, on the other hand, seem to show some decrease in cloud amounts, in conjunction with the modest GSM drying at these levels apparent from Case I in Figure 12. On a positive note, the 85 and 70 kPa levels in Figure 36 also show vivid formation of distinct frontal bands in response to the spin-up of the divergence and vertical velocity fields, yielding a more binary RH forecast distribution, as shown in Figure 19. Finally, there is a large increase in cloud amount at the 100 kPa level, where the low-level moist bias of the GSM forecast over oceans (notably subtropical and tropical oceans) manifests itself.

The study of MW⁶ also used the GSM/A scheme, though arbitrarily imposing zero cloud on the GSM forecast levels of 100, 40, and 30 kPa to circumvent the above biases. In so doing, MW obtained total cloud forecast accuracy scores rivaling those of the GSM/GL schemes in Tables 12-13. Such an approach, though enlightening, is too ad hoc for operational use, as it fails in particular those users who need forecasts of high cloud.

It is central to this study to further consider the 0-hour layer cloud fields of the GSM/A scheme in Figure 36, in conjunction with the 0-hour 20/20 scores for this scheme Tables 12-13. It is puzzling at first that (1) the 0-hour 20/20 scores in Case I and II are so low for the GSM/A scheme and (2) the 0-hour GSM/A cloud fields in Figure 36 do not better resemble the RTNEPH layer cloud fields of Figure 31, especially in RAOB sparse areas. After all, the hallmark of the AFGWC initial moisture analyses used here to initialize the GSM moisture in Cases I and II is the use of a 3-hour 5LAYER CPS forecast, from the 21Z RTNEPH, as the first-guess for the 00Z humidity analysis. In fact, as the reader will recall from Section 2.1.1, this study effort went to great lengths to use the particular AFGWC moisture analysis that used the RTNEPH/5LAYER first-guess, in order to reduce the short-range forecast advantage of 5LAYER stemming from 5LAYER's RTNEPH-based moisture initialization method of Figure 7.

The 3-hour 5LAYER CPS first-guess forecast valid at 00Z will be a virtual persistence of the 21Z initial 5LAYER CPS field, obtained directly from the 21Z RTNEPH, also according to Figure 7. Most notably, here in the GSM/A scheme we are using the same CPS curves to invert the initial GSM humidity fields back to a "synthesized" 0-hour cloud analysis. (We use the term "synthesized" here with the GSM 0-hour "cloud" fields to mean the GSM inferred or derived cloud analysis obtained by all the static preprocessing and postprocessing steps involved in the humidity/cloud forecast calculations of the GSM, short of actually taking a forward time integration step in the model. Hence the label "SYN" shown with all GSM 0-hour cloud "analyses" in Figures 35-47). Therefore, insofar as we can view the 3-hour 5LAYER CPS forecast from 21Z as a very close surrogate (similar to persistence) of the CPS fields obtained directly from the 00Z RTNEPH, the 00Z synthesized GSM cloud analysis should closely resemble the 00Z RTNEPH cloud analysis, at least in RAOB sparse areas.

But this expectation is not borne out by the distressingly low 0-hour 20/20 score for the GSM/A scheme or by subjective comparison of the RTNEPH and 0-hour GSM/A cloud fields. This 0-hour 20/20 score penalty in all the GSM cloud schemes reflects the severe penalty

incurred from the totality of the various vertical interpolation and horizontal spectral transformation steps of the GSM pre- and postprocessing circuit, which is schematically illustrated in Figure 38, summarized in Section 3.1.1 (for postprocessing only) and discussed in full detail by Mitchell and Yang.¹⁴

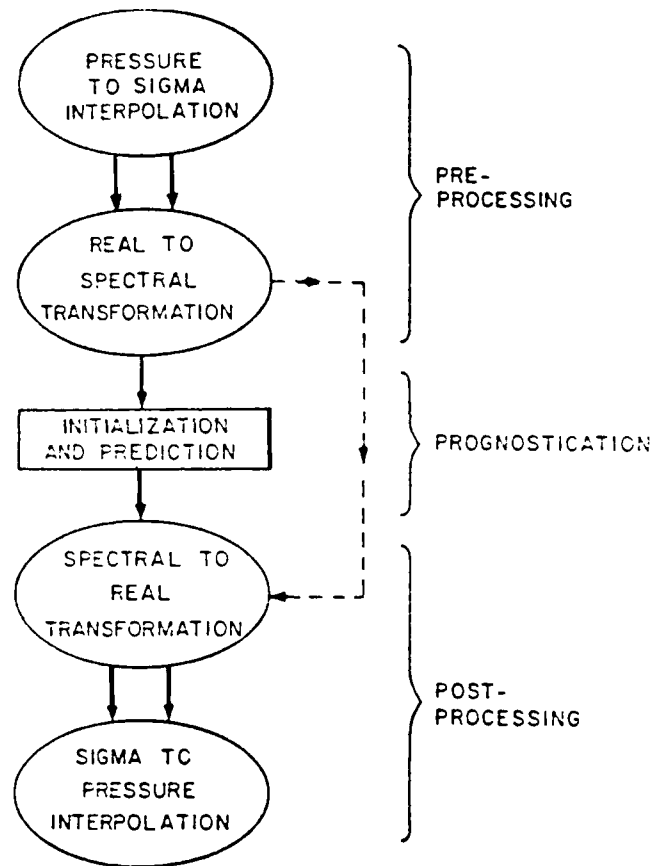


Figure 38. Schematic Illustration of the Major GSM Static Preprocessing and Postprocessing Steps, which when Applied (Along with the Chosen Cloud Scheme as the Last Step) to an Input Humidity Analysis on Mandatory Pressure Levels Yield the So-called "Synthesized" GSM 0-hour Cloud Forecast.

Some of the reduction of the 0-hour GSM/A 20/20 score is also due to some correction of the RTNEPH/5LAYER-based CPS first guess (with its upper-level dry bias) by the actual RAOBs of humidity. The 0-hour GSM/A mean NH octagon cloud amount of 58.8 percent versus the lower verifying cloud amount of 48 percent surely reflects some of the RAOB correction, especially at the upper levels. Nevertheless, we contend that a major cause of the low 0-hour 20/20 scores for all GSM cloud schemes in Tables 12 and 13 is the accumulated static error from the GSM pre- and postprocessing steps.

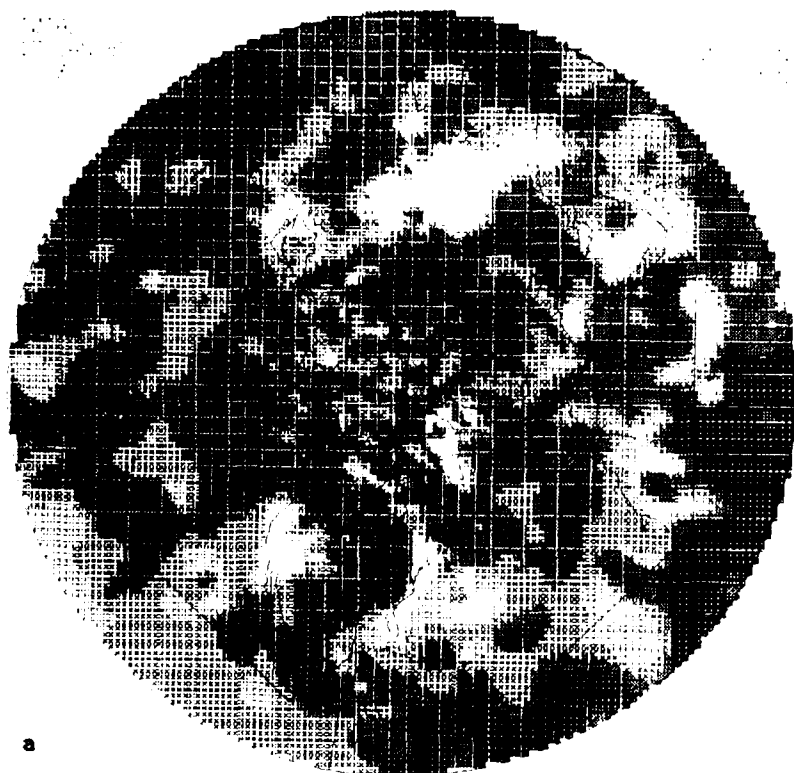
Should AFGWC in the future embark on an attempt to include pseudo or inferred moisture observations from the RTNEPH in its present-day HIRAS global moisture analysis for the purpose of improving GSM short-range cloud forecasts, it must drastically reduce the steps and substantially increase the horizontal resolution in the pre- and postprocessing of the GSM moisture fields. Details of one such streamlining in postprocessing were already given in Section 3.1.1. In streamlining preprocessing, an analog of Figure 7 must be followed as closely as possible, that is, (1) vertically and horizontally compact the RTNEPH to the GSM internal grid (GSM sigma layers and Gaussian grid -- where the latter grid and corresponding spectral resolution are carried at sufficiently high resolution to retain 1/2-mesh initial detail) and 2) directly convert this GSM-compacted RTNEPH cloud analysis to humidity using the humidity-to-cloud curves tuned specifically for the asymptotic GSM-preferred RH forecast distribution (like the GL scheme curves of Section 3.1.3).

As an alternative (not applied in this study), the so-called "trending" approach demonstrated in the study of MW can be used with substantial success to increase the short-range GSM cloud forecast accuracy. In the trending approach, as applied, for example, to obtain a 12-hour GSM cloud forecast, a 12-hour GSM cloud change field would be derived at each of the six moist GSM pressure levels by subtracting the synthesized 0-hour initial layer cloud field from the 12-hour forecast layer cloud field. Then these GSM layer cloud trends (which isolate trends from the forward time integration of the GSM) would be added to the original compacted RTNEPH layer cloud fields, followed by the stacking algorithm to obtain total cloud.

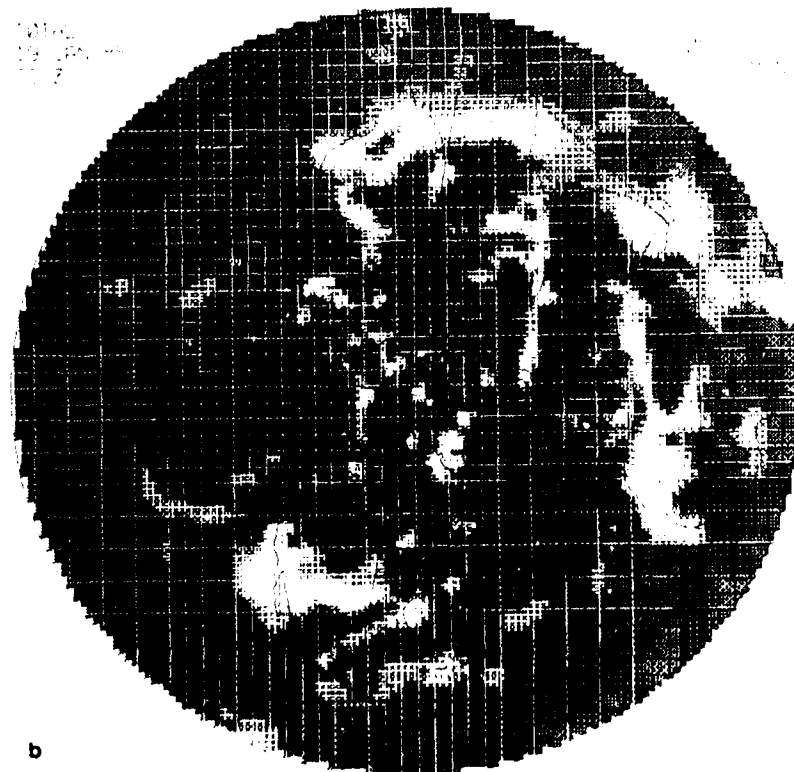
Although usable with any diagnostic cloud scheme, the trending approach is especially suited to a cloud scheme, like the GL schemes, having little or no short-term spin-up in forecast mean cloud amounts. The trending approach in the MW study, applied in conjunction with the GSM/A or CPS scheme, yielded 20/20 accuracy scores surpassing those of 5LAYER at 12 hours. The trending approach in conjunction with the GL4 cloud scheme represents in our view the best possible approach to short-range GSM cloud forecasting. The lack of tests of the trending approach here is probably the present study's most serious shortfall.

We next briefly examine displays of the Case I 48-hour GSM cloud forecasts from the GSM/N scheme (Figure 23) in Figure 39 (total cloud) and Figure 40 (layer cloud). Tables 9, 10A, and 11A and Figure 39 show that, like the GSM/A scheme, this second, temporally fixed scheme, also suffers a dramatic spin-up to total cloud forecast fields having large positive biases. In the GSM/N scheme, this positive bias occurs not from low critical values of RH_c for the onset of nonzero cloud, but rather from the low critical values of RH_m for the mostly cloudy and overcast thresholds, namely critical values RH_m of 75 and 65 percent for the onset of overcast at the 70 kPa and 30-50 kPa levels, respectively. Thus, the GSM/N cloud scheme

specifies mostly cloudy or overcast at RH values well below 100 percent at mid and upper levels. Figure 40, for example, shows widespread areas of virtual overcast at the 70 kPa and 30 kPa levels (similarly for the 50 and 40 kPa levels not shown).



a



b

Figure 39. For the NMC Cloud Scheme, the GSM (a) 0-hour and (b) 48-hour Forecast of NH Total Cloud Amount Valid at 00Z on 17 and 19 January 1985, Respectively.

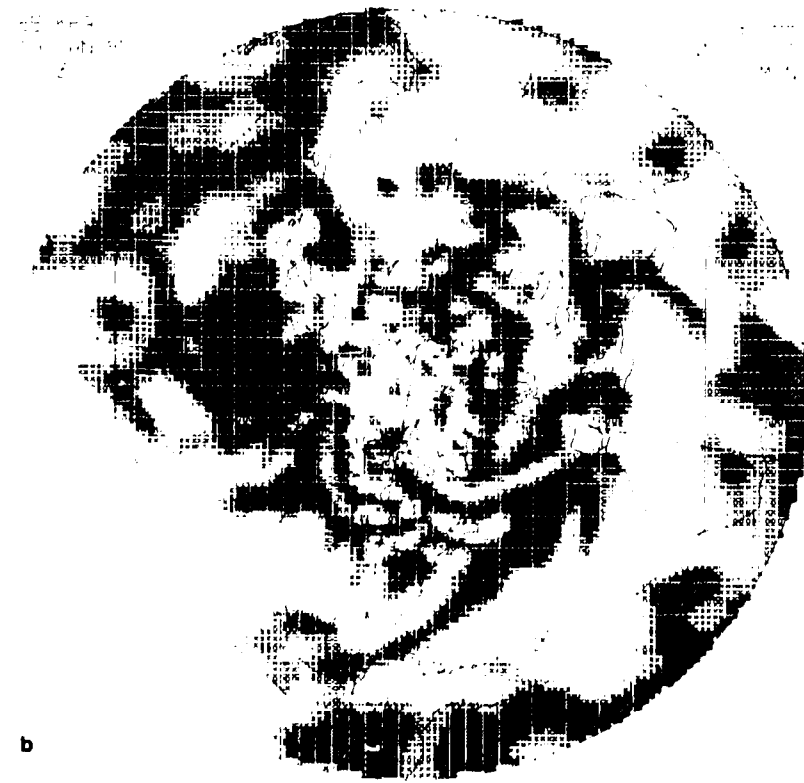
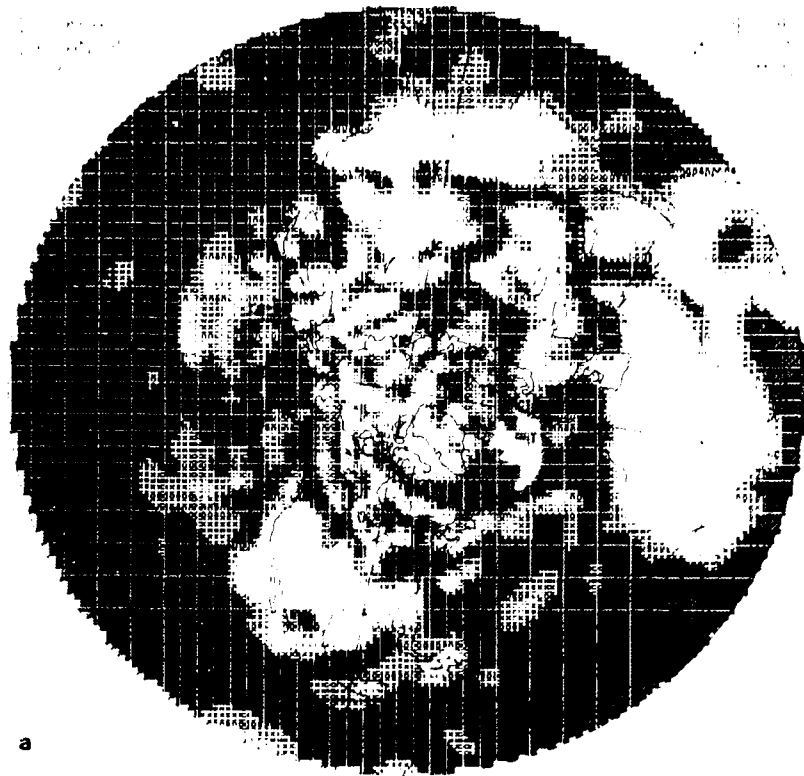
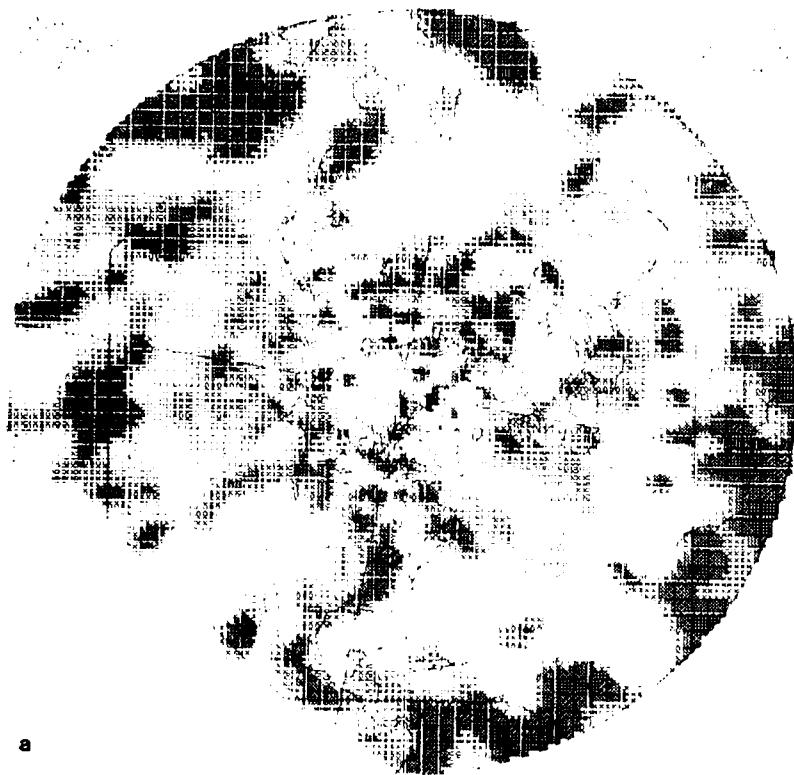


Figure 40. For the NMC Cloud Scheme, the GSM 48-hour Forecast of NH Layer Cloud Amount Valid at 00Z on 19 January 1985 for Layers Nominally Centered at the (a) 100, (b) 85, (c) 70 and (d) 30 kPa Pressure Levels.

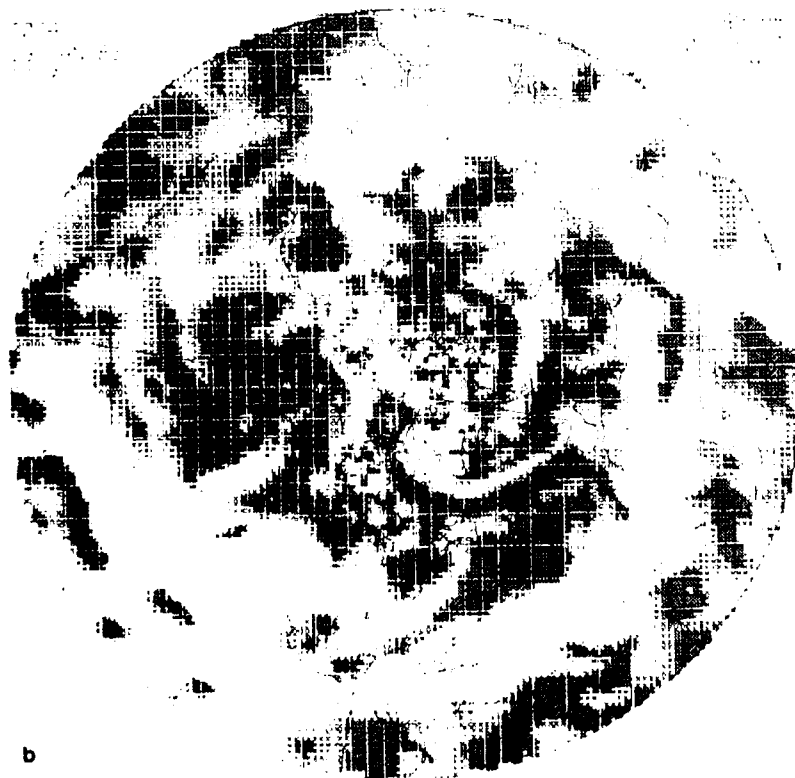


Finally, the small RH spread or interval of only 20 percent between the RH_c and RH_m values (clear and overcast RH thresholds) of the GSM/N scheme (see Section 3.1.2) for the 30, 40, and 50 kPa levels yields upper-level layer cloud patterns in Figure 40 that are overly "sharp". That is, the upper-level cloud patterns are too binary in character, dominated by large pervasive areas of strictly clear or strictly overcast.

Turning now to the final previous diagnostic cloud scheme, which is also a temporally-fixed scheme, we consider displays of Case I cloud forecasts from the GSM/E scheme (Figure 20) in Figure 41 (total cloud) and Figure 42 (layer cloud). A review of Figure 21 reminds us that this scheme has the largest low- and upper-level critical values of RH for the onset of nonzero cloud. Figure 42 correspondingly shows the small amounts of cloud yielded by this scheme at the 100 kPa and 30 kPa levels. The large upper-level critical values of the GSM/E scheme are especially ill-suited for the initial upper-level AFGWC humidity analyses, which are erroneously very dry over most of the octagon. Correspondingly then, the 0-hour total cloud fields from the GSM/E scheme show very large negative biases. As the low- and upper-level moistening trends set in during the GSM forecast, this initial negative bias decreases to a range of -10 to -20 percent at 48 hours in Tables 10-11, a significantly smaller bias magnitude than the 20-35 percent positive bias at 48 hours for the GSM/A and GSM/N schemes. More importantly, the GSM/E scheme showed higher 20/20 scores than the GSM/A and GSM/N schemes in more than half the areas at 36 and 48 hours for all three cases.



a



b

Figure 41. For the ECMWF Cloud Scheme, the GSM (a) 0-hour and (b) 48-hour Forecast of NH Total Cloud Amount Valid at 00Z on 17 and 19 January 1985, Respectively.

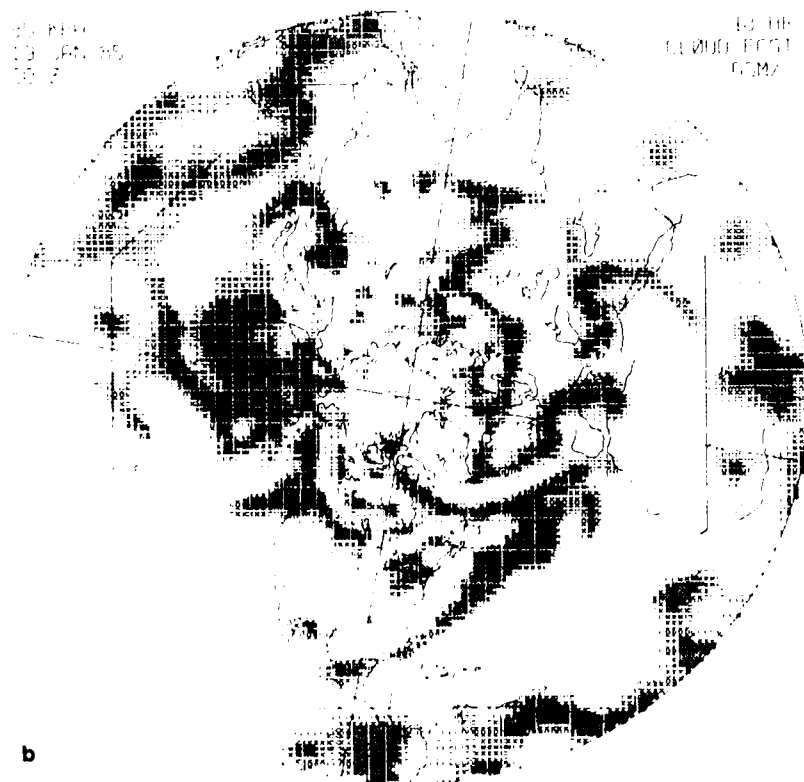
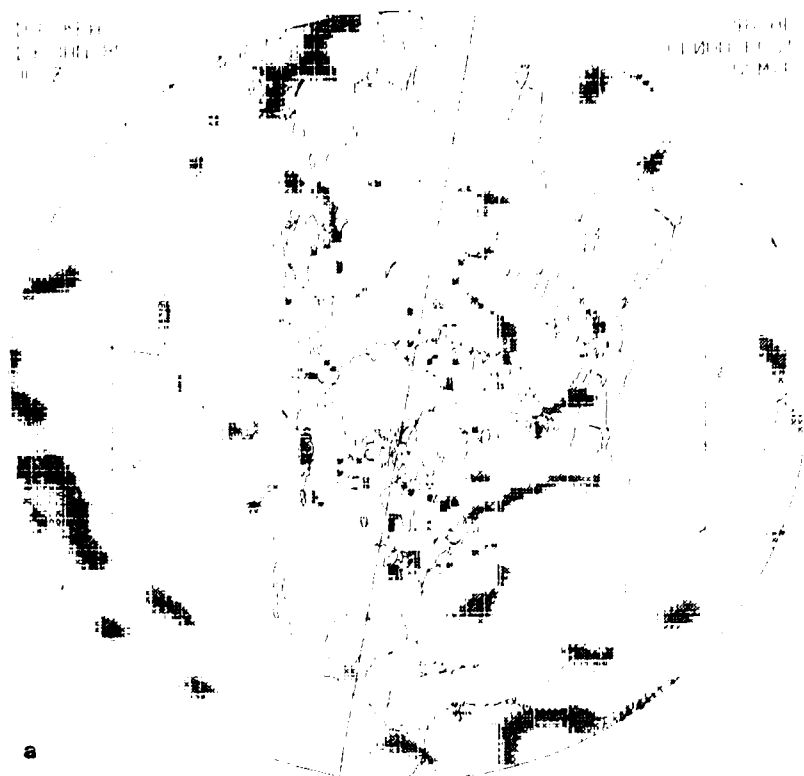
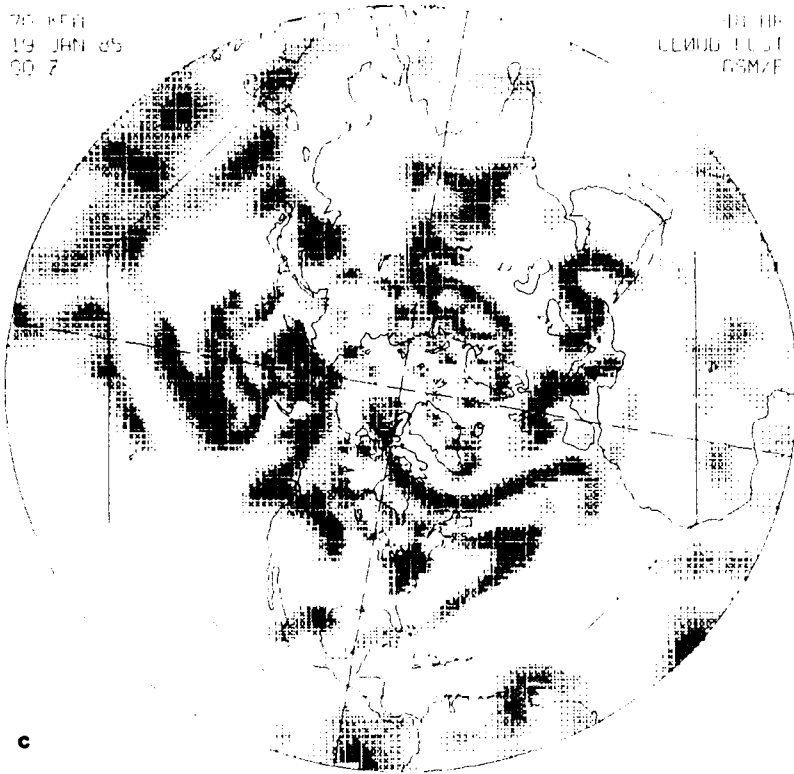


Figure 42. For the ECMWF Cloud Scheme, the GSM 48-hour Forecast of NH Layer Cloud Amount Valid at 00Z on 19 January 1985 for Layers Nominally Centered at the (a) 100, (b) 85, (c) 70 and (d) 30 kPa Pressure Levels.

70 KPA
19 JAN 85
00 Z

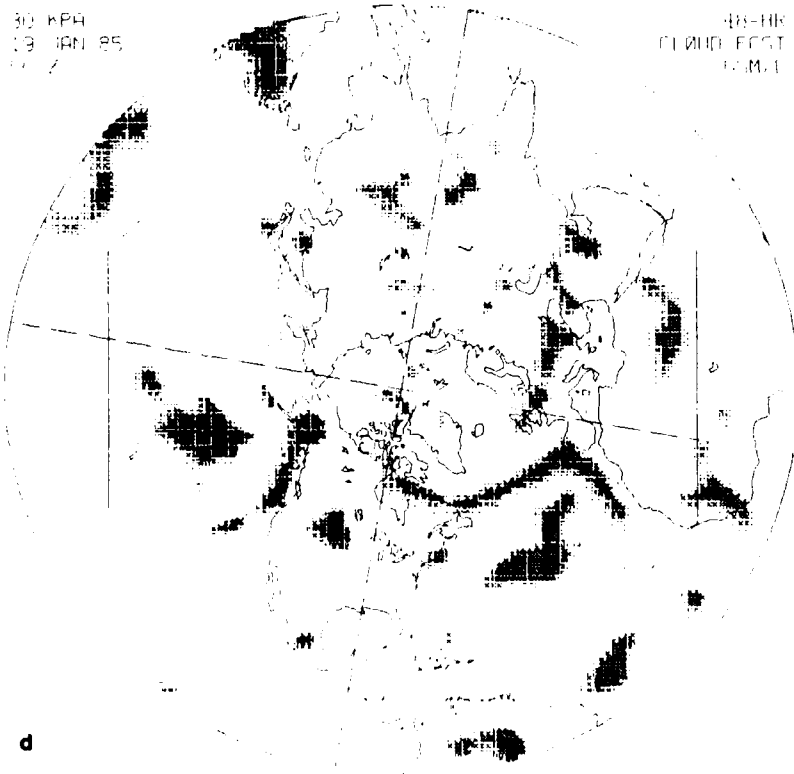
10-HP
CLOUD FCT
GSM/F



c

30 KPA
19 JAN 85
00 Z

48-HP
CLOUD FCT
GSM/F



d

The latter somewhat encouraging results with the GSM/E scheme led to numerous trial and error experiments at subjectively tuning the critical RH values, RH_c , and nonlinear exponent, P_k (see Eqs. 1 and 6). The most promising result was obtained with no change in the exponent, and modest changes in the RH_c critical values as given in Table 7. The given changes in these values clearly are not radical; yet experiments with more radical changes yielded poorer 20/20 scores, albeit not necessarily poorer bias scores. The impacts of the RH_c changes in Table 7 on the GSM/E bias and 20/20 scores are evident in Tables 9-13 under the designation GSM/EM (for modified). The improvement of GSM/EM over GSM/E scores is not notable.

3.2.3 THE NEW GL DIAGNOSTIC CLOUD SCHEME

The disappointing performance of the previous diagnostic cloud schemes led to a resolute search for a new diagnostic cloud scheme specifically tuned to the present GSM forecast model and verifying RTNEPH cloud analysis. The earlier results showed it was important to find a scheme with temporal degrees of freedom to compensate for the early GSM spin-up period. The early attempts to modify the GSM/E scheme for this purpose via trial and error tests proved almost endless owing to the number of degrees of freedom in Eq. (6). Hence, it became clear that an objective approach was necessary. The routine gridded objective cloud analyses of the RTNEPH provide the crucial discretized 3-D cloud database needed for such an effort. Section 3.1.3 described the development and procedures of the new GL objective cloud-scheme methodology, yielding first the GSM/GL6 cloud scheme, which utilizes all six moist pressure levels output by the GSM.

The cloud forecasts in Case I from the GSM/GL6 scheme (Figure 27) are displayed for the 0- and 48-hour forecast times in Figure 43 (total cloud) and Figures 44-45 (layer cloud). (We must note that all GSM/GL forecasts displayed here in Figures 43-47 and listed in Tables 9-13 used the so-called "aggregate" curves - see discussion of Figure 25 - derived from the combined Case I and II cumulative frequency distributions of RTNEPH clouds and GSM RH forecasts.) The 0-hour and 48-hour GSM/GL6 total cloud fields in Figure 43 appear at first glance to be rather cloudy, especially in the tropics outside the octagon. However, we recall in Section 3.1.3 that the GL6 cloud curves in Figure 27 were derived by mapping RTNEPH cloud and GSM RH layer cumulative frequency distributions derived only from grid points inside the octagon (the RTNEPH outside the octagon was not available). Within the octagon, Table 9 shows that the 0-hour GL6 mean cloud amount (50.9) agrees closely with that of the RTNEPH (48.0).

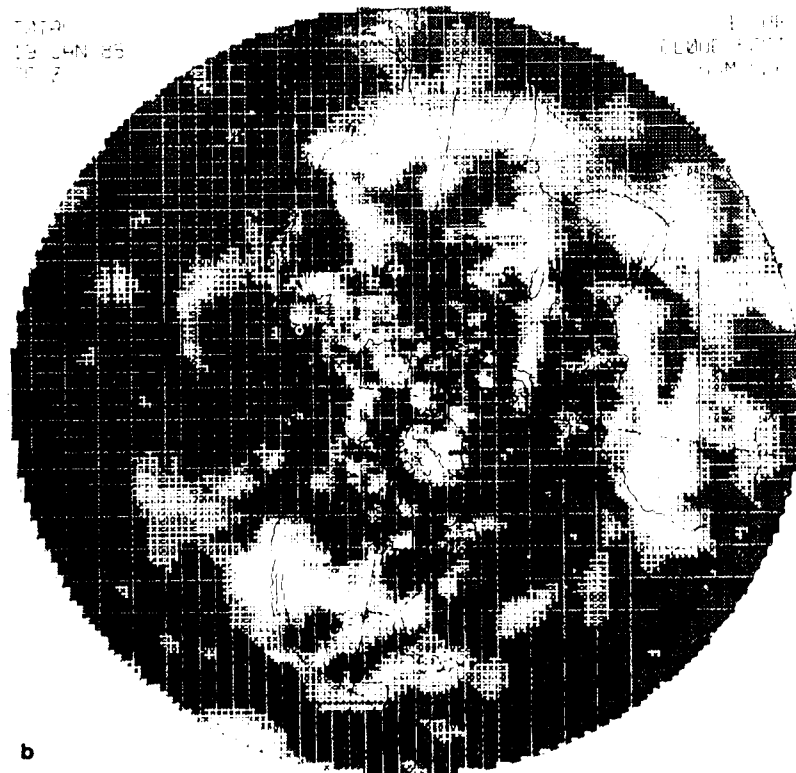
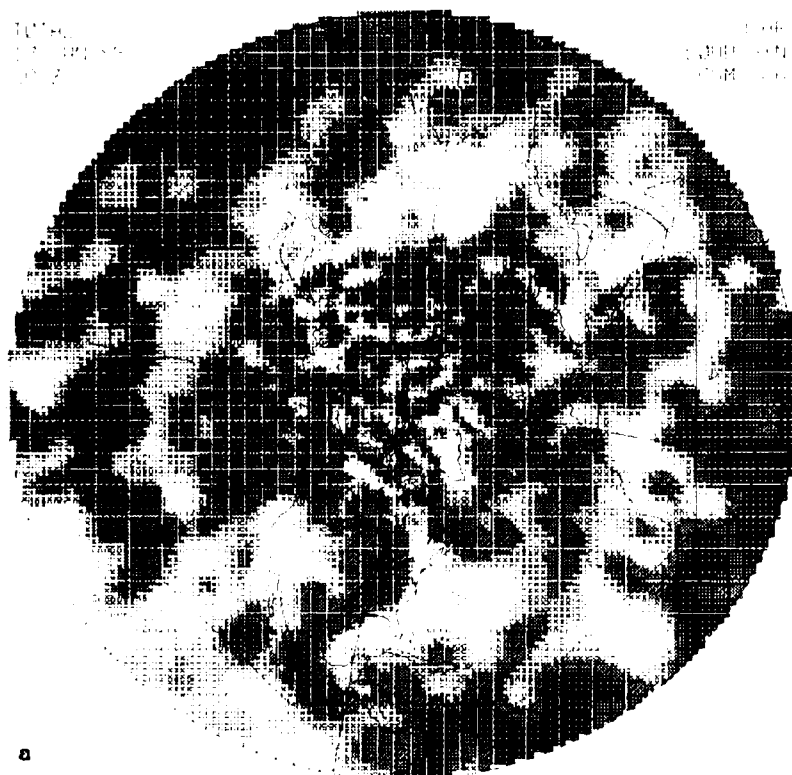
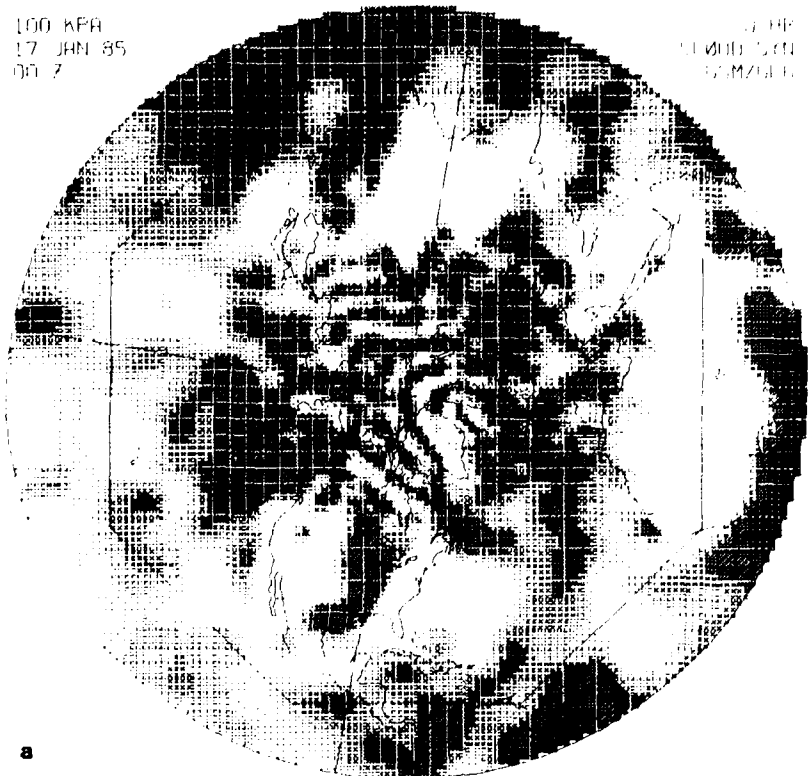


Figure 43. For the GL6 Cloud Scheme, the GSM (a) 0-hour and (b) 48-hour Forecast of NH Total Cloud Amount Valid at 00Z on 17 and 19 January 1985, Respectively.

100 KPA
17 JAN 85
00Z

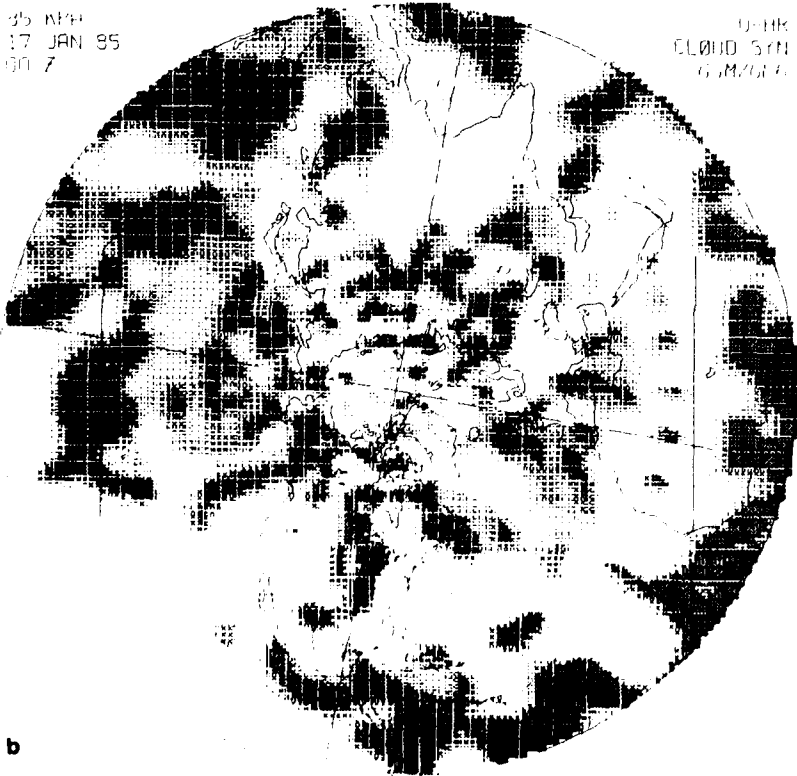
0-6H
CLOUD SYN
G.M.Z. 85



a

85 KPA
17 JAN 85
00Z

0-6H
CLOUD SYN
G.M.Z. 85

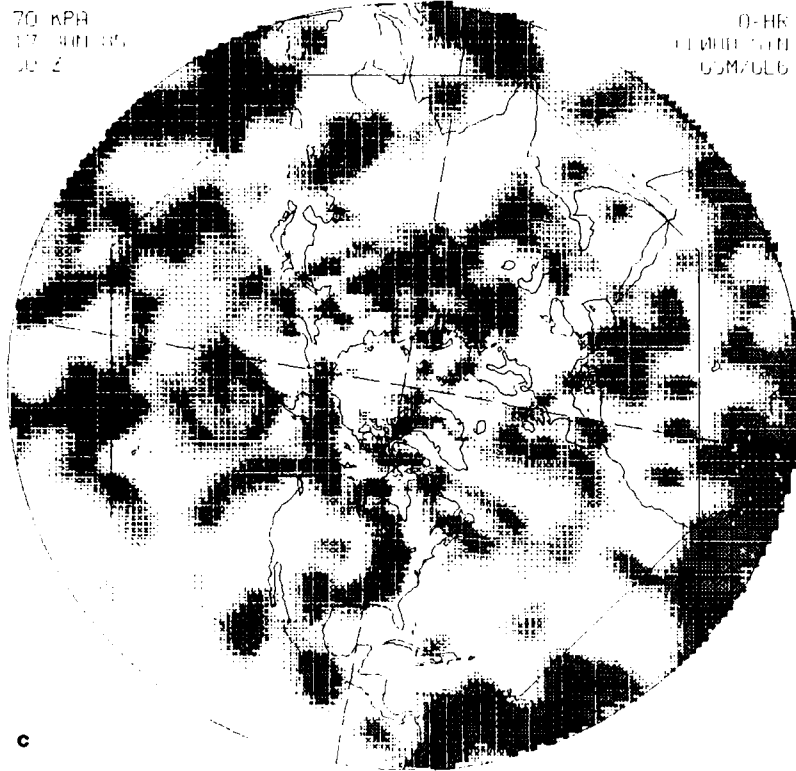


b

Figure 44. For the GL6 Cloud Scheme, the GSM 0-hour Forecast of NH Layer Cloud Amount Valid at 00Z on 17 January 1985 for Layers Nominally Centered at the (a) 100, (b) 85, (c) 70 and (d) 30 kPa Pressure Levels.

70 KPA
17 JAN 85
00 Z

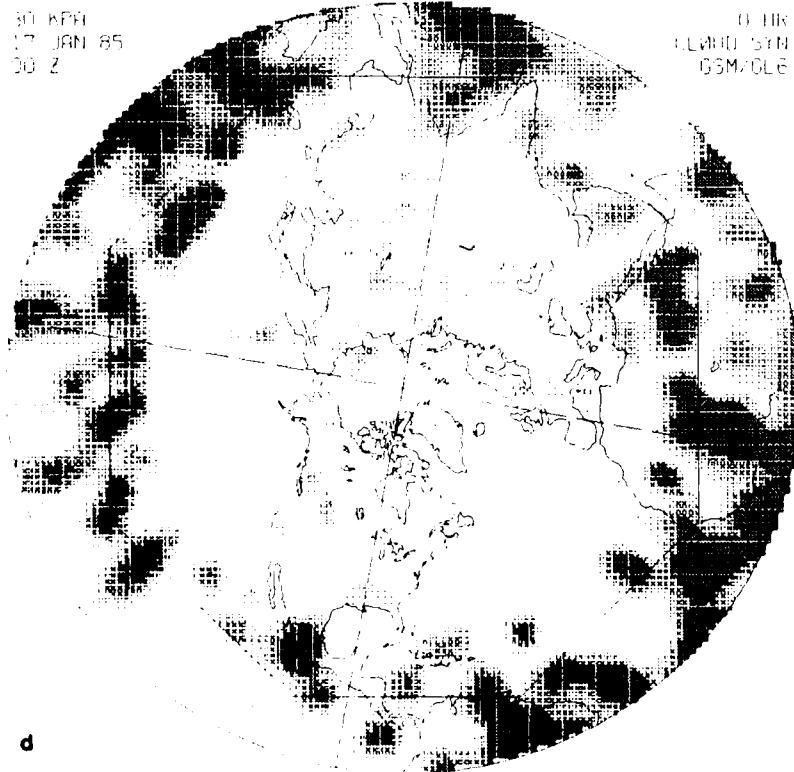
0-HR
CLMNH STR
OSM/OLE



c

30 KPA
17 JAN 85
00 Z

0-HR
CLMNH STR
OSM/OLE



d

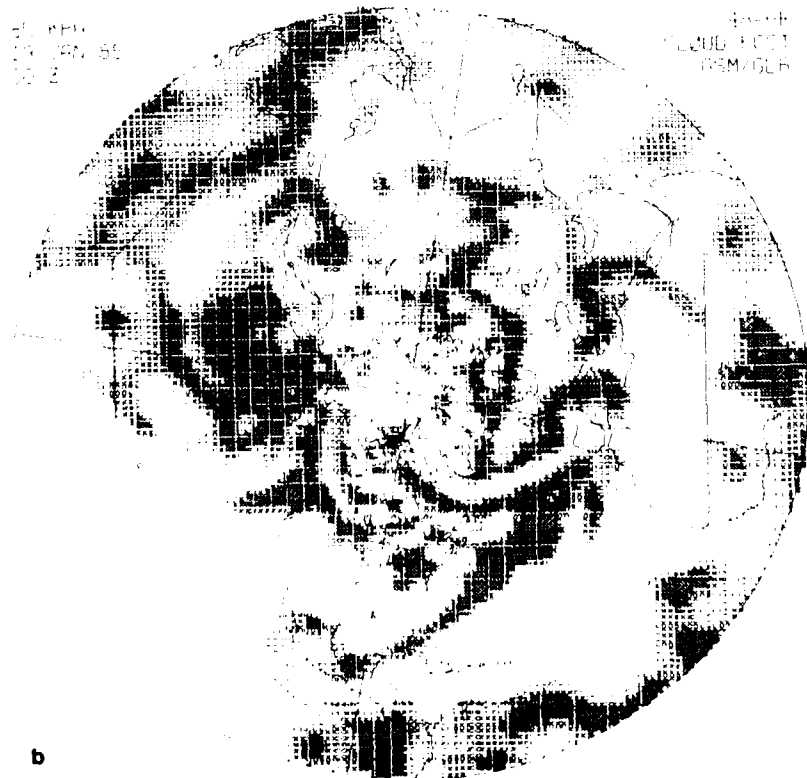
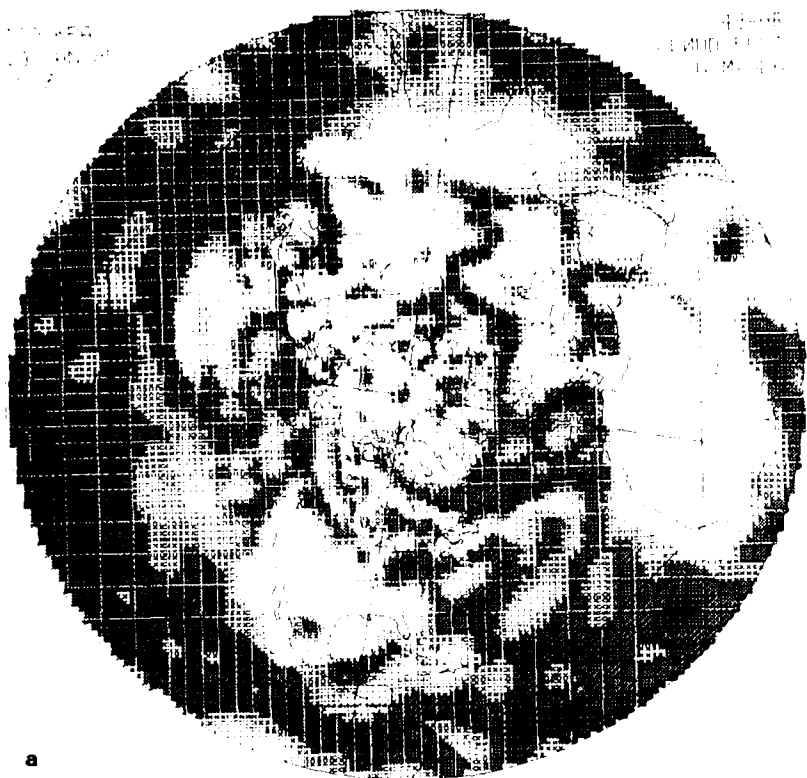
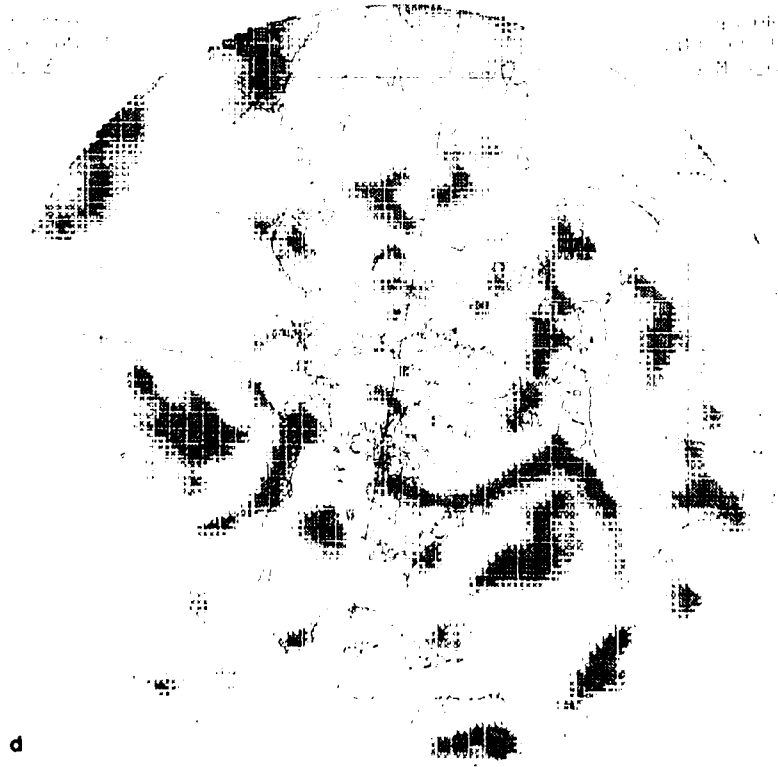


Figure 45. For the GL6 Cloud Scheme, the GSM 48-hour Forecast of NH Layer Cloud Amount Valid at 00Z on 19 January 1985 for Layers Nominally Centered at the (a) 100, (b) 85, (c) 70 and (d) 30 kPa Pressure Levels.





a

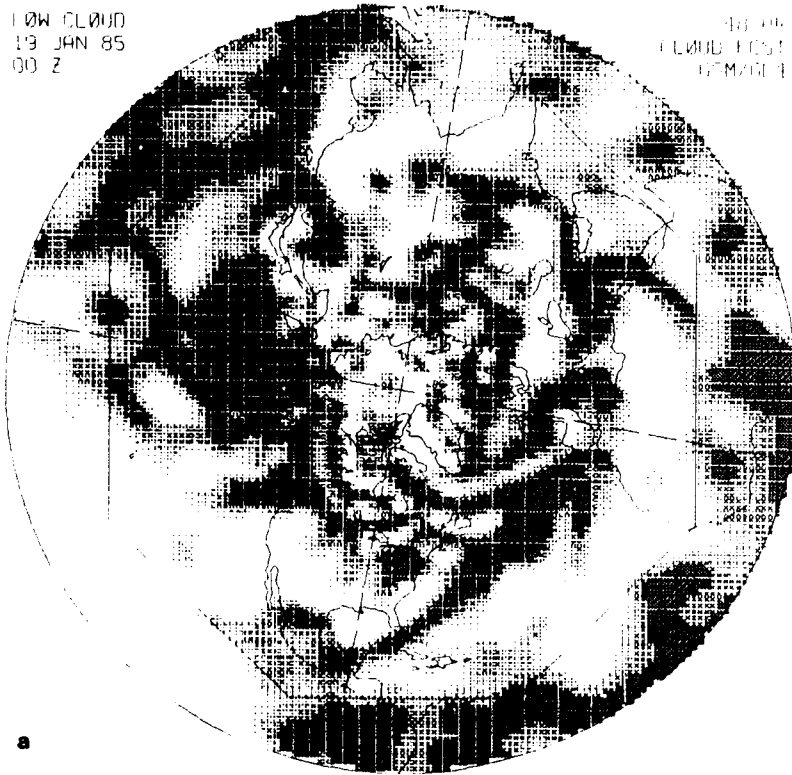


b

Figure 46. For the GL4 Cloud Scheme, the GSM (a) 0-hour and (b) 48-hour Forecast of NH Total Cloud Amount Valid at 00Z on 17 and 19 January 1985, Respectively.

LOW CLOUD
19 JAN 85
00 Z

48-HR
CLOUD FST
G.M.O.P.



HIGH CLOUD
19 JAN 85
00 Z

48-HR
CLOUD FST
G.M.O.P.

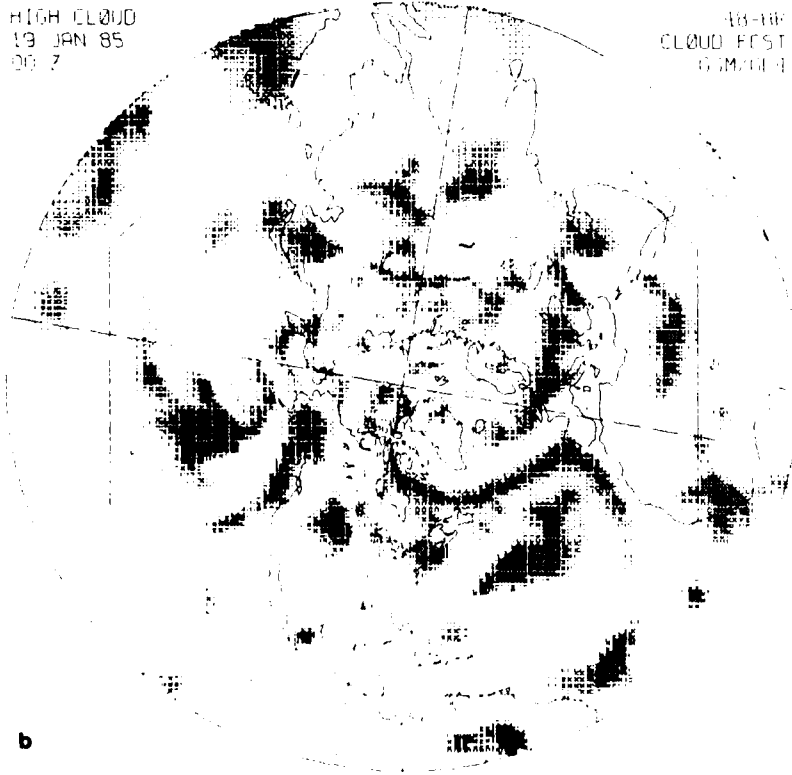


Figure 47. For the GL4 Cloud Scheme, the GSM 48-hour Forecast of NH Layer Cloud Amount Valid at 00Z on 19 January 1985 for Layers Nominally Centered at the (a) Low and (b) High Cloud.

This points out that in routine global applications of the GL6 cloud scheme, the curves should probably be stratified by region. Such a stratification might include tropical, midlatitude, and polar domains, each further divided according to water and land points. Access to just two independent cases here provided too small a sample to test areal stratification of the curves in this study.

While the octagon-mean total cloud amounts of the 0-hour GL6 and RTNEPH agree closely, the GL6 cloud field lacks the "ragged" detailed appearance of the RTNEPH analysis or 5LAYER forecast fields, that is, it fails to preserve the perceived distinct fractal geometry of the relatively high resolution, albeit compacted, RTNEPH. This failure again is due to the greater pre- and postprocessing penalty or synthesis penalty encountered in the GSM versus 5LAYER frameworks. The 0-hour 20/20 scores for all the GSM/GL schemes in Tables 12-13 suffer this very substantial synthesis penalty though not as severely as the previous schemes. The failure of the GSM synthesis to preserve the detail of definition in the initial RTNEPH is also recognized when comparing the 0-hour GL6 layer cloud fields in Figure 44 with those of the RTNEPH in Figure 31.

Turning to a new matter, we next consider the 0-hour GL6 and RTNEPH 30 kPa cloud fields in Figures 44d and 31d, which illustrate inherent limits to the ability of the GL cloud scheme to overcome forecast or analysis systematic position error. From the AFGWC initial RH analysis at 30 kPa in Figure 17f, we recall that the "boundary-area" blending of the erroneous, very dry, 5LAYER first guess dependent moisture analysis with the independent and more realistic tropical moisture analysis (see Table 3) yields an unnatural ring of maximum humidity (with respect to the octagon interior) along the inside of the octagon boundary. The frequency distribution of RH derived from the octagon interior of Figure 17f will contain no "memory" of the predominant location of this high humidity. Most importantly, the position of this ring of relative maximum of humidity is an analysis artifact; and it does not correlate well with the location of cloudy areas in the RTNEPH analysis of Figure 31d, because the ring coincides with the generally cloud-free subsiding subtropical trade wind zone.

Hence, when the underlying diagnostic cloud-scheme assumption of high correlation between locations of high humidity and large cloud amount breaks down due to gross mislocations of relative maximums of RH in the analysis or forecast, the humidity-inferred location of the clouds will break down also. This limitation is true of any type-1 humidity-to-cloud scheme and is thus a limitation not overcome by the particular derivation method for the GL schemes. However, the real culprit in the wrong location of cloudiness in Figure 44d is not the cloud scheme, but rather the total breakdown of the initial AFGWC humidity analysis at this level in Figure 17f. We nevertheless have duly noted that whenever the distribution of relative maximums in humidity assumes an unnatural character in the GSM initial state or forecast, then the GL cloud schemes, like any type-1 scheme, will also reflect that unnatural character.

What may be more significant here is that even in Figure 44, the GL6 scheme does continue to reproduce the correct octagon-mean 30 kPa cloud amount and the correct octagon-domain frequency distribution of the range of cloud amounts as provided by the RTNEPH analysis in Figure 31d. Furthermore, by 48 hours, when the GSM forecast has largely corrected the

erroneous dry bias of the initial state, the GSM 30 kPa 48-hour cloud forecast and verifying RTNEPH cloud analysis now appear much more similar (Figures 45d and 32d).

A similar problem of this type is observed again to a lesser, but nonetheless detrimental, degree in the GSM RH forecast and GL6 diagnosed cloud amount at 100 kPa in Figure 45a. Here, the GSM's large positive RH forecast bias over subtropical oceans (but still inside the octagon) has led to a predominance of diagnosed cloud cover over the subtropical oceans at the expense of midlatitude oceanic cloud, almost opposite the oceanic latitudinal cloud distribution of the RTNEPH in Figure 32. Thus, while the GL6 scheme ensures the proper octagon-mean cloud amount at every layer, the GSM systematic error in the location of high RH has resulted in layer cloud at the 100 kPa level in the wrong location.

Consequently, in the vertical stacking steps of Appendix A, the derived total cloud cover in the GL6 scheme is somewhat positively biased, despite the enforced zero layer biases, because the GSM initial and forecast cloud layers have an unobserved vertical alignment. Tables 9, 10A, and 11A show the tendency of the GL6 total cloud analysis and the forecast to be positively biased. The culprit early in the forecast is the aforementioned mislocation of high RH in the 30 kPa analysis, and later in the forecast the mislocation of high RH in the 100 kPa forecast. Both the 30 kPa and 100 kPa problems could be alleviated substantially, we speculate, by a stratification of the GL curves by area as suggested earlier.

Unable to pursue areal stratification here owing to the two-case limit, to overcome the 100 kPa problem we tested various alternative vertical stacking strategies in schemes GL6A, GL6B, GL6C, GL4, and GL4A. Scheme GL6B simply imposes a forecast of zero cloud at 100 kPa. As expected, the total cloud bias of the GL6B scheme is negative. The 20/20 accuracy score of the GL6B scheme is mixed, occasionally showing improvement. Next, the GL6C scheme also ignores the 100 kPa GSM cloud forecast, but additionally assumes random cloud-layer overlap ($R=1$ in stacking Combinations I, II, and III of Appendix A). As a random stacking reference case, the GL6A scheme also assumes random overlap in stacking, but retains the 100 kPa GSM cloud forecast. Predictably, the GL6A scheme shows a definite positive bias over the octagon. Though mixed, the 20/20 scores of these GL6 scheme variations showed occasional superiority over the original GL6 scheme.

Thus in a final attempt to circumvent the poor GSM 100 kPa cloud forecasts over low-latitude oceanic areas, the four-layer GL4 scheme was developed (Figure 28) and tested (Figures 46-47). As described in detail in Section 3.1.3, this scheme also ignores the GSM 100 kPa RH forecast and handles the 30 and 40 kPa GSM RH forecasts differently in deriving frequency distributions of forecast RH at upper levels (to better deal with the lack of compacted RTNEPH layer cloud at 40 kPa). Lastly, the GL4A scheme once again assumes random layer overlap in the derivation of total cloud. For overall consistency in terms of small steady bias and competitive 20/20 scores in Tables 9-13, the GL4 scheme appears to be the best choice among all GL cloud schemes, virtually all of which clearly surpass the previous GSM diagnostic cloud schemes.

From the results of this section on GL cloud schemes, it is clear that the objective tuning procedure and temporal degree of freedom embraced in the GL scheme do indeed achieve the desired goals of a small forecast bias and negligible spin-up in large-area mean cloud amounts. These strengths do not overcome the penalties in forecast accuracy incurred by a

poor initial humidity analysis and the complex, multiple, and relatively low resolution of the numerous static steps of GSM pre- and postprocessing. These penalties are so severe that the 20/20 accuracy scores of both the GL schemes and previous schemes actually increase over 12 hours, often over 24 hours or longer, indicating that the full potential for GSM forecast accuracy in the 12-24 hour range has not been achieved. By 36 hours and beyond, the present GSM/GL schemes regularly surpass the cloud forecast accuracy of 5LAYER, sometimes by a significant margin. Recommended approaches for achieving GSM cloud forecast superiority over 5LAYER at shorter forecast ranges are reiterated in the following conclusion section.

4.0 SUMMARY AND CONCLUSIONS

Automated objective cloud forecasts (especially in the 0-24 hour range) have been important products of AFGWC for at least two decades,²⁹ in support of various world-wide Air Force missions. During this period, AFGWC's primary cloud forecast model has been the 5LAYER model, and its direct predecessors. This family of cloud models has always required input wind forecasts from a prior execution of a separate dynamic NWP model, which prior to 1985 at AFGWC were dry models (non-moisture bearing). In October 1985, AFGWC implemented the AWAPS, including a moist global spectral model from NMC,⁸ which for the first time afforded AFGWC the possibility of producing global cloud forecasts directly from a single, global, moist dynamic model. In response to this opportunity and at the request of AWS, GL initiated a program to develop cloud forecast schemes suitable for use in AFGWC's present and future global (and regional) model.

The purpose of this study was to develop and test a skillful scheme for forecasting layer and total fractional cloud cover in AFGWC's presently operational GSM (also GL's baseline GSM) and to compare these GSM cloud forecasts with the corresponding forecasts from AFGWC's traditional 5LAYER model. One specific objective was to determine the shortest forecast length, T, if any, at which the cloud forecast skill of the GSM equalled or surpassed that of 5LAYER. Thus this study had to be particularly cognizant of the preeminent source of 5LAYER's rather good short-range cloud forecast skill -- namely 5LAYER's timely and direct use (via a minimum of static preprocessing steps) of AFGWC's RTNEPH global 3-D high-resolution cloud analysis to empirically derive initial CPS (5LAYER's moisture variable). Thus, to minimize the time T cited above, the central GSM forecasts in this study were purposely executed from AFGWC global moisture analyses that also heavily utilized RTNEPH clouds to infer the first-guess fields for the moisture analysis.

As a precursor to the GSM cloud forecasts, we first examined these AFGWC relative humidity (RH) analysis fields, along with the follow-on GSM RH forecasts. We established that the above RTNEPH-influenced AFGWC moisture analyses were much too dry in the upper half of the troposphere owing to (1) overly low zero-cloud humidity thresholds in the cloud-to-humidity inference scheme (that is, the 5LAYER CPS-cloud scheme) and (2) underestimation of high cloud amounts in the RTNEPH. Unlike the 5LAYER model, which maintains this

substantial, initial upper-level dry bias during its forecast (and therefore still yields reasonable forecast mean cloud amounts when it applies the CPS-to-cloud scheme at forecast time), the GSM moistens these upper levels during its forecast and largely corrects the erroneous initial dry bias. The large magnitude of this upper-level GSM spin-up, which is an artifact of the poor AFGWC upper-level moisture analysis, severely degrades the GSM short-range cloud forecast skill.

Separate GSM RH forecasts from more realistic NMC moisture analyses demonstrated much less spin-up. Additionally, these latter GSM forecasts, together with the GSM forecasts from the AFGWC analyses, showed that the GSM in 24 hours evolves quickly toward its own model-preferred zonal mean humidity state and model-preferred RH frequency distribution, largely irrespective of the chosen initial moisture analysis. As a class, large-scale moist NWP models characteristically show distinct drift toward a model-preferred moisture state and a concomitant model-preferred hydrological balance. However, these model-preferred moisture states differ from observations and from model to model to various degrees depending on the veracity of the model's physical parameterizations. The GSM preferred moisture state here exhibits a small upper-level moist bias and a modest mid- and lower-level dry bias, except for a substantial lowest-level moist bias over tropical (warm) oceans.

To produce cloud forecasts with the GSM, we sought an appropriate diagnostic or empirical scheme to infer cloud cover from standard model output. Because the baseline GSM here substantially underestimates convective precipitation rate and lacks parameterized physics for (1) radiation, (2) a surface energy budget, and (3) land surface and PBL moisture fluxes, we considered only the simplest diagnostic cloud schemes (here called type-1 schemes), which diagnose fractional cloud cover using only the model's RH forecast. In these simplest diagnostic cloud schemes, the conceptual physical picture is as follows: On spatial resolutions typical of a GSM, clouds are frequently subgrid scale, both horizontally and vertically. Hence, although the forecast volume-average RH for a given grid box volume may be somewhere below 100 percent, we may expect some fractional cloud cover in the grid box since the local variance about the average will yield subgrid regions of saturation (and hence clouds).

In type-1 diagnostic cloud schemes, the crucial empirical parameter is the critical threshold of humidity, or critical humidity (RH_c), at which nonzero fractional cloud cover is first inferred. In more complex diagnostic cloud schemes (type-2), which we recommend be tested in follow-on studies when the GSM has improved convection, radiation, and PBL physics, other model output fields such as convective precipitation rate, vertical velocity, and static stability should be utilized, since the magnitude of the humidity variance within a grid volume is undoubtedly a function of these variables (for example, stable stratification or descending motion will likely be associated with a decrease in subgrid moisture variance and hence imply an increase in the RH_c parameter).

In the GSM, we first tested several pre-existing type-1 diagnostic cloud schemes (for example, the scheme used by ECMWF prior to May 1985). It was found that because type-1 cloud schemes from another model usually use RH_c values tuned for that model's preferred moisture state, such schemes perform poorly when applied to an independent model and yield large cloud forecast biases and unacceptable spin-up behavior.

Thereafter, we developed a new methodology, herein called the GL cloud scheme, to objectively derive a type-1 diagnostic cloud scheme tuned specifically for any given NWP model. The methodology provides a cloud scheme that manifests (1) negligible bias and (2) negligible spin-up in the forecast cloud amounts. The method derives explicit RH-to-cloud conversion functions or "curves" layer by layer. The method does so by calculating the cumulative frequency distribution of the model's RH forecasts for a given forecast length at a given layer (over a sample of forecast cases spanning several weeks) and mapping this distribution onto the cumulative frequency distribution of RTNEPH observed cloud amounts at that layer for the same time period. By mapping the model's RH frequency distribution to observed cloud amounts at each regular interval of model forecast length (say 6-hourly), one can account for the model's changing RH frequency distribution during the spin-up period. The resulting forecast-time dependent RH-to-cloud curves eliminate spin-up biases in the derived forecast cloud amounts.

Because the cumulative frequency distribution of model forecast RH or RTNEPH cloud amounts can vary substantially over various climatological regions (owing to natural factors, failures in model physics, or breakdowns in the RTNEPH cloud retrieval algorithms), we recommend that the above methodology be carried out separately over large climatologically homogeneous regions (say tropical, midlatitude, and polar areas, each stratified by land and water). To account for the seasonal cycle in these areas, we recommend a real-time update of the respective RH and cloud frequency distributions based on a continuously updated running sample over a period of several weeks, coupled to a corresponding update of the RH-to-cloud curves. Such a continuous update would also account for changing RH or cloud amount distributions stemming from ongoing developmental changes in model resolution, numerics, and physics or RTNEPH cloud retrieval algorithms.

Regarding the cloud forecast performance of the GL cloud scheme, in two separate winter cases, the GSM cloud forecast accuracy as verified against the RTNEPH showed the GL cloud scheme consistently outperformed three previous type-1 cloud schemes, including the pre-1985 ECMWF scheme. However, even with the GL cloud scheme, the GSM performance relative to 5LAYER was less than hoped, but not surprising after investigating the impacts of the poor AFGWC initial humidity analyses. Indeed, the accuracy of the GSM cloud forecasts with the GL and other type-1 schemes actually increases in the first 24 hours, as the GSM corrects and recovers from the poor AFGWC initial moisture state. Hence, usually in the 24- to 36-hour range, the GSM cloud forecast skill with the GL scheme surpasses that of 5LAYER over the U.S. and European areas.

In addition to the poor AFGWC initial moisture analysis, another cause of poor GSM short-range cloud forecast accuracy is the substantial 0-hour GSM error incurred in the numerous, complex, and relatively low-resolution GSM static pre- and postprocessing steps. Section 3.1.1 describes straightforward ways of reducing the postprocessing steps for cloud forecast purposes. The reduction of preprocessing steps is less straightforward and more challenging.

The approaches one might take to reduce preprocessing error hinge on whether the moisture forecasts from the GSM must support multiple users of several model moisture outputs (RH, precipitation, etc.) or users only interested in explicit short range (0-24 hour) cloud forecasts. In the latter rather unlikely situation, the GSM's initial moisture field could

be initialized directly on the GSM's internal grid (model sigma layers and Gaussian grid) from the RTNEPH's cloud analysis by inverting the RH-to-cloud curves derived for the model's long term (96-hour) preferred asymptotic mean humidity state. In the more likely event of multiple users of various GSM moisture outputs, one must utilize a more conventional 4-D assimilation of explicit moisture observations from RAOBs (possibly folded in with moisture estimates derived from the RTNEPH in the manner explored by Norquist^{12,28}), using an OI (or other) objective analysis scheme and a GSM first-guess moisture forecast.

The latter approach would again suffer the full short-range cloud forecast penalty incurred by the GSM's complex 0-hour preprocessing suite. The only viable method known to us at present for overcoming this 0-hour penalty from the full GSM static preprocessing is the trending technique described in Section 3.2.1 and demonstrated in the forerunner study of MW⁶.

Since the archiving period of this study, AFGWC has vastly improved its global moisture analysis (in HIRAS - see Section 2.1.1), from the point of view of providing a suitable initial moisture state for a GSM moisture forecast intended for multiple users. This HIRAS RH analysis is now based on a 4-D assimilation using a GSM first-guess, RAOB humidity measurements, and an OI objective analysis. RTNEPH-based moisture estimates are presently ignored. Given the improved status of the HIRAS moisture analysis, a follow-on GL-funded study is now underway at AFGWC to test the GL cloud scheme in the AFGWC GSM environment on a continuous real-time basis over a period of about 9 months. This follow-on study will test all the above recommendations regarding the type-1 GL cloud scheme, including continuous real-time updating of the RH-to-cloud curves, areal stratification of the curves, reduced postprocessing steps, and the trending approach to reduce initial 0-hour static processing error.

References

1. Geleyn, J.-F. (1981) *Some diagnostics of the cloud/radiation interaction in the ECMWF forecasting model*, ECMWF Workshop on Radiation and Cloud-Radiation Interaction in Numerical Modeling, 15-17 October 1980, European Centre for Medium Range Weather Forecasts, Reading, Berkshire, U.K., 135-162.
2. Stoble, J.G. (1986) *AFGWC's Advanced Weather Analysis Prediction System (AWAPS)*, AWS/TN-86-001, Air Weather Service, Scott AFB, IL, pp. 61.
3. Slingo, J. and Ritter, B. (1985) *Cloud Prediction in the ECMWF model*, ECMWF Tech. Rep. No., 46, European Centre for Medium Range Weather Forecasts, Reading, Berkshire, U.K., pp. 48.
4. Crum, T.D. (1987) *AFGWC Cloud Forecast Models*, AFGWC/TN-87-001, Air Force Global Weather Central, Offutt AFB, NE, pp. 66.
5. Tarbell, T. and Hoke, J. (1979) *The AFGWC Automated Analysis/Forecast Model System*, AFGWC-TN-79/004, Air Force Global Weather Central, Offutt AFB, NE, pp. 52.
6. Mitchell, K. and Warburton, J. (1983) *A comparison of cloud forecasts derived from the NMC and AFGWC operational hemisphere forecasts of moisture*, Proceedings of AMS Sixth Conference on Numerical Weather Prediction, 6-9 June 1983, Omaha, NE, pp. 66-73.
7. Brenner, S., Yang, C.-H., and Mitchell, K. (1984) *The AFGL Global Spectral Model: Expanded Resolution Baseline Version*, AFGL-TR-84-0308, ADA160370.
8. Sela, J. (1980) Spectral modeling at the National Meteorological Center, *Mon. Wea. Rev.*, **108**:1279-1292.
9. Kless, R. and Cox, W. (1988) *The AFGWC Automated Real-Time Cloud Analysis Model*, AFGWC/TN-88-001, Air Force Global Weather Central, Offutt AFB, NE, pp. 82.
10. Kuo, H.L. (1965) On formation and intensification of tropical cyclones through latent heat release by cumulus convection, *J. Atmos. Sci.*, **22**:40-63.

11. Halberstam, I.M. (1988) *Objective Nephology, Section 1: Improved Regional Cloud Forecast Model*, AFGL-TR-88-0109, pp. 1-46, ADA200500.
12. Norquist, D. (1986) *Alternative forms of moisture information in 4-D data assimilation*, AFGL-TR-86-0194, pp. 139, ADA179792.
13. Kaplan, L.D., Hoffman, R.N., Isaacs, R.G., Rosen, R.D., Salstein, D.A., and Wang, W.-C. (1983) *Outlook for Improved Numerical Weather Prediction Using Satellite Data with a Special Emphasis on the Hydrological Variables*, AFGL-TR-83-0305, pp.183, ADA141233.
14. Mitchell, K. and Yang, C.-H. (1985) *A Comparison of Moisture Variables in the Vertical Interpolations of a 4-D Assimilation System*, AFGL-TR-85-0090, pp. 77, ADA160464.
15. Liou, K.-N., Ou, S.C., Kinne, S., and Koenig, G. (1984) *Radiation Parameterization Programs for Use in General Circulation Models*, AFGL-TR-84-0217, ADA148015.
16. Soong, S.-T., Ogura, Y., and Kau, W.S. (1985) *Study of Cumulus Parameterization in a Global Circulation Model*, AFGL-TR-85-0160, pp. 122, ADA170137.
17. Mahrt, L., Pan, H.-L., Paumier, J. and Troen, I. (1984) *A Boundary Layer Parameterization Scheme for a General Circulation Model*, AFGL-TR-84-0063, pp. 169, ADA144224.
18. Yang, C.-H., Norquist, D., Yee, S.Y.K., and Mitchell, K. (1989) *Diagnostics for and Evaluations of New Physical Parameterization Schemes for Global NWP Models*, GL-TR-89-0158.
19. Sundqvist, H. (1981) Prediction of stratiform clouds: results from a 5-day forecast with a global model, *Tellus*, **33**:242-253.
20. Bergman, K.H. (1979) Multivariate analysis of temperature and winds using optimum interpolation, *Mon. Wea. Rev.*, **107**:1423-1444.
21. Stackpole, J.D. (1978) *The NMC 9-Layer Global Primitive Equation Model on a Latitude-Longitude Grid*, NMC Office Note 178, National Meteorological Center, Washington, D.C.
22. McPherson, R.D., Bergman, K.H., Kistler, R.E., Rasch, G.E., and Gordon, D.S. (1979) The NMC operational global data assimilation system, *Mon. Wea. Rev.*, **107**:1445-1461.
23. Flattery, T. (1971) *Spectral methods for global analysis and forecasting*, Proc. Sixth AWS Technical Exchange Conference, U.S. Naval Academy, 21-24 September 1970, AWS-TR-242, Air Weather Service, Scott AFB, IL, 42-54.
24. Dey, C.H. and Morone, L.L. (1985) Evolution of the National Meteorological Center global data assimilation system: January 1982-December 1983., *Mon. Wea. Rev.*, **113**:304-318.
25. Fye, F.K. (1978) *The AFGWC Automated Cloud Analysis Model*, AFGWC-TM-78-002, Air Force Global Weather Central, Offutt AFB, NE, pp. 97.
26. Stobie, J.G., Lewis, M.D., Langford, M.A., Tuell, J.P., and Carr, E.L. (1985) The use of optimum interpolation at AFGWC, *Preprints Seventh Conference on Numerical Weather Prediction*, Montreal, P.Q., Canada, Amer. Meteor. Soc., 43-49.
27. Cressman, G.P. (1959) An operational objective analysis system, *Mon. Wea. Rev.*, **87**:367-374.
28. Norquist, D. (1988) Alternative forms of humidity information in global data assimilation, *Mon. Wea. Rev.*, **116**:452-471.
29. Edson, H. (1965) *Numerical Cloud and Icing Forecasts*, Scientific Services Technical Note 13, 3rd Weather Wing, Offutt AFB, NE, pp. 44.
30. Hughes, N.A. and Henderson-Sellers, A. (1985) Global 3-D nephanalysis of total cloud amount: climatology for 1979, *J. Climate Appl. Meteor.*, **24**:669-686.

31. Henderson-Sellers, A. (1986) Layer Cloud Amounts for January and July 1979 from 3D-Nephanalysis, *J. Climate Appl. Meteor.*, **25**:118-132.
32. Staff (1986) *Daily Global Analyses: Operational Data Assimilation System, January - March 1985*, European Center for Medium Range Weather Forecasts, Reading, Berkshire, U.K.
33. Lejenas, H. (1979) Initialization of moisture in primitive equation models, *Mon. Wea. Rev.*, **107**:1299-1305.
34. Slingo, J. (1980) A cloud parametrization scheme derived from GATE data for use with a numerical model, *Q.J.R. Met. Soc.*, **106**:747-770.
35. Slingo, J. (1987) The development and verification of a cloud prediction scheme for the ECMWF model, *Q.J.R. Met. Soc.*, **113**:899-927.
36. Chu, R. and Parrish, D. (1977) *Humidity analyses for operational prediction models at the National Meteorological Center*, NMC Office Note 140, National Meteorological Center, Washington, D.C.
37. Tibaldi, S. (1982) The ECMWF humidity analysis and its general impact on global forecasts and on the forecast in the Mediterranean area in particular, *Rivista di Meteorologia Aeronautica*, **42**:309-328, (portion used in this report also available in the book *Atmospheric Water Vapor* (1980) Academic Press, ISBN 0-12-208440-3).
38. Rasmussen, R.G. (1982) *Some Techniques for the Objective Analysis of Humidity for Regional Scale Numerical Weather Prediction*, Ph. D. thesis, NCAR/CT-67, National Center for Atmospheric Research, Boulder, CO.

List of Acronyms

AFGWC	Air Force Global Weather Central
AFSCC-K	Air Force Supercomputer Center-Kirtland AFB
AWAPS	Advanced Weather Analysis and Prediction System
AWS	Air Weather Service
CPS	condensation pressure spread
ECMWF	European Centre for Medium Range Weather Forecasts
FGGE	First GARP Global Experiment
GARP	Global Atmospheric Research Program
GDAS	Global Data Assimilation System
GL	Geophysics Laboratory
GSM	global spectral model
HIRAS	High Resolution Analysis System
ITCZ	inter-tropical convergence zone
MULTAN	Multi-level Analysis Model
NH	Northern Hemisphere
NMC	National Meteorological Center
NWP	numerical weather prediction
OI	optimum interpolation
PBL	planetary boundary layer
PE	primitive equation
RAOB	radiosonde observation
RH	relative humidity
RTNEPH	Real-time Nephanalysis Model

SH	Southern Hemisphere
TROPUA	Tropical Upper-air Analysis Model
USAF	United States Air Force
3DNEPH	Three-dimensional Nephanalysis Model
5LAYER	Five-layer Cloud Forecast Model

APPENDIX A

The Vertical Cloud Stacking Algorithm

To obtain a forecast of total cloud from a forecast of cloud cover at several layers, a vertical cloud stacking algorithm must be used. Cloud stacking algorithms usually fall into one of two categories, adhering either to the assumption of (1) maximum layer overlap or (2) random layer overlap. In the more general algorithm applied here, taken from that used in the AFGWC 5LAYER model, a free parameter referred to as the stacking factor R (detailed shortly) is introduced to permit maximum overlap, random overlap, or any degree in between.

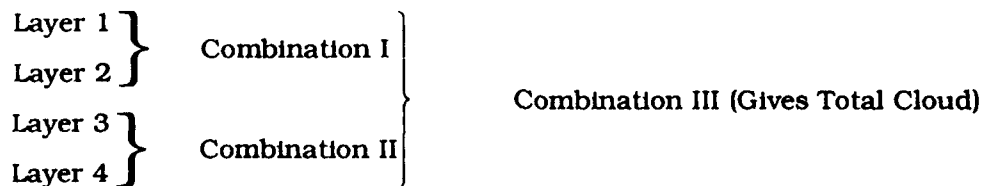
The various cloud forecast schemes and models addressed in this study yield layer cloud forecasts at six layers (in the schemes GSM/A, GSM/N, GSM/E, GSM/EM, GSM/GL6), five layers (in the 5LAYER model), and four layers (in the scheme GSM/GL4). To most easily describe the application of the stacking algorithm to these various numbers of layers, it is convenient to present the scheme as a four-layer scheme, which in cases of more than four input layers is preceded by a preliminary step that combines one or more pairs of neighboring cloud layers using maximum overlap. Table A1 shows the preliminary step in the six-, five-, and four-layer cases encountered in this study. In the four-layer case of scheme GSM/GL4, the preliminary step is really a null or "do nothing" step, with the exception of terrain masking described next.

Table A1. Preliminary Step of the Vertical Cloud Stacking Algorithm.

GSM/A, N, E, EM, GL6 CLOUD SCHEMES	5LAYER MODEL CLOUD TEST	GSM/GL4 CLOUD SCHEME	OUTPUT LAYER CLOUD AMNT
100 kPa } MAX Cld 85 kPa } Amnt	Gradient } MAX Cld 85 kPa } Amnt	LOW Cld Amnt	Layer 1
70 kPa Cld Amnt	70 kPa Cld Amnt	70 kPa Cld Amnt	Layer 2
50 kPa Cld Amnt	50 kPa Cld Amnt	50 kPa Cld Amnt	Layer 3
40 kPa } MAX Cld 85 kPa } Amnt	30 kPa Cld Amnt	HIGH Cld Amnt	Layer 4

During the preliminary step for all columns outlined in Table A1, at grid points where the terrain height is above one or more of the listed standard pressure surfaces, the cloud amount is set to zero at each terrain-filled surface. For this purpose, the 5LAYER 1/2-mesh field of terrain heights is used, for both the 5LAYER and GSM cloud layers. This terrain field never extends to 40 kPa, so at least Layer 4 in Table A1 is an active layer at every grid point. Overall, very few points are terrain-filled at 70 kPa and above. Finally, as noted in the main text, the "Gradient" layer cited in the 5LAYER column of Table A1 denotes a terrain-following layer centered at 6 kPa above the terrain-surface pressure. Thus in the 5LAYER case of Table A1, whenever the 85, 70, or 50 kPa levels are terrain-filled, the MAX operation with the Gradient layer shifts to Layer 2, 3, or 4 respectively in Table A1.

After the preliminary step, the stacking algorithm operates on the four input layer cloud amounts according to the three successive pairings or combinations shown below:



To perform each Combination I, II, or III, one begins with two layer cloud amounts, identified generically as amounts A and B, expressed in percent, with A denoting the largest. The amounts A and B are divided by 100 to get fractional amounts CA and CB in the range 0 to 1. By way of background, if cloud presence in one layer is considered an event independent of cloud presence in the other layer (that is, the vertical alignment is random), then the

vertically superimposed overlap of the two layers is the product $CA*CB$. The total or combined sky-cover fraction, CC , of the two layers is then given by

$$CC = CA + CB - CA*CB, \tag{A1}$$

or equivalently

$$CC = CA + (1-CA)*CB \tag{A2}$$

Eq. (A2) shows that CC can be viewed as the cloud fraction from layer A plus that part of cloud layer B randomly aligned over the clear area of layer A. Actual experience shows, however, that cloud presence in one layer is often positively correlated with cloud presence in another layer, the correlation being greater for smaller layer separation distances. To account for this observation, the stacking algorithm applied in this study generalizes Eq. (A2) by introducing a "stacking factor" R according to

$$CC = CA + (1-CA)*CB*R, \tag{A3}$$

$$CA \geq CB, \quad 0 \leq R \leq 1$$

The two limiting cases of $R=0$ and $R=1$ yield the combined cloud amount, respectively, for maximum overlap (giving the smallest CC) and random overlap (giving the largest CC). Intermediate values of R give combined cloud amounts falling between these limiting values. It can be rigorously proved that CC in Eq. (A3) is bounded in all cases by 0 and 1.

It remains only to specify the values of R used in this study for the three combinations I, II, and III diagrammed above. Although the details are somewhat tedious, overall we allow for larger R values for increasing distances between cloud layers. In the "MAX" operations listed in the preliminary stacking step of Table A1, we implicitly applied Eq. (A3) with $R=0$, that is we assumed adjacent layers were maximally overlapped. In Combination I of Layers 1 and 2, we use $R=0.2$, with the exception of $R=0.3$ if the 100 kPa or Gradient layer is chosen in the MAX operation in the preliminary step giving Layer 1 in Table A1. In Combination II of Layers 3 and 4, we use $R=0.3$, with the exception of $R=0.4$ if the 30 kPa layer cloud amount is chosen in the MAX operation in the preliminary step giving Layer 4 in Table A1. In Combination III, which combines the resulting cloud amounts of I and II, R takes one of the nine values given by $R = RM(I,J)$ from the 3 X 3 RM matrix below:

